

1981

Berg Porphyry
Copper - Molybdenum Deposit

Geologic Setting, Mineralization,
Zoning, and Pyrite Geochemistry

By Andrejs Panteleyev

Bulletin 66



**Province of
British Columbia**
Ministry of Energy,
Mines and
Petroleum Resources

Canadian Cataloguing in Publication Data

Panteleyev, Andrejs, 1942—
Berg porphyry copper-molybdenum deposit.

(Bulletin / Province of British Columbia, Ministry of Energy,
Mines and Petroleum Resources, ISSN 0226-7497 ; 66)

Bibliography: p.
ISBN 0-7718-8269-6

1. Copper ores — British Columbia — Tahtsa Ranges. 2. Molybdenum ores — British Columbia — Tahtsa Ranges. 3. Geology, Economic — British Columbia — Tahtsa Ranges. I. British Columbia. Ministry of Energy, Mines and Petroleum Resources. II. Title. III. Series: Bulletin (British Columbia. Ministry of Energy, Mines and Petroleum Resources) ; 66.

TN444.C32B76 553.4'3'09711 C81-092343-2

**MINISTRY OF ENERGY, MINES AND PETROLEUM RESOURCES
VICTORIA, BRITISH COLUMBIA
CANADA**

JULY 1981



Frontispiece

Berg deposit, view to northeast.

Berg Porphyry Copper - Molybdenum Deposit

Geologic Setting, Mineralization, Zoning, and Pyrite Geochemistry

SUMMARY

Berg copper-molybdenum deposit is in mountainous terrain of the Tahtsa Ranges in west-central British Columbia. Of the major porphyry copper-molybdenum prospects discovered in the Canadian Cordillera (see Sutherland Brown, 1976) it is the one that possibly most closely resembles the idealized porphyry copper model of Lowell and Guilbert (1970).

Berg deposit is found in thermally metamorphosed and hydrothermally altered Jurassic Hazelton volcanic rocks and Tertiary quartz diorite adjacent to a weakly mineralized Eocene stock. The stock is about 640 metres in diameter and consists of four quartz monzonitic phases. A major intrusive breccia body is associated with the stock. Weakly mineralized volcanic rocks and barren sedimentary strata of the Lower Cretaceous Skeena Group crop out east of the deposit. These are overlain to the north by rocks of the Upper Cretaceous Kasalka Group.

Hydrothermal alteration and sulphide minerals are arranged in concentric, annular zones around the composite stock. From the interior outward pervasive alteration zones are potassic, phyllic, biotitic, and propylitic. Argillic alteration is rare. The biotitic zone surrounding the stock is a thermal aureole (biotite hornfels) that has been enhanced by an overlapping hydrothermal biotite overprint.

A multistage vein stockwork is superimposed on the pervasively altered rocks. Early veins, both with and without alteration envelopes, were deposited from saline fluids at temperatures in excess of 400 degrees celsius. Later veins were deposited from cooler, less saline fluids and commonly have retrograde alteration envelopes or bleached margins. A gypsum-filled subhorizontal fracture cleavage cuts all alteration minerals and veins.

The molybdenite zone (> 0.05 per cent MoS_2) closely follows the intrusive contact where quartz stockworks are well developed. Chalcopyrite is most abundant outside the stock in the zone of biotitic alteration. Pyrite is concentrated 200 to 300 metres from the intrusive contact but is abundant throughout a broad halo that extends outward from the stock for at least 600 metres.

Leaching and supergene mineralization cause pronounced vertical zoning in the deposit. In the leached capping copper has been removed to a depth of 38 metres but molybdenum remains and is locally concentrated in limonite. In the supergene zone which overlies the entire deposit and is as much as 91 metres in thickness, copper is enriched by a factor of 1.25 over primary grade. Supergene mineralization is a contemporary ongoing process that was initiated after Pleistocene glaciation.

Minor elements in pyrite are concentrated in disseminated pyrite from the zone of best copper mineralization. Pyrite from all veins, including early molybdenum-bearing veins, has less minor element concentration. This bimodal distribution can be demonstrated by univariate and bivariate statistical analyses and implies a different origin for vein as opposed to disseminated pyrites. Zoning patterns of minor elements in disseminated pyrite are similar to alteration and sulphide zoning around the composite stock. Q-mode factor analysis duplicates individual element zoning patterns and, more significantly, accentuates the well-mineralized zone.

RÉSUMÉ

Le gisement de cuivre-molybdène de Berg se situe dans la chaîne des Tahtsa, dans le centre-ouest de la Colombie Britannique. De tous les grands gisements porphyriques de cuivre-molybdène découverts dans la Cordillère Canadienne (*voir* Sutherland Brown, 1976), c'est celui qui semble se rapprocher le plus du modèle théorique de Lowell et Guilbert (1970).

Le gisement se présente dans des roches adjacentes à un stock faiblement minéralisé d'âge Eocène. Ces roches sont des volcanites Hazelton, du Jurassique, qui ont subi un métamorphisme de contact et une altération hydrothermale, et une diorite quartzique, du Tertiaire. Le stock, d'environ 640 mètres de diamètre, comprend quatre phases de monzonite quartzique; une importante brèche intrusive lui est associée. Des volcanites faiblement minéralisées et des strates sédimentaires stériles du groupe de Skeena, du Crétacé inférieur, affleurent à l'est du gisement. Elles sont recouvertes, au nord, par des roches du groupe de Kasalka, du Crétacé supérieur.

L'altération hydrothermale et les sulfures se présentent en zones concentriques, annulaires, autour du stock. Du centre vers la périphérie, les zones sont potassiques, phylliques, biotitiques, et propylitiques. L'altération argileuse est rare. A noter que la zone biotitique est une auréole thermique (cornéenne à biotite) à laquelle s'adjoint une altération hydrothermale à biotite.

Un stockwerk à stades multiples se superpose aux roches profondément altérées. Les premières veines, avec ou sans auréoles d'altération, résultent de fluides salins déposés à des températures dépassant 400° C. Les veines subséquentes, de causalité moins saline et de températures plus basses, sont généralement accompagnées d'auréoles d'altération régressive ou de bordures blanchies. Un clivage cassant, subhorizontal et à remplissage de gypse, recoupe tous les minéraux d'altération et les veines.

La zone de molybdénite ($>0.05\% \text{ MoS}_2$) s'accroche au contact intrusif là où les stockwerks quartzifères sont bien développés. La chalcopyrite est fort abondante dans la zone

biotitique, en dehors de stock. La pyrite se concentre à 200 ou 300 metres du stock mais elle continue à abonder dans un halo qui se manifeste sur une distance d'au moins 600 metres.

La lixiviation et la minéralisation supergène se traduisent par une zonalité verticale marquée. Dans le capucon lixivié, le cuivre a été éliminé jusqu'à une profondeur de 38 metres; le molybdène, qui y est demeuré, a localement été concentré dans la limonite. Dans la zone supergène, qui recouvre complètement le gisement et atteint 91 metres d'épaisseur, la teneur originelle en cuivre est multipliée par 1.25. L'enrichissement de la minéralisation, un processus qui a commencé après la glaciation du Pléistocène, se continue encore.

La pyrite qui renferme le plus d'éléments est celle essaimée dans la zone à minéralisation cuprifère maximum. La pyrite associée aux veins, y compris les veines précoces à molybdène, en renferme moins. Cette distribution bimodale, démontrable par analyses statistiques univariées et bivariées, implique que les deux pyrites ont des origines différentes. La zonation des éléments dans la pyrite disséminée ressemble à celle de l'altération et des sulfures autour du stock. L'analyse factorielle à mode Q reproduit les zonations individuelles des éléments et, surtout, fait ressortir la zone bien minéralisée.

TABLE OF CONTENTS

	Page
SUMMARY	5
RÉSUMÉ	7
1 INTRODUCTION	15
Location and Access	15
Weather	17
History of Exploration	17
Physiography	19
Glaciation	20
Acknowledgments	21
Bibliography	21
2 GEOLOGY	29
Regional Geology of Tahtsa Ranges	29
Geology of Berg Map-area	29
Hazelton Group (Middle Jurassic; Fig. 3, Unit 1)	30
Skeena Group (Lower Cretaceous; Fig. 3, Units 2 and 3) ..	31
Kasalka Group (Upper Cretaceous; Fig. 3, Units 4 and 5) ..	32
Quartz Diorite	33
Quartz Monzonite Porphyry	36
Minor Intrusions	37
Structure	37
Geology of Berg Copper-Molybdenum Deposit	39
Bedded Rocks	42
Intrusive Rocks	44
Quartz Diorite (Fig. 7, Unit 2)	45
Mineralized Quartz Monzonite Stock and Dykes (Fig.	
7, Units 3 to 5)	46
Quartz Monzonite Porphyry Phase (QMP; Fig.	
7, Unit 3)	46
Sericitized Quartz Plagioclase Porphyry Phase	
(QPP; Fig. 7, Unit 4)	47
Plagioclase Biotite Quartz Porphyry (PBQP;	
Fig. 7, Unit 5)	48
Quartz Monzonite-Granodiorite Dykes (Horn-	
blende quartz feldspar porphyry, hbde	
QFP; Fig. 7, Unit 6)	49
Basic Dykes	50
Chemical Composition	50
Distribution and Geometry of Porphyries (Fig. 7) ...	50

2	GEOLOGY (CONTINUED)	
	Geology of Berg Copper-Molybdenum Deposit (<i>Continued</i>)	
	Intrusive Rocks (<i>Continued</i>)	
	Age of Intrusions	53
	Breccias	54
	Intrusive Breccia (Pebble Breccia Pipe)	54
	Other Breccias (Observed Only in Diamond-drill Core)	55
	Breccia 1	55
	Breccia 2	55
	Breccia 3	55
	Breccia 4	56
	Structure	56
3	HYDROTHERMAL ALTERATION	59
	Introduction	59
	Definition of Alteration Facies and Zones	61
	Potassic Alteration	62
	Biotitic Alteration	62
	Phyllic Alteration	64
	Propylitic Alteration	64
	Argillic Alteration	65
	Veins	65
	Hydrothermal Processes in the Formation of Berg Deposit	67
4	MINERALIZATION	89
	Introduction	89
	Primary Mineralization and Lateral Zoning	90
	Secondary Mineralization and Vertical Zoning	97
	Extent of Leaching and Supergene Mineralization	99
	Mineralogy and Processes of Formation	103
	Zone of Oxidation and Sulphide Leaching	103
	Zone of Supergene Enrichment	107
5	MINOR ELEMENTS IN PYRITE	115
	Introduction	115
	Univariate Analysis	117
	Frequency Distribution Plots (Histograms)	117
	F and t Tests	121
	Cumulative Probability Plots	124
	Bivariate Analysis	127
	Correlation and Simple Regression	127
	Cobalt-Nickel Ratios	131
	Multivariate Analysis	133

5	MINOR ELEMENTS IN PYRITE (CONTINUED)	
	Minor Element Zoning in the Deposit	136
	Introduction	136
	Univariate Minor Element Zoning	138
	Zoning of Factors (Multivariate Analysis)	143
	Summary of Minor Element Study	147

APPENDICES

A.	Elements Detected in Berg Pyrite	151
B.	Analytical Results – Minor Elements in Pyrite	154
C.	Data Parameters and Computed Chi Square Values	156
D.	Varimax Factor Matrix, Disseminated Pyrite	157
E.	Varimax Factor Matrix, Vein Pyrite	158

TABLES

1.	Mineralogical composition of intrusive rocks, Berg deposit	46
2.	Chemical compositions and norms	51
3.	Potassium-argon ages, Berg deposit	53
4.	Partial analyses of iron ores and Berg ferricrete	105
5.	Analytical precision	116
6.	Comparison of spectrographic and atomic absorption analyses of pyrite concentrates	117
7.	Summary – mean and standard deviation	121
8.	Calculated t and F probability of vein pyrite versus disseminated pyrite	122
9.	F and t tests – Ni in pyrite	123
10.	Summary of t and F tests for all elements	125
11.	Correlation of paired variables	128
12.	R ² and F ratios for all data of all pairs of variables having significant correlation	129
13.	Characteristic Co and Ni concentrations in ppm	132
14.	Successive Q-mode varimax factor components – disseminated pyrite	134
15.	Q-mode varimax factor scores – disseminated pyrite	134
16.	Successive Q-mode varimax factor components – vein pyrite	135
17.	Vertical variation of minor elements in pyrite	138
18.	Spectrographic analysis of pyrite	152
19.	Minor element content of chalcopyrite	152

FIGURES

1.	Berg property location map	16
2.	Geology of Tahtsa Ranges	28
3.	Geology of Berg map-area	In pocket
4.	Air photograph interpretation of fracture trends	38
5.	Geology – Berg deposit	40

FIGURES (CONTINUED)

6.	Geologic cross sections (view looking northerly)	41
7.	Geology and drill hole location map	In pocket
8.	Subdivision of Hazelton Group volcanic succession at Berg deposit	42
9.	Modal composition of intrusive rocks, Berg deposit	48
10.	Generalized alteration zones, Berg deposit	60
11.	Mineral assemblages in thermally metamorphosed andesite, quartz diorite, and quartz monzonite	69
12.	Primary minerals – pyrite	91
13.	Pyrite-chalcopyrite ratio	92
14.	Primary mineralization – Cu	93
15.	Primary mineralization – Mo	94
16.	Primary Cu and MoS ₂ grade in relation to distance from main intrusive contact	96
17.	Vertical zoning of Cu and MoS ₂ grades in diamond-drill cores	98
18.	Trend surface elevation marking start of gypsum in fractures	100
19.	Trend surface isopach map, strongly oxidized rocks (Cu leached)	101
20.	Trend surface isopach map, supergene Cu mineralization	102
21.	Mineral stability at 25° C and 1 ATM:	
	A. Cu-Fe-S-O-H modified from Garrells (1960)	108
	B. Mo-Fe-S-O-H after Barakso and Bradshaw (1971)	108
	C. Fe-S-O-H in presence of K ⁺ after Brown (1971)	108
22.	Stability fields in Cu-H ₂ O-CO ₂ -O ₂ -S system (including chalcopyrite) at 25° C and 1 ATM	109
23.	Mineral compositions showing possible phase relationships	111
24.	Primary and supergene copper minerals	112
25.	Berg deposit, idealized geologic sections	113
26.	Ni and Zn content of pyrite	118
27.	Pb and Ag content of pyrite	119
28.	Frequency distributions of As, Co, and Ti	120
29.	Bimodal distribution containing vein and disseminated pyrite populations	122
30.	Distribution of Ni in pyrite	123
31.	Cumulative probability; minor elements in disseminated pyrite	127
32.	Linear least squares regression line (Y = a + bX) for Co:Ni(A) and Pb:Zn(B)	130
33.	Cobalt-nickel scatter diagram showing pyrite according to source	131
34.	Co-Ni ratios of pyrite	132
35.	Zoning of minor elements in pyrite, Co and Ni	139
36.	Zoning of minor elements in pyrite, Co and Ni and Co/Ni	140
37.	Composite of maximum minor element values	142
38.	Contoured plan of Q-mode factor values – factors 1 and 2	144
39.	Contoured plan of Q-mode factor values – factors 3 and 4	145
40.	Composite of factors 1 to 4	146

PLATES

Berg deposit, view to northeast	Frontispiece
I. Berg camp (lower left) and Mount Ney	34
II. Skeena sedimentary rocks overlain by Kasalka volcanic rocks	35
III. Mount Ney, elevation 2 469.8 metres (8,103 feet)	35
IV. Berg deposit, view looking northerly	73
V. Berg deposit, Tahtsa Ranges, view to east-northeast	74
VI. Berg camp viewed to the west (VIA) down 'Red Creek' and south-west (VIB) across Bergeland Creek	75
VII. Berg camp looking northeast along quartz monzonite ridge: vivid jarositic clay-rich soil (VIIA); fibrous jarositic limonite precipitation from springs (VIIB)	76
VIII. Quartz monzonite porphyry (Fig. 7, unit 3; QMP)	77
IX. Quartz monzonite porphyry	78
X. Detail in quartz monzonite porphyry of anhedral resorbed quartz phenocryst with vermicular plagioclase and K-feldspar inclusions	79
XI. Sericitized quartz plagioclase porphyry (Fig. 7, unit 4, QPP)	80
XII. Quartz plagioclase porphyry with quartz veining (unstained specimen) and silicified alteration envelopes on fractures (stained specimen)	81
XIII. Plagioclase biotite quartz porphyry (Fig. 7, unit 5; PBQP)	82
XIV. Hornblende quartz feldspar porphyry (Fig. 7, unit 6; hbde QFP)	83
XV. Quartz diorite (Fig. 7, unit 2) with quartz and K-feldspar veining	84
XVI. Pervasive phyllic alteration and quartz veining in bleached hornfels (left specimen) and quartz plagioclase porphyry (right specimen)	85
XVII. Veining in biotite hornfels	86
XVIII. Potassic alteration in biotite hornfels	87
XIX. Biotite hornfels with relict pale lapilli	88

INTRODUCTION

Berg deposit is a major copper-molybdenum prospect in the Canadian Cordillera that very closely resembles the idealized porphyry copper model of Lowell and Guilbert (1970).

Copper and molybdenum sulphides are associated with a small Tertiary quartz monzonite porphyry stock that intrudes Mesozoic volcanic rocks. The stock has a number of intrusive phases and associated breccia bodies. Hypogene mineralization resulted in: (1) fracture-controlled and disseminated pyrite and chalcopyrite; (2) quartz stockworks with pyrite, molybdenite, and chalcopyrite; and, less commonly, (3) quartz and quartz-carbonate veins containing pyrite, sphalerite, galena, chalcopyrite, and sulfosalt minerals. Sulphide zoning is evident within a broad annulus of hydrothermally altered rocks about a weakly mineralized intrusive core. Weathering has produced a leached capping that is underlain by a laterally extensive supergene copper zone. Hypogene copper and molybdenum sulphides below the supergene zone are locally of ore grade. Geological reserves are in the order of 400 million tonnes containing 0.4 per cent copper and 0.05 per cent molybdenite (Panteleyev, Drummond, and Beaudoin, 1976).

LOCATION AND ACCESS

Berg deposit is in Omineca Mining Division in west-central British Columbia at latitude 53 degrees 49 minutes north, longitude 127 degrees 25.5 minutes west (Figs. 1 and 2). It lies in the Tahtsa Ranges approximately midway between Tahtsa, Nanika, and Kid-price Lakes in the northwestern corner of Whitesail map-area (NTS 93E/14W). Except for some habitation at Kemano to the southwest and Ootsa Lake to the east, the closest centres of commerce are Houston, 93 kilometres (57 miles) to the northeast, and Smithers, 118 kilometres (73 miles) to the north. The property is about 585 kilometres (365 miles) north of Vancouver.

The area of economic interest is on moderate to steep, south and west-facing slopes in generally rugged, mountainous terrain. The claim group containing Berg deposit lies

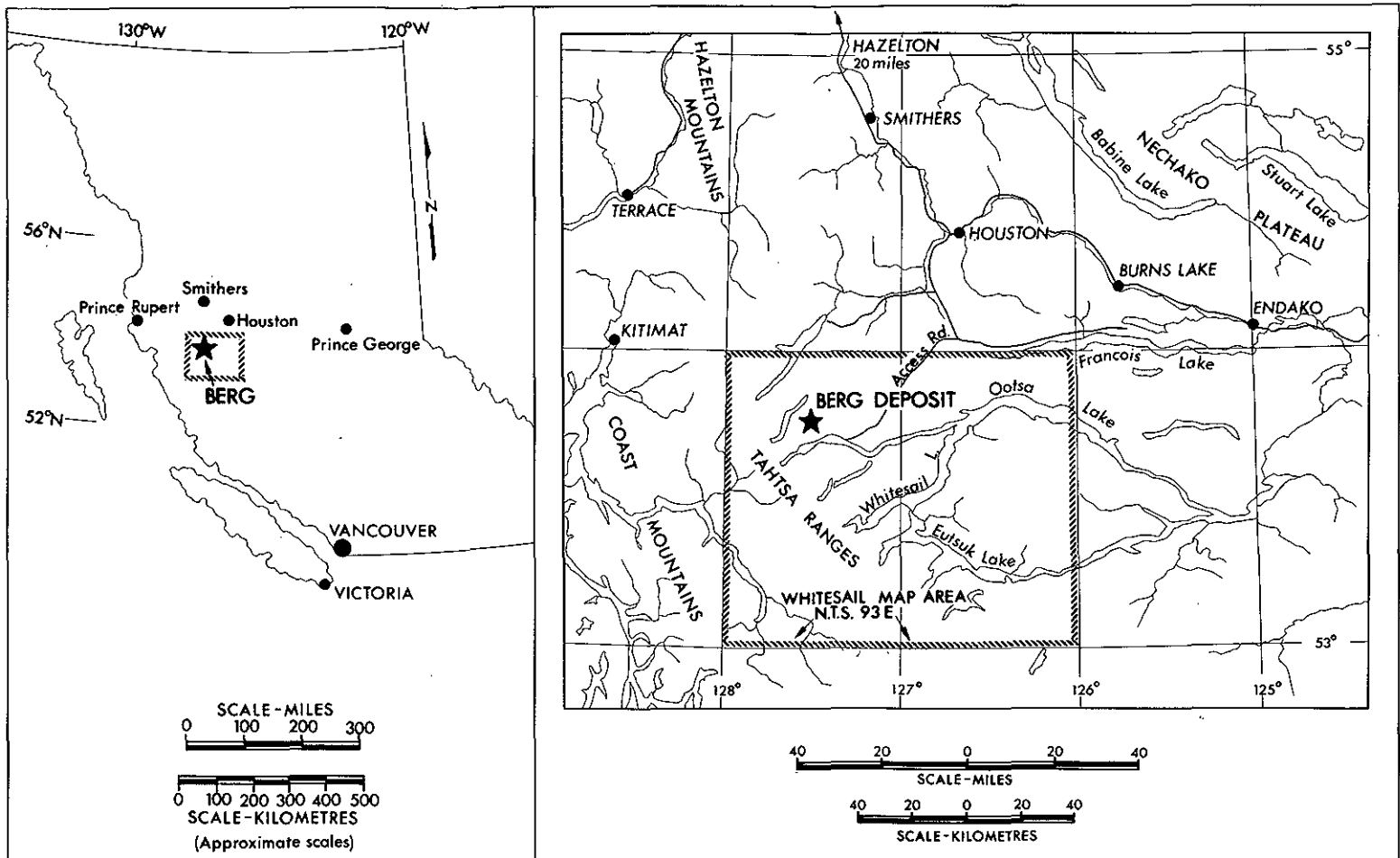


Figure 1. Berg property location map.

between elevations of 1 375 and 2 275 metres (4,500 and 7,450 feet), mainly to the north of the east fork of Bergeland Creek.

Access for most personnel during early exploration was by helicopter from bases at Smithers and Houston, but later a 42-kilometre (26-mile) bulldozer road was built to the camp from Twinkle Lake on the Tahtsa Lake forest access road. The access road traverses the northern flank of Sibola Peak and then follows Kidprice Creek to its headwaters where it crosses a 1 740-metre (5,700-foot) pass and descends to camp at an elevation of 1 555 metres (5,100 feet).

During the early stages of exploration most drill equipment and supplies were brought to the property on sleds with a bulldozer but work on the access road has upgraded it to the point where, since 1970, with some annual maintenance it is usually possible during summer months to reach the property with a four-wheel-drive vehicle and occasionally with a two-wheel-drive vehicle. Access for about six winter months is restricted to vehicles capable of travel in snow, but winter travel requires prudence because of avalanche hazards. Spring thaw and resulting breakup render the property inaccessible by road for up to one month. Alternate access routes from the north and west may be *feasible if mining development continues.*

WEATHER

The weather, typical of mountainous terrain along the east flank of the Coast Mountains, is unsettled with rapid changes. Short, generally cool summers are punctuated with numerous showers. Midsummer temperatures in excess of 20 degrees celsius are common but hail or sleet storms of short duration can occur on any day. The region is in the rain shadow of the Coast Mountains and thus has relatively light precipitation of about 100 centimetres per year. However, rainfall can accumulate very rapidly during short, violent storms. In winter, snow is generally less than 1 metre deep on the valley floors and open sidehills but deeper snow accumulations, drifts, and avalanche areas on northern and eastern slopes give rise to small permanent snowfields that sustain numerous small glaciers. Possibly the most adverse weather conditions for work in the area are caused by high winds that occasionally reach gale and hurricane force. Company records also show that dense fog sometimes enveloped the area for days at a time and reduced visibility to a few tens of metres.

HISTORY OF EXPLORATION

Prospecting in the Whitesail map-area started soon after the settlers arrived in the early 1900's and resulted in the discovery of a number of lead-zinc-silver, silver, gold-tungsten, copper, and molybdenum deposits. In 1913, 'Kid' Price found placer gold and its source

veins on Sibola Peak and precipitated a small rush to the area in 1914. From 1915 to the late 1920's, a number of lead-zinc-silver and copper deposits were located, the most notable being the Emerald Glacier deposits on Mount Sweeney approximately 13.7 kilometres (8.5 miles) southeast of Berg property. In 1929 lead-zinc-copper-silver veins peripheral to the Berg copper-molybdenum deposit were first staked.

Prospecting activity declined during the 1930's but was renewed during 1943 to 1947 by discoveries of gold-tungsten mineralization on Lindquist Peak (Duffel, 1959). General activity in the area increased after 1947 when the Aluminum Company of Canada, Limited—Aluminium du Canada, Limitée (Alcan) started engineering studies for its Kitimat project and the Geological Survey of Canada initiated a program of systematic regional mapping. The Francois-Tahtsa Lake access road built by Alcan and the raised water level in a number of lakes provided improved access to many regions and prompted a period of renewed exploration and property development in the late 1940's and early 1950's. In 1948 the Lead Empire Syndicate relocated claims first staked in 1929 on the lead-zinc-copper-silver veins along what is now the northern boundary of the Berg deposit. The first significant mineral production in the district was attained from the Emerald Glacier mine during 1951 to 1953. Mining resumed in 1966 and 1967; total production ending in 1967 was 9,196 tons of ore with gross metal content of 49 ounces gold, 83,494 ounces silver, 19,872 pounds copper, 1,689,456 pounds lead, 1,996,407 pounds zinc, and 3,713 pounds cadmium.

The main brunt of exploration activity and an appreciation for the tremendous mineral potential of the area began in the early 1960's when exploration philosophy became oriented toward large tonnage deposits amenable to open-pit mining. Highly mobile, helicopter-supported exploration teams with geochemical and geophysical facilities and assisted by a newly published geological map (Duffel, 1959, Geological Survey of Canada, Map 1064A), found a large number of significant deposits and occurrences of copper-molybdenum and molybdenum. These include: Berg, Huckleberry, Whiting Creek, Ox Lake, Red Bird, Coles Creek, Lucky Ship, Troitsa, Bergette, Nanika, and others (*see* Carter, 1974, 1976).

Berg copper-molybdenum prospect was located as the 28 BERG mineral claims in 1961. The property name 'Berg' is derived from nearby geographic features Bergeland Creek and Mount Bergeland. Evidence of Berg deposit has been known for a long time because a large, brightly coloured capping, most of which is above tree line, marks the mineralized zone. In the centre of Berg property exploration pits predating the 1961 staking were found on a quartz-molybdenite vein. The lead-zinc-silver vein deposits located first in 1929 and again in 1948 are peripheral to the zone of copper-molybdenum mineralization along the northeast margin of the vivid colour anomaly.

The Berg claim group was located to cover the prominent capping developed on and around a small stock that is the locus of a strong geochemical anomaly. Stream sediment samples at the confluence of two forks of Bergeland Creek, about 2 miles downstream

from the deposit, are said to have contained as much as 47 000 parts per million copper and 60 parts per million molybdenum (H. Goddard, 1974, personal communication). In spite of such a strong geochemical expression, prospecting results were discouraging. Molybdenite is widespread, but generally sparse, in the intrusive rocks; in outcroppings copper minerals are absent except as secondary oxides and carbonates along borders of some basalt dykes.

In 1963 geologists with experience in the southwestern United States were the first to appreciate the ore potential of the extensively leached rocks. Increased exploration expenditure in 1964 enabled bulldozer trenching and diamond drilling that demonstrated the profound effects of surface leaching and revealed the widespread presence of supergene minerals, a feature not common in the Canadian Cordillera. Subsequent work showed that rocks are leached in places to depths in excess of 30 metres, and these rocks are underlain by an extensive 'blanket' of supergene copper enrichment.

Drilling during 1965 and 1966 delineated two main mineralized zones. A northeast zone contains primary (hypogene) and some supergene mineralization, and a southeast zone has widespread supergene mineralization. At the end of the 1966 field season the property consisted of 108 mineral claims on which there had been a total of 3 770.7 metres (12,371 feet) of diamond drilling in 23 holes. During 1967 a 3 461.6-metre (11,357-foot) drill program tested the southeast zone on a widely spaced grid and three holes explored areas peripheral to the main area of interest. From 1968 to 1970 the property was dormant but metallurgical testing was done on composite samples of drill core. In 1971 three additional holes were drilled in the northeast zone. At the end of the 1971 exploration program a total of 49 diamond-drill holes of mainly NQ and BQ core had been completed with a total depth of 7 980.9 metres (26,184 feet).

In 1972 exploration and development of the property were taken over by Canex Placer Limited (Placer Development Limited) under agreement with Kennco Explorations, (Western) Limited. From 1972 to 1975 an additional 25 drill holes of NQ core totalling 7 083.2 metres (23,239 feet) and 19 drill holes of BQ core totalling 1 843.7 metres (6,049 feet) were completed. In total, 16 907.8 metres (55,472 feet) of drilling was completed in 93 diamond-drill holes. In 1976 work was again suspended and the property is dormant at this time of writing.

PHYSIOGRAPHY

Berg deposit is in the Tahtsa Ranges, a 16 to 24-kilometre-wide (10 to 15-mile) belt of mountains within the Hazelton Mountains (Holland, 1964). The Hazelton Mountains lie along the eastern flank of the Kitimat Ranges of the Coast Mountains and form part of the Skeena Arch, a northeasterly trending area that was tectonically positive and was a locus for intrusive activity throughout much of the Mesozoic. Duffel (1959) referred to the Tahtsa Ranges as 'transitional ranges' because they represent a transitional zone

between the rugged, predominantly granitic Coast Mountains to the west and the rolling hill region of sedimentary and volcanic rocks that underlie the Nechako Plateau to the east. This terrane would correspond to a 'highland' region as described by Holland (1964).

The Tahtsa Ranges are further subdivided into east-west to northeasterly trending ranges called, from north to south, the Tahtsa, Sibola, Whitesail, and Chikamin Ranges. These are separated by major valleys whose floors range in elevation from 795 to 945 metres (2,600 to 3,100 feet) and which are occupied by long lakes; from north to south these are Morice, Nanika, Tahtsa, Troitsa, Whitesail, and Eutsuk Lakes. All drain eastward into waterways of the Skeena or Fraser Rivers drainage systems.

The highest peak in the Tahtsa Ranges is a previously unnamed 2 469.8-metre (8,103-foot) peak east of Nanika Lake and about 4 kilometres (2.5 miles) north-northeast of the Berg camp. As of January 1979, the Canadian Permanent Committee on Geographic Names has recommended that the peak is to be known as Mount Ney after the eminent Cordilleran geologist and alpinist, Charles S. Ney.

A number of other mountains and ridges 2 135 metres (7,000 feet) and higher in elevation occur as serrate peaks formed by cirque glaciation. Many of the highest and most rugged peaks are underlain by granitic cores. Mountain flanks and valley walls generally have more subdued, glacially rounded profiles with small benches, dissected plateau-like areas, and hanging valleys at various elevations.

GLACIATION

The Tahtsa Ranges have undergone extensive glaciation. According to Tipper (1971), multiple glaciation is probable over much of central British Columbia. In the Berg area there is evidence for three types of glaciation: a continental or mountain ice sheet, valley glaciation, and alpine cirque glaciation.

During the main (Wisconsin) glaciation and possibly a second ice advance that was localized in north-central British Columbia (Fraser glaciation), ice from the Coast Mountains flowed northeasterly and easterly along the existing major valleys into the Nechako Plateau. As ice depths increased, glaciers overrode valley walls and all but the highest peaks were glaciated. In Berg area there is ample evidence from erratic boulders on small, dissected plateaus and beveled ridge crests to show that ice reached elevations of at least 1 675 metres (5,500 feet).

During deglaciation [*circa* 15 000 BP and later, as shown by Prest (1970)] valley glaciation, or surges during wasting and over-all recession of the ice sheet, further modified valley walls. Evidence of valley glaciation is preserved as terraces and ridges at various elevations along sidehills bounding the larger valleys.

Cirque glaciation has been the dominant influence in sculpturing present topography above 1 525 metres (5,000 feet). Small active cirque glaciers and snowfields are found on eastern and northern slopes at elevations above 1 830 metres (6,000 feet). At present, cirque glaciers are wasting and receding so that most cirques, alpine valleys, and gullies are mantled by recently deposited debris from terminal and recessional moraines and by fluvio-glacial deposits. Between the period of 1967 and 1974 there was a noticeable melt-back of glacier ice and a decrease in the size of snowfields in Berg map-area.

ACKNOWLEDGMENTS

This report is a summary of a dissertation submitted to the Faculty of Graduate Studies, University of British Columbia, in 1976. Fieldwork was done while the writer was employed by Kennco Explorations, (Western) Limited during 1967, 1969, and 1971. A visit to the deposit in 1974 and discussions with geologists of Placer Development Limited kept the writer up-to-date with recent developments.

BIBLIOGRAPHY

- Allen, D. G. (1971): The Origin of Sheet Fractures in the Galore Creek Copper Deposits, British Columbia, *Can. Jour. Earth Sci.*, Vol. 8, No. 6, pp. 704-711.
- Baas Becking, L.G.M., Kaplan, I. R., and Moore, D. (1960): Limits of Natural Environments in Terms of Eh and pH and Oxidation-Reducing Potentials, *Jour. Geol.*, Vol. 68, pp. 243-284.
- Barakso, J. J. and Bradshaw, B. A. (1971): Molybdenum Surface Depletion and Leaching in Geochemical Exploration, *C.I.M.*, Special Vol. No. 11, pp. 78-84.
- Barr, D. A. (1966): The Galore Creek Copper Deposits, *C.I.M.*, Bull., Vol. 59, pp. 841-853.
- Barton, P. B., Jr. (1973): Solid Solutions in the System Cu-Fe-S, Part 1: The Cu-S and Cu-Fe-S Joins, *Econ. Geol.*, Vol. 68, pp. 455-465.
- Beaudoin, P. and Mortensen, E. (1973): Final Report Berg Property Exploration Activity, 1973, unpublished private rept., *Canex Placer Limited*, 10 pp.
- Blanchard, R. (1968): Interpretation of Leached Outcrops, *Nevada Bureau of Mines*, Bull. 66, 196 pp.
- Brown, J. B. (1971): Jarosite-Goethite Stabilities at 25° C, 1 ATM, *Mineral. Dep.*, Vol. 6, pp. 245-252.
- Burnham, C. W. (1962): Facies and Types of Hydrothermal Alteration, *Econ. Geol.*, Vol. 57, pp. 768-784.
-(1975): Annual Report, 1974-1975, *Geophysical Laboratory*, p. 627.
- Carpenter, R. H. (1968): Geology and Ore Deposits of the Questa Molybdenum Mine Area, Taos County, New Mexico, *in Ore Deposits in the United States, 1933-1967*, *A.I.M.E.*, pp. 1328-1350.

- Carson, D.J.T. and Jambor, J. L. (1974): Mineralogy, Zonal Relationships and Economic Significance of Hydrothermal Alteration at Porphyry Copper Deposits, Babine Lake Area, British Columbia, *C.I.M.*, Bull., Vol. 67, pp. 110-133.
- Carter, N. C. (1974): Geology and Geochronology of Porphyry Copper and Molybdenum Deposits in West-Central British Columbia, Ph.D. thesis, *University of British Columbia*, 236 pp., and Bulletin 64, *B.C. Ministry of Energy, Mines & Pet. Res.*, in preparation.
-(1976): Regional Setting of Porphyry Copper Deposits in West-Central British Columbia, *C.I.M.*, Special Vol. 15, pp. 227-238.
- Creasey, S. C. (1959): Some Phase Relations in the Hydrothermally Altered Rocks of Porphyry Copper Deposits, *Econ. Geol.*, Vol. 54, pp. 351-373.
-(1966): Hydrothermal Alteration, in Geology of the Porphyry Copper Deposits, in Southwestern North America, *University of Arizona Press*, pp. 51-74.
- Dahl, C. L. and Norton, D. (1967): Mineralogical and Petrographic Service Report, Berg Project, private rept., *Kennco Explorations, (Western) Limited*, 15 pp.
- Daly, R. A. (1933): Igneous Rocks and the Depths of the Earth, *McGraw-Hill Book Company Inc.*, New York, N.Y., 598 pp.
- Dawson, K. M. (1972): Geology of Endako Mine, British Columbia, Ph.D. thesis, *University of British Columbia*, 337 pp.
- Dawson, K. M. and Sinclair, A. J. (1974): Factor Analysis of Minor Element Data for Pyrites, Endako Molybdenum Mine, British Columbia, Canada, *Econ. Geol.*, Vol. 69, pp. 404-411.
- Dixon, W. J. and Massey, F. J. (1969): Introduction to Statistical Analysis, Third Edition, *McGraw-Hill Book Company Inc.*, New York, N.Y., 638 pp.
- Drummond, A. D. and Godwin, C. I. (1976): An Empirical Evaluation of Alteration Zoning, *C.I.M.*, Special Vol. 15, pp. 52-63.
- Duffel, S. (1959): Whitesail Lake Map-area, British Columbia, *Geol. Surv., Canada*, Mem. 299, 119 pp.
- Garrels, R. M. (1954): Mineral Species as Functions of pH and Oxidation-Reduction Potentials with Special Reference to the Zone of Oxidation and Secondary Enrichment of Sulphide Ore Deposits, *Geochim. et Cosmochim. Acta*, Vol. 5, pp. 153-168.
-(1960): Mineral Equilibria, *Harper Bros.*, New York, 254 pp.
- Garrett, R. G. (1969): The Determination of Sampling and Analytical Errors in Exploration Geochemistry, *Econ. Geol.*, Vol. 64, pp. 568, 569.
- Godwin, C. I. (1973): Shock Brecciation, An Unrecognized Mechanism for Breccia Formation in the Porphyry Environment?, *Geol. Assoc., Can., Proc.*, Vol. 25, pp. 9-12.
-(1975): Geology of Casino Porphyry Copper-Molybdenum Deposit, Dawson Range, Y.T., Ph.D. thesis, *University of British Columbia*, 245 pp.
- Gosh-Dastidar, P. (1970): Syntheses of Sulfide Standards for Quantitative Spectrochemical Analyses, *Econ. Geol.*, Vol. 65, pp. 56-59.
- Guilbert, J. M. and Lowell, J. D. (1974): Variation in Zoning Patterns in Porphyry Ore Deposits, *C.I.M.*, Bull., Vol. 67, No. 742, pp. 99-109.

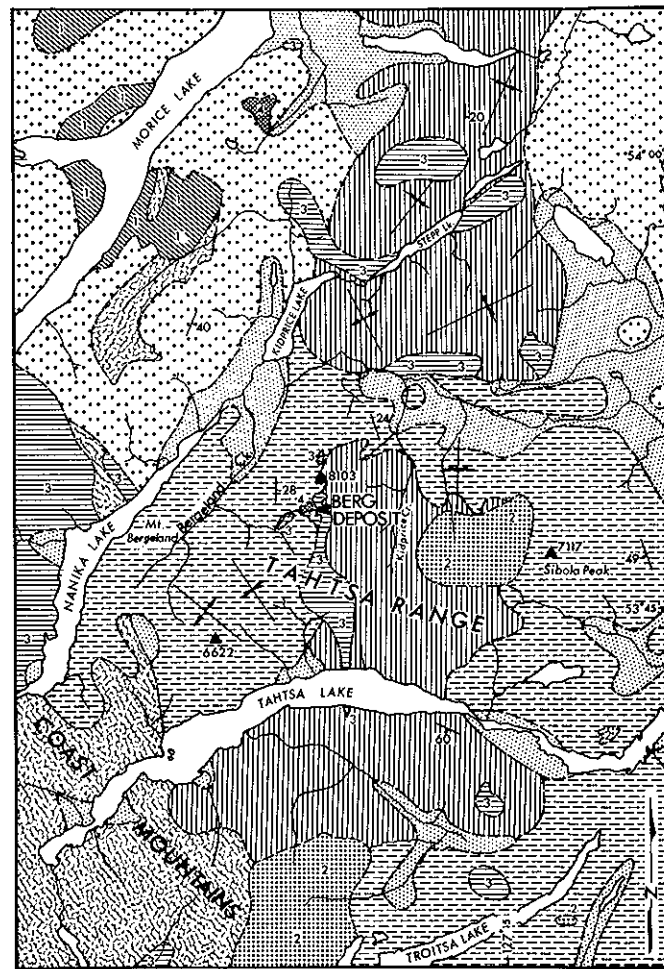
- Gustafson, L. B. and Hunt, J. P. (1975): The Porphyry Copper Deposit at El Salvador, Chile, *Econ. Geol.*, Vol. 70, pp. 857-912.
- Hansuld, J. A. (1966): Eh and pH in Geochemical Exploration, *C.I.M., Bull.*, Vol 59, pp. 315-322.
- Hemley, J. J. (1959): Some Mineralogical Equilibria in the System $K_2O-Al_2O_3-SiO_2-H_2O$, *Am. Jour. Sci.*, Vol. 257, pp. 241-270.
- Hemley, J. J., Mercer, C., and Richter, D. H. (1961): Some Alteration Reactions in the System $Na_2O-Al_2O_3-SiO_2-H_2O$, *U.S.G.S., Prof. Paper 424D*, pp. 338-340.
- Hemley, J. J., Montoya, J. W., Nigrini, A., and Vincent, H. A. (1970): Some Alteration Reactions in the System $CaO-Al_2O_3-SiO_2-H_2O$, *Soc. Min. Geol., Japan*, Special Issue No. 2, pp. 58-63.
- Holland, H. D. (1967): Gangue Minerals in Hydrothermal Deposits, in *Geochemistry of Hydrothermal Ore Deposits*, H. L. Barnes, editor, *Holt, Rinehart, and Winston*, Montreal, pp. 382-436.
- Holland, Stuart S. (1964): Landforms of British Columbia, A Physiographic Outline, *B.C. Ministry of Energy, Mines & Pet. Res.*, Bull. 48, 138 pp.
- Howell, F. H. and Molloy, S. S. (1969): Geology of the Braden Orebody, Chile, *Econ. Geol.*, Vol. 55, pp. 863-905.
- Imbrie, J. and Van Andel, T. H. (1964): Vector Analysis of Heavy-Mineral Data, *Geol. Soc. Am., Bull.*, Vol. 75, pp. 1131-1156.
- Jaeger, J. C. (1959): Temperatures Outside a Cooling Intrusive Sheet, *Am. Jour. Sci.*, Vol. 257, pp. 44-54.
-(1964): Thermal Effects of Intrusion, *Rev. Geophysics*, Vol. 2, pp. 443-466.
- Jäger, W., Rahmal, A., and Becker, K. (1959): Investigations of the Tertiary System Iron-Molybdenum-Oxygen, *Arch. Eisenhüttenw.*, Vol. 30, No. 7, pp. 435-439.
- Jambor, J. L. and McMillan, W. J. (1976): Distribution and Origin of the 'Gypsum Line' in the Valley Copper Porphyry Copper Deposit, Highland Valley, British Columbia, *Geol. Surv., Canada*, Paper 76-1B, pp. 335-341.
- James, W. R. (1966): FORTRAN IV, Programs Using Double Fourier Series for Surface Fitting of Irregularly Spaced Data, Computer Contribution 5, State Geological Survey, *University of Kansas*, D. F. Merriam, editor, 19 pp.
- Jolliffe, A. W. (1955): Geology and Iron Ores of Steep Rock Lake, *Econ. Geol.*, Vol. 50, pp. 373-398.
- Kiovan, J. E. (1968): Selection of Target Areas by Factor Analysis, Proc. of the Symposium on Decision-making in Exploration, I, Vancouver, *University of British Columbia*, Extension Dept., pp. 19-27.
- Kurz, S. L., Brownlow, A. H., and Park, W. C. (1975): Properties of Pyrites from Ore and Non-ore Environments, *Geol. Soc. Am.*, Annual Meeting, Abstract, Salt Lake City, Utah.
- Locke, A. (1926): Leached Outcrops as Guides to Copper Ore, *Williams and Wilkins Co.*, Baltimore, 175 pp.
- Loftus-Hills, G. and Solomon, M. (1967): Cobalt, Nickel, and Selenium in Sulphides as Indicators of Ore Genesis, *Mineral. Dep.*, Vol. 2, pp. 228-242.

- Lovering, T. S. (1948): Geothermal Gradients, Recent Climatic Changes and Rate of Sulfide Oxidation in the San Manuel District, Arizona, *Econ. Geol.*, Vol. 43, pp. 1-20.
-(1955): Temperatures In and Near Intrusions, *Econ. Geol.*, 50th Anniversary Vol., pp. 249-281.
- Lowell, J. D. and Guilbert, J. M. (1970): Lateral and Vertical Alteration – Mineralization Zoning in Porphyry Ore Deposits, *Econ. Geol.*, Vol. 65, pp. 373-408.
- MacIntyre, D. G. (1976): Evolution of Upper Cretaceous Volcanic and Plutonic Centres and Associated Porphyry Copper Occurrences Tahtsa Lake Area, British Columbia, Ph.D. thesis, *University of Western Ontario*, 149 pp.
- McAndrew, R. T., Wang, S. S., and Brown, W. R. (1975): Precipitation of Iron Compounds from Sulphuric Acid Leach Solutions, *C.I.M.*, Bull., Vol. 68, pp. 101-110.
- Meyer, C. and Hemley, J. J. (1967): Wall Rock Alteration in Geochemistry of Hydrothermal Ore Deposit, H. L. Barnes, editor, *Holt, Rinehart, and Winston*, Montreal, pp. 166-235.
- Morimoto, N. and Koto, K. (1970): Phase Relations of the Cu-S System at Low Temperatures: Stability of Anilite, *Am. Min.*, Vol. 55, pp. 106-117.
- Ney, C. S. (1972): Berg Prospect, in Copper and Molybdenum Deposits of the Western Cordillera, Field Excursion A09-C09, Guidebook, *24th International Geological Congress*, Montreal, pp. 25-27.
- Nichol, I., Garrett, R. G., and Webb, J. S. (1969): The Role of Some Statistical and Mathematical Methods in the Interpretation of Regional Geochemical Data, *Econ. Geol.*, Vol. 64, pp. 204-220.
- Nockolds, S. R. (1954): Average Chemical Compositions of Some Igneous Rocks, *Geol. Soc. Am.*, Bull., Vol. 65, pp. 1007-1032.
- Norton, D. L. (1975): Porphyry Pluton Environments: Fluid-Rock Interactions Predicted from Theoretical Models of Heat and Mass Transfer, *Geol. Soc. Am.*, Annual Meeting, Abstract, Salt Lake City, Utah.
- Norton, D. L. and Mariano, A. N. (1967): Sibolaite, MoO₂, A New Mineral from the Sibola Mountains, British Columbia, in Berg Examination, Progress Rept., 1966, Appendix B, 7 pp.; private report, *Kennco Explorations, (Western) Limited*.
- Ovchinnikov, L. N. (1967): Impurity Elements as Indicators of the Process of Ore Formation and Application of the Patterns of their Distribution to Search and Prospecting for Ore Deposits, in Chemistry of the Earth's Crust, Vol. II (*Vernadsky Commen. Vol.*), A. P. Vinogradov, editor.
- Owens, D. (1968): Mineralogical Investigation of a Sample of a Copper-Molybdenum Ore from Kennco Explorations, (Western) Limited, British Columbia, Mines Branch Investigation Report., IR 68-30, *Dept. of Energy, Mines & Res.*, 8 pp.
- Panteleyev, A. (1976): Geologic Setting, Mineralization, and Aspects of Zoning at the Berg Porphyry Copper-Molybdenum Deposit, Central British Columbia, Ph.D. thesis, *University of British Columbia*, 235 pp.
- Panteleyev A., Drummond, A. D., and Beaudoin, P. G. (1976): Berg in Porphyry Deposits of the Canadian Cordillera, *C.I.M.*, Special Vol. 15, pp. 274-283.
- Phillips, W. J. (1972): Hydraulic Fracturing and Mineralization, *Geol. Soc. London, Jour.*, Vol. 128, No. 4, pp. 337-359.

-(1973): Mechanical Effects of Retrograde Boiling and its Probable Importance in the Formation of Some Porphyry Ore Deposits, *Trans. Inst. Min. Met.*, Vol. 82, pp. B90-B98.
- Pokalov, V. T. and Orlov, V. G. (1974): Behaviour of Molybdenum in the Oxidation Zone, *Geochemistry International*, Vol. 11, No. 1, pp. 447-452.
- Prest, V. K. (1970): Quaternary Geology, in *Geology and Economic Minerals of Canada, Geol. Surv., Canada*, Econ. Geol. Rept. No. 1, R.J.W. Douglas, editor, pp. 675-764.
- Price, B. J. (1972): Minor Elements in Pyrite from the Smithers Map-area, British Columbia and Exploration Applications of Minor Element Studies, M.Sc. thesis, *University of British Columbia*, 270 pp.
- Richards, T. A. (1974a): Hazelton East-Half (93M East Half), *Geol. Surv., Canada*, Paper 74-1, Pt. A, pp. 35-37.
-(1974b): Low Grade Alteration Assemblages and Their Relation to Stratigraphy of the Hazelton and Skeena Groups, Central British Columbia in *Volcanic Geology and Mineral Deposits of the Canadian Cordillera, Geol. Assoc. Can., Cordilleran Section, Programme and Abstracts, Vancouver*.
- Roberts, H. M. and Bartley, M. W., (1943): Hydrothermal Replacement in Deep Seated Iron Ore Deposits of the Lake Superior Region, *Econ. Geol.*, Vol. 38, pp. 1-24.
- Roedder, E. (1962): Studies of Fluid Inclusions I: Low Temperature Applications of a Dual Purpose Freezing and Heating Stage, *Econ. Geol.*, Vol. 57, pp. 1045-1061.
-(1963): Studies of Fluid Inclusions II: Freezing Data and Their Interpretation, *Econ. Geol.*, Vol. 58, pp. 167-211.
-(1967): Fluid Inclusions as Samples of Ore Fluids, in *Geochemistry of Hydrothermal Ore Deposits*, H. L. Barnes, editor, *Holt, Rinehart, and Winston*, Montreal, pp. 515-574.
-(1971): Fluid Inclusion Studies on the Porphyry-Type Ore Deposits at Bingham, Utah, Butte, Montana, and Climax, Colorado, *Econ. Geol.*, Vol. 66, No. 1, pp. 98-120.
- Rose, A. W. (1970a): Zonal Relations of Wallrock Alteration and Sulfide Distribution at Porphyry Copper Deposits, *Econ. Geol.*, Vol. 65, pp. 920-936.
-(1970b): Origin of Trace Element Distribution Patterns in Sulphides of the Central and Bingham Districts, Western United States of America, *Mineral. Dep.*, Vol. 5, pp. 157-163.
- Roseboom, E. H., Jr. (1966): An Investigation of the System Cu-S and Some Natural Copper Sulfides Between 25° and 700° C, *Econ. Geol.*, Vol. 61, pp. 641-672.
- Runnells, D. D. (1969): The Mineralogy and Sulfur Isotopes of the Ruby Creek Copper Prospect, Bornite, Alaska, *Econ. Geol.*, Vol. 64, pp. 75-90.
- Ryall, W. R. (1977): Anomalous Trace Elements in Pyrite in the Vicinity of Mineralized Zones at Woodlawn, New South Wales, Australia, *Jour. Geochem. Expl.*, Vol. 8, pp. 73-83.
- Sato, M. (1960): (a) Oxidation of Sulphide Orebodies – I, Geochemical Environments in Terms of Eh and pH, *Econ. Geol.*, Vol. 55, pp. 928-961. (b) Mechanisms of Sulphide Orebodies – II, Oxidation of Sulphide Minerals at 25° C, *Econ. Geol.*, Vol. 55, pp. 1202-1231.

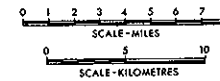
- Sawkins, F. J. (1969): Chemical Brecciation, an Unrecognized Mechanism for Breccia Formation?, *Econ. Geol.*, Vol. 64, pp. 613-617.
- Shearman, D. J., Mossop, G., Dunsmore, H., and Martin, M. (1972): Origin of Gypsum Veins by Hydraulic Fracture, *Trans. Inst. Min. Met.*, Vol. 81, No. 789, pp. 149-155.
- Sillitoe, R. H. and Sawkins, F. J. (1971): Geologic, Mineralogic, and Fluid Inclusion Studies Relating to the Origin of Copper-bearing Tourmaline Breccia Pipes, Chile, *Econ. Geol.*, Vol. 66, No. 7, pp. 1028-1041.
- Sinclair, A. J. (1974): Selections of Threshold Values in Geochemical Data Using Probability Graphs, *Jour. Geochem. Expl.*, Vol. 3, pp. 129-150.
-(1976): Application of Probability Graphs in Mineral Exploration, *Assoc. of Expl. Geochemists*, Special Vol. No. 4, 95 pp.
- Skoček, V., Al-Qaraghuli, N., and Saadallah, A. (1971): Composition and Sedimentary Structures of Iron Ores from the Wadi Husainiya Area, Iraq, *Econ. Geol.*, Vol. 66, pp. 995-1004.
- Steiger, R. H. and Hart, S. R. (1967): The Microcline-orthoclase Transition Within a Contact Aureole, *Am. Mineralogist*, Vol. 52, pp. 87-116.
- Stewart, G.O.M. (1967): Berg Examination, Progress Report, 1966, private rept., *Kennco Explorations, (Western) Limited*, 88 pp.
- Streckeisen, A. L. (1967): Classification and Nomenclature of Igneous Rocks, *Neues Jahr. Miner. Abh.*, Vol. 107, No. 2, pp. 144-214.
- Sutherland Brown, A. (1960): Geology of Rocher Deboule Range, *B.C. Ministry of Energy, Mines & Pet. Res.*, Bull. 43, 78 pp.
-(1967): Berg, *B.C. Ministry of Energy, Mines & Pet. Res.*, Ann. Rept., 1966, pp. 105-111.
-(1969): Mineralization in British Columbia and the Copper Molybdenum Deposits, *C.I.M.*, Bull., Vol. 62, No. 681, pp. 26-40.
-(1974): Metallic Resources of the Canadian Cordillera, preprint, *Circum-pacific Mineral Resources Conference*, Honolulu.
-(1976): Morphology and Classification, in *Geology of Porphyry Copper Deposits of the Canadian Cordillera*, *C.I.M.*, Special Vol. 15, pp. 44-51.
-(1976): Porphyry Deposits of the Canadian Cordillera, A. Sutherland Brown, editor, *C.I.M.*, Special Vol. 15, 510 pp.
- Thompson, M. and Howarth, R. J. (1978): A New Approach to the Estimation of Analytical Precision, *Jour. Geochem. Expl.*, Vol. 9, pp. 23-30.
- Tipper, H. W. (1971): Multiple Glaciation in Central British Columbia, *Can. Jour. Earth Sci.*, Vol. 8, pp. 743-752.
-(1972): Smithers Map-area, British Columbia (93L), in *Rept. of Activities, April to October 1971*, *Geol. Surv., Canada*, Paper 72-1A, pp. 39-41.
- Tipper, H. W. and Richards, T. A. (1976): Jurassic Stratigraphy and History of North-Central British Columbia, *Geol. Surv., Canada*, Bull. 270, 73 pp.
- Titley, S. R. (1963): Some Behavioral Aspects of Molybdenum in the Supergene Environment, *Soc. Min. Eng.*, Trans., Vol. 15, pp. 199-204.
-(1972): Intrusion, and Wall Rock, Porphyry Copper Deposits, *Econ. Geol.*, Vol. 67, pp. 122, 123.

-(1975): Geological Characteristics and Environment of Some Porphyry Copper Occurrences in the Southwestern Pacific, *Econ. Geol.*, Vol. 70, pp. 499-514.
- White, D. E., Muffler, L.J.P., and Truesdell, A. H. (1971): Vapour-dominated Hydrothermal Systems Compared with Hot-water Systems, *Econ. Geol.*, Vol. 66, pp. 75-97.
- Whitney, J. A. (1975a): Vapour Generation in a Quartz Monzonite Magma: A Synthetic Model with Application to Porphyry Copper Deposits, *Econ. Geol.*, Vol. 70, pp. 346-358.
- (1975b): The Effects of P, T, and xH₂O on Phase Assemblages in Four Synthetic Rock Compositions, *Jour. Geol.*, Vol. 83, No. 1, pp. 1-32.
- Wilson, J.D.S. and Sinclair, A. J. (1969): Q-mode Factor Analysis Applied to Mineral Exploration Data, in Proc. of Symposium on Decision-making in Mineral Exploration, II, *University of British Columbia*, Extension Dept., pp. 244-257.
- Winkler, H.G.F. (1965): Petrogenesis of Metamorphic Rocks, *Springer-Verlag New York Inc.*, New York, N.Y., 220 pp.



GEOLOGY OF TAHTSA RANGE

BASED ON DUFFEL, 1959, MAP 1064A (WHITESAIL LAKE)
AND UNPUBLISHED REVISIONS BY
N. C. CARTER, H. TIPPER, A. PANTELEYEV, AND D. MacINTYRE



INTRUSIVE ROCKS

TERTIARY

MIDDLE TO UPPER EOCENE

3 COAST PLUTONIC COMPLEX:
GRANITIC ROCKS (MAY BE OLDER
IN PART)

MIDDLE EOCENE

4 QUARTZ MONZONITE PORPHYRY, SOME
FELSITE INTRUSIONS; Cu AND Mo-
BEARING STOCKS

CRETACEOUS AND TERTIARY

UPPER CRETACEOUS - PALEOCENE

2 'BULKLEY INTRUSIONS' (IN PART): MAINLY PORPHYRITIC QUARTZ MONZONITE, Mo-Cu,
AND Mo-W-BEARING STOCKS

JURASSIC

LOWER AND MIDDLE JURASSIC

1 'OMINECA INTRUSIONS' (IN PART): GRANODIORITE, QUARTZ DIORITE, SYENITE

BEDDED ROCKS

QUATERNARY

PLEISTOCENE AND RECENT

5 ALLUVIUM, GLACIAL OUTWASH, TILL, MORaine

CRETACEOUS 'SKEENA GROUP'

LATE LOWER CRETACEOUS AND ? YOUNGER

6 GREYWACKE, SILTSTONE, CONGLOMERATE; INCLUDES UNITS OF PORPHYRITIC
ANDESITE, DACITE, RHYOLITE FLOWS, BRECCIA, TUFF, AND RELATED SUBVOLCANIC
INTRUSIONS

JURASSIC HAZELTON GROUP

MIDDLE JURASSIC (MAY INCLUDE SOME LOWER CRETACEOUS)

7 GREEN, GREY, MAROON VOLCANIC BRECCIA, TUFF, FLOWS; SOME SEDIMENTARY
ROCKS

LOWER JURASSIC

8 GREEN, RED, PURPLE VOLCANIC BRECCIA, CONGLOMERATE, GREYWACKE; SOME INTER-
CALATED SEDIMENTARY ROCKS

TRIASSIC AND EARLIER

9 GNEISS COMPLEX

Figure 2. Geology of Tahtsa Ranges.

2

GEOLOGY

REGIONAL GEOLOGY OF TAHTSA RANGES

Berg deposit is about 12 kilometres (8 miles) east of the Coast Plutonic Complex in a region of bedded volcanic and sedimentary rocks of Jurassic and Cretaceous age. Bedded rocks have been intruded by a number of Jurassic, Cretaceous, and Tertiary stocks (Carter 1974, 1976). Mapping by Duffel (1959, Whitesail Lake Map-area, Map No. 1064A) provides a geological framework for the area but is currently being extensively revised as a result of recent and ongoing work.

Duffel's 'Hazelton Group' includes rocks of pre-Middle Jurassic to Early Cretaceous age. Recent work in the Whitesail Lake and other map-areas to the north, mainly by geologists of the Geological Survey of Canada (Tipper, 1972; Richards, 1974a; Tipper and Richards, 1976) has permitted subdivision of Hazelton rocks into Early and Middle Jurassic units and has shown that Cretaceous rocks are more widespread than previously recognized. The Cretaceous rocks, now called Skeena Group, are part of an extensive draping of interbedded marine and nonmarine sedimentary and volcanic rocks over Hazelton rocks. According to Tipper and Richards (1976) Early Cretaceous to ? earliest Late Cretaceous (Hauterivian to Albian or ? Cenomanian) Skeena rocks are now known to extend from south of Tahtsa Lake to Hazelton where they include the Brian Boru and Red Rose Formations of Sutherland Brown (1960). In Tahtsa Lake vicinity rocks of the Skeena Group are unconformably overlain by volcanic rocks which MacIntyre (1976) believes to be strictly Late Cretaceous and for which he proposes the name 'Kasalka Group.'

Considerable refinement of intrusive history in the region has been done by Carter (1974). A revised geological map of the area is shown on Figure 2.

GEOLOGY OF BERG MAP-AREA

This report describes a 50-square-kilometre area that surrounds Berg deposit. The map is shown as Figure 3 (in pocket) and is hereafter referred to as Berg map-area.

In Berg map-area bedded rocks can be readily subdivided into three lithologically distinct assemblages: upper and lower volcanic units and an intervening sedimentary unit. On Whitesail Lake map all these rocks are shown as Hazelton Group and are described as '(mainly) Middle Jurassic' volcanic and sedimentary rocks. The possibility that some Cretaceous rocks are included in this sequence is suggested in the accompanying text (Duffel, 1959).

During regional reconnaissance in 1966 C. S. Ney observed an angular discordance between volcanic and sedimentary units at the head of Kidprice Creek south of Berg deposit. Thus, correlation of a similar lithologic succession near Berg deposit with the Hazelton Group became suspect and subsequent mapping revealed the presence of at least two angular unconformities in Berg map-area. The presence of Cretaceous Skeena rocks in Berg map-area was substantiated in 1972 and stratigraphic relationships clarified when ammonites from rocks of the sedimentary (middle) assemblage (locality shown on Fig. 3) were identified by H. W. Tipper as *Cleoniceras*, a zone fossil of the Middle Albian stage (latest Early Cretaceous).

Detailed mapping in Berg map-area revealed a gentle angular unconformity between volcanic units near the top of the lower volcanic assemblage (Fig. 3, units 1 and 2). The underlying Hazelton rocks are moderately eastward-dipping red and green fragmental volcanic rocks. They crop out along the western half of Berg map-area (Fig. 3, unit 1). To the east the overlying rocks are more gently eastward-dipping grey and green amygdaloidal flows which form the basal part of the Skeena Group (Fig. 3, unit 2). These volcanic rocks are conformably overlain by the Albian sedimentary rocks which form an eastward-thickening prism or clastic wedge (Fig. 3, unit 3). The youngest volcanic assemblage (Fig. 3, units 4 and 5) unconformably overlies Albian sedimentary rocks (unit 3) in the east and volcanic rocks (unit 2) in the west where the clastic wedge has pinched out.

Intrusive rocks have been grouped into three map units as shown on Figure 3: a diorite/quartz diorite stock and related intrusions in the centre of the map-area that are satellitic bodies of the Coast Intrusions; a small multiphase mineralized stock of quartz monzonite porphyry that is part of the Eocene 'Nanika Intrusions' of Carter (1974); and numerous minor dykes and sills of various affinities and ages.

HAZELTON GROUP (Middle Jurassic; Fig. 3, Unit 1)

Hazelton rocks comprise a predominantly andesitic pyroclastic assemblage in which about 1 675 metres (5 500 feet) of strata are exposed in the mineralized area, Bergeland Creek valley, and ridges to the west. The rocks are green, grey, red, and maroon lithic tuff, tuff breccia, and lesser units of volcanic flows, flow breccia, and tuffaceous or epiclastic sedimentary rocks.

Base of the map unit is not exposed but oldest strata are thick beds of flow breccia, massive flows, and tuff that pass into a sequence of thinly bedded shale, chert, and

tuffaceous siltstone and sandstone. These well-bedded sedimentary rocks are seen mainly in the lower reaches of the north fork of Bergeland Creek. They are overlain by the principal ridge forming pyroclastic members in Berg area. These are disorganized to weakly graded beds of coarse to fine-grained tuffs (lapilli to fine ash sized) with some units of massive, rarely porphyritic flows, thin units of breccia, and reworked tuffaceous sedimentary members. About 3 kilometres west of Berg deposit the succession contains siliceous volcanic rocks. Many of these appear to be compacted or welded dacitic lithic-crystal tuff and lapilli tuff. Youngest beds are, in part, subaerial but are mainly shallow marine (intertidal or littoral). A number contain well-developed accretionary lapilli, mud pellets, and at least one locality with oscillation ripple marks. Many of the porous, fragmental rocks have a limy or ferruginous red-coloured, silt-sized matrix. Near the top of the sequence a few cobble beds with predominantly andesitic clasts and a reworked volcanic sandstone matrix were noted. None was seen to contain any clasts of intrusive rocks; exotic rocks are mainly chert and a few pieces of crystalline limestone.

Regional metamorphic grade is sub-greenschist facies (Richards, 1974b). In Berg map-area no prehnite nor pumpellyite and only one hydrothermal zeolite locality were noted. Epidote and chlorite are most common; calcite, quartz, tremolite, montmorillonite, albite, K-feldspar, and muscovite are widespread. Small amounts of garnet, tourmaline, amphibole, scolecite, magnetite, hematite, pyrite, and rutile are present in xenoliths within quartz diorite. The latter minerals are of apparent hydrothermal origin and formed in broad propylitic zones or small skarn zones associated with intrusive rocks.

SKEENA GROUP (Lower Cretaceous; Fig. 3, Units 2 and 3)

The basal Cretaceous volcanic unit (unit 2) is found along a north-south-trending belt up to 2.5 kilometres wide through the centre of Berg map-area. Best outcrop exposures are on steep slopes east of the main granitic intrusions and west of Kidprice Creek. A maximum of about 600 metres (2,000 feet) of strata is present.

The rocks are typically amygdaloidal and rarely vesicular or massive flows and flow breccias of andesitic or basaltic composition. They are grey to purple and dark green in colour and are composed predominantly of small laths and microlites of plagioclase in a chloritic groundmass. Slight orientation of feldspars imparts a trachytic texture in some of the porphyritic rocks. Amygdules contain abundant chlorite, commonly as radiating fibrous spherulites, or as concentric layers with calcite, quartz, epidote, and montmorillonite. Calcite with crystalline and chalcedonic quartz is common in vesicles and cavities.

The contact of the basal volcanic beds with Hazelton rocks is not well exposed. Throughout much of Berg map-area the contact is intruded by quartz diorite or is covered. Immediately north of the main quartz diorite body, the contact is exposed in a cliff face but is inaccessible. It appears that in this area the contact is strongly epidotized and rocks are hydrothermally altered.

Sedimentary rocks (unit 3) crop out in most of the eastern half of Berg map-area where they form a clastic wedge that overlies feldspathic amygdaloidal flow rocks of the Cretaceous basal volcanic unit (unit 2). At the southeast corner of Berg map-area a maximum of about 500 metres of sedimentary strata is exposed. The clastic unit thins northward and to the west; the pinchout can be traced along the northern boundary of the area mapped and just east of Mount Ney (*see* cross-sections, Fig. 3).

The sedimentary rocks are mainly fine-grained sandstone. They form massive grey to buff outcrops with individual members up to 50 metres in thickness. Monotony in the succession is broken by a few pebble conglomerate beds and thin units of graded, thinly bedded siltstone and shale having crossbedding, rip-up clasts, and slump structures. The sandstone is composed of subrounded quartz, plagioclase, and K-feldspar grains and small rock fragments in a fine-grained micaceous matrix. Abundance of detrital mica is a useful criterion for distinguishing Cretaceous sedimentary rocks from older rocks in Smithers and Hazelton map-areas (H. W. Tipper, 1972, personal communication). Some sandstone beds contain spherical concretions up to 35 centimetres in diameter. One cherty argillite unit yielded a few specimens of the ammonite *Cleoniceras* which established a mid-Albian age for the strata. The top of the map unit is marked by 40 metres of flaggy siltstone and dark brown shale beds.

KASALKA GROUP (Upper Cretaceous; Fig. 3, Units 4 and 5)

Kasalka volcanic rocks unconformably overlie Skeena rocks and cap two ridges in the north and northeastern part of Berg map-area. Kasalka rocks have been studied extensively in Tahtsa Lake area by MacIntyre (1976) who proposed the name 'Kasalka Group' and subdivided the assemblage into a basal conglomerate and three formations: the Mount Baptiste, Swing Peak, and Bergette. On the basis of their discordant relationship with Skeena rocks, a number of Late Cretaceous radiometric dates from volcanic and related intrusive rocks, and despite one whole rock date of 105 Ma from the Mount Baptiste Formation, MacIntyre (1976) considers Kasalka rocks to be strictly Late Cretaceous in age.

In Berg map-area and according to MacIntyre (1976) throughout the Tahtsa Lake region, the basal member of the Kasalka Group is a red to maroon conglomerate that contains ferruginous sandstone lenses. The conglomerate is commonly 5 to 10 metres thick and composed of mainly pebbles and cobbles of Hazelton and Skeena volcanic rocks in a ferruginous sand matrix. In the eastern part of Berg map-area the conglomerate is up to 12 metres thick and overlies flaggy siltstone and dark brown shale beds of the Skeena Group (Fig. 3, unit 3). In the west where the Skeena sedimentary wedge has pinched out the conglomerate rests on epidotized amygdaloidal Skeena flows (Fig. 3, unit 2). In the most westerly part of Berg map-area the basal conglomerate is a dark-grey to brown cobble conglomerate that forms two small flat-lying ridge cappings on eastward-dipping Hazelton volcanic rocks (*see* Fig. 3, cross-section B-B').

Overlying the red conglomerate are rocks correlated with the Swing Peak Formation of MacIntyre (1976). The sequence consists of a basal strongly jointed hornblende feldspar porphyry member and overlying fragmental unit (Fig. 3, unit 4). Maximum thickness in this map unit is 190 metres. The feldspar porphyry member was mapped by this writer as a sill but has been interpreted by MacIntyre to be an andesite-latitude flow unit (his 'Member A'). In the eastern part of Berg map-area the feldspar porphyry unit is up to 43 metres thick. A similar (probably the same) feldspar porphyry sill (?) 1.5 kilometres to the north is 4 metres thick (see Fig. 3, cross-section D—D') and 2.3 kilometres to the south it is 48 metres thick (see Fig. 3, cross-section C—C'). In the northeasterly area the feldspar porphyry unit is overlain by about 10 metres of red to purple conglomerate (lahar ?) that is similar to the basal Kasalka conglomerate. The upper conglomerate is overlain by up to a 90-metre-thick disorganized prism of north and eastward-thinning, dark grey-green, calcite-rich basalt or andesitic breccia. This is overlain in turn, by a 75-metre layered succession of purple, grey, and violet vitric flows (see Plate II). To the west in the central part of Berg map-area the feldspar porphyry unit is absent and red conglomerate is overlain by an alternating sequence of red to maroon lahar units interbedded with grey to purple and reddish brown volcanic sandstone, lithic tuff, breccia, and numerous porphyritic sills, commonly less than 1 metre in thickness.

The youngest Kasalka rocks are shown on Figure 3 as map units 5a and 5b. Rocks of map unit 5a are cream to pale grey rhyolite breccia and flows that are equivalent to MacIntyre's Bergette Formation. In the northeast part of Berg map-area rocks of unit 5a are up to 100 metres in thickness and conformably overlie rocks of map unit 4. Locally rhyolite of map unit 5a is in fault contact with older rocks (see Fig. 3, cross section A—A'). In contrast, 3 kilometres to the west on the peak of Mount Ney and on the ridge leading northeast of the peak, the youngest Kasalka rocks (Fig. 3, unit 5b) are a lithologically diverse assemblage of fragmental and massive flow rocks that unconformably overlie rocks of map unit 4 (see Plate III).

Rocks of map unit 5b range widely in composition and appearance, from intermediate to felsic, dark to pale, and fragmental to massive. On the ridge northeast of Mount Ney dense, glassy, purple to dark grey dykes are abundant and fragmental rocks appear to be agglomerate. It is the presence within this succession of pale rhyolite members similar to rocks of map unit 5a that permits map unit 5b to be considered as a lateral equivalent to map unit 5a. However, if the gentle angular unconformity near the peak of Mount Ney (see Plate III) is of regional rather than local extent, map unit 5b may not be part of the Bergette Formation (unit 5a) and is part of a yet unnamed assemblage.

QUARTZ DIORITE

Quartz diorite forms the largest intrusive body mapped, a northward-trending stock at least 600 metres wide in the centre of Berg map-area. The body has steep walls and forms the core of the Tahtsa Ranges. The intrusion has been traced by the writer at least 6.5 kilometres to the south of Berg camp where it widens to about 2 750 metres along the southern edge of Berg map sheet. The stock was mapped by Duffel (1959) as



Plate I. Berg camp (lower left) and Mount Ney, view in late June looking north. Eastward dipping Hazelton (H) rocks are overlain on Mount Ney by Skeena (Sk) and Kasalka (Ks) rocks.

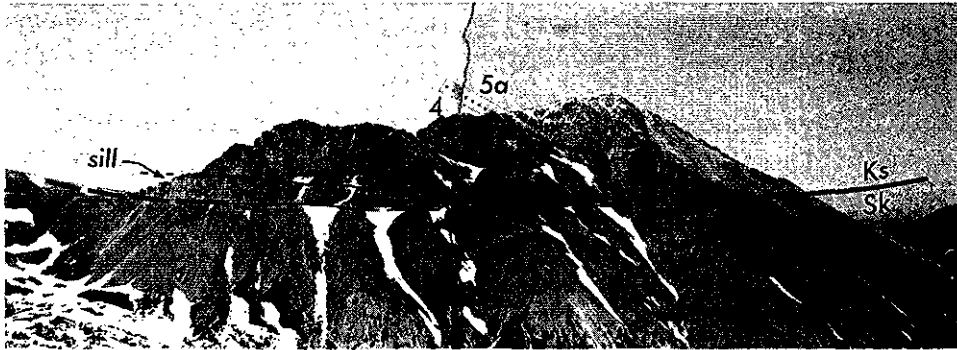


Plate II. Skeena sedimentary rocks overlain by Kasalka volcanic rocks, 2.5 kilometres east of Mount Ney. Approximately 400 metres of strata are exposed.

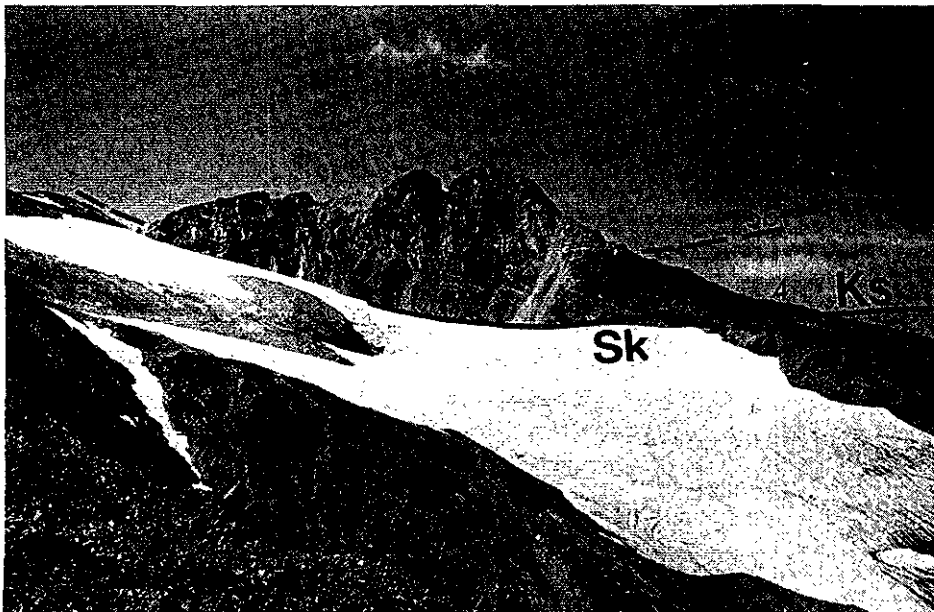


Plate III. Mount Ney, elevation 2 469.8 metres (8,103 feet), view looking northerly. Red lahar, unit 4, and breccia, unit 5, of Kasalka Group overlie Skeena volcanic rocks, unit 2, Figure 3. Approximately 500 metres of strata are shown.

'gabbro' which 'closely resembles many of the diorites associated with the main mass of the coast intrusion.' More detailed mapping has shown the intrusion to be texturally and compositionally zoned, ranging from fine-grained, equigranular to locally porphyritic, biotite hornblende quartz diorite or diorite. A minor hornblende-rich contact phase is found where brecciated microporphyritic andesite has been metasomatized along the intrusive contact.

About 1.6 kilometres south-southeast of camp, the core of the quartz diorite intrusion is composed of a porphyritic, pink, sericite-rich granodiorite and quartz monzonite. The quartz monzonite phase is a coarser grained porphyritic rock and has a gradational contact zone about 30 metres wide with the quartz diorite. The porphyritic phase is seen as a 180-metre-wide zone of rusty, hydrothermally altered rock surrounded by less altered, jointed quartz diorite typical of the main intrusive mass.

Small intrusions of biotite hornblende diorite and hornblende diorite/quartz diorite related to the main intrusion are found to the north and peripherally around the stock. These smaller intrusions occur as small stocks and dykes that penetrate Hazelton and Skeena strata as jagged intrusive plugs without any appreciable disruptive effects on bedding. The largest of the peripheral bodies intrudes west of the Berg camp and is found along an east-northeast trend that is perpendicular to the main quartz diorite stock.

Thermal metamorphic effects due to intrusion of the main diorite mass are evident as zones of purplish brown biotite hornfels formed across widths of up to 120 metres (commonly 30 metres or less) from the contact. Small areas and local patches of coarsely recrystallized amphibole and biotite-bearing metasomatized rocks have a 'dioritized' look. Along the north and northeast contact, patches of garnet-epidote skarn have formed locally in calcite-bearing amygdaloidal flows of Skeena volcanic units.

QUARTZ MONZONITE PORPHYRY

The most economically significant intrusive body in the map-area is a small composite stock of quartz monzonite porphyry about 460 metres in diameter that intrudes pyroclastic rocks near the northwest margin of the quartz diorite intrusion (*see* Figs. 3, 5, 6, and 7). All phases of quartz monzonite are hydrothermally altered and mineralized.

The main mass of the quartz monzonite stock is roughly equidimensional at surface with fairly regular contacts. Exceptions are along the south and southwest contact and at depth where dykes and sill-like bodies project into or along volcanic strata. The main intrusive mass is a composite of at least three phases of coarse-grained biotite quartz feldspar porphyry that are intruded by at least one distinctly crosscutting phase of porphyry, namely hornblende quartz feldspar porphyry. This porphyry forms a northeasterly trending dyke that bisects the main quartz monzonite mass and intrudes hornfels and quartz diorite to the northeast. The main phases of quartz monzonite have not been observed to intrude quartz diorite and are separated from it by a screen of hornfelsed

volcanic rock, on average about 90 metres wide. Quartz diorite close to quartz monzonite is strongly altered and mineralized. An intrusive breccia body that is similar to quartz monzonite in composition and alteration intensity underlies a large area about 450 metres southeast of the quartz monzonite stock.

Potassium-argon dating by Carter (1974) of biotite from the quartz monzonite stock, altered quartz diorite, and whole rock specimens from the mineralized hornfels surrounding the stock indicates Eocene ages with a mean value of about 50 million years.

MINOR INTRUSIONS

A number of minor intrusions are shown on Figure 3 (unit C). Columnar-jointed feldspar porphyry sills (flows ?) near the base of the Kasalka successions consist of plagioclase and chloritized hornblende phenocrysts in a fine-grained matrix of plagioclase, K-feldspar, rare pyroxene, and fine-grained alteration products clay-chlorite-epidote. In Berg map-area the three main exposures of the feldspar porphyry unit are shown on Figure 3, cross-sections A, C, and D. The feldspar porphyries are part of the Kasalka Group and are intrusive, possibly extrusive, equivalents of volcanic rocks.

Pale grey to cream-coloured, weakly layered, massive to microporphyrific rhyolite dykes (part of unit C) form small irregular intrusions, mainly southwest of Berg camp and northeast of Mount Ney. These dykes are compositionally similar to rhyolite of the Bergette Formation (unit 5a) of the Kasalka assemblage.

The most abundant porphyry dykes in the region are biotite quartz feldspar porphyries. These form predominantly northwesterly trending dykes, commonly 2 to 15 metres wide that have been found in all but the youngest (map unit 5) Kasalka rocks. The porphyry dykes intrude quartz diorite and are, therefore, Tertiary in age and part of the quartz monzonite intrusive suite.

Basalt dykes of Miocene (and younger ?) age, shown on Figure 3 as unit D, intrude all major rock units throughout the map-area. They are commonly less than 3 metres wide although dykes up to 25 metres in width are known. Basalt dykes are abundant and occur randomly except in the mineralized zone where a greater number than the regional average has been intersected in drill holes.

STRUCTURE

Bedded rocks in the map-area form an easterly dipping succession, commonly with 10 to 30-degree dips. Gentle folding is evident in Hazelton rocks where large-scale undulations and flexures about north to north-northeasterly fold axes can be seen. Cretaceous rocks are flatter lying except where they are tilted by faulting and in local areas where contorted strata and slumped blocks are associated with small-scale décollements. Such

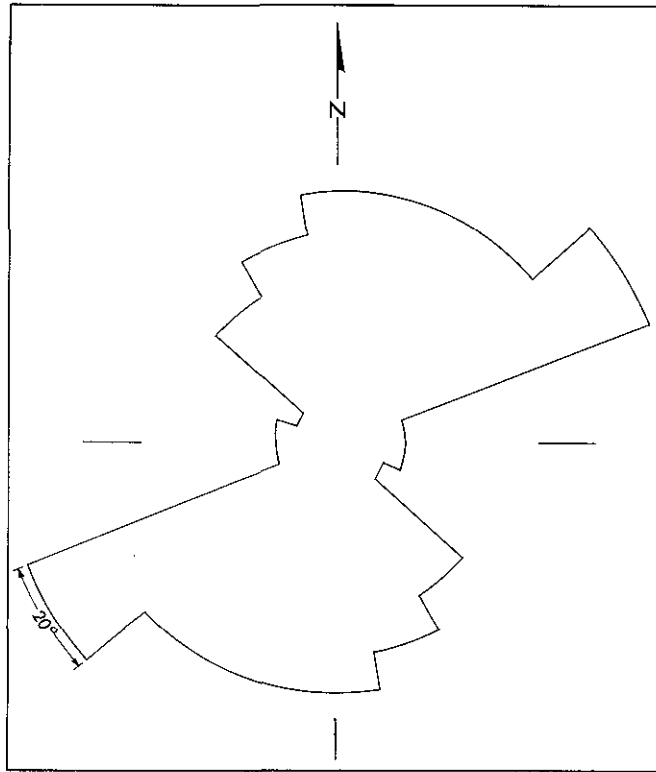


Figure 4. Air photograph interpretation of fracture trends.

décollement structures are seen over a 70-metre succession on the west flank of Mount Ney (Plate III).

Fracture patterns, as shown on Figure 4, indicate predominance of east-northeast and north to northeasterly trends. This is in contrast to dominantly northwesterly trends described in the Tahtsa Lake region by MacIntyre (1976). He suggests that north to northeasterly trends are subsidiary trends within fault blocks bounded by northwesterly faults. Where fault displacements or offsets can be measured in Berg map-area the most significant movements are, at most, some tens of metres in magnitude and appear to have taken place along northwesterly breaks. Age of faulting is uncertain but Miocene ? basalt dykes that commonly invade the most intensely fractured zones rarely show any significant offsets. This implies that post-Miocene movements may have been minor relative to those during Cretaceous or Early Tertiary time.

Structural controls on the emplacement of intrusive bodies are suggested by north-south elongation of the main quartz diorite stock and alignment of small diorite intrusions along the northern extension of the stock. Subsidiary, possibly younger, northeasterly trending structures or zones of weakness appear to have controlled emplacement of mineralized quartz monzonite intrusions and dykes. The youngest structural breaks are northwesterly zones that are intruded by unmineralized quartz feldspar porphyry dykes

and basalt dykes. The basalt dykes are emplaced in northwesterly fault zones that cut and displace older northeast-trending quartz monzonite intrusions.

GEOLOGY OF BERG COPPER—MOLYBDENUM DEPOSIT

Geology of the mineralized zone at Berg deposit was studied extensively and first described in detail by George O. M. Stewart (1967). Stewart, aided by some bulldozer trenching and some diamond drilling, mapped highly weathered surface exposures. His interpretation of general geology, major map units, and locations of intrusive contacts is still essentially valid. Stewart described five main map units: hornfelsed and hydrothermally altered Hazelton Group volcanic and sedimentary rocks; a diorite/quartz diorite stock thought to be a satellite of the Coast Plutonic Complex; a composite quartz monzonite porphyry stock about which copper-molybdenum mineralization is localized; a cross-cutting 'quartz latite' post-ore dyke phase; and an intrusive breccia pipe. Recent diamond drilling in previously untested areas, principally in the core and near margins of the quartz monzonite stock, indicates that a number of porphyry phases can be distinguished and internal intrusive relations are more complex than first thought. Recent revisions of Stewart's mapping are shown on Figures 5 and 6, and also Figure 7 (in pocket).

Surface exposures are limonite-stained, deeply weathered, crumbly outcrops that are strongly oxidized and leached. Slopes are generally devoid of vegetation and are mantled by slide debris and talus. The centre of the mineralized area is underlain by a quartz monzonite porphyry stock containing generally less than 2 per cent sulphide minerals. This stock is a roughly equidimensional plug about 640 metres in diameter and has a splayed northwesterly trending lobe in the southwest. It is transected by a northeasterly trending porphyry dyke that forms a spine-like ridge. Porphyritic intrusive rocks weather pale to yellow brown and form an elongate northeasterly trending mound in the centre of a broad, west-facing embayment that is carved into the prominent north-trending ridge of quartz diorite and Hazelton volcanic rocks.

A broad horseshoe-shaped low-weathering area that opens into Bergeland Creek tributary on the southwest surrounds the ridge of somewhat more resistant porphyry stock. This is the zone of strongly fractured, mineralized, and altered volcanic rocks. Rapid erosion of hydrothermally altered and highly fractured rocks abetted by percolation of acidic groundwater that removes gypsum from fractures has probably been more important than glacial scouring in development of low-lying areas about the stock. The most highly eroded zones have relief of about 215 metres relative to the porphyry ridge crest and are occupied by 'Red' Creek on the southeast and 'Pump' Creek on the northwest (Fig. 7).

Rocks containing economically significant sulphide minerals extend outward for at least 600 metres beyond the quartz monzonite contact and adjoining deeply eroded volcanic rocks. Rocks with sulphide minerals are marked by dark brown limonite-stained outcrops. To the north of the quartz monzonite stock these are volcanic and sedimentary rocks, and to the northeast and east, quartz diorite. Topography reflects changes in rock

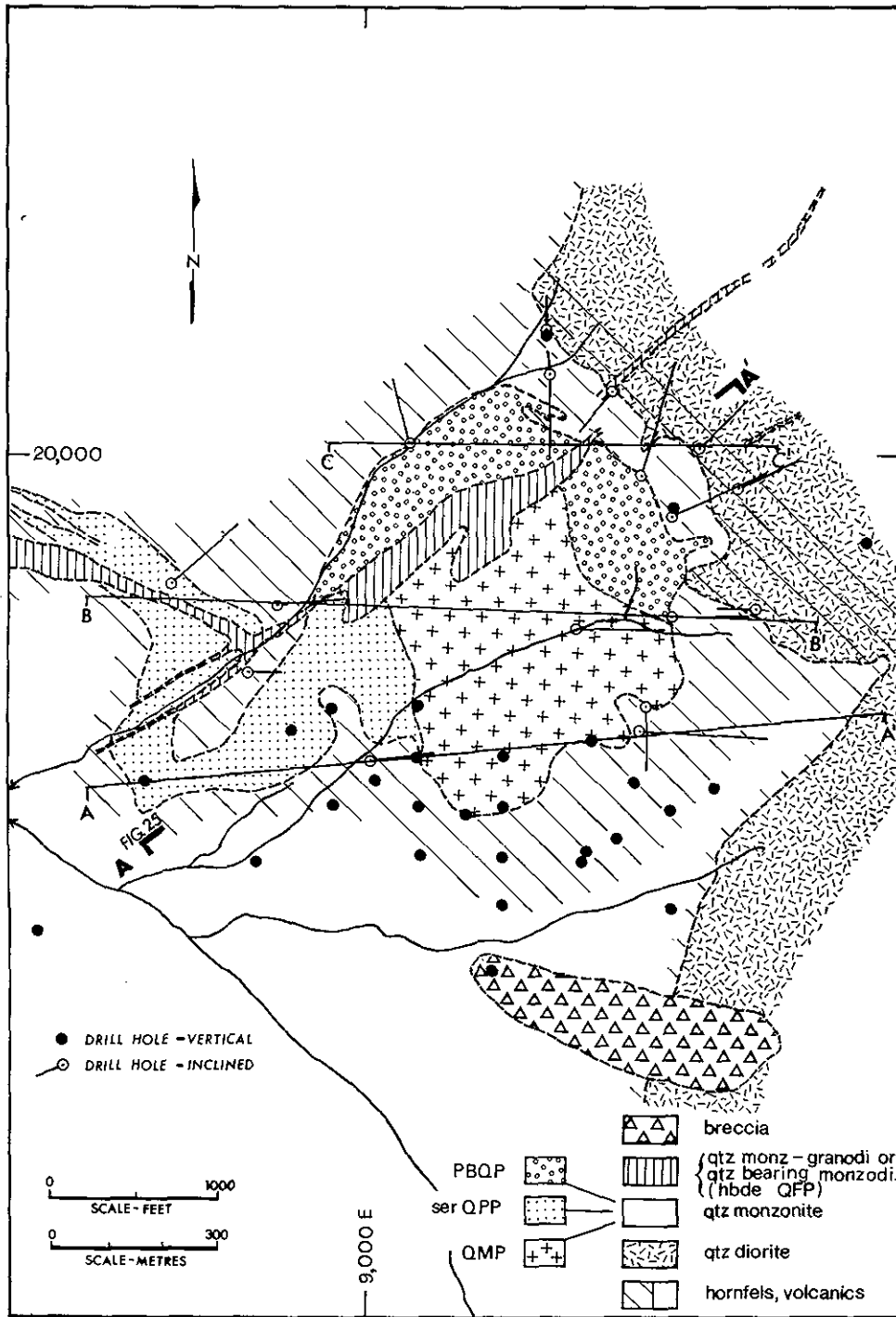


Figure 5. Geology — Berg deposit.

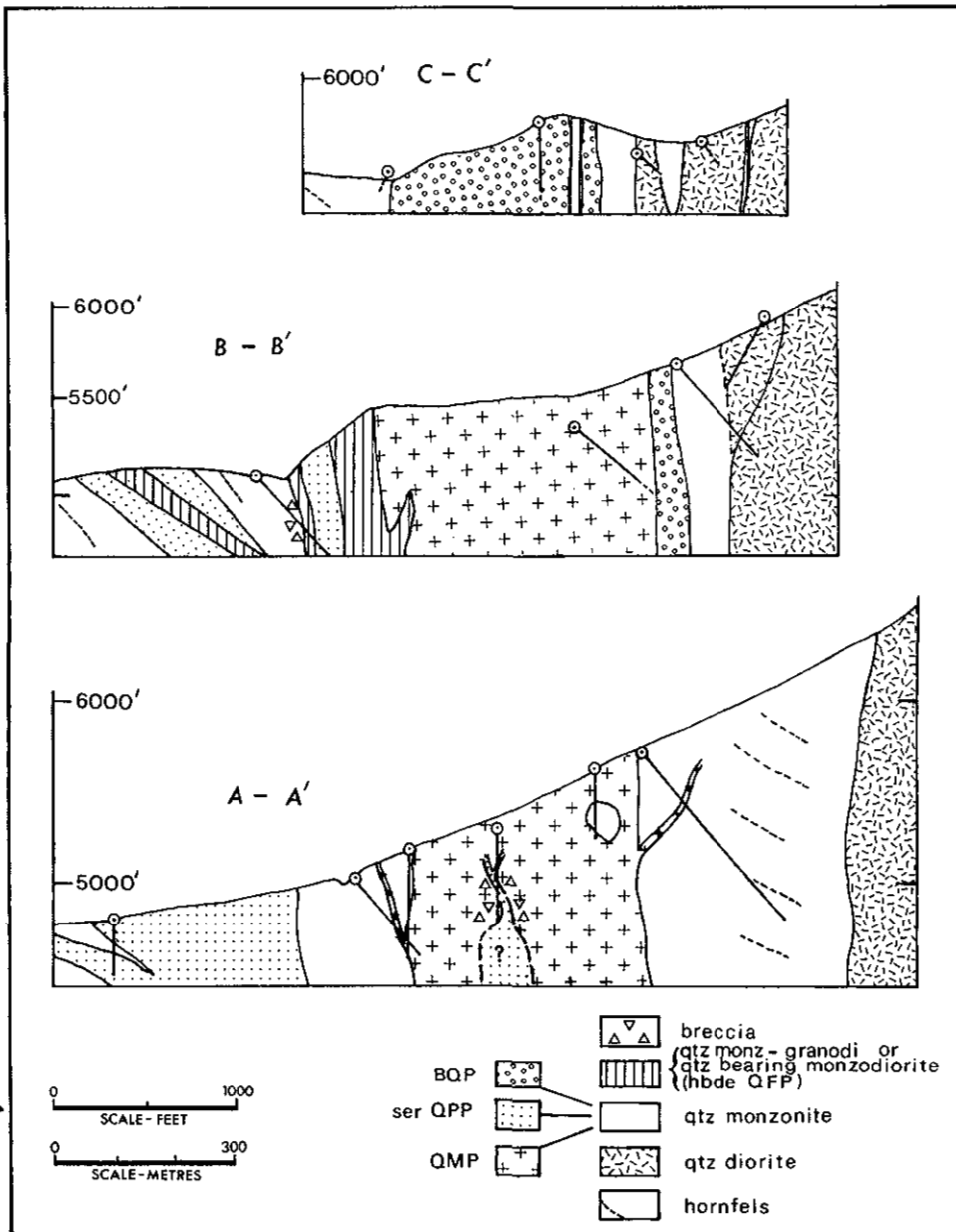


Figure 6. Geologic cross sections (view looking northerly).

type and alteration. Slopes are relatively gentle near the stock, steepen to about 30 degrees on flanking hillsides, and at the outer edge of the limonite-stained zone steepen abruptly to about 45 degrees. Weakly altered and sparsely mineralized volcanic rocks on the north and quartz diorite on the east form ridge crests that tower over the mineralized zone. Maximum relief is approximately 550 metres on the ridge to the north and 730 metres on the ridge to the east of the quartz monzonite stock.

BEDDED ROCKS

Host rocks for intrusions and mineral deposits are Middle Jurassic Hazelton Group volcanic rocks (Figs. 3 and 7, unit 1) that are predominantly subaerial erupted volcanic rocks and lesser interbedded sedimentary rocks. These are mainly coarse to medium-grained (lapilli) tuffs of andesitic composition as well as subordinate flows, breccias, epiclastic volcanic rocks (reworked volcanic source sandstones or 'greywackes'), and minor amounts of marine shale and siltstone. Outside the area of mineralization volcanic rocks are dark grey, grey-green, purple, and red in colour with obvious fragmental textures and well-defined bedding. Closer to intrusions the volcanic rocks are recrystallized to dark grey-brown and black rocks in which original fragments are seen as relict clasts or are totally obliterated in homogeneous-looking hornfels.

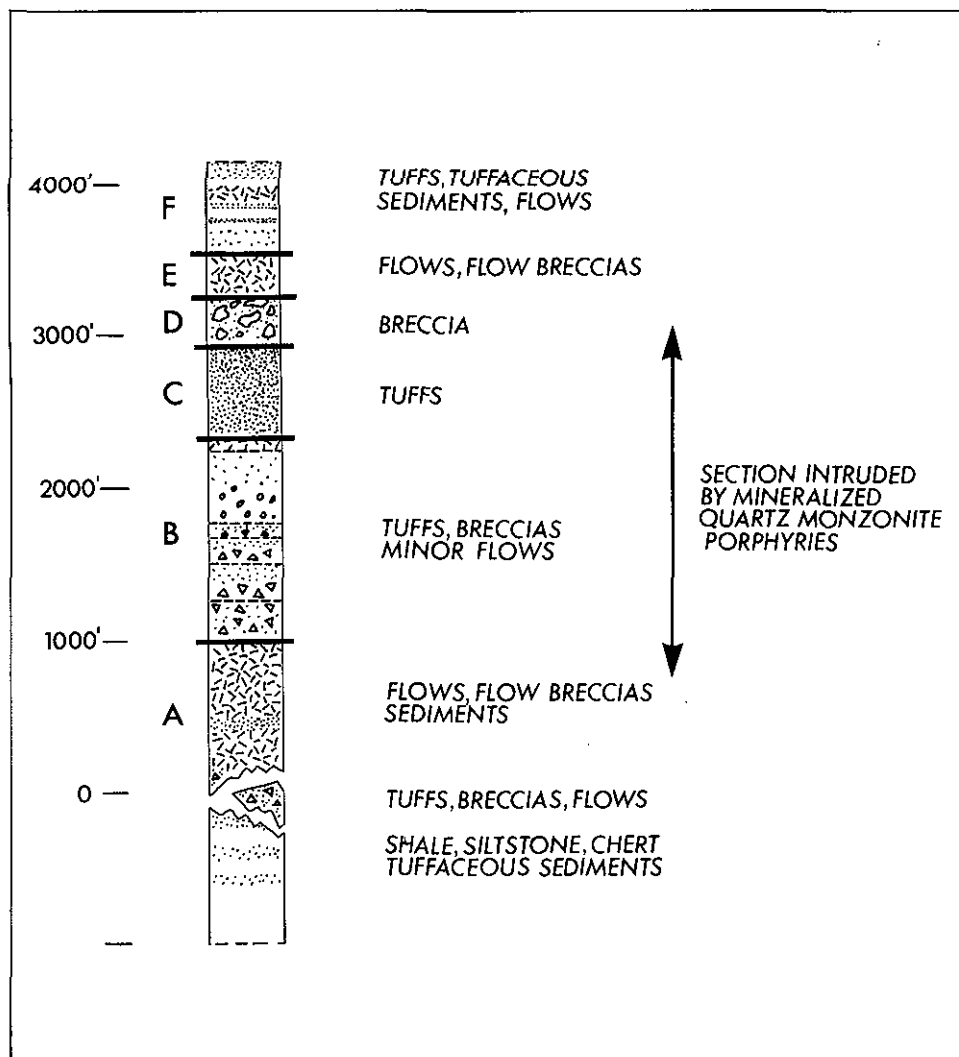


Figure 8. Subdivision of Hazelton Group volcanic succession at Berg deposit.

The volcanic succession strikes approximately north-south and is tilted eastward at about 30 degrees. There is no apparent repetition by faulting or other structural complications. Thus, an east-west section measured along Bergeland Creek and the ridge immediately north of Berg deposit represents a reasonably true geologic cross-section with younger rocks or 'tops' to the east. A generalized succession subdivided into six units representing about 1 530 metres of strata is shown on Figure 8. Oldest rocks are on the west and are shown on Figure 8 as unit A. The base of the succession is not exposed and the upper contact with rocks of the Skeena Group is intruded by quartz diorite or is inaccessible.

Rocks of map unit A form a 300-metre-thick sequence of grey and grey-green, fine-grained to weakly porphyritic andesites, flow breccias, and intercalated fine-grained sedimentary layers. The tuffs, tuff breccias, and flows are seen along the north bank of upper Bergeland Creek and overlie about 300 metres of thinly bedded shale, siltstone, chert, and tuffaceous sedimentary rocks exposed further downstream. Unit B consists of a 400-metre-thick pile of tuffs, minor breccias, and a few flow units including three paired units of purple lapilli tuff overlain by grey and mauve ash tuff. Purple members are made up of pale grey and cream lapilli-sized porphyritic fragments constituting from 10 to 30 per cent of the rock in a dense vitric groundmass. Overlying grey and mauve rocks are lithic tuffs in which there is sorting of fragments. Most beds are graded and there is much alternation between beds containing either fine ash or coarse ash together with lapilli fragments. The three paired units are successively thinner; the older being over 60 metres in thickness, the middle 45 metres, and the upper only 18 metres thick. Individual members within these map units are 2 centimetres to 2 metres in thickness. Above the paired purple-grey units are mainly dark purple, mauve, and grey, loosely packed, lithic lapilli and ash tuffs that contain a few crystalline limestone fragments. The top of unit B is taken to be a 12-metre-thick succession of massive fine-grained flow volcanic rocks.

Map unit C consists of about 200 metres of red, purple, and grey lithic tuffs. The succession is made up of thinly bedded lapilli tuffs with fragments up to 5 centimetres in size, 0.5 to 1.5-centimetre fragments being most common in an ash matrix. These tuffs are very porous with loosely packed fragments in a relatively homogeneous nonsorted ash matrix. Some beds contain fragments of cindery and pelleted accretionary lapilli in a ferruginous matrix and were probably deposited in a subaerial accumulation. Other beds consist of reworked tephra with a limy mud matrix and formed in an apparently shallow subaqueous environment. Unit D consists of about 90 metres of pale and medium grey volcanic breccia with fragments up to 5 centimetres in size. This unit is overlain unconformably by a thin capping of Cretaceous boulder conglomerate of unit 4 on the ridge northwest of the camp. Unit E is a 90-metre succession of 'greenstone' flows and flow breccias which is overlain by unit F, a heterogeneous assemblage of tuffs, fine-grained tuffaceous sedimentary rocks including limy siltstones, volcanic sandstones, and volcanic flows totalling at least 150 metres in stratigraphic thickness.

Strata of units B, C, and upper part of A have been intruded, altered, and mineralized. The resulting rocks have been described as 'hornfels.' However, there has been consider-

able metasomatism and, thus, the term 'hornfels' is used in an informal sense. At Berg deposit, Sutherland Brown (1967) distinguished between biotitic hornfels in a thermal aureole and hydrothermally metasomatized rocks he termed skarn, containing recrystallized quartz, biotite, and K-feldspar. He further subdivided hydrothermally altered rocks into a third group of mottled 'greisen-like' (quartz sericite) rocks. However, origin of biotite cannot always be ascribed on the basis of appearance to either purely contact metamorphism or metasomatism and the term 'hornfels' will be retained in this report for purely descriptive purposes. Thus, biotite hornfels refers to all the massive, dark, fine-grained metamorphosed rocks surrounding Berg intrusions. While some epidote and rare garnet occur in altered calcareous beds along the quartz diorite contact or in pendants in quartz diorite, no skarn assemblages are present within Berg deposit.

INTRUSIVE ROCKS

Two distinctive intrusive bodies are seen at Berg deposit. They differ in composition, texture, shape, and effect on intruded rocks. The older rock is a fine-grained quartz diorite that has no inherent mineralization and has recrystallized intruded rocks into a dense, compact hornfels. The quartz diorite is part of a large intrusive body at least 600 metres wide that extends for at least 8 kilometres to the south of Berg deposit. The intrusive contact is steeply dipping, somewhat serrated in plan, but continuous without known offshoots or projections. Two small satellitic bodies of porphyritic hornblende quartz diorite intrude 1.5 and 3 kilometres to the north of the main intrusion and another quartz diorite plug intrudes 1 kilometre west of Berg camp.

The younger intrusion is a composite stock of quartz monzonite porphyry that is no more than 640 metres in diameter. Every intrusive phase is mineralized to some degree and adjoining volcanic rocks and quartz diorite are altered and mineralized extensively. The core of the quartz monzonite stock is plug like and is flanked to the south and southwest by dykes, sills, and irregular apophyses. Quartz monzonite does not intrude quartz diorite, but has altered and mineralized it. Both rock types are cut by one large and a number of smaller porphyry dykes related to quartz monzonite.

The absolute age difference and genetic relationships between the two main intrusive types are not certain. Porphyritic quartz monzonite is found in a zone a few hundred metres wide within quartz diorite 3.5 kilometres south of Berg deposit. The zone is within the centre and widest part of the quartz diorite intrusion and appears to have gradational contacts with quartz diorite. Thus, porphyritic quartz monzonite may be a more highly differentiated phase of a parent quartz diorite magma. The mineralized quartz monzonite porphyry and quartz diorite in Berg map-area might be cogenetic.

Description of intrusive rocks in Berg map-area at a regional scale has been done by Duffel (1959), and at the property by Kennco Explorations, (Western) Limited geologists (Stewart, 1967), Sutherland Brown (1967), and more recently, Canex Placer Limited geologists. Nomenclature used in this study is a modification of the descriptive classification

used by Canex Placer Limited geologists (1974, personal communication). It is based largely on diamond drilling in the core of the quartz monzonite stock since 1972.

Quartz diorite was mapped by Duffel as gabbro. Along the contact the rock in places contains less than 10 per cent quartz, has some pyroxene, and is melanocratic due to an abundance of hornblendes. However, average plagioclase composition is that of calcic andesine (An_{50}), quartz content slightly exceeds 10 per cent, and biotite accompanies hornblende everywhere as a mafic constituent. The rock is better classified as quartz diorite and has been so described by investigators subsequent to Duffel.

The mineralized stock of quartz monzonite porphyry consists of at least two distinct types of porphyry. The two are distinguished on the basis of texture, mineralogy, fracture intensity, degree of alteration, and most readily by differences in their weathering characteristics in outcrop. The younger porphyry dyke is less altered and forms a resistant ridge crosscutting the main mass of porphyry.

From field observations Kenenco Explorations, (Western) Limited geologists (Stewart, 1967) called the main mass 'quartz monzonite porphyry' and the crosscutting dyke 'quartz latite porphyry.' Sutherland Brown (1967), on the basis of field mapping and microscopic examinations, classed rocks as 'quartz monzonite porphyry' and 'quartz-bearing monzonite porphyry.' Both Stewart and Sutherland Brown recognized the presence of more than one phase of quartz monzonite in the main stock and inferred that intergradational relationships exist between the phases.

Recent drilling by Canex Placer Limited has revealed that the mineralized stock (Fig. 7) is composed of two phases of quartz monzonite, called in this report quartz monzonite porphyry (QMP, Fig. 7, unit 3), and sericitized quartz plagioclase porphyry (QPP, Fig. 7, unit 4), as well as a third phase of quartz monzonite or quartz-bearing monzonite called plagioclase biotite quartz porphyry (PBQP, Fig. 7, unit 5). The phases are most apparent on the basis of texture. Differences in type, amount, and proportion of minerals are slight and are recognized only by careful point counts and examination of rocks in thin section. The porphyry dyke (QFP, Fig. 7, unit 6) that crosscuts the quartz monzonite stock is distinct on the basis of mineralogy and texture. Descriptions of rock types as determined from point counts on phenocrysts in large stained slabs and matrix in thin section are given below, summarized in Table 1, and illustrated by a ternary plot on Figure 9.

QUARTZ DIORITE (Fig. 7, Unit 2)

Quartz diorite is a pale grey, fine to medium-grained, and locally porphyritic rock in which plagioclase, hornblende, and biotite are the most obvious components. Specimens range in composition from diorite to granodiorite but quartz diorite is most common. Laths of plagioclase about 1 millimetre in size are randomly oriented in a matrix of hornblende, fine-grained biotite, and very fine anhedral grains of quartz and orthoclase. Some

TABLE 1: MINERALOGICAL COMPOSITION OF INTRUSIVE ROCKS BERG DEPOSIT (Mean values of modal analyses, not recalculated to 100 per cent)					
Figure 7	Unit 3 OMP N=8	Unit 4 Sericitic OPP N=4	Unit 5 PBOP N=4	Unit 6 hbde QFP N=4	Unit 2 Qtz dio N=9
Phenocrysts					
Orthoclase	3.1	---	0.8	0.2	---
Quartz	6.4	5.7	5.3	5.1	---
Plagioclase	27.3	25.9	28.1	26.0	---
Matrix	54	65	59	63	
Total					
Orthoclase	26.1	25.8	26.7	20.2	5.3
Quartz	27.1	26.7	15.1	10.4	12.6
Plagioclase	35.6	32.2	41.4	43.0	61.2
Mafics	7.5	5.2	13.8	19.9	16.8
Accessories (including sericite)	3.6	10.1	3.7	6.0	4.1
Mafics	bio	bio (sericitized)	bio >hbde	hbde >bio	variable hbde >bio
Plagioclase An	~30	~31	31±3	38±4	50±8

subhedral crystals of hornblende are up to 5 millimetres and more in size. A few specimens from near the intrusive contact contain rare pyroxene, have less than 10 per cent quartz, and have weak orientation of plagioclase laths and hornblende crystals. Plagioclase is oscillatory normal-zoned calcic andesine to labradorite ($An_{4.2-5.8}$). Chlorite has formed after hornblende and, less commonly, biotite. Other alteration minerals include sericite, epidote, and calcite. Magnetite, sphene, and apatite are accessory minerals. In the zone of mineralization near quartz monzonite porphyry, chalcocopyrite, pyrite, some molybdenite, and quartz veining are evident. Replacement of original mafic minerals by fine-grained felted biotite and magnetite by pyrite is common.

MINERALIZED QUARTZ MONZONITE STOCK AND DYKES (Fig. 7, Units 3 to 5)

Quartz Monzonite Porphyry Phase (QMP; Fig. 7, Unit 3): Quartz monzonite porphyry is a grey to pink, coarse-grained, two-feldspar quartz porphyry. It contains about 45 per cent phenocrysts of mainly oligoclase-andesine ($An_{3.0}$), quartz, biotite, and some orthoclase in a fine-grained quartz feldspar matrix. Plagioclase phenocrysts are chalky white to cream, grey, buff, and grey-green subhedral, blocky laths 2 to 8 millimetres, averaging about 5 millimetres, in size. Quartz and myrmekitic quartz-oligoclase forms large, deeply embayed, anhedral grains averaging 4 to 6 millimetres, in a few cases up to 1 centimetre, in size. Perthitic orthoclase is seen as scattered poikilitic phenocrysts about 5 millimetres in size and as sparse, squat megacrysts up to 2 centimetres in length. A few grains have rims of plagioclase around orthoclase. Biotite as tabular books 6 millimetres in length

and 4 millimetres in cross-section is the sole remaining magmatic mafic constituent. A small amount of hornblende that was originally present is now totally replaced by biotite, sericite, and chlorite. The matrix is an allotriomorphic-granular mosaic of 0.04-millimetre grains of plagioclase, slightly in excess of equal amounts of similarly sized quartz and orthoclase.

In thin section quartz phenocrysts are distinctive with a myrmekitic appearance. Grains are strongly corroded with deep embayments and contain inclusions of small oligoclase ? grains. Grain boundaries appear to be resorbed resulting in reaction rims of microcrystalline quartz. Large grains are sutured composite crystals that appear to be cumulates of a number of smaller grains, or may simply be fractured megacrysts. Plagioclase phenocrysts are strongly sericitized and locally argillic. Crystals are strongly zoned in an oscillatory-normal manner but twinning is largely obscured by alteration and plagioclase determinations are difficult. On the basis of a few determinations plagioclase appears to be oligoclase-andesine (approximately An_{30}). Hornblende which was originally present in small amounts is commonly totally replaced by fine-grained felted biotite. Fine-grained secondary biotite is also scattered throughout the matrix. In addition to sericite, biotite, chlorite, calcite, and opaque minerals, some kaolinite and montmorillonite are alteration products. Sphene, apatite, and zircon are accessory minerals. Quartz veins and gypsum-filled fractures are common.

A dyke phase of similar quartz monzonite porphyry commonly displays chilled contacts and can be seen to intrude quartz monzonite porphyry and possibly plagioclase biotite quartz porphyry in a number of drill holes. The dyke rock contains about 40 to 45 per cent coarse-grained phenocrysts of plagioclase (An_{30-33}) with biotite, some quartz, and orthoclase, in a fine-grained matrix of mainly quartz and orthoclase. Quartz megacrysts up to 1 centimetre in size are the largest grains seen. Matrix is a distinctive pinkish grey to orange-tinted grey or brown colour and is considerably less altered than in other porphyry phases. Biotite and plagioclase phenocrysts are also little altered and fresh looking. Secondary biotite and other alteration minerals are of minor abundance but fine-grained disseminated magnetite is more abundant than in other porphyries. In addition to chilled contacts and weak alteration, strong magnetic response and paucity of ore minerals set this rock type apart from other quartz monzonite porphyries.

Sericitized Quartz Plagioclase Porphyry Phase (QPP; Fig. 7, Unit 4): This quartz monzonite is a medium-grained porphyry, the finest grained of all the types of porphyry recognized at Berg deposit. The rock is strongly sericitized, leucocratic buff to grey, rarely grading to medium brown in colour. It contains about 35 per cent phenocrysts, mainly plagioclase (An_{30-32}) and some quartz. Orthoclase phenocrysts are notably rare or absent as are large grains of biotite. Grain size of plagioclase and quartz phenocrysts varies from 1 millimetre to a maximum of 5 millimetres, 2 to 3 millimetres being the average. Fine-grained plagioclase phenocrysts are equant subhedral crystals that are evenly distributed to produce a rock with homogeneous appearance. Coarser phenocrysts vary in size and are rounded, thereby giving a seriate texture to some of the porphyry. Quartz grains average 2 millimetres in size and are strongly corroded.

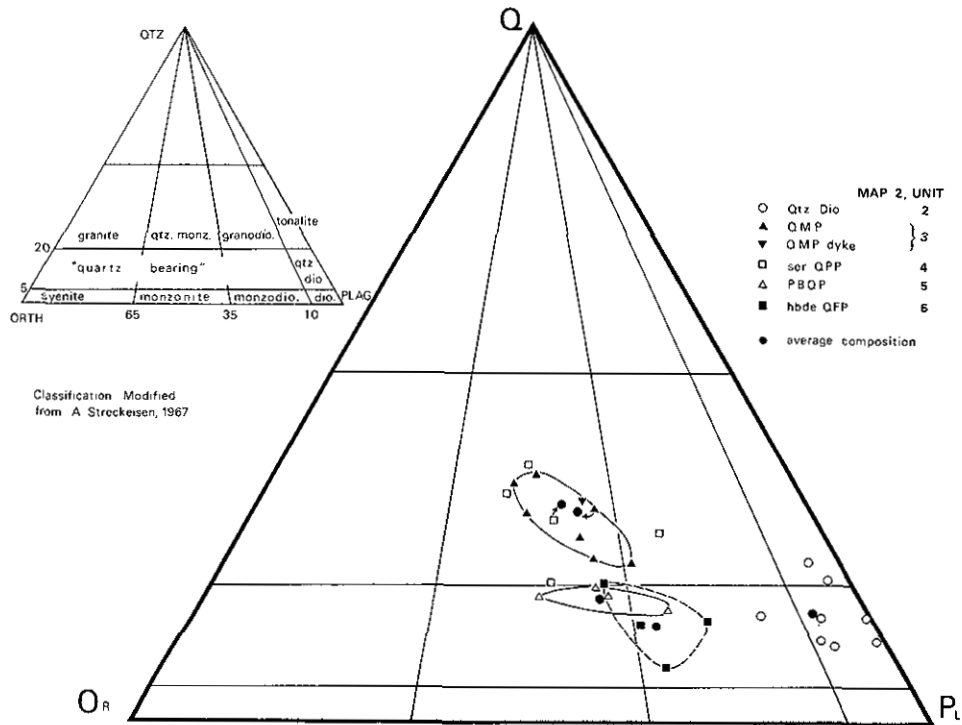


Figure 9. Modal composition of intrusive rocks, Berg deposit.

In thin section the matrix can be seen to be composed of 0.01 to 0.03-millimetre grains of plagioclase, orthoclase, and quartz. Plagioclase is slightly more abundant than orthoclase and appears to be the same composition as phenocrysts (An_{30-32}). Quartz content is variable, probably due to different degrees of secondary silicification. Where abundant, quartz in the matrix is an accumulation of rounded, possibly overgrown, grains. Quartz veins are common. Sericite is abundant and pervasive; it replaces both plagioclase and orthoclase. Together with kaolinite, lesser chlorite, and montmorillonite, sericite comprises up to 10 per cent and more of the rock. It has formed mainly after feldspars but is also found with pyrite, chlorite, and calcite replacing primary biotite (and hornblende?). Almost all biotite now seen in the rock is present in the matrix as scattered, shredded, fine-grained secondary biotite. Where abundant, fine-grained biotite imparts a brownish cast to the matrix of the rock.

Strong sericitization, medium-sized phenocrysts, absence of orthoclase phenocrysts, and lack of large biotite grains readily set this porphyry apart from other phases of quartz monzonite.

Plagioclase Biotite Quartz Porphyry (PBQP; Fig. 7, Unit 5): This rock type has less quartz and more plagioclase than the two quartz monzonite phases (units 3 and 4) and straddles the boundary of quartz monzonite and quartz-bearing monzonite compositional fields (Fig. 9). Hand specimens are relatively homogeneous in appearance with grey to

pinkish grey or brown matrix in which evenly distributed fine and medium-grained phenocrysts form about 40 per cent of the rock. Plagioclase phenocrysts form about 40 per cent of the rock. Plagioclase phenocrysts are pale grey in colour and are of two sizes. Larger ones 4 to 7 millimetres, averaging 5 millimetres in size, comprise about 80 per cent of the feldspar phenocrysts; smaller ones are 1 to 2 millimetres in size. Quartz phenocrysts are anhedral grains 3 millimetres and smaller in size. Orthoclase is seen as rare phenocrysts that are the same size or smaller than surrounding plagioclase grains. In a few crystals orthoclase forms rims or mantles on plagioclase. Biotite is unaltered looking, fresh euhedral platelets or short, stubby books about 2 millimetres in cross-section. These contrast markedly with elongate, coarse books of biotite in quartz monzonite porphyry (QMP) and highly sericitized biotite in quartz plagioclase porphyry (QPP).

In thin section the matrix is a 0.02-millimetre-sized mosaic of mainly plagioclase with lesser orthoclase and quartz. Plagioclase phenocrysts and matrix grains are sericitized but twinned crystals, mainly albite and combined Carlsbad-albite types, are common and only moderately affected by alteration. Crystals are zoned in an oscillatory normal manner, commonly with four to six cycles. Measured plagioclase composition ranges from calcic oligoclase to andesine (An_{28-34}). Over-all, mafic minerals in this rock type are about twice as abundant as in quartz monzonite porphyry (QMP) and sericitized quartz plagioclase porphyry (QPP). The amount of secondary biotite is less than in other porphyries but this reduction is compensated by the presence of increased amounts of fine-grained hornblende. Biotite to hornblende ratio varies from 2:1 to 5:1. All fine-grained original biotite and hornblende grains in the matrix are chloritized to some degree. Hornblende is replaced extensively by biotite or chlorite, sericite, calcite, and opaque minerals.

Quartz Monzonite-Granodiorite Dykes (Hornblende quartz feldspar porphyry, hbde QFP; Fig. 7, Unit 6): This variety of dyke-forming quartz feldspar porphyry is a pale to medium grey coarse porphyry that superficially is similar to quartz monzonite phases of the mineralized stock that it intrudes (units 3 to 5). Large phenocrysts of cream to pinkish buff plagioclase, as well as quartz, biotite, and very sparse orthoclase, make up about 35 per cent of the rock. Near intrusive contacts the rock is chilled and has small phenocrysts commonly 2 millimetres or smaller of plagioclase, quartz, mafic minerals, and some orthoclase in medium grey microcrystalline matrix. In the main mass of porphyry, equant rounded phenocrysts of plagioclase are 5 to 7 millimetres in size. Strongly corroded and resorbed quartz grains average 6 millimetres in size, but are up to 1.2 centimetres across in some large cumulate grains. Orthoclase crystals are interspersed sporadically throughout the rock as squat, euhedral megacrysts up to 1.8 centimetres in length. Most orthoclase phenocrysts are altered and extensively replaced by epidote. Mafic minerals are present as large elongate books of biotite up to 7 millimetres in length and small laths of hornblende. Large grains of sphene are common as well as matted patches and clots of epidote up to 6 millimetres in size.

The most obvious difference between this rock type and other phases of porphyry is in the matrix where quartz is relatively sparse, ranging from 6 to 12 per cent in specimens

examined. The matrix is mostly plagioclase, poikilitic almost intersertal orthoclase, and fine-grained hornblende, biotite, opaque grains, and alteration minerals. Hornblende is abundant, well in excess of biotite, and total mafic content of the rock is about 20 per cent.

Plagioclase phenocrysts are only slightly altered. They are combined crystals that display complex twins and simple normal zoning with rarely more than three or four cycles. Anorthite content ranges from $An_{3.4}$ to an observed maximum of $An_{4.2}$. Secondary biotite is present but in minor amounts compared to quartz monzonite porphyries. Hornblende is seen as small to medium-sized relict crystals partially or totally replaced by chlorite, epidote, calcite, or fine-grained biotite. Over-all, secondary biotite, sericite, quartz veins, and gypsum are weakly developed and epidote, chlorite, and calcite are main alteration minerals.

BASIC DYKES

Dykes, shown as unit D on Figure 3, are all similar medium to dark grey fine-grained basalt. They form thin steeply dipping sheets generally up to 3 metres in thickness. A number contain up to 5 per cent small phenocrysts of plagioclase but more commonly are massive with small amygdules of calcite. In thin section basic dyke rocks are fine-grained feldspathic to trachytoid intergrowths of plagioclase and hornblende with abundant accessory, opaque minerals, and alteration products, mainly chlorite and calcite.

CHEMICAL COMPOSITION

Chemical compositions, reported by Carter (1974), of representative samples of quartz monzonite porphyry (QMP, Fig. 7, unit 3) and plagioclase biotite quartz porphyry (PBQP, Fig. 7, unit 5), determined by wet chemical silicate analyses, are given in Table 2. Analytical results and calculated norms for plagioclase biotite quartz porphyry correspond very closely to Daly's and Nockold's average quartz monzonite or adamellite whereas quartz monzonite is more akin to granite. This is probably due to increased amount of K_2O through orthoclase metasomatism and SiO_2 due to quartz veining.

DISTRIBUTION AND GEOMETRY OF PORPHYRIES (Fig. 7)

The roughly equidimensional core of the mineralized stock is made up of two phases: quartz monzonite porphyry (unit 3) and plagioclase biotite quartz porphyry (unit 5). Sericitized quartz plagioclase porphyry (unit 4) forms irregular bodies adjacent to the core in the southwest. All three phases are transected by a northeasterly trending hornblende quartz feldspar porphyry dyke (unit 6) which is the only porphyry phase that intrudes quartz diorite (unit 2). The three main phases of quartz monzonite porphyry (units 3 to 5) are separated from quartz diorite by a screen of hornfelsed volcanic rocks.

Quartz monzonite porphyry (unit 3) is found as a subcircular mass forming the southern and southeastern portion of the mineralized stock. The porphyry is thought to be a

TABLE 2. CHEMICAL COMPOSITIONS AND NORMS					
	1	2	3	4	5
Oxides Recalculated to 100%—					
SiO ₂	70.73	67.76	67.41	69.67	72.60
TiO ₂	0.53	0.55	0.51	0.56	0.37
Al ₂ O ₃	16.36	16.39	15.76	14.74	13.96
Fe ₂ O ₃	1.21	1.78	1.93	1.23	0.87
FeO	0.80	0.92	1.96	2.29	1.68
MnO	0.02	0.07	0.06	0.06	0.06
MgO	1.09	1.62	1.43	1.00	0.52
CaO	1.07	2.59	3.54	2.47	1.34
Na ₂ O	2.89	3.39	3.45	3.37	3.10
K ₂ O	5.30	4.93	3.76	4.61	5.50
Oxides as Determined—					
P ₂ O ₅	0.30	0.18	0.19	0.20	0.18
H ₂ O	1.32	2.18	1.15	0.54	0.53
SO ₃	1.92	4.53	---	---	---
CO ₂	0.02	---	---	---	---
BaO	0.12	---	---	---	---
CuO	0.38	---	---	---	---
Molecular Norm—					
Quartz	30.5	24.7	21.7	24.8	29.2
Orthoclase	31.2	29.1	22.5	27.2	32.2
Albite	25.9	30.4	31.3	28.3	26.2
Anorthite	3.2	7.7	16.6	11.1	5.6
Pyroxene	3.0	4.8	5.1	4.7	3.0
Magnetite	1.4	2.0	2.0	1.9	1.4
Ilmenite	0.3	0.1	0.7	1.1	0.8
Unassigned	4.5	1.2	0.1	0.9	1.6

- 1 — Berg quartz monzonite porphyry (Fig. 7, unit 3), NC-67-10 (DDH 19), S. Metcalfe, Analyst, *B.C. Ministry of Energy, Mines & Pet. Res.*, 1968.
- 2 — Berg plagioclase biotite quartz porphyry (Fig. 7, unit 5), NC-67-11 (DDH 1), S. Metcalfe, Analyst, *B.C. Ministry of Energy, Mines & Pet. Res.*, 1968.
- 3 — Average quartz monzonite, 20 analyses, Daly, 1933.
- 4 — Average adamellite, 121 analyses, Nockolds, 1954.
- 5 — Average calc-alkalic granite, 72 analyses, Nockolds, 1954.

small, vertical, plug-like body that is possibly the most voluminous phase present. Vertical drill holes (diamond-drill holes 19, 27, and 34) collared a few metres from the contact pass in and out of porphyry. The contact is sharp but appears to undulate and protrude outward in places, and locally splays to form arborescent dyke and sill-like projections. Rocks near the contact are highly altered by intense sericitization and quartz veining, and hornfels at the contact is brecciated in places.

Plagioclase biotite quartz porphyry (unit 5) is slightly less abundant than quartz monzonite porphyry and forms a shell up to 180 metres wide across the northern half of the stock. On the basis of limited diamond drilling, intrusive contacts with hornfels appear to be vertical and simple with few (possibly no) related dykes and breccias. Horn-

fels adjacent to plagioclase biotite quartz porphyry is black, biotite-rich rock with some quartz veining. Relationship to sericitized quartz plagioclase porphyry in the southwest is uncertain and possibly complex.

Sericitized quartz plagioclase porphyry (unit 4) intrudes as an irregular mass or group of coalescing bodies peripheral to the main stock on the southwest. The largest portion of this rock type appears to form a northwesterly trending dyke, or possibly a laccolith, in the vicinity of drill hole 13 (Fig. 7). The intrusion may have a small pipe-like core in the vicinity or northeast of drill holes 7, 30, and 31. It is flanked by splaying elaborate dykes and sills, two of which are intersected by drill holes 15 and 17. Two other areas in which sericitized quartz plagioclase porphyry may be present are at the north margin of the stock by drill hole 1 and in the main mass of quartz monzonite porphyry (unit 3) near drill hole 69. In the vicinity of drill hole 1, 'hybridized' rocks resembling quartz plagioclase porphyry were noted as breccia clasts in hornfels near the contact with plagioclase biotite quartz porphyry. Near diamond-drill hole 69 a poorly defined and little understood metasomatized breccia zone may contain zones or fragments of quartz plagioclase porphyry.

A hornblende quartz feldspar porphyry dyke (unit 6) crosscuts the three other porphyry phases and is located, at least in part, along the quartz monzonite porphyry-plagioclase biotite quartz porphyry contact. Exact shape of the intrusion is uncertain. In the centre of the mineralized stock, hornblende quartz feldspar porphyry forms a steep-walled dyke or northeasterly elongated plug up to 70 metres wide with a lobe to the south. Distal parts of the intrusion are tabular, dyke-like sheets with chilled margins. The dyke splays into three branches at its southwest extremity. In the northeast, it is offset by faults and may branch into a number of subparallel dykes, two of which are seen at surface in quartz diorite (unit 2).

Internal contact relationships between phases are not known mainly because surface exposures are poor and diamond drilling is limited. No distinct contacts have been recognized in drill core between the three main quartz monzonite phases. This may be because differences are subtle, rock types are intergradational, or alteration and metasomatism mask original textural and compositional differences. On the other hand, contacts simply may not be intersected by drilling to date. There is some evidence from outcrop data that contacts of plagioclase biotite quartz porphyry (unit 5) with quartz monzonite porphyry (unit 3) are sharp. In other places drill-hole data suggest that contacts may be metasomatized breccia zones, especially where contacts trend northwesterly. The hornblende quartz feldspar porphyry dyke (unit 6) can be distinguished from other phases in outcrop but no sharp contacts are known in drill cores. The only rock type seen that has chilled margins in drill cores is a quartz monzonite porphyry dyke that is included in unit 3.

AGE OF INTRUSIONS

Relative ages of intrusive phases cannot be determined unequivocally as only one rock type has been demonstrated to crosscut others. Hornblende quartz feldspar porphyry (unit 6) intrudes quartz diorite (unit 2) and all three main quartz monzonite phases (units 3 to 5). At least one quartz monzonite dyke intrudes quartz monzonite porphyry of the main stock; both rock types are included in unit 3, Figure 7, because of their similar composition and texture. Dykes of what appear to be plagioclase biotite quartz porphyry (unit 5) intrude sericitized quartz plagioclase porphyry (unit 4) but this classification of the dykes is not a certainty. These few observed relationships and the presence of sericitized quartz plagioclase porphyry breccia fragments in quartz monzonite porphyry, as well as considerable geological intuition, suggest the following sequence from oldest to youngest:*

- (a) Quartz diorite (Fig. 7, unit 2).
- (b) Quartz monzonite porphyry including similar dykes with chilled margins that may be considerably younger (QMP, unit 3).
- (c) Sericitized quartz plagioclase porphyry (ser QPP, unit 4).
- (d) Plagioclase biotite quartz porphyry (PBQP, unit 5).
- (e) Hornblende quartz feldspar porphyry (hbde QFP, unit 6).

Sample No.	Location	Rock Type	Material Sampled	Age (Ma)
NC-67-12	DDH 20	Biotite hornfels	Whole rock	52.0±3
NC-67-11	DDH 1	Plagioclase biotite quartz porphyry	Biotite	52.0±2
NC-67-13	DDH 9	Mineralized quartz diorite	Biotite	49.9±2.1
NC-67-9	DDH 70	Dyke quartz monzonite porphyry	Biotite	48.0±3
NC-67-10	DDH 19	Quartz monzonite porphyry	Biotite	47.0±3
NC-67-8	13,000E 21,000N	Quartz diorite	Chloritized biotite	46.8±1.5
			Mean	49.0±2.4

Absolute ages of rocks at Berg deposit have been determined by Carter (1974) using potassium-argon dating of biotite and whole rock specimens. Results ranging from 52.0 to 46.8 million years with a mean of 49.0±2.4 million years are listed in Table 3. No resolution of intrusive events or stages is possible from these data as all ages determined

* Drilling (A. D. Drummond, 1975, personal communication) has revealed that fragments of quartz monzonite porphyry (unit 3) are found in sericitized quartz plagioclase porphyry (unit 4). The breccia fragments of sericitized quartz plagioclase porphyry (unit 4) referred to above are intruded into quartz monzonite porphyry (unit 3) in a 'volcanic neck.' Also plagioclase biotite quartz porphyry (unit 5) contains fragments said to be quartz monzonite porphyry (unit 3) and sericitized quartz plagioclase porphyry (unit 4).

are within limits of analytical error of the mean age. Age of quartz diorite is not reliable as biotite sampled was chloritized and yielded only 2.64 per cent potassium. Quartz diorite may be considerably older as biotite might have been reset or crystallized during intrusion of quartz monzonite bodies.

BRECCIAS

In this report the term 'breccia' is used to describe fragmented rocks in which fragments can be demonstrated to be displaced relative to their original position. Intensely fractured rocks surrounding the stock at Berg deposit have been described as 'crackle zones' or 'crackle breccias' but are not included in this discussion because rocks are shattered *in situ* and fragments display insignificant displacement. Only one large body of breccias in bedrock, an intrusive breccia pipe, is known to crop out. A number of other breccia bodies have been intersected in drill holes but their geometry is not known and origin is speculative. Newly formed, thin surficial deposits of ferruginous concretionary breccias (ferricrete) mantle small areas but these actively forming deposits are discussed elsewhere.

INTRUSIVE BRECCIA (PEBBLE BRECCIA PIPE)

The centre of the intrusive breccia pipe is about 750 metres to the southeast of Berg camp. The breccia mass is elliptical in plan, approximately 580 metres along its longer east-southeast axis and about 175 metres wide. It intrudes quartz diorite and pyritic volcanic rocks at the outer edge of the zone of mineralization. Outcrops of breccia are deeply weathered, pale cream to yellow, and contrast sharply with surrounding darker brown outcrops and debris.

Breccia, intersected for 150 metres in diamond-drill hole 21, is relatively uniform in appearance with a cream to light grey colour. It is composed of approximately equal amounts of strongly milled fragments, finely comminuted groundmass, and pervasive alteration minerals. Fragments are subangular to subrounded grains commonly 1 to 4 millimetres in size of quartz, feldspar, and a few rock fragments. Some rock fragments (pebbles) are larger than 1 centimetre, 3.2 centimetres being the largest seen. Rock fragments are quartz monzonite porphyry, one or more porphyritic species not recognized elsewhere, andesite, and siltstone. Matrix is a cream to buff, finely comminuted mass of quartz and alkali feldspars with interspersed alteration minerals. Both matrix and fragments are extensively altered by carbonate, clays (mainly montmorillonite), sericite, and chlorite. Pyrite, much of which is present as small euhedral grains in the matrix, constitutes about 3 per cent of the rock. Sulphide and accessory minerals including apatite, zircon, topaz, rutile, and possibly sphene constitute 4 to 6 per cent of the rock, mainly in the matrix.

The breccia pipe is thought to be explosive in origin and formed by venting of volatiles related to magma intrusion or by phreatic explosion of groundwater. Abundance of

porphyry fragments and presence of a few myrmekitic quartz grains indicate that the breccia is related genetically to the mineralized stock. C. S. Ney (1969, personal communication) and Sutherland Brown (1967) have suggested that the breccia pipe is a late structure related to emplacement of young intrusive phase(s) possibly 'quartz latite porphyry' (now called hornblende quartz feldspar porphyry). However, the breccia may be older. Brecciation postdates at least one period of mineralization as quartz veinlets with molybdenite were seen in one milled breccia fragment.

OTHER BRECCIAS (OBSERVED ONLY IN DIAMOND-DRILL CORE)

Breccia 1: A shatter breccia is seen in the bottom 7 metres of diamond-drill hole 35 but the extent of this breccia is not established. This breccia is composed of weakly abraded but over-all angular fragments up to 5 centimetres in size of altered volcanic rocks in a pulverized matrix that forms not more than 10 per cent of the rock. Alteration minerals are similar to those in the intrusive breccia pipe although quartz flooding is more abundant. Alteration is not as intense as in the pebble breccia as many of the larger fragments have weakly altered cores surrounded by more altered rims. Fine to medium-sized grains of pyrite constitute about 8 per cent of the rock examined. Chalcopyrite and molybdenite are rare but irregular grains of sphalerite, tetrahedrite, and traces of galena were noted in the matrix. Brecciation post-dates deposition of molybdenite in fractures and quartz veinlets. The breccia may be an incipient diatreme or a weakly vented channelway of hydrothermal fluid streaming.

Breccia 2: Breccias in which fragmented country rocks are engulfed in a magmatic matrix are developed along the main contact of quartz monzonite porphyry phase, adjacent to related dykes, and possibly with parts of the sericitic quartz plagioclase porphyry intrusion(s). Their origin is not from collapse or removal of magma support but rather by hydraulic ramming during magma pulsations that cause brecciation and invasion of brecciated country rocks by magma. This apparently takes place most commonly at Berg deposit where dykes splay outward from the main intrusive body. Breccia zones form envelopes a few metres thick surrounding porphyry dykes. Generally, volume of intrusive rock in breccia decreases progressively outward from massive intrusive dyke cores as proportion, size, and angularity of country rock fragments increase. Examples of this type of breccia were noted in diamond-drill holes 14, 25, and 35. Similar breccia, but lacking a massive intrusive core, was seen in a 60-metre drill intercept in diamond-drill hole 71. In this breccia weakly assimilated fist-sized fragments of mineralized biotite hornfels are contained in an approximately equal amount of sparsely mineralized quartz monzonite porphyry matrix. Molybdenite mineralization took place during at least two periods, one before and the other after brecciation. Early generation quartz molybdenite veinlets are seen in transported breccia fragments whereas younger quartz molybdenite veinlets crosscut both hornfels fragments and quartz monzonite matrix.

Breccia 3: Breccias within the stock are poorly documented; their origin and composition are uncertain. Apparently breccias are most common in quartz monzonite

porphyry (unit 3) and sericitic quartz plagioclase porphyry (unit 4) whereas plagioclase biotite quartz porphyry (unit 5) and dyke rocks are not known to be brecciated except near faults. One breccia has been intersected in diamond-drill hole 69 where a strongly altered 'hybridized' zone at least 30 metres thick contains a number of types of porphyry fragments in the hangingwall of altered sericitic quartz plagioclase porphyry. Canex Placer Limited geologists (P. G. Beaudoin, 1974, personal communication) have suggested that a 'neck' of sericitic quartz plagioclase porphyry may be present within the quartz monzonite porphyry phase in this vicinity.

Breccia 4: Tectonic breccias are present; most are related to northwesterly and northeasterly trending faults. These breccias, as seen in a number of diamond-drill cores, are crushed or silicified zones, some with abundant gouge. Fault-related breccias are commonly centimetres to a few metres in width and form steeply dipping tabular bodies. A number of such breccia zones are bounded or intruded by basalt dykes.

STRUCTURE

Outcrops at Berg deposit are so highly altered, leached, and disintegrated that few *in situ* structural features can be measured. Detailed observations and measurements can be made only from drill core and much of this is highly fractured and crushed. For these reasons structural data are minimal and additional information from large-diameter drill core or underground openings is desirable.

Intrusive rocks forming small stocks, plugs, dykes, and sills have been described in a previous section. The intrusions were forcefully emplaced into genetically unrelated host rocks with no evidence of any structural controls. There was little apparent disruption of the moderately eastward dipping homoclinal succession of volcanic and locally derived sedimentary rocks. Beds were truncated without any discernible development of foliation or folding. Room for intrusive rocks was made by shouldering aside country rocks, brecciation, some magmatic stoping, and assimilation along with intense fracturing, metasomatism, and extensive recrystallization near the stock. On the basis of structure and style of emplacement of porphyries, Sutherland Brown (1969) classified Berg deposit as a 'simple porphyry deposit'; more recently (1974, 1976) he has described it as typical of a class of porphyry deposits called 'phallic porphyry deposits.'

Fracturing of rocks is widespread in the area of the Berg deposit and is most intense adjacent to the main intrusive contact. This corresponds to the zone of best copper-molybdenum mineralization in which numerous generations of fractures have reduced the rock to a 'crackle breccia' of 1 to 3-centimetre fragments (Ney, 1972). Early generation fractures include reticulate quartz stockworks, fractures filled with sulphide grains or veinlets, and fractures both with and without alteration envelopes. Younger fractures filled with gypsum crosscut early fractures, sulphide grains, gangue, and alteration mineral grains as a subhorizontal fracture cleavage.

The subhorizontal cleavage is a closely spaced set of parallel hairline fractures that has been called sheeting, poker chip cleavage, and sheet fractures (Allen, 1971). Sixty to 100 fractures per metre are most common at Berg deposit, although rocks with as many as 300 or more fractures per metre are known. In detail, fractures splay and interconnect resulting in a reticulate pattern although subhorizontal fractures are dominant. Cleavage fractures have no visible alteration effect on the rocks they crosscut and are filled with the low-temperature mineral gypsum. Thus, fracture cleavage appears to be much younger than other fractures. The sequence of events resulting in fracturing would be as follows: (1) intrusions of porphyries accompanied by invasion of hydrothermal fluids; (2) early fracturing and quartz veining to form crackled zones; (3) widespread hydrothermal alteration, additional quartz veining, brecciation, and some fracturing of intrusive rocks; and (4) development of subhorizontal fracture cleavage and gypsum fracture filling (possibly at a much later date).

The presence of subhorizontal fracture cleavage with gypsum fracture filling is known in a number of deposits in the Canadian Cordillera (Barr, 1966; Godwin, 1975; Jambor and McMillan, 1976) as well as elsewhere in North and South America (Howell and Molloy, 1960; Lowell and Guilbert, 1970). A number of theories have been proposed to explain *origin of sheet fracture cleavage in porphyry deposits but no single explanation seems satisfactory nor can be applied to Berg deposit*. The problem is threefold: firstly, to explain the subhorizontal fracture cleavage; secondly, to explain presence of gypsum in these late fractures; and thirdly, to explain the high frequency of fracture.

Allen (1971) has developed a model for the Galore Creek copper deposits in which sheet fractures are formed along with concomitant deposition of gypsum as a consequence of near surface hydration of anhydrite. *In situ* hydration of anhydrite is accompanied by up to 63-per-cent increase in volume that results in fracturing parallel to the topographic surface, perpendicular to stress relief. Fractures are further opened by mechanical force of crystallization as gypsum is redeposited from saturated meteoric solutions. The model is attractive for the deposits studied by Allen as rocks at depth contain up to 20 per cent pervasive anhydrite and near surface where sheet fractures are most abundant the anhydrite is totally hydrated to gypsum. The model is not convincing for Berg deposit where anhydrite is found in only small amounts together with quartz and calcite as a vein constituent. The anhydrite-bearing veins occur from surface to depth mainly as late-stage veins near the periphery of the porphyry stock. Independent of depth, anhydrite in these veins shows only erratic, patchy hydration to form bassanite (hemihydrate) and yet the veins are consistently cut by gypsum-bearing sheet fractures.

Other investigators discuss alternate origins of fracture cleavage that place little or no emphasis on hydration of anhydrite as a causative process. Suggested mechanisms of cleavage development include explosive brecciation, chemical brecciation, and hydraulic fracturing.

Godwin (1973) has suggested that explosive brecciation might be accompanied by development of subhorizontal fracture cleavage caused by reflection of shock waves from the

air-rock interface. However, at Berg deposit no young breccia body has been recognized in the core of the mineralized area to which the late cleavage can be spatially and genetically related. Rocks surrounding the large intrusive pebble breccia lack sheet cleavage. Also the mechanism does not explain why well-mineralized and altered volcanic rocks close to the intrusive stock are strongly cleaved and veined by gypsum whereas the adjoining intrusive rocks are only weakly fractured and veined. Chemical brecciation as discussed by Sawkins (1969) and Sillitoe and Sawkins (1971) has been used to relate vertical sheeting and associated flat-lying cleavage to breccia pipes. Similar to explosive brecciation, the mechanism is possibly adequate to explain certain fractures proximal to breccia bodies but is inadequate to explain the very widespread and late development of subhorizontal fracture cleavage at Berg deposit.

The third, possibly most promising, theory advanced to explain fracture cleavage is that of hydraulic fracture. It suggests that subhorizontal fracture cleavage may be formed by near surface fracturing perpendicular to the direction of stress relief in the presence of a fluid (Phillips, 1972, 1973; Shearman, *et al.*, 1972). Differential stress could be imposed on intruded rocks by increasing pore pressure in response to a thermal gradient caused by emplacement of intrusive rocks or magma. Phillips (1972) describes this as a process involving nonpenetrative fluids. At the same time fluid pressure in intruded rocks could be increased by penetrative fluids such as magmatic fluids or magmatically heated groundwater. Hydraulic fracturing would take place in stressed rocks surrounding the intrusive stock when a large increase in fluid volume took place due to rapid expulsion of fluid from the crystallizing magma or adiabatic expansion took place as tensile strength of rock was exceeded and fractures opened. This magma-related process has been termed a 'hydromagmafract' process by Burnham (1975).

3

HYDROTHERMAL ALTERATION

INTRODUCTION

Alteration patterns at Berg deposit, as defined by changes in non-sulphide mineralogy observed in diamond-drill cores, are grossly similar to those in porphyry copper models described by Lowell and Guilbert (1970) and Rose (1970a). Refinements by Guilbert and Lowell (1974), Carson and Jambor (1974), Gustafson and Hunt (1975), and Drummond and Godwin (1976) embellished older models and made them more appropriate for Berg and other Cordilleran deposits where volcanic rocks host major portions of the porphyry deposits. These deposits exemplify the wallrock or combined wallrock-intrusion porphyry copper-type deposits of Titley (1972).

This study is concerned primarily with defining hypogene alteration types and zoning patterns. At Berg deposit the distinction between rocks with solely hypogene or combined hypogene-supergene alteration is indicated clearly in drill core by fractures filled with gypsum that mark the limit to which present day groundwaters have circulated. Supergene alteration has taken place only near surface where gypsum is leached. In the zone with gypsum-healed fractures, groundwater flow following hydrothermal activity has been minimized and all alteration can be assumed to be hydrothermal and hypogene.

Supergene alteration caused by weathering, oxidation, hydration, hydrolysis, recrystallization, and leaching by acidic solution is extensive and has resulted in a thick leached capping containing mainly quartz, limonite, sericite, chlorite, and clay minerals. Thin section and X-ray diffraction analyses of clay-sized minerals in the capping reveal marked increases in amounts of quartz, kaolinite, sericite (illite), chlorite, and amorphous hydrates compared to rocks subjected only to hypogene alteration.

At Berg deposit hypogene alteration zones with dominant quartz-orthoclase and quartz-sericite alteration are developed centrally in the weakly mineralized quartz monzonite stock and are surrounded by alteration aureoles containing first, biotitic cupriferous

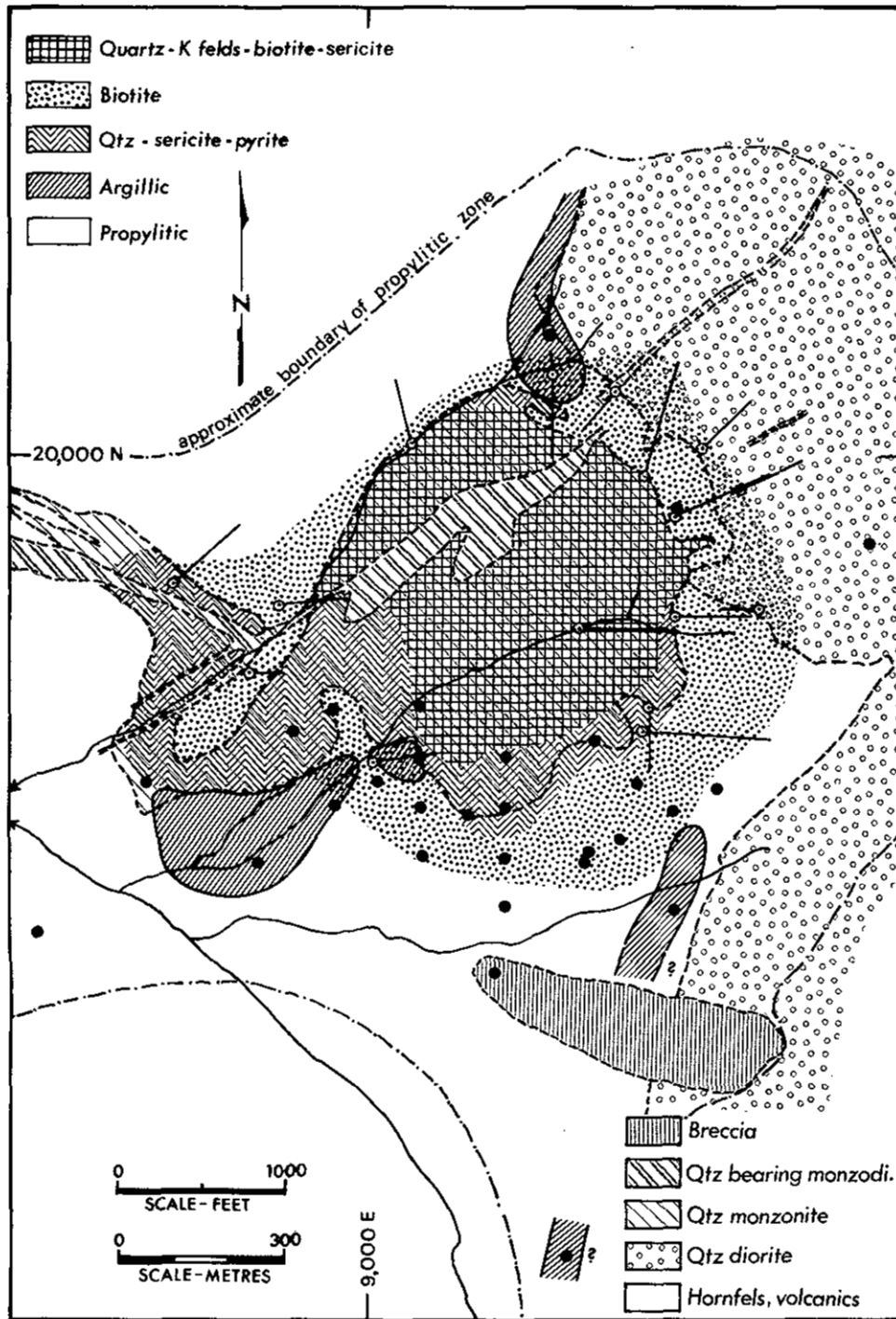


Figure 10 Generalized alteration zones, Berg deposit.

rocks, then, pyritic chlorite-calcite-epidote-bearing rocks. Quartz-sericite-pyrite zones occur extensively along the intrusive contact of the quartz monzonite stock and clay-bearing zones are developed locally in positions intermediate between the intrusive core and pyritic periphery.

Quantities and associations of alteration minerals in 3.05-metre (10-foot) sections of drill core were recorded in descriptive and graphic drill logs. All diamond-drill core available to 1971 (7 980.9 metres in 49 drill holes) was catalogued by the writer with particular regard for: quartz, orthoclase, biotite, sericite (muscovite), magnetite, calcite, epidote, anhydrite, and gypsum. Clay minerals were identified later in the laboratory by X-ray diffraction. Location of gypsum was noted and number of cleavage fractures per foot of core was recorded. Limonite minerals, where present, were described in terms of colour, abundance, and character. An estimate based on limonite colour was made of the proportions of goethite, jarosite, and hematite.

Significant differences in appearance of diamond-drill core and hand specimens were used to define various alteration types and alteration intensities. A standardized cataloguing procedure enabled alteration intensities to be ranked and thereby quantified. Ranked values of alteration intensities were plotted and contoured on a geologic plan and were used to define hypogene zoning patterns (Fig. 10).

DEFINITION OF ALTERATION FACIES AND ZONES

Diagnostic alteration minerals and mineral associations can be used to define a number of alteration types or facies (Creasey, 1959, 1966; Burnham, 1962; Meyer and Hemley, 1967). All commonly used types are recognized at Berg deposit (Fig. 10) including potassic, phyllic, propylitic, and argillic facies. A variant of the potassic alteration facies, biotitic alteration (biotite hornfels), is possibly the most important alteration type because it is more closely associated with chalcopyrite concentrations than are other alteration types. Because of this important relationship, biotitic alteration is considered here separately rather than included in discussion of the potassic (K-silicate) zone as done by some authors.

Alteration effects are most obvious in volcanic rocks surrounding the quartz monzonite stock, close to the intrusive contact. Alteration of quartz monzonite varies in intensity in different zones and rock types within the stock. Most intensely altered rock types are quartz monzonite porphyry (Fig. 7, unit 3) and sericitized quartz plagioclase porphyry (Fig. 7, unit 4). Most subtle alteration is in plagioclase biotite quartz porphyry (Fig. 7, unit 5) and hornblende quartz feldspar porphyry (Fig. 7, unit 6). Intrusive contacts in the southern part of the stock and northwesterly trending fracture or breccia zones are the most highly altered zones within the stock.

POTASSIC ALTERATION

Potassic (quartz-orthoclase) alteration can be found within the mineralized stock where it appears to be restricted to the quartz monzonite porphyry phase (Fig. 7, unit 3). However, recent drilling (A. D. Drummond, 1975, personal communication) indicates that strong sericitization is more widespread (probably as an overprint) than originally thought and potassic alteration might not be as extensive in the stock as shown on Figure 10.

Orthoclase, quartz, sericite, and biotite are main alteration minerals together with some anhydrite, sulphide minerals, chlorite, magnetite, kaolinite, and montmorillonite. Potassic alteration is seen as a pervasive pink colouration in the rock matrix caused by orthoclase flooding. In thin section it is seen as a fine-grained mosaic of orthoclase-quartz-plagioclase-sericite, or as patchy aplitic intergrowths of orthoclase and quartz. In specimens examined (all from drill holes 1 and 6) about 5 per cent orthoclase appears to have been added during potash metasomatism, generally replacing plagioclase or rarely as orthoclase rims on plagioclase phenocrysts. In the most strongly altered rocks, quartz veins exceed 10 per cent, and plagioclase phenocrysts proximal to quartz veins are sericitized and, in rare cases, are altered to clay minerals (mainly kaolinite). Altered plagioclase has a characteristic pale green to buff colour. Where quartz veins are less than 10 per cent of the rock volume, plagioclase crystals are unaltered or slightly clouded in appearance. Mafic phenocrysts (originally biotite and hornblende) in strongly altered rocks are replaced totally by fine-grained, felted biotite and less commonly by sericite, magnetite, sulphide minerals, and chlorite. In weakly altered zones of porphyry, only hornblende is replaced by secondary biotite and biotite phenocrysts are either partially replaced or remain as euhedral crystals.

BIOTITIC ALTERATION

Biotitic alteration, also referred to as biotite hornfels, is most intensely developed in volcanic rocks adjacent to quartz monzonite (Fig. 10). Biotitic alteration coincides with zones of most intense copper mineralization. This intimate association of copper sulphides with a zone of hydrothermal biotite development is characteristic of many porphyry deposits and, therefore, makes recognition and definition of biotitic alteration zones a useful product of alteration studies in ore search.

Rocks with biotitic alteration at Berg deposit are predominantly andesitic volcanic rocks which are easily recognized by their dark brown to black colour and velvety hornfelsic texture. Biotitic alteration is also seen in quartz diorite which has a spotted 'salt and pepper' appearance where it is biotitized near quartz monzonite. As much as 50 per cent of some volcanic rocks is made of fine-grained hydrothermal biotite but most commonly biotite content ranges from 10 to 35 per cent. Other alteration minerals associated with biotite are: quartz, orthoclase, plagioclase, sericite, chlorite, magnetite, epidote, and minor calcite, clay minerals, anhydrite, and rutile. Chlorite from the biotitic zone at Berg appears to be a magnesium clinocllore, leuchtenbergite (Dahl and Norton, 1967) whereas outlying propylitic rocks have been noted to contain iron-rich thuringite.

The biotite hornfels can be classified as part of either the potassic or propylitic alteration facies depending on which alteration minerals accompany biotite. Titley noted in 1972 that the distinction between potassic and propylitic alterations is not always obvious and depends on whether potash metasomatism can be demonstrated to have taken place. Ideally biotite-bearing rocks in which potash enhancement can be observed belong to the potassic alteration type. Where isochemical conditions prevailed (especially with respect to K_2O) rocks were simply recrystallized and the product would be a biotite hornfels. Superimposed veining and related hydrothermal alteration in such hornfels could render the rock compatible with propylitic alteration assemblages. Such is the case at Berg deposit where the zone of biotitic alteration occupies an intermediary position between a core of potassic (quartz-orthoclase) or phyllic alteration in quartz monzonite and the peripheral propylitic zone formed in volcanic rocks and quartz diorite. A similar situation is described at the El Salvador deposit by Gustafson and Hunt (1975) who consider the potassic and propylitic alteration assemblages in altered andesite to be contemporaneous and zonally related.

In the southern half and parts of the northern contact of the quartz monzonite stock at Berg deposit, the biotitic rocks also contain quartz, plagioclase (albite), chlorite, epidote, magnetite, clays, and calcite. The observed 10 to 20 per cent biotite by volume is the amount of biotite that would be expected to form in a hornfels derived from a typical Hazelton andesitic rock containing between about 1 and 1.5 per cent K_2O . Thus no potash enrichment is evident and the rocks are compatible with propylitic alteration type. The zoning sequence from the porphyry core outward is: potassic (quartz-orthoclase-sericite), then phyllic, and finally propylitic in the biotite hornfels, a normal zoning reference.

In contrast, along the northeast and east contact of the quartz monzonite stock in the screen of hornfelsed volcanic rocks between quartz monzonite and quartz diorite intrusions (and possibly also along the northwestern quartz monzonite contact), phyllic alteration is poorly developed or is absent. In these zones biotitic rocks adjoin intrusive rocks with potassic alteration and contain up to 50 per cent biotite. In addition, the rocks are veined by quartz-orthoclase-anhydrite, quartz-orthoclase, and orthoclase veins (see Plate XVII) as well as abundant quartz-molybdenite veins. The abundance of biotite as well as orthoclase veining is proof of K_2O enhancement and; therefore, the rocks are compatible with the potassic alteration facies. In these areas the zoning sequence is: potassic (vein and pervasive orthoclase) in quartz monzonite, potassic (orthoclase-veined biotitic alteration) in hornfels near the porphyry stock, and finally a transition to propylitic alteration in quartz diorite and hornfelsed volcanic rocks further from the quartz monzonite contact.

At Berg deposit the presence of hornfels with potassic alteration might be restricted to that zone in which volcanic rocks have been first thermally metamorphosed by quartz diorite and then overlapped by vein stockworks and hydrothermal biotite alteration closely related to quartz monzonite. Elsewhere along the quartz diorite contact where

hydrothermal fluids had travelled further from the source quartz monzonite, the hornfels formed by quartz diorite was retrogressively altered, mainly by degeneration of biotite to chlorite, to a rock of propylitic aspect.

PHYLIC ALTERATION

Phyllic (quartz-sericite-pyrite) alteration of rocks is easily recognized by a bleached and chalky weathered appearance (Plate XVI). Bleaching is caused by thorough quartz-sericite alteration of plagioclase and orthoclase, as well as breakdown of mafic minerals to dominantly sericite and lesser amounts of biotite, quartz, chlorite, and pyrite. Magnetite is absent but pyrite and small amounts of hematite are present. In thin section rocks with phyllic alteration appear as a fine-granular, mosaic intergrowth of quartz-sericite among relict, sericitized, and weakly kaolinized feldspar phenocrysts. Scattered, shredded grains of secondary biotite and minor chlorite are mafic constituents. In sericitized quartz plagioclase porphyry (Fig. 7, unit 4) fine-grained biotite is locally abundant (up to 6 per cent) and imparts a tan to medium-brown colour to the rock matrix. Topaz, first reported to be present at Berg deposit by Dahl and Norton (1967), is a minor alteration mineral in phyllic assemblages.

The zone of phyllic alteration is developed most extensively along the southern and southwestern intrusive contacts. It is discontinuous around the northeast contact close to quartz diorite and plagioclase biotite quartz porphyry, which is little altered (Fig. 10). The phyllic alteration zone overlaps the quartz monzonite contact on the south and southeast and extends outward for a few metres into highly fractured volcanic rocks. A small zone with phyllic alteration was also intersected at depth in drill hole 1 along with the northern boundary of the stock. Phyllic alteration is developed peripherally to the core zone potassic alteration but the zone of phyllic alteration can be seen to encroach on the potassic zones. A highly irregular contact following interconnected zones of intense fracturing and brecciation locally isolates 'islands' of rocks with potassic alteration within the phyllic porphyry stock.

PROPYLITIC ALTERATION

Propylitic alteration coincides with strongly pyritized volcanic rocks and quartz diorite next to either phyllic alteration zones in quartz monzonite porphyry or biotite hornfels (Fig. 10). Presence of sulphide minerals, mainly pyrite, was the main criterion used to distinguish rocks with hydrothermal propylitic alteration from those subjected to regional (sub) greenschist metamorphism.

Propylitic alteration is recognized by an over-all green colouration in rocks caused by pervasive chlorite, abundant epidote, and calcite. Locally propylitized rocks have a mottled appearance due to bleached borders of fractures and veins (Plates XVII and XIX). Where fractures are abundant, crosscutting, and interconnected, propylitic rocks are pervasively bleached to a pale grey-green to drab olive colour. Possibly the best indicator of propy-

litic alteration and most reliable criterion for distinguishing propylitized rocks from chloritic biotite hornfels is presence of calcite. Invariably, abundant calcite coincides with rocks in which chlorite exceeds biotite in abundance, and epidote as well as magnetite is common. In addition to the chlorite, calcite, and magnetite above, albitized plagioclase, sericite, epidote, and pyrite are abundant along with lesser quantities of montmorillonite, kaolinite, dolomite, tremolite/actinolite, gypsum, rutile, leucosene, and hematite. Detailed examination of propylitized rocks reveals three common mineral associations: (1) chlorite-epidote-calcite (widespread), (2) chlorite-epidote-tremolite (in basic volcanic rocks), and (3) chlorite-kaolinite-dolomite (localized in three small zones of argillic alteration).

Bleached margins of quartz-pyrite veins consist of very fine-grained mixtures of calcite-montmorillonite (and rare gypsum), as well as chlorite-albite and possibly sericite. Bleached vein margins in the propylitic zone are distinguished from phyllic alteration by sparseness of sericite and presence of calcite.

Pervasive propylitic alteration is also found in hornblende quartz feldspar porphyry (Fig. 7, unit 6), the youngest phase of the quartz monzonite stock. However, unlike volcanic rocks and quartz diorite in the propylitic zone peripheral to the composite stock, quartz feldspar porphyry is only weakly pyritized but contains abundant sphene (up to 1 per cent by volume) and scattered large grains of epidote.

ARGILLIC ALTERATION

Argillic (clay) alteration is recognized at Berg by presence of abundant montmorillonite and kaolinite. Argillic rocks are known to occur in three zones (Fig. 10). The zones appear to be small and limited to a few tens of metres in width, but their extent is poorly documented due to limited subsurface information. One zone is associated with the altered southwestern contact of sericitized quartz plagioclase porphyry (Fig. 7, unit 4). *The argillic zones lie between phyllic and propylitic alteration zones in the position predicted by porphyry copper models.* The two other zones are in propylitized volcanic rocks north and southeast of the composite stock and along the quartz diorite contact. In all three zones containing clay minerals, calcite and epidote are present. Strong calcium leaching, one of the main requirements of the argillic alteration facies according to Creasey (1966), is therefore not evident. The clay-bearing rocks at Berg deposit might be regarded simply as clay-bearing, aluminous subfacies of propylitic alteration. These clay-rich zones might mark the main passageways for late CO₃-rich hydrothermal fluids that flowed mainly along the quartz diorite contact into the central alteration area.

VEINS

Veins are abundant throughout the hydrothermally altered and mineralized zone. Most commonly they are 1 millimetre to 1 centimetre-wide quartz veins, many with pyrite

and/or molybdenite, that form quartz stockworks near the main contact of the quartz monzonite stock. Abundance of quartz veins decreases both inward and outward from the intrusive contact. In the outlying biotite hornfels and propylitic alteration zone pyritic veins and veinlets predominate.

The alteration facies described in preceding pages represent large pervasive alteration zones. Veins, on the other hand, are only partly synchronous with pervasive alteration processes. They are in many cases superimposed on pervasively altered rocks and reflect changes in hydrothermal fluids that passed through and were confined to fractures and other channelways. Hydrothermal fluids from which some vein minerals were deposited caused little alteration of enclosing rocks and veins cut host rocks without appreciable alteration effects. In other host rocks reactions with fluids in fractures resulted in alteration envelopes in which minerals adjacent to veins were metasomatized or recrystallized and made over to mainly quartz, K-feldspar, sericite, and biotite. Still other veins have bleached vein margins in which relict primary textures are maintained, and rock-forming minerals are broken down to mainly quartz, chlorite, clay minerals, carbonate, sericite, and gypsum (Plate XVII). Thus, where significant metasomatism (most obviously orthoclase-quartz) has taken place, altered vein borders are referred to as envelopes; where retrograde breakdown of rock-forming constituents has taken place but original textures remain, altered vein borders are referred to as alteration margins.

In zones of extensive fracturing away from the stock, bleached margins on veins result in a mottled appearance or coalesce to form large bleached zones. In general, alteration envelopes are most abundant on veins within the stock and along its contacts where quartz stockworks are best developed. Veins with alteration envelopes decrease in abundance away from the composite stock and are exceeded by veins with bleached margins. Bleached alteration margins are most noticeable in pyritic hornfels and propylitic rocks.

All three vein types (with alteration envelopes, without envelopes, and with bleached margins) can be found in the same rock. They have formed in sequence as a staged vein series. The sequence is complicated to decipher and cannot be resolved completely without additional detailed study. The following sequence from oldest to youngest is suggested; it bears a remarkable similarity to the vein sequence described at El Salvador by Gustafson and Hunt (1975).

- Stage 1.**
- A. Quartz-pyrite-chalcopyrite-molybdenite veins with alteration envelopes of quartz-sericite (common), chlorite (less common), or K-feldspar (rare).
 - B. Quartz-pyrite-chalcopyrite-molybdenite veins without envelopes.

The above associations are modified by presence of other minerals including chlorite, anhydrite (purple and clear), epidote, carbonate, clay minerals, and magnetite.

- Stage 2.**
- Quartz-molybdenite (or molybdenite alone) veins without envelopes.

- Stage 3.** Quartz-pyrite veins and pyritic veinlets with or without envelopes, many with bleached margins. Veins may also contain chalcopyrite, rare epidote, and magnetite.
- Stage 4.** Quartz-carbonate (common) and quartz-anhydrite-carbonate (rare) veins, many with bleached margins. These veins can contain pyrite, chalcopyrite, sphalerite, tetrahedrite, galena, and epidote. Anhydrite is partially to completely hydrated (hemihydrate to gypsum).
- Stage 5.** Gypsum-filled fractures.

Crosscutting relationships permit at least five periods of stage 1 veining to be postulated (A. D. Drummond, 1975, personal communication). However, as a rule, stage 1 veins display complex relationships and suggest that stage 1 veins have filled a previously crackled zone rather than generated an oriented, sequential, crosscutting stockwork system. Stage 1 veins generally consist of massive quartz intergrowths although many have cockscomb structures and vugs with drusy lining. In some veins vugs are filled with anhydrite; in others, cavities are open and quartz crystals are overgrown by fine-grained chlorite. Stage 2 veins are massive and composed of compact, fine-grained quartz or are ribboned with granulated quartz grains interspersed by bands of fine-grained molybdenite. Stage 3 veins are ubiquitous and are possibly the most abundant veins in the stockworks. Except where they are clearly crosscutting, stage 3 quartz veins are indistinguishable from stage 1 or any other quartz-pyrite veins. Stage 4 veins up to 3 millimetres in width have been noted in diamond-drill core but are rare over-all. In pyritic rocks surrounding the composite stock a number of quartz-carbonate-pyrite-sphalerite-galena-tetrahedrite veins a few tens of centimetres in width are known to occur. Stage 5 gypsum-filled fractures form a subhorizontal fracture cleavage that crosscuts all primary alteration and ore minerals and possibly formed long after veins of stages 1 to 4.

HYDROTHERMAL PROCESSES IN THE FORMATION OF BERG DEPOSIT

With the preceding description of alteration facies, zoning, and vein development in mind, origin of zoning can be considered. In essence alteration and zoning are a response to temperature, pressure, and chemical gradients caused by: (1) emplacement of the four batches of quartz monzonite magma, (2) cooling and crystallization of the stock, (3) generation and flow of hydrothermal fluids (both magmatic and heated groundwater) in and around the stock, (4) supply, transport, and redeposition of metals and other substances by hydrothermal fluids, and (5) changes in fluids or interaction between fluids and wallrocks. The hydrothermal regime acted as a dynamic fluid system which caused heat and mass transport in and around the quartz monzonite stock. The resulting large-scale zoning is a remnant imprint of pervasive regional pressure, temperature, and chemical gradients whereas the veining is an overprint of fracture-controlled fluid-rock disequilibrium conditions.

The most striking alteration zone is the annular biotite hornfels that surrounds the quartz monzonite stock. The biotite hornfels extends at least 185 metres from the intrusive contact. The larger quartz diorite intrusion to the north and east has similar biotite hornfels along its intrusive contact but the hornfels there is commonly 30 metres or less in width. Conductive thermal effects of igneous intrusions have been described by Lovering (1955), Jaeger (1959, 1964), and Whitney (1975a).

Based on their models, temperature at the contact of a stock the size of Berg intrusion containing quartz monzonite magma at 800 degrees celsius would be 400 to slightly in excess of 500 degrees celsius. Temperatures would decrease outward from the contact *but the limit to which purely conductive heat transfer would cause biotite hornfels to form is uncertain.* Heat flow models are imprecise and allow great latitude in determinations of conductive heat flow. For example, at Copper Canyon, Nevada, a granodiorite stock was suggested to impose temperatures by conduction of only 150 degrees celsius (Steiger and Hart, 1967), whereas Winkler (1965, pages 61-63) suggested temperatures equal to 60 per cent of magma temperature (for example, a maximum of about 480 degrees celsius in this case) could be maintained by conduction over a distance of up to 60 metres from the contact of a stock such as that at Berg deposit. In any case, even if thermal conduction is as effective as suggested by Winkler, the extensive zone of biotite hornfels surrounding Berg deposit could not have formed solely by thermal metamorphism due to conduction alone. It must have been expanded by a more efficient heat transfer involving outward-flowing and convecting fluids in the manner discussed by Rose (1970a) and Norton (1975). Thus the presence of a heated fluid in fractures and pores must have abetted heat transfer and recrystallization of andesite to hornfels. The presence of this heated fluid can be regarded to mark the onset of hydrothermal alteration regardless of whether mass transfer occurred. The entire zone outside the stock in which recrystallized biotite is present is referred to as a biotite hornfels or a biotitic alteration zone because products of contact metamorphism (purely conductive heating) cannot be distinguished in the field from those of pervasive hydrothermal alteration (convective heat flow).

Imposition of heat on the various rocks at Berg deposit (quartz monzonite, andesite, quartz diorite) resulted in a number of alteration assemblages that reflect differences in bulk rock composition as illustrated (Fig. 11) by ACF and A'KF diagrams (Winkler, 1965). Under the same elevated temperature conditions andesite and quartz diorite will alter similarly to biotite-quartz-plagioclase-chlorite-epidote-calcite assemblages (biotite hornfels) whereas quartz monzonite will consist of a quartz-K-feldspar-plagioclase-biotite-muscovite-chlorite-epidote-clay assemblage (K-feldspar stable, plagioclase degenerative alteration). The importance of rock composition in determining alteration assemblages has been discussed by Guilbert and Lowell (1974).

The foregoing discussion is used to explain observed zoning that can be related to the simplest (idealized) geologic situation — increase in temperature within closed chemical systems. In addition to re-equilibration of minerals due simply to elevated temperature,

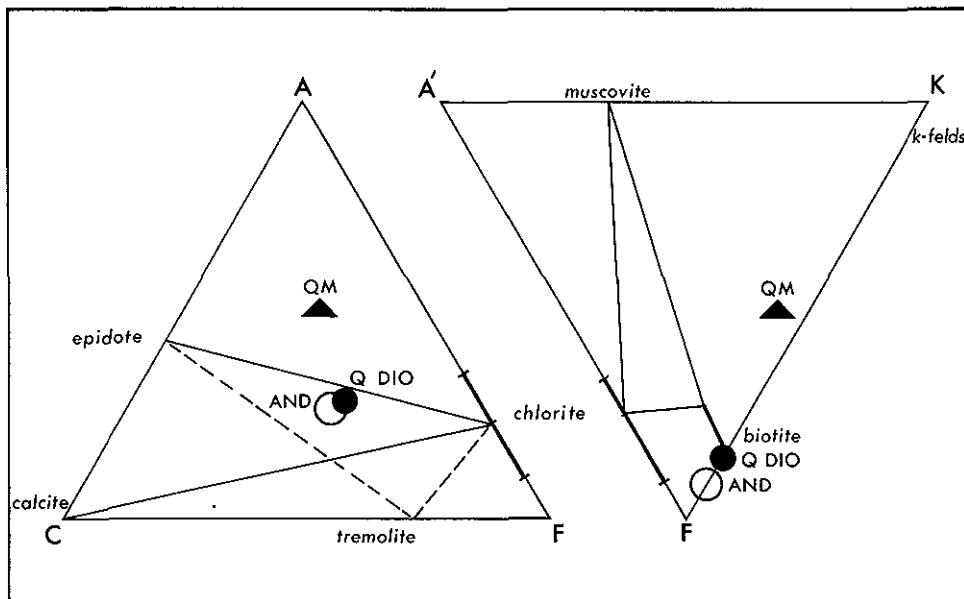


Figure 11. Mineral assemblages in thermally metamorphosed andesite, quartz diorite, and quartz monzonite.

chemical reactions involving mass transfer occur when passage of hydrothermal fluids takes place. One type of pervasive change in rocks is most evident in feldspars and results from hydrolysis reactions. In the core of the stock K-feldspar is unaltered; in the margin of the stock, throughout the quartz plagioclase porphyry and in highly fractured zones within the stock, K-feldspar is sericitized; and at the extremity of the sheet-like quartz plagioclase intrusion in the southwest, K-feldspar is sericitized and argillic. Plagioclase in the core of the stock contains minor montmorillonite and in the periphery of the stock is kaolinized or locally sericitized. These changes can be interpreted on the basis of feldspar stabilities in a regime with outward decreasing temperature and increasing ratio of hydrogen ion activity with respect to potassium ion activity as illustrated in the now familiar hydrolysis equilibria studies of Hemley (1959) and Hemley, *et al.* (1961, 1964, 1970).

Veins and fracture-associated alteration suggest the fluids changed in composition during the alteration sequence. The staged sequence of veins and fractures reveals that they initially (stages 1 and 2) had little effect on host rocks and fluids were evidently in equilibrium with minerals present. Later veins and fractures (stages 3 and 4) superimposed local conditions of disequilibrium on areas of pervasive alteration and older fracture-controlled alteration, each younger stage causing retrogressive breakdown of rock-forming and older alteration minerals.

Early veins (stages 1 and 2) are vuggy, ribboned, or massive and commonly contain molybdenite. Vuggy and massive coarsely granular quartz veins that contain anhydrite commonly have orthoclase associated with them whereas ribboned and finely granular quartz veins rarely have orthoclase envelopes. Most stage 1 and 2 veins are bereft of alteration envelopes or bleached margins and crosscut host rocks without apparent

alteration effects. Therefore, early veins and fractures formed under conditions in which biotite and feldspars were stable, probably at elevated temperatures during recrystallization to form hornfels. Where alteration envelopes are present about stage 1 veins, the envelopes are sericitic or have silicified metasomatic selvages containing orthoclase and rare anhydrite.

Most younger veins (stages 3 and 4) alter enclosing rocks and therefore have alteration envelopes or bleached margins. Such alteration can be interpreted in terms of localized hydrolysis reactions and feldspar-mafic mineral instability, in the same manner as pervasive alteration zoning. At Berg deposit minerals adjacent to late fluid-filled fractures or veins were unstable and recrystallized to form silicified sericitic alteration envelopes (Plate XIX), or degenerated to form bleached argillic (quartz-clay-chlorite-carbonate-gypsum) vein margins, or formed combined sericitic envelopes with argillic margins. The zoned sequence: orthoclase-sericite-clay has not been recognized in any altered vein margin. This suggests that quartz-orthoclase metasomatism of stage 1 and 2 veins was prograde and did not change in the same vein into retrogressive sericite-clay alteration such as that in stage 3 and 4 veins. Evidently early (stages 1 and 2) and late (stages 3 and 4) vein-forming processes were distinct and mutually exclusive. Additional support for presence of unique solutions during various vein stages and changes during the vein sequence is provided by vein mineralogy as was described in preceding paragraphs.

The nature of fluids involved in alteration processes can be deduced from examination and heating of fluid inclusions. In this study 20 samples of various vein types were examined in detail and 20 of the better fluid inclusions from four samples of molybdenite-bearing stage 1 veins were heated on a microscope heating stage. The heating stage was a Unitron-500 model mounted on a petrologic microscope equipped with a long focal length objective. Temperature was controlled by varying electric current to the stage with a rheostat and recorded on a chart recorder linked to a thermocouple. The system was calibrated with spec-pure lead and three temperature-sensitive crayons. The temperature of homogenization was taken to be the mean temperature between disappearance of the gas bubble during heating and reappearance during subsequent cooling. Maximum temperature that could be determined with this apparatus was 406 degrees celsius with precision of roughly ± 20 degrees celsius.

Fluid inclusions are abundant in all quartz veins at Berg deposit and can be seen also in anhydrite and pale-coloured zones in sphalerite. Fluid inclusions commonly are less than 2 microns and rarely up to 20 microns in size. In quartz they are particularly abundant and occur as two or three-phase negative crystal cavities, spheres, ovoids, or irregularly shaped bodies of primary and secondary origin as defined by Roedder (1962, 1963, 1967). In anhydrite, fluid inclusions are thin rod-like bodies that probably formed as *secondary inclusions along cleavage intersections*. They contain only liquid or rarely are two phase with minute vapour bubbles. In outer growth zones of sphalerite crystals, fluid inclusions were seen as negative crystal cavities. Two-phase inclusions are present in sphalerite but in some samples the vapour bubble contains a small amount of liquid CO₂.

Detailed examination of quartz reveals that two and three-phase fluid inclusions are abundant in quartz from stage 1 veins. The solid phase in three-phase inclusions is halite which forms small cubic crystals generally smaller than 2 per cent by volume. In addition, a few samples contain minute tabular crystals (gypsum ?) and equant opaque grains (sulphides or hematite ?). The few specimens of stage 2 veins examined contain only two-phase inclusions but three-phase inclusions might be present if additional samples were examined. Stage 3 and 4 veins appear to contain only two-phase inclusions although two species of liquid are present (brine and CO₂) in sphalerite from stage 4 veins. From these data it can be concluded that initially vein-forming fluids were saturated or close to saturation by NaCl and that salinity decreased as younger veins were deposited.

Volume of vapour observed in inclusions from stage 1 and 2 veins varies from 1 to 70 per cent. Vapour volumes vary widely even in the same vein or vein specimen although most fluid inclusions contain 10 to 30 per cent vapour. Such variability and high vapour content are considered to be evidence for boiling if homogenization temperatures are consistently similar (Roedder, 1967, 1971). At Berg deposit the inclusions tested behaved similarly upon heating to 406 degrees celsius but no filling temperatures were possible to determine above this temperature. Thus these observations to 406 degrees celsius are compatible with evidence for boiling but do not prove it. If indeed boiling occurred at Berg deposit it took place during early vein development and hydrothermal fluids were maintained at hydrostatic pressure. Based on present-day topographic relief the minimum depth at which mineralization occurred was about 700 metres; this corresponds to a maximum (lithostatic) pressure of about 200 bars.

The 20 fluid inclusions examined during heating from four specimens of stage 1 veins include: 14 inclusions in quartz from three quartz-anhydrite-molybdenite-pyrite-chalcocopyrite-bearing veins in well-mineralized biotite hornfels, and six fluid inclusions from terminated quartz crystals in a vuggy, coarsely crystalline quartz-molybdenite vein from quartz monzonite porphyry with strong phyllic (quartz-sericite-pyrite) alteration. Size of fluid inclusions ranged from 5 to 15 microns, most being 10 to 12 microns in size and containing about 10 per cent vapour. Only one of the 20 fluid inclusions contained a readily visible halite crystal. Some of the other inclusions are believed to contain minute salt crystals that could not be confirmed with the available optical apparatus.

Upon heating to 406 degrees celsius, 18 of the 20 fluid inclusions tested did not homogenize and a reduction in vapour volume of only about 10 per cent was achieved. Therefore stage 1 veins appear to have been deposited at temperatures well in excess of 406 degrees celsius. One two-phase negative crystal cavity includes anhydrite-bearing stage 1 vein homogenized at 392 ± 15 degrees celsius. This indicates that secondary inclusions are present in stage 1 veins or that a considerable decrease in temperature might have taken place during development of stage 1 veins. Another two-phase fluid inclusion, that is associated with a number of high temperature inclusions in a stage 1 quartz-anhydrite-molybdenite-pyrite-chalcocopyrite vein, appears to be primary but homogenized at 284 ± 2

degrees celsius. This was assumed to be a secondary inclusion or indicates that leakage or necking down has taken place in these veins.

Gypsum-filled subhorizontal fractures of stage 5 do not have any apparent alteration effects on host rocks or minerals along fracture selvages. This is in marked contrast to stage 4 carbonate veins in which anhydrite is partially to totally hydrated to hemihydrate (bassanite) or gypsum and the veins have clay-carbonate alteration margins. Gypsum in the fracture cleavage appears to have been deposited as open-space filling and there is no suggestion, even from deep drill holes (to 610-metre depth), that anhydrite was precipitated first and then hydrated to gypsum. Fracture cleavage filling by gypsum (the last stage of veining) therefore took place at temperatures below 57 degrees celsius because at higher temperature anhydrite is precipitated by itself or along with gypsum from aqueous solution (Holland, 1967).

The widespread presence of gypsum in late-stage cleavage fractures in the mineralized zone and all but the youngest intrusive phase of the composite stock might be because solubility of gypsum (and carbonate) in aqueous solution decreases with increasing temperature and decreasing pressure (Holland, 1967). Thus gypsum was probably deposited by heating of circulating, possibly inward-flowing sulphate-bearing fluids, during late cooling of the stock. The association of these late-forming gypsum-filled fractures with the zone of mineralization and intrusion is possibly the best available evidence at Berg deposit that convective flow involving meteoric sulphate-bearing hydrothermal fluids has taken place as described in the model of White, *et al.* (1971).



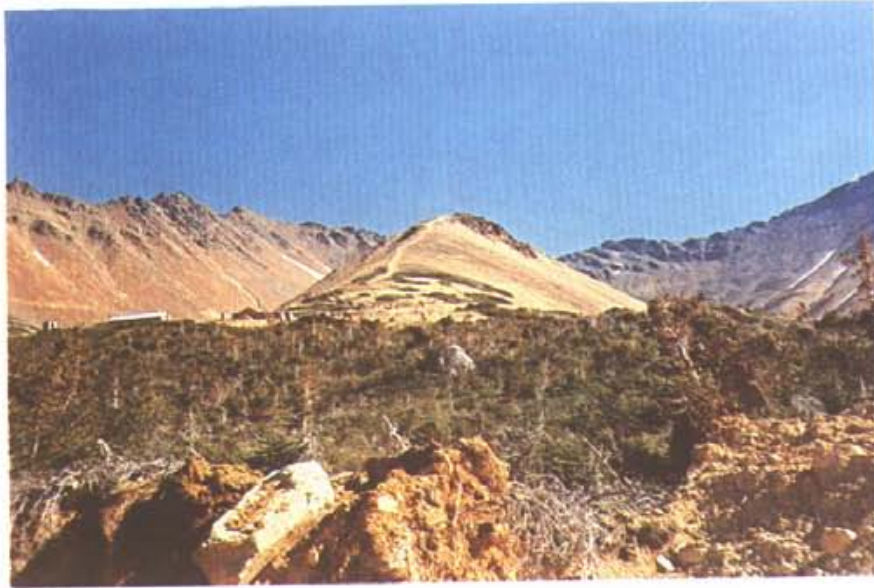
Plate IV. Berg deposit, view looking northerly, September 1974. Quartz monzonite underlies the central ridge. Drill access roads outline the area of economic interest. Berg camp is at elevation 1 560 metres (5,120 feet) in the lower left of the photograph.



Plate V. Berg deposit, Tahtsa Ranges, view to east-northeast. Nadina Lake is at top left. Photo by G.O.M. Stewart, 1971.



Plates VIA and VIB. Berg camp viewed to the west (VIA) down 'Red Creek' and southwest (VIB) across Bergeland Creek. Note the marked colour contrast between the limonitic mineralized rocks (foreground and centre) and Hazelton volcanic rocks (background).



Plates VIIA and VIIB. Berg camp looking northeast along quartz monzonite ridge. Note the vivid jarositic clay-rich soil (VIIA). Fibrous jarositic limonite precipitation from springs (VIIB), felt pen for scale.

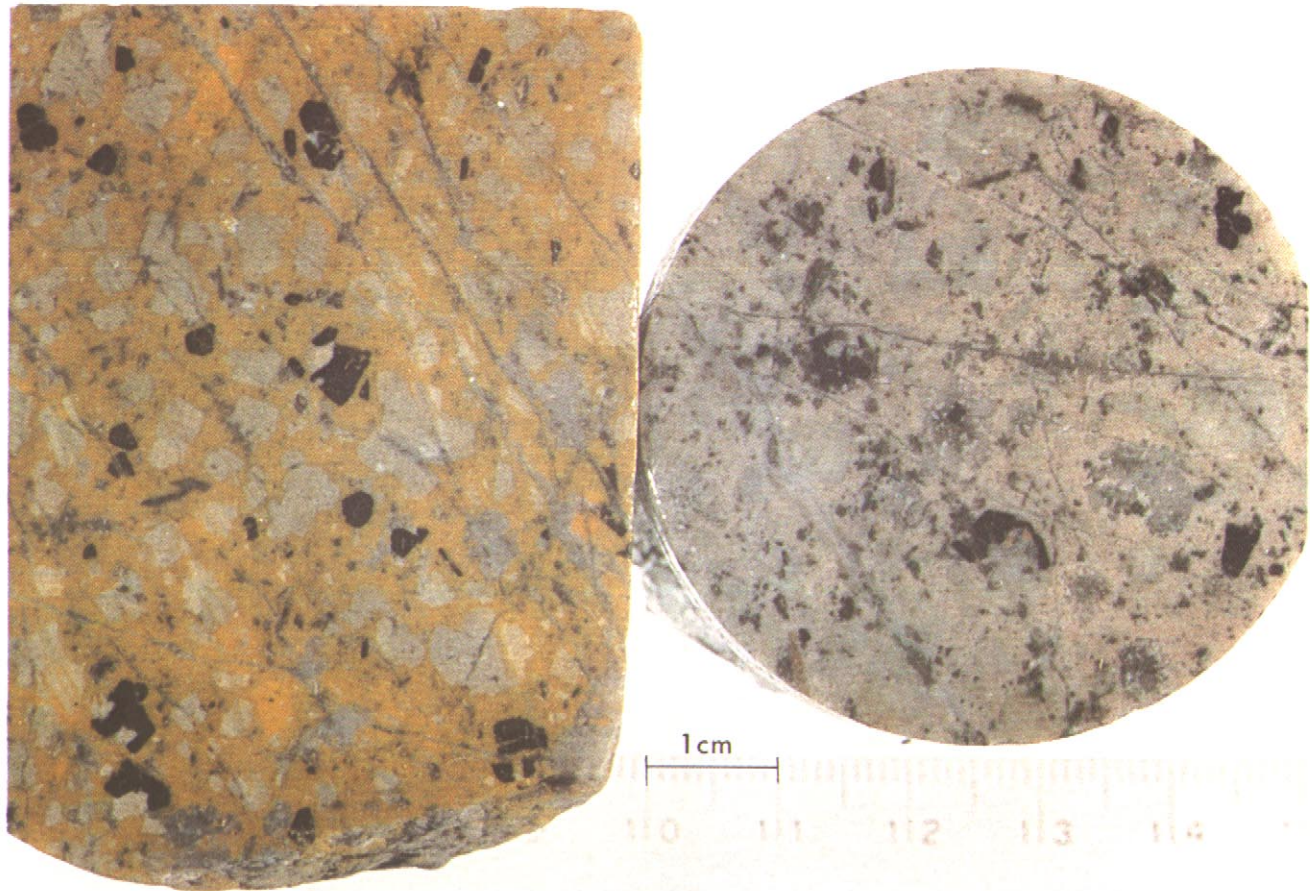


Plate VIII. Quartz monzonite porphyry (Fig. 7, unit 3; QMP). Minor veinlets contain quartz-K-feldspar or gypsum. Left specimen stained for K-feldspar; scale in centimetres.

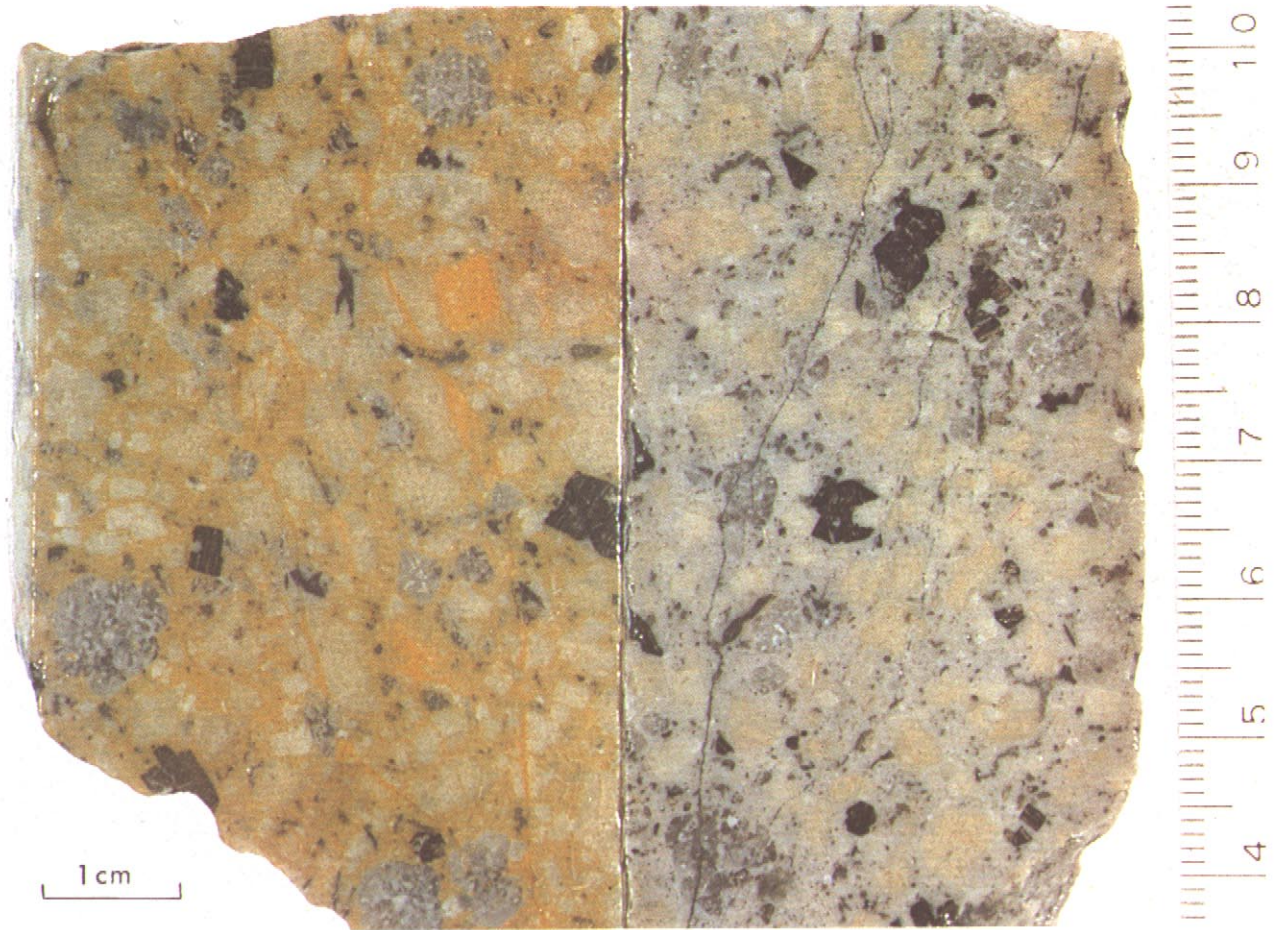


Plate IX. Quartz monzonite porphyry. Note resorbed quartz phenocrysts and incipient alteration of biotite.

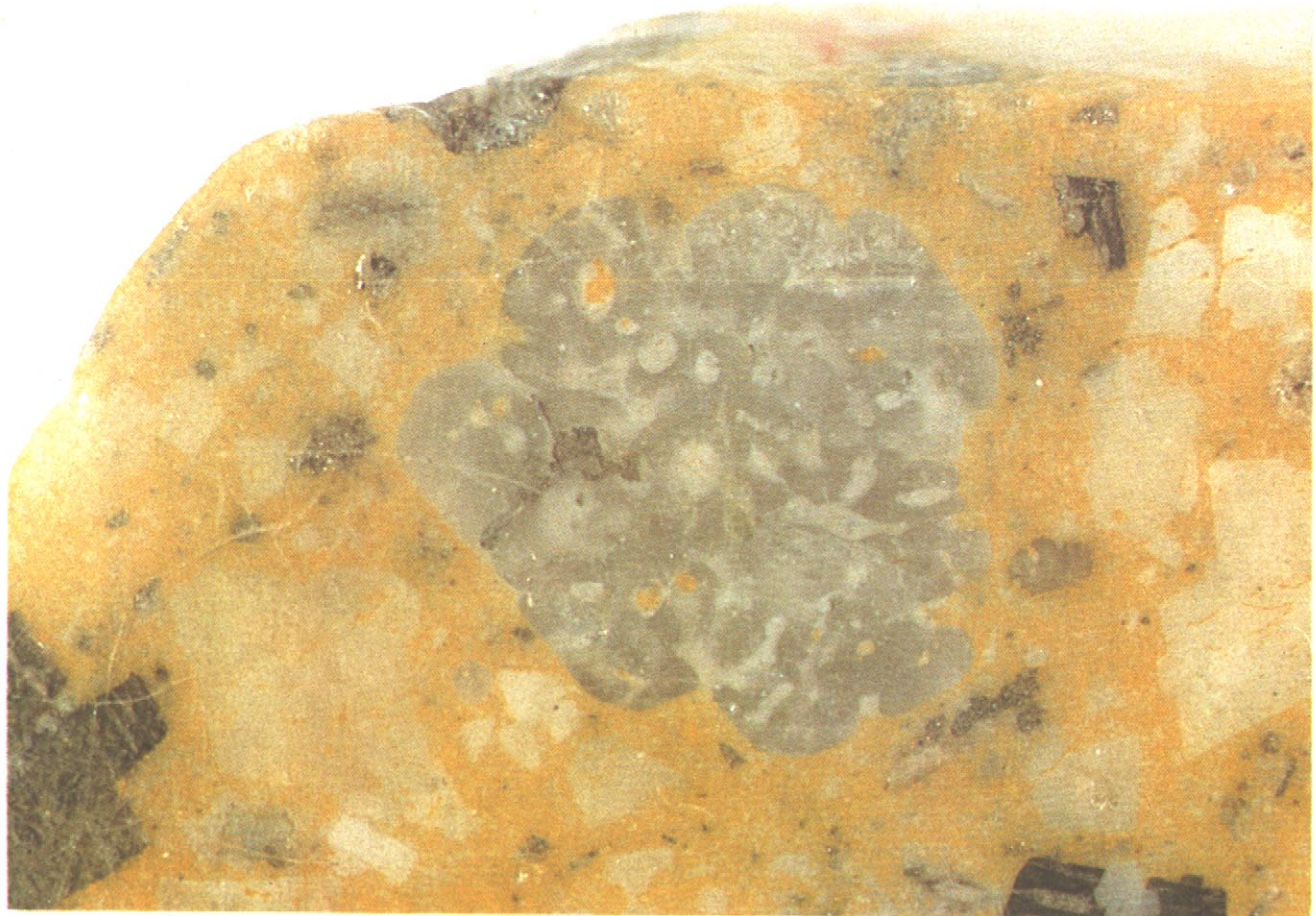


Plate X. Detail in quartz monzonite porphyry of anhedral resorbed quartz phenocryst with vermicular plagioclase and K-feldspar inclusions. Width of quartz grain, 8 millimetres.

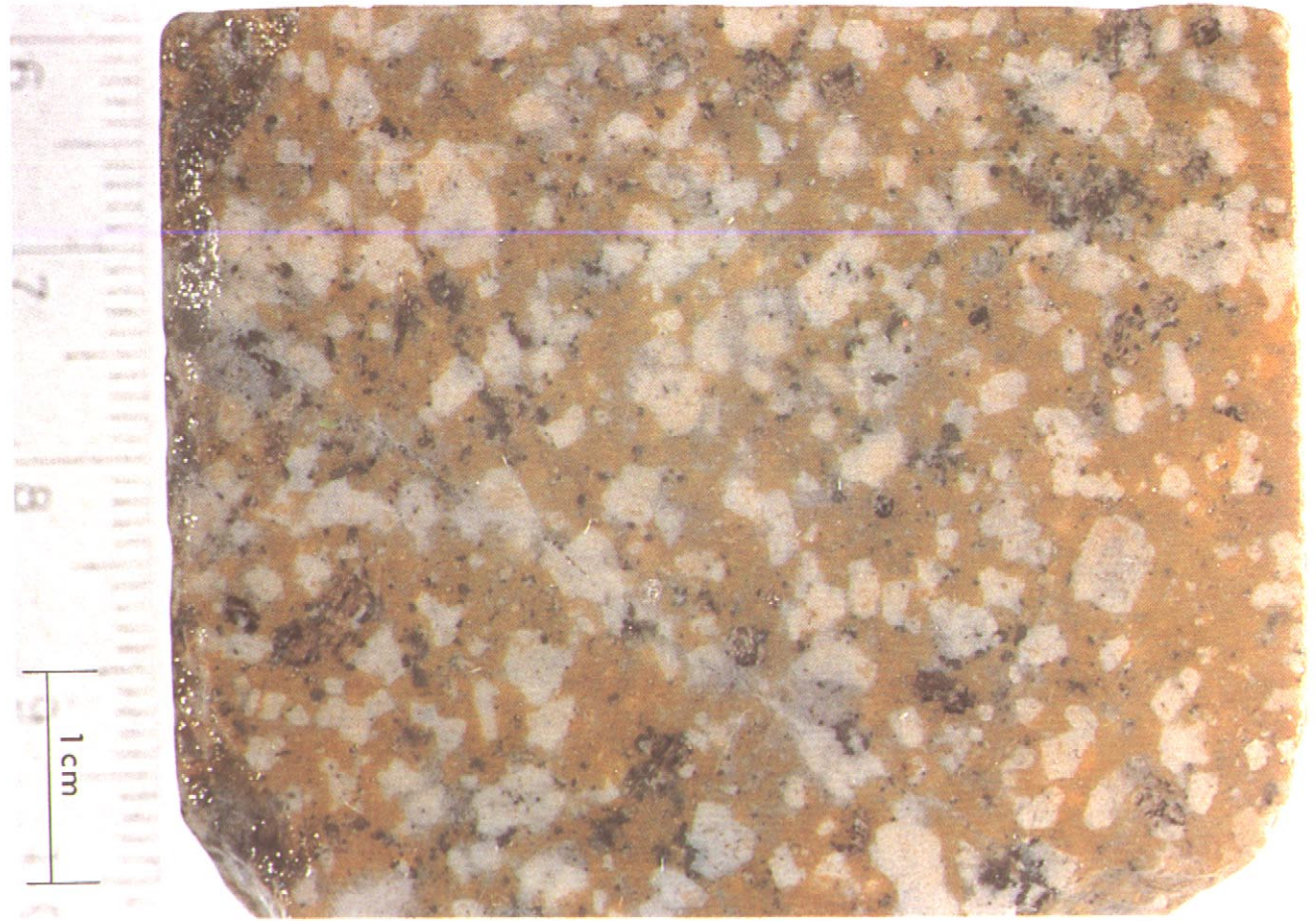


Plate XI. Sericitized quartz plagioclase porphyry (Fig. 7, unit 4, QPP) stained for K-feldspar.



81

Plate XII. Quartz plagioclase porphyry with quartz veining (unstained specimen) and silicified alteration envelopes on fractures (stained specimen).



Plate XIII. Plagioclase biotite quartz porphyry (Fig. 7, unit 5; PBQP). Right specimen stained for K-feldspar.



Plate XIV. Hornblende quartz feldspar porphyry (Fig. 7, unit 6; hbde QFP).

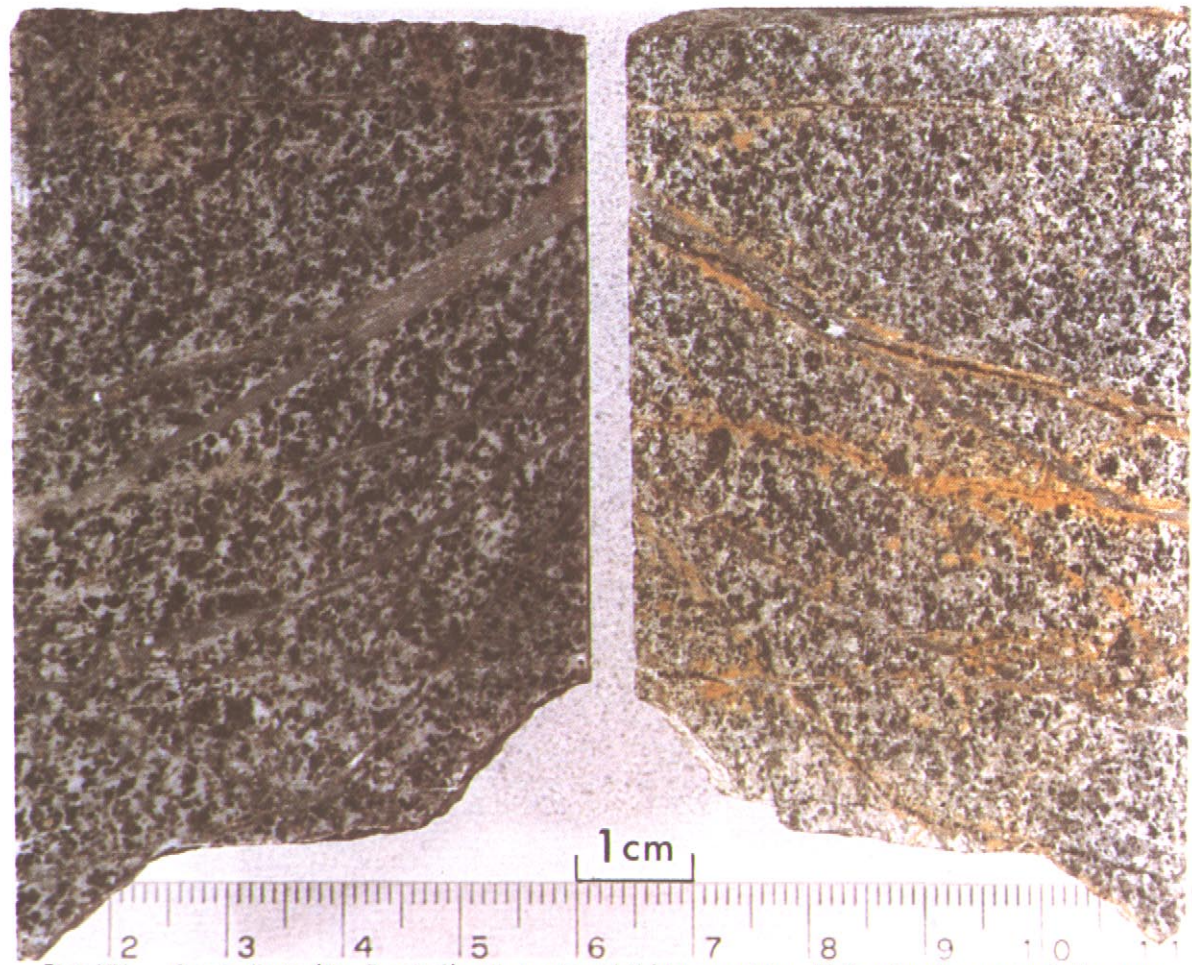


Plate XV. Quartz diorite (Fig. 7, unit 2) with quartz and K-feldspar veining. Mafic minerals are extensively recrystallized to fine-grained secondary biotite.

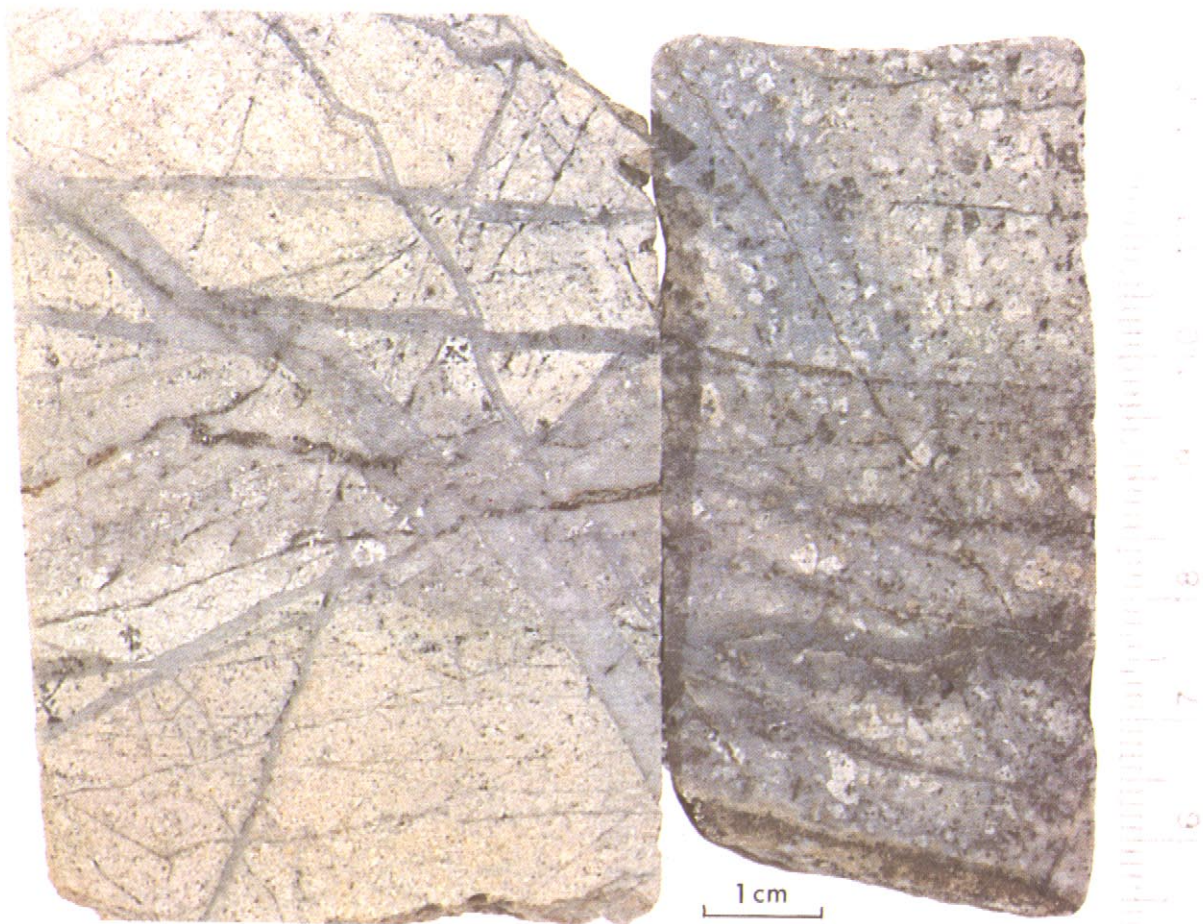


Plate XVI. Pervasive phyllic alteration and quartz veining in bleached hornfels (left specimen) and quartz plagioclase porphyry (right specimen).

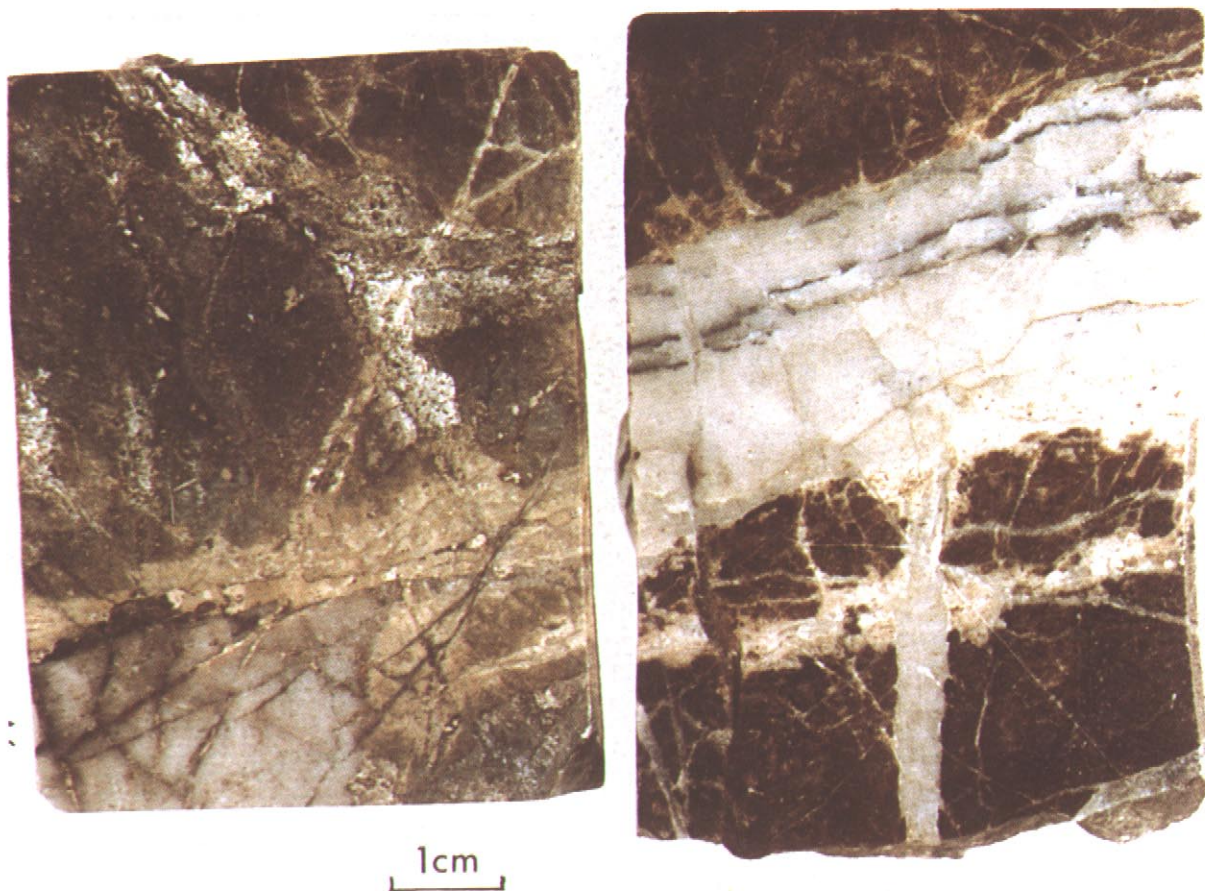


Plate XVII. Veining in biotite hornfels. Right specimen has a ribboned quartz-K-feldspar-molybdenite vein that shows little effect on the adjacent rock (potassic zone alteration). Left side has propylitic alteration of biotite hornfels by fracture-related quartz-calcite-chlorite-pyrite-clay.

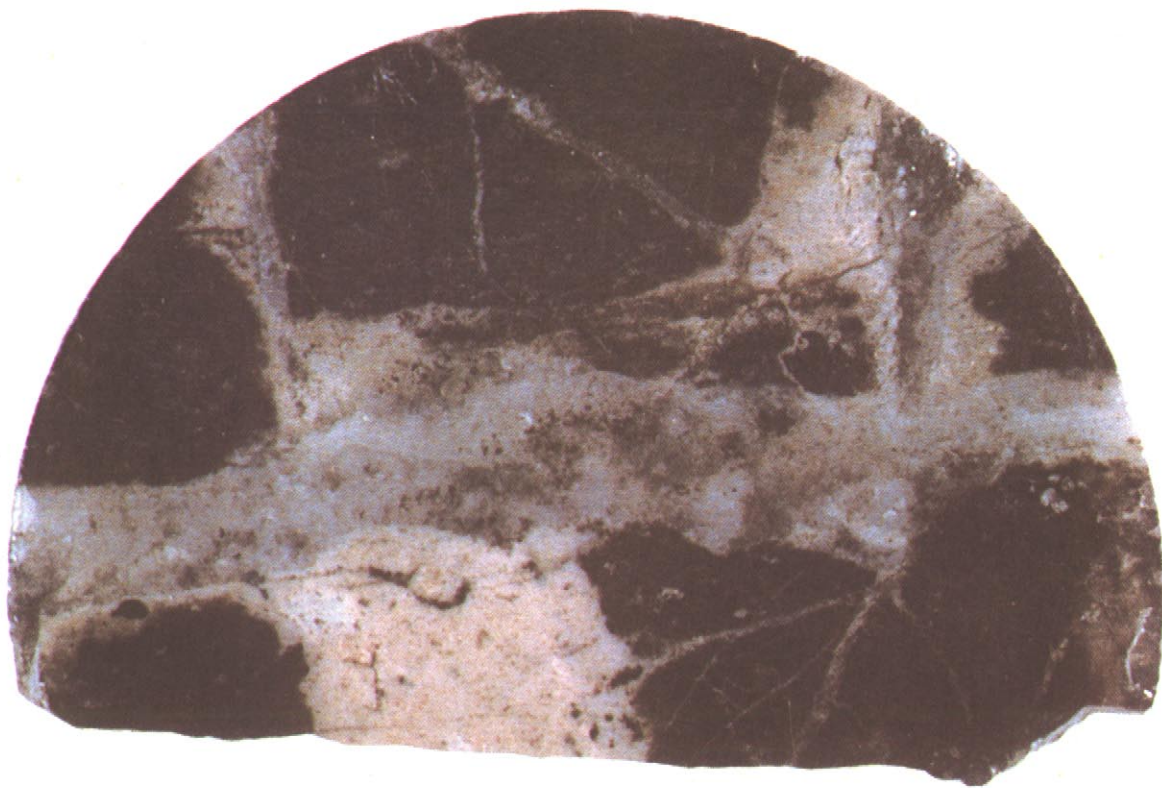


Plate XVIII. Potassic alteration in biotite hornfels. K-feldspar (pink) veins are cut by quartz-anhydrite-biotite veins. Note how little the veins alter the hornfels.

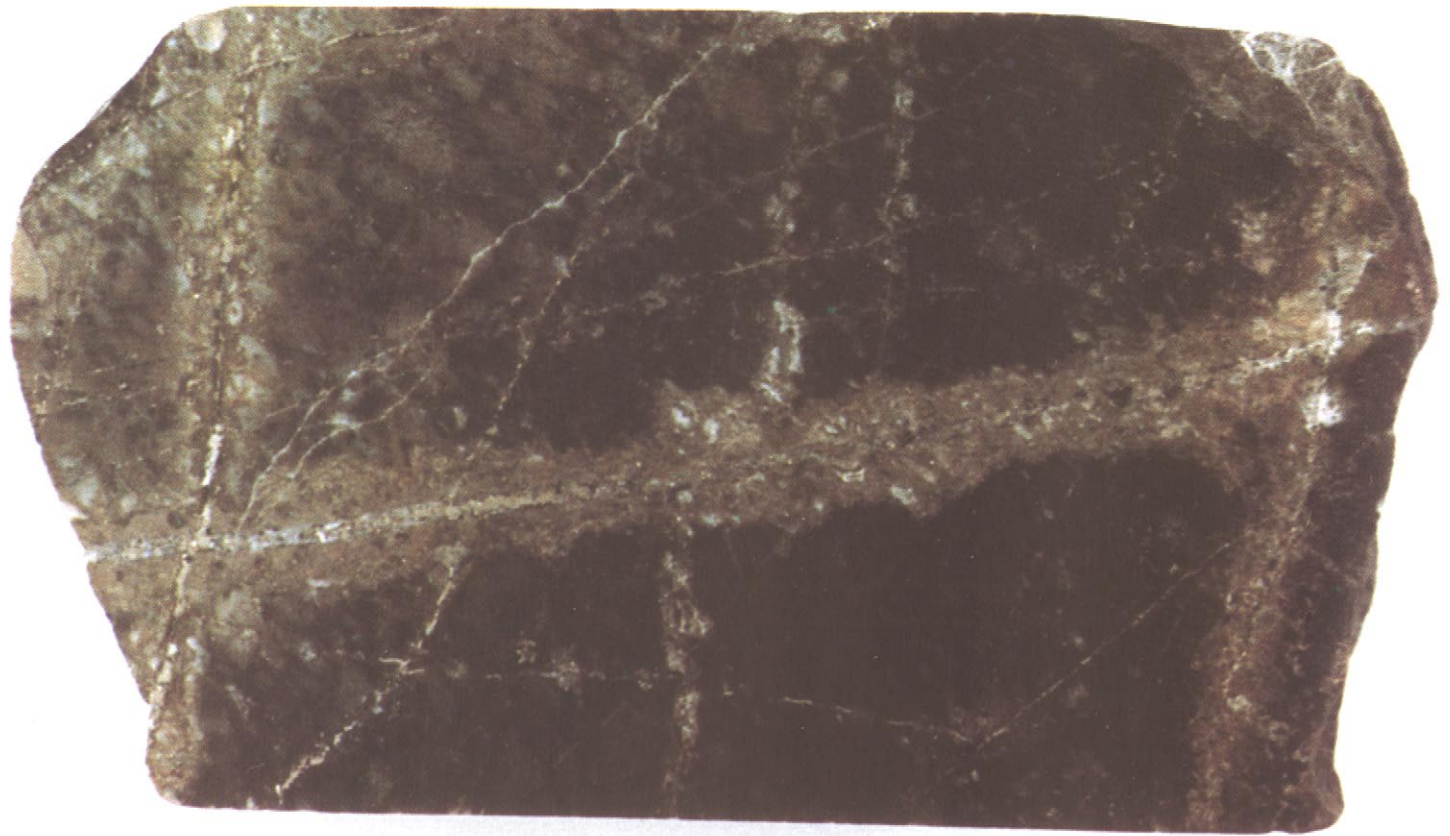


Plate XIX. Biotite hornfels with relict pale lapilli. The hornfels is cut and altered by pyritic veinlets with phyllic margins.

MINERALIZATION

INTRODUCTION

Widespread copper-molybdenum mineralization is associated with rocks intruded by quartz monzonite. Drill-indicated geological reserves are in the order of 400 million tonnes containing 0.4 per cent copper and 0.05 per cent molybdenite. Computed geological reserves taken to information limits (the projected 3,325-foot bench) and assuming stripping ratios in the order of 2:5 to 3:1 waste to ore, range from about 90 million tonnes containing 0.51 per cent copper and 0.050 per cent molybdenite at a 0.40-per-cent copper cutoff, to approximately 485 million tonnes containing 0.30 per cent copper and 0.048 per cent molybdenite at a 0.15-per-cent copper-equivalent cutoff (Beaudoin and Mortensen, 1973).

Pyrite and chalcopyrite are the most abundant sulphide minerals and occur primarily in fractures, in quartz veins, and as disseminations. Molybdenite is contained mainly in quartz veins. Secondary copper sulphides are found in an enrichment blanket over most of the deposit. 'Chalcocite' (probably mainly digenite) and covellite are the most important secondary copper minerals. They occur as thin coatings on pyrite and chalcopyrite and are deposited in a large, well-defined zone of supergene enrichment. Near surface sulphide minerals are extensively leached and secondary copper minerals are present in small amounts as copper oxides or carbonates and native copper.

Primary ore minerals are most abundant in an asymmetrical annular zone of biotitic hornfels surrounding the quartz monzonite stock. Best grades of copper and molybdenum are found in biotitic quartz diorite in the northeast sector of the deposit; weakest mineralization is found along the western margin of the intrusion. Copper-molybdenum mineralization decreases in intensity away from the main quartz monzonite contact. Outward from the contact, pyrite increases to form a pyritic halo around the zone of copper-molybdenum mineralization, then decreases abruptly. Within the quartz monzonite stock copper and molybdenum grades decrease away from the contact and rarely exceed 0.15 per cent copper and 0.02 per cent molybdenite. Sphalerite with pyrite and some

tennantite and galena are found in veins within and peripheral to the pyritic halo as well as in small late-forming quartz and quartz carbonate veinlets in the main copper-molybdenum zone.

Distribution of primary minerals is not readily seen in outcrop due to weathering and sulphide leaching. At surface rocks are bleached, crumbly masses commonly stained and cemented by limonite in an extensive capping. Sulphide minerals are strongly corroded or leached to a maximum depth of about 38 metres (125 feet). Secondary copper minerals are deposited below the oxidized and leached rocks in a zone of supergene copper mineralization with a maximum thickness of about 90 metres (300 feet). The combined effects of oxidation, leaching, and supergene enrichment impart a pronounced vertical zoning to the deposit that overlaps, and to a large degree, masks primary zoning patterns. Vertical zoning is illustrated on Figure 17 which shows copper depletion and molybdenum concentration in the strongly oxidized zone near surface, copper enrichment beginning approximately at the present water table and primary mineralization at depth below the 'gypsum line,' the elevation below which fractures are tightly cemented by gypsum and groundwater circulation has been minimal.

PRIMARY MINERALIZATION AND LATERAL ZONING

Primary (hypogene) ore minerals are mainly pyrite, chalcopyrite, and molybdenite. In addition to the three main ore minerals, magnetite, sphalerite, tennantite, and galena are present as well as trace amounts of arsenopyrite, pyrrhotite, scheelite, ilmenite, hematite, and rutile. Bornite has been reported (Owens, 1968) in minute amounts as 2 to 10-micron-sized inclusions in pyrite but does not contribute significantly to ore value. Precious metal content, as indicated by eleven 50-foot composite samples from five representative drill holes, averages 4.6 ppm silver and less than 0.2 ppm gold (Beaudoin and Mortensen, 1973).

Zoning patterns, as defined by variable amounts of the main ore minerals, are illustrated on Figures 12, 13, 14, 15, and 16. These patterns are based on all information available to 1971 and some selected data from more recent drilling. No vertical zoning can be demonstrated in primary mineralization within 300 metres (1,000 feet) of surface but deeper drilling suggests that molybdenite grades increase slightly at depths greater than 450 metres (1,500 feet) whereas copper grades decrease below 600 metres (2,000 feet) from surface (P. G. Beaudoin, 1975, personal communication).

Pyrite is present as fracture-controlled and disseminated grains averaging about 1 millimetre in size as well as coarser euhedral grains and aggregates in a number of successive generations of pyrite and quartz-pyrite veins. Chalcopyrite is intimately associated with pyrite but is finer grained and commonly present as discrete 0.1 to 0.3-millimetre grains. A significant proportion is found as 10 to 50-micron inclusions in pyrite. Some blebs of chalcopyrite 10 microns and smaller in size are scattered throughout and totally enclosed in pyrite and less commonly magnetite. Such chalcopyrite might be difficult to liberate

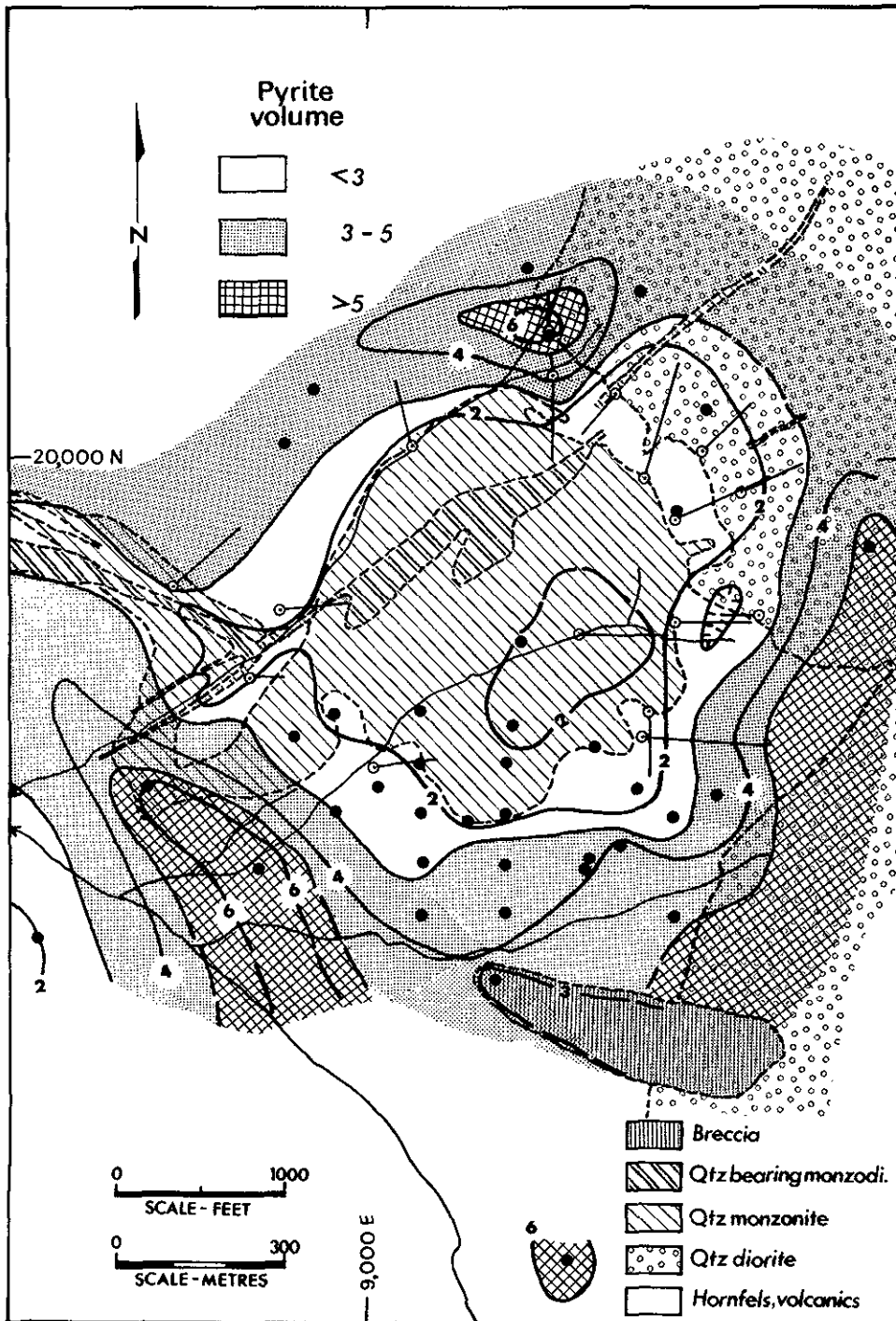


Figure 12. Primary minerals — pyrite.

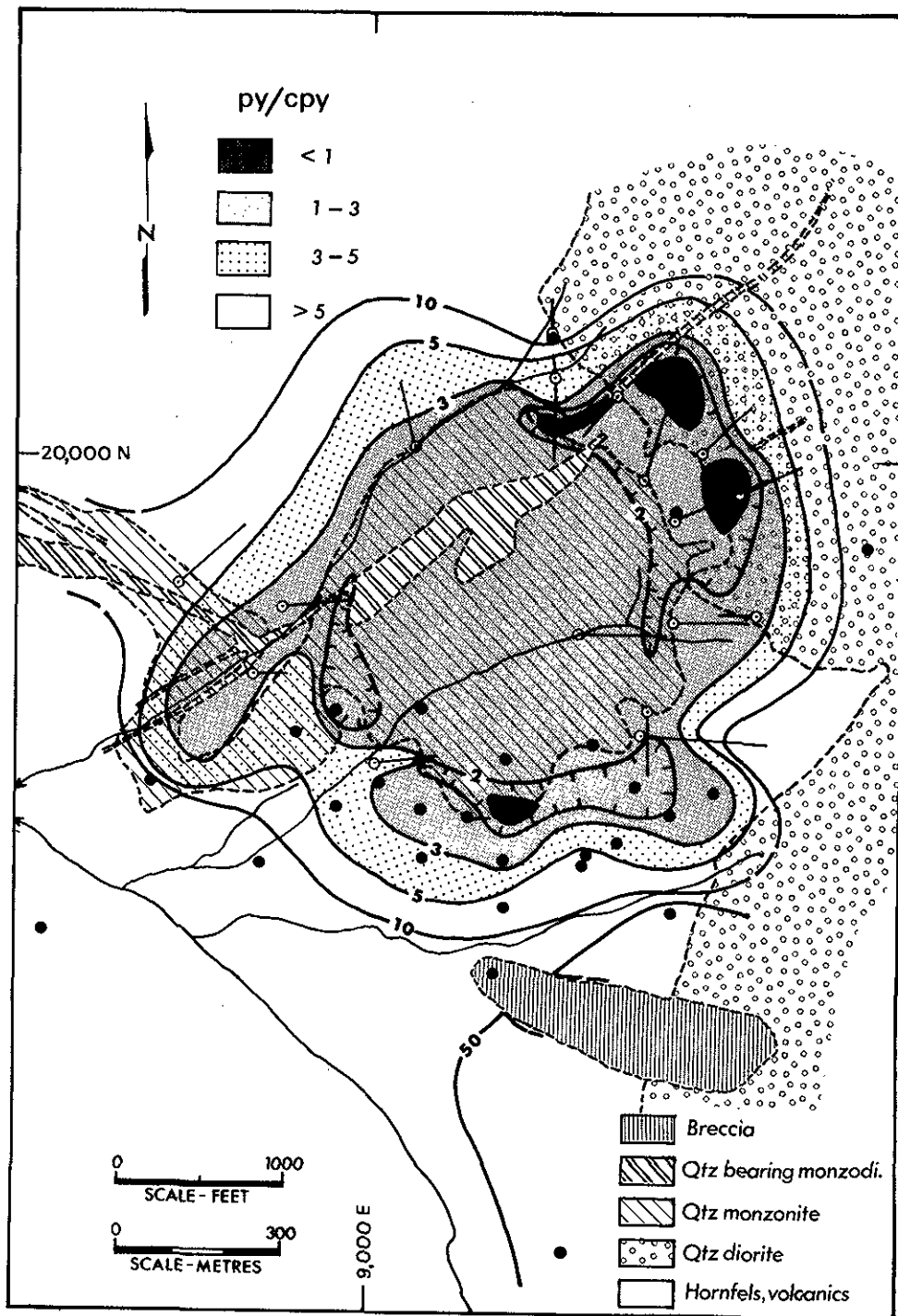


Figure 13. Pyrite—chalcopyrite ratio.

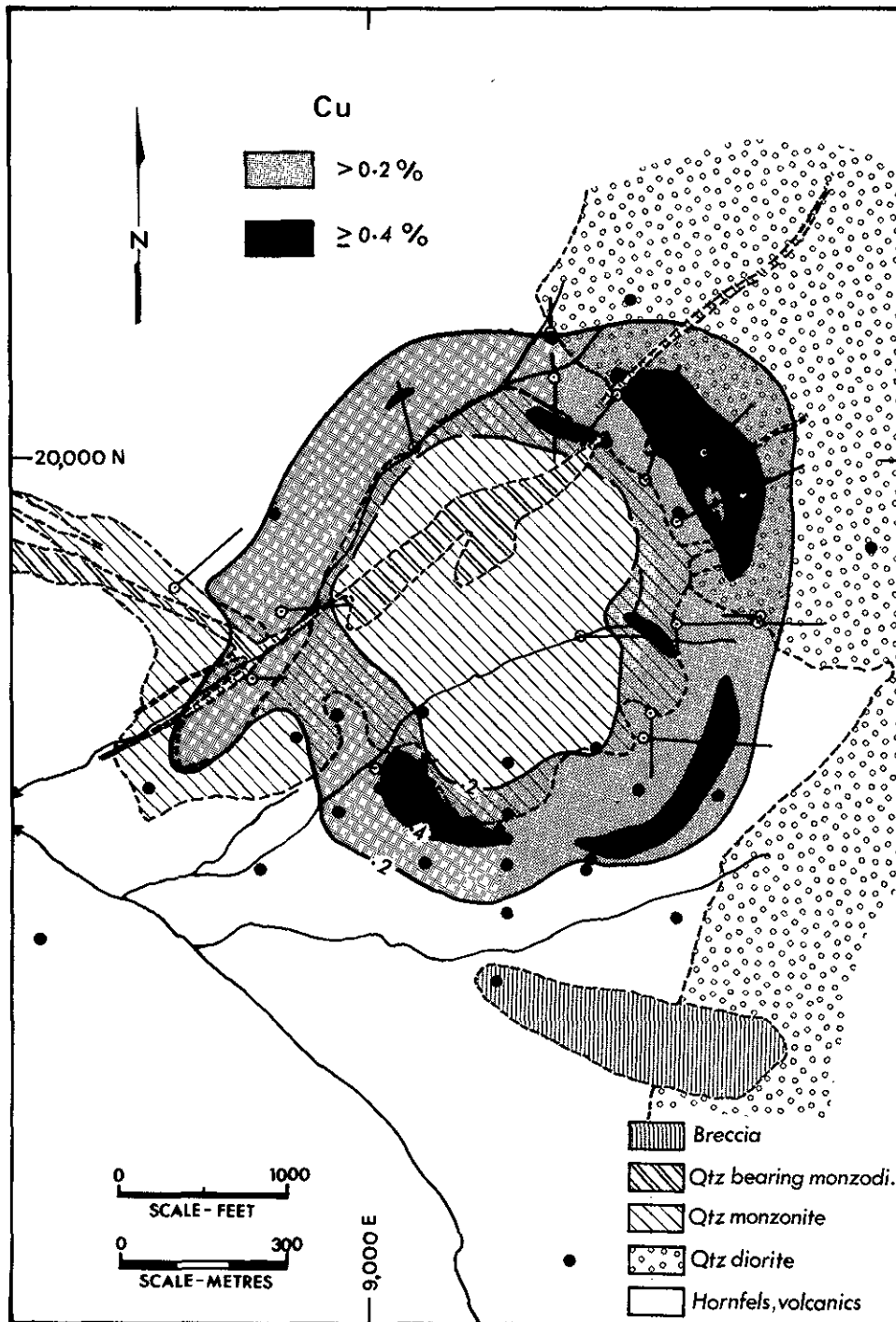


Figure 14. Primary mineralization – Cu.

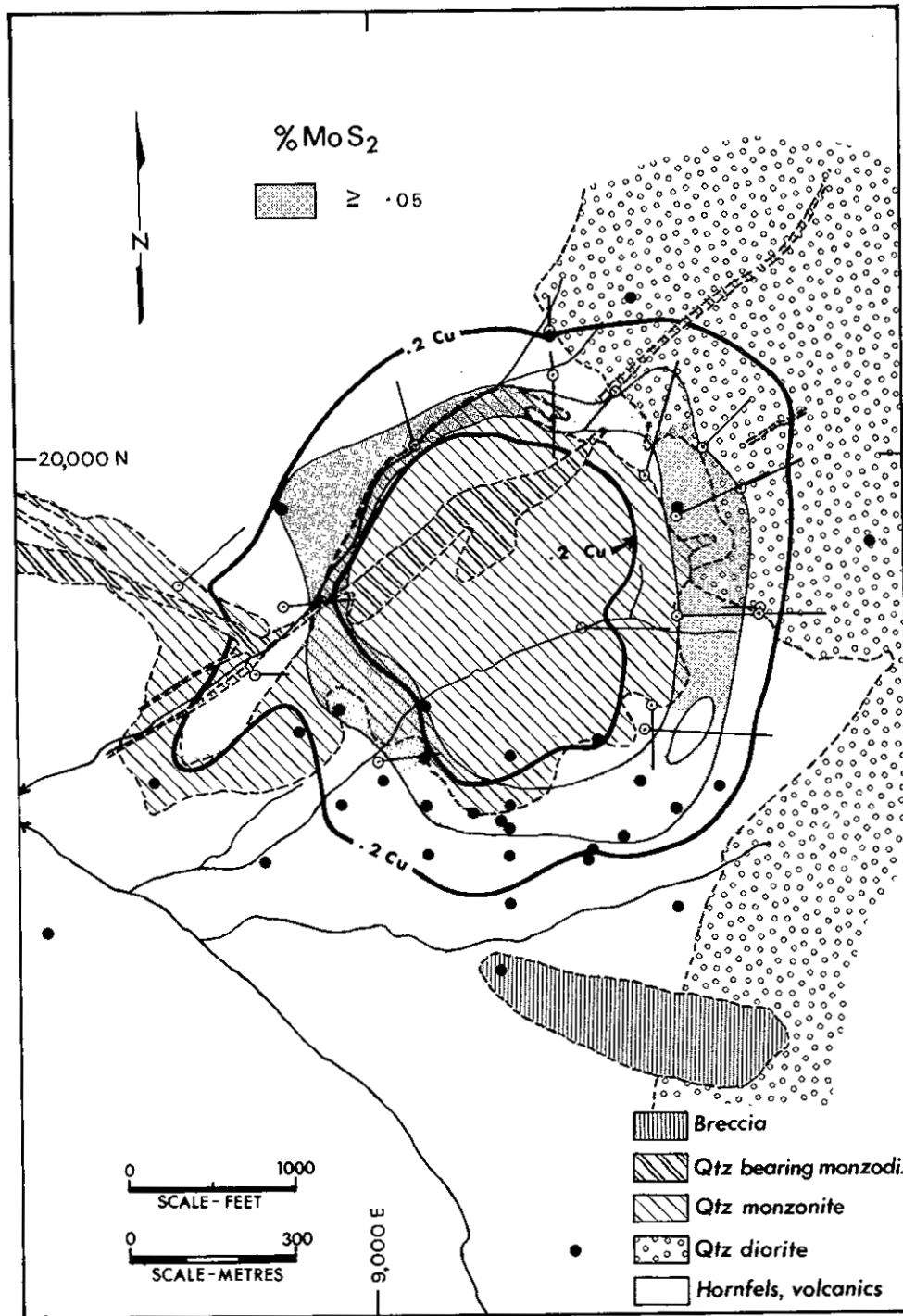


Figure 15. Primary mineralization — Mo.

by conventional milling of ore. Molybdenite is most commonly found as fine-grained flakes within several generations of quartz-bearing veinlets. It also occurs as very fine grains or 'paint' in ribboned quartz veins, as crystals along quartz vein selvages, and less commonly in fractures with pyrite and/or chalcopyrite. Some coarse crystals of molybdenite are engulfed and mechanically transported by gypsum within late-stage veins.

Distribution of pyrite represented as mean volume per cent calculated over long drill intercepts is shown on Figure 12. Pyrite in quartz monzonite averages 2 per cent or less by volume and increases progressively outward everywhere except in the northeast sector of the deposit where the zoning symmetry is interrupted by a zone with little pyrite in biotitic quartz diorite. Pyrite increases to a maximum of about 6 per cent or more in the pyrite halo about 150 metres (500 feet) or more from the main quartz monzonite contact. The pyrite halo envelopes the zone of best copper-molybdenum mineralization with best grades corresponding to a pyrite content of about 2 to 3 per cent.

Chalcopyrite is most concentrated in biotitic hornfels adjacent to the quartz monzonite stock and in biotitized quartz diorite in the northeast zone. Chalcopyrite content decreases progressively away from the main intrusive contact in an inverse manner to pyrite. Relationship of chalcopyrite to pyrite is illustrated as a pyrite-chalcopyrite ratio on Figure 13. Chalcopyrite exceeds pyrite in abundance only in quartz diorite of the well-mineralized northeast sector and in a low pyrite zone encountered in a single drill hole at the southern contact of the quartz monzonite intrusion. Outward from the intrusive contact a pyrite-chalcopyrite ratio of 4:1 signifies the inner margin of the pyrite halo and a rapid increase in amount of pyrite. Within the pyrite halo, pyrite-chalcopyrite ratio exceeds 10:1 and locally is greater than 50:1. Pyrite-chalcopyrite ratio remains fairly constant in any given zone even where total volume of sulphides varies.

Chalcopyrite and molybdenite concentrations expressed as per cent copper and molybdenite are shown on Figures 14 and 15. The annular pattern of mineralization and intimate relationship of copper-molybdenite mineralization with intensely fractured and hydrothermally altered rocks along the quartz monzonite contact are evident. The pattern and zoning trends are remarkably consistent throughout the mineralized area. Areas underlain by zones at least 6.1 metres thick with >0.4 per cent copper within the larger zone of >0.2 per cent copper are shown on Figure 14. The >0.4-per-cent copper grade is an arbitrary value used to indicate zones of better copper mineralization. A 6.1-metre (20-foot) thickness is taken to be the minimum thickness of rock from which a bench of ore could be developed. In plan view small areas underlain by rocks with better copper grades cluster around the quartz monzonite stock or are localized in biotitic quartz diorite in the northeast sector.

Grades of copper and molybdenite, when averaged over long drill intercepts and plotted in relation to distance from the main quartz monzonite contact (Fig. 16), document be-

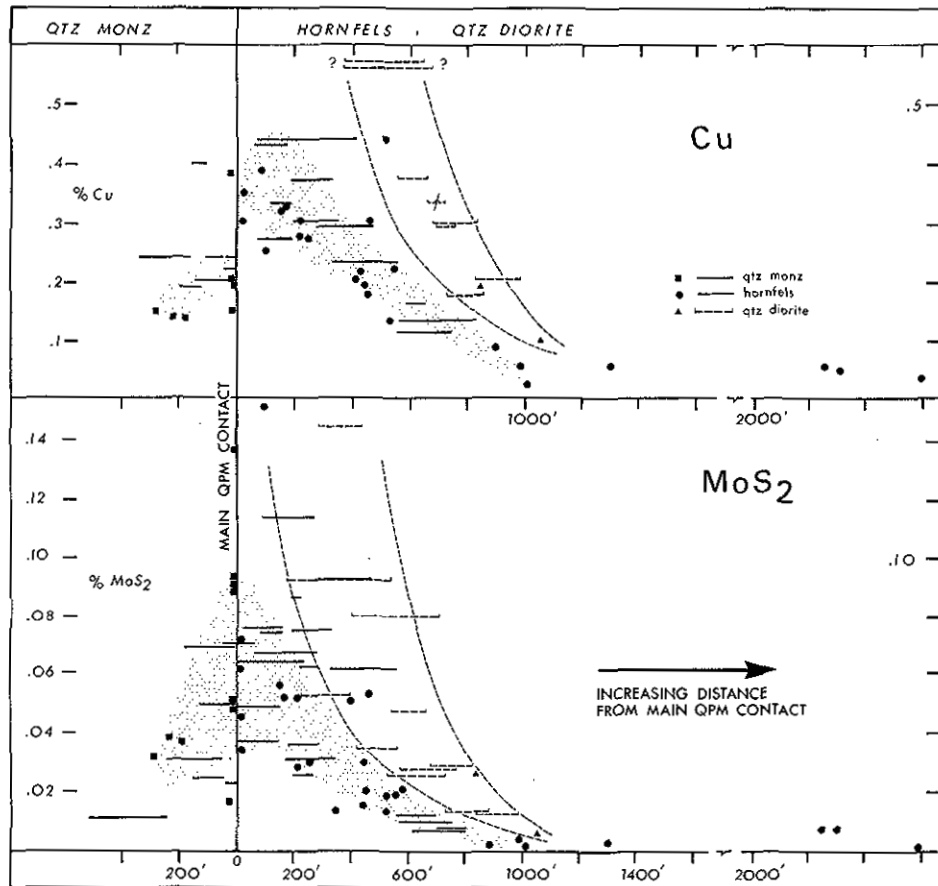


Figure 16. Primary Cu and MoS₂ grade in relation to distance from main intrusive contact.

haviour of chalcopyrite and molybdenite more explicitly. Both copper and molybdenum decrease in intensity in a regular manner away from the quartz monzonite contact but two separate regimes are evident — hornfels and quartz diorite. Quartz diorite is superior to hornfels as a host for copper and molybdenum sulphides, even though in many localities it is some distance from the quartz monzonite stock. The same grade is developed in quartz diorite twice as far from the quartz monzonite contact as hornfels. Conversely, at the same distance from the quartz monzonite contact, grades of copper and molybdenite in quartz diorite are about double those in hornfels. Best grades of copper discovered to date are in quartz diorite, but some of the higher values shown on Figure 16 (marked by ?) might not be representative as they are based on poor core recoveries (from 10 to 25 per cent).

Trends of copper-molybdenum mineralization shown on Figure 16 are similar but some differences are indicated. Best mineralization has taken place in hornfels near the quartz monzonite stock. Copper is most concentrated in hornfels a slight distance from the

main contact whereas molybdenum mineralization straddled the intrusive contact and molybdenite is maximized along it. Copper values exhibit two distinct levels of concentration with quartz monzonite having only about one-half the copper content of well-mineralized hornfels. A similar observation was noted in breccia bodies outside the main intrusive mass where copper was derived mainly from well-mineralized hornfels fragments and copper grades were diluted as the amount of quartz monzonite matrix increased.

These patterns (Fig. 16) indicate that molybdenite mineralization was superimposed on the main intrusive contact zone and grades diminish in a regular manner away from the contact. The main control for molybdenite is fracture intensity and quartz veining. Copper grades, on the other hand, diminish abruptly within intrusive rocks and in addition to fracture intensity appear to be influenced more than molybdenite by rock composition.

SECONDARY MINERALIZATION AND VERTICAL ZONING

Vertical zoning defined by progressive changes in mineralogy and ore tenor with depth is a result of oxidation, sulphide leaching, and supergene processes. At surface, in subcrop, and at relatively shallow depths, abundance of sulphide minerals and ore value are reduced due to oxidation and leaching by acidic solutions. In this environment copper is mobile whereas molybdenum is immobile (Garrels, 1954; Sato, 1960; Titley, 1963; Hansuld, 1966). Thus, when sulphide minerals break down copper is depleted but molybdenum remains and may be concentrated.

Figure 17 illustrates vertical zonation as defined by ore tenor. Copper is consistently depleted from rocks near surface except near basic dykes where copper oxides and hydrated copper carbonates are deposited (for example, diamond-drill hole 23). Molybdenum is more variable in its behaviour. Molybdenite grades of oxidized outcrops commonly compare with those of primary mineralization zones at depth (for example, diamond-drill hole 74). In certain areas of strongly oxidized rocks, molybdenum is in the form of molybdates and complexes with ferric hydroxide as well as molybdenite in quartz veins where it was protected from leach solutions. Mineralogy of strongly oxidized rocks will be discussed in more detail in a succeeding section.

Supergene copper mineralization resulting in enrichment of primary grade ore takes place below the zone of oxidation in the zone containing groundwater. Copper contained in downward-percolating acidic leach solutions replaces chalcopyrite, and pyrite as solutions becomes neutralized at depth and forms secondary copper sulphides. Enrichment of primary copper grade averages about 25 per cent (that is, 1.25 to one enrichment factor) and is maximized near the top of the groundwater table immediately below zones of oxidizing primary mineralization as in diamond-drill hole 23. Increase in intensity of enrichment with depth shown by diamond-drill hole 19 is only apparent and reflects

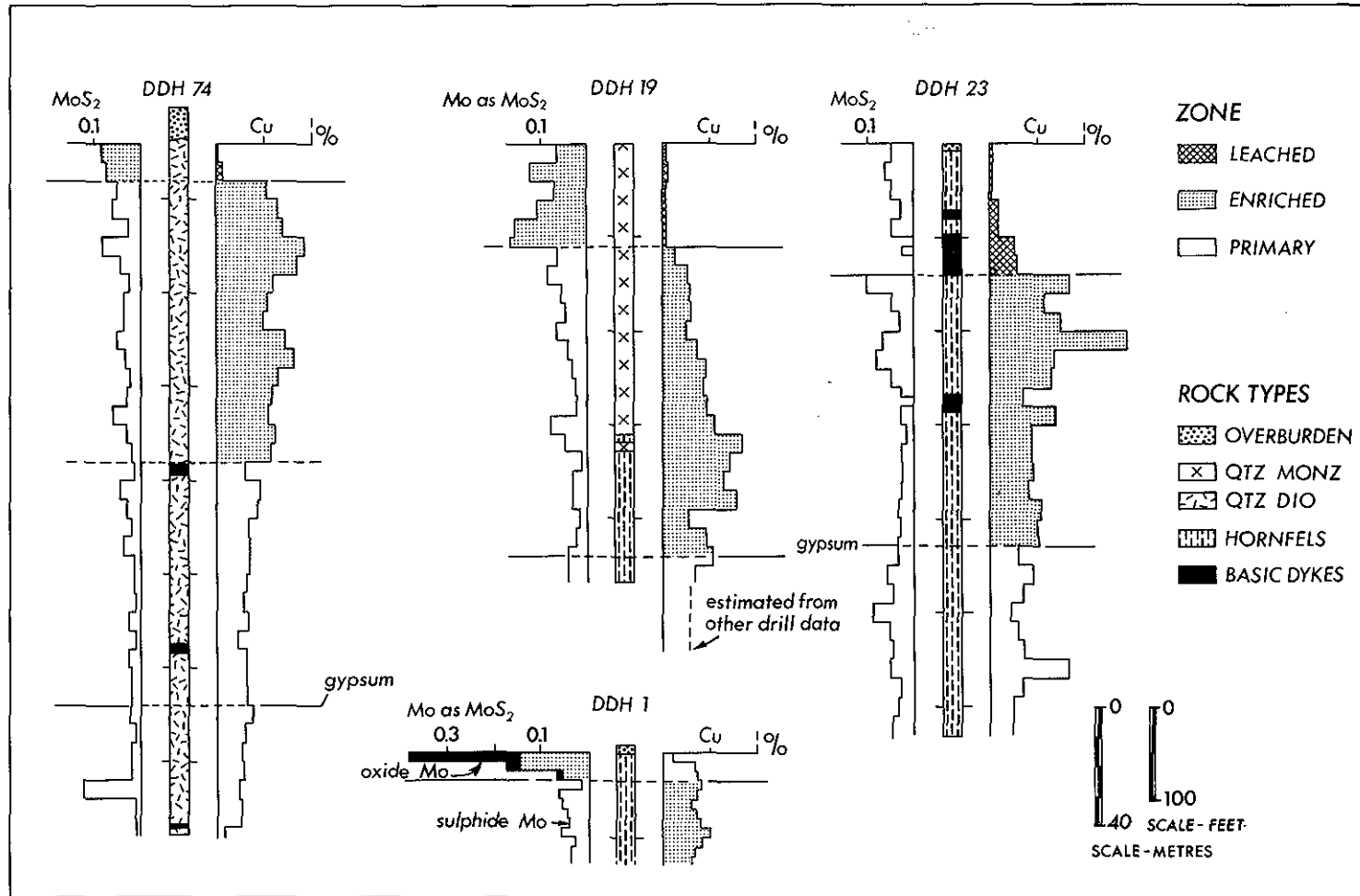


Figure 17. Vertical zoning of Cu and MoS₂ grades in diamond-drill cores.

increasing primary grade as the intrusive contact is approached. Away from the contact (at greater depth) primary grade diminishes as does the amount of supergene copper enrichment.

EXTENT OF LEACHING AND SUPERGENE MINERALIZATION

Maximum thickness of the strongly oxidized zone with sulphide leaching is about 38 metres (125 feet); the supergene zone is up to 100 metres (325 feet) thick. Base of the strongly oxidized zone is clearly shown by marked increases in copper grade and amount of sulphide minerals, presence of secondary copper sulphides, and minor amounts of copper oxides and native copper, as well as a decrease in the amount of limonite and a noticeable change in limonite colour from yellow-brown or orange to dark brown. Base of supergene copper mineralization is clearly marked in drill holes by the 'gypsum line' — the limit of groundwater circulation below which fractures are tightly cemented by gypsum.

Depth of strong oxidation with sulphide leaching and thickness of the supergene copper zone are illustrated as isopach maps on Figures 19 and 20. The elevation below which gypsum is present (the gypsum surface), that defines the start of primary mineralization at depth, is shown on Figure 18. The isopachs and gypsum surface are trend surface maps computed using double Fourier series analyses of irregularly spaced data after a method described by James (1966). Data input from 54 locations was utilized using a wavelength of 670 or 700 metres (2,200 or 2,300 feet) and 25 terms in series representing a second harmonic surface. The waveform generated approximates the present topographic profile at Berg deposit (shown on Fig. 18) to which the depth of oxidation and supergene mineralization are related. A wavelength of about 670 metres (2,200 feet) is compatible with the dimensions of the intrusive system, zone of hydrothermal alteration and mineralization, and topographic relief. The 'goodness of fit' of trend surfaces generated are about 63, 70, and 88 per cent, thus achieving an acceptable and geologically useful degree of smoothing of the observed data.

Contours relative to sea level marking the start of gypsum in fractures define a 'gypsum plane.' This surface is shown on Figure 18, and unequivocally defines the base of groundwater circulation below which oxidation and supergene effects are minimal and confined to a few narrow zones of intense fracturing or faulting. Depth of gypsum solution is a function of groundwater flow patterns and acidity. Flow patterns in bedrock are influenced at Berg deposit mainly by topography, major and subsidiary surficial drainage patterns within the cirque-like basin, and intensity of fracturing. The zone of gypsum leaching defined by diamond drilling forms a northeasterly elongate depression that rises in elevation to the northeast roughly following present topography. The zone of deepest gypsum leaching is coaxial with mineralized intrusions parallel to 'Red' and 'Pump' Creeks but perpendicular to the north fork of Bergeland Creek, the major drainage system.

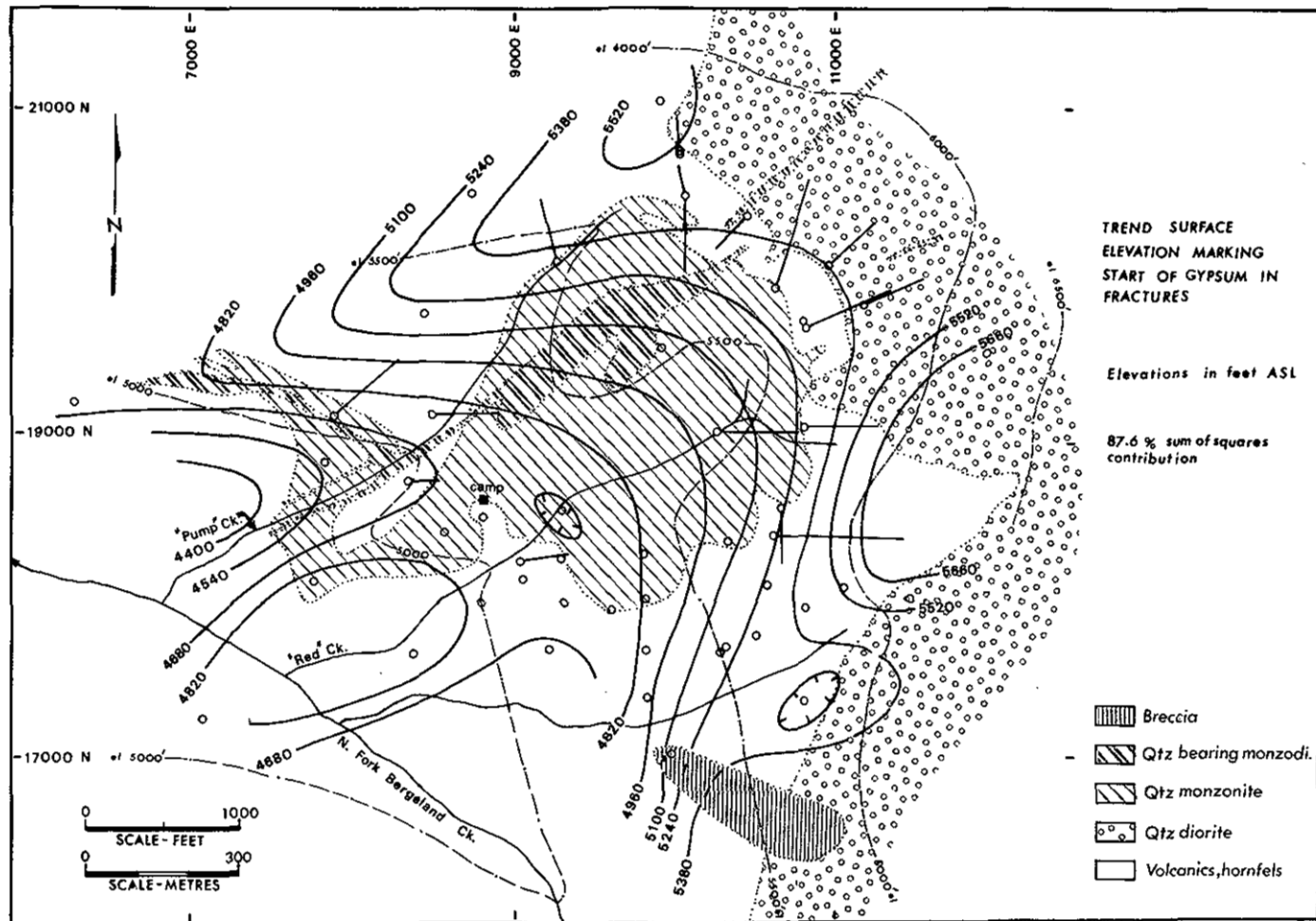


Figure 18. Trend surface elevation marking start of gypsum in fractures.

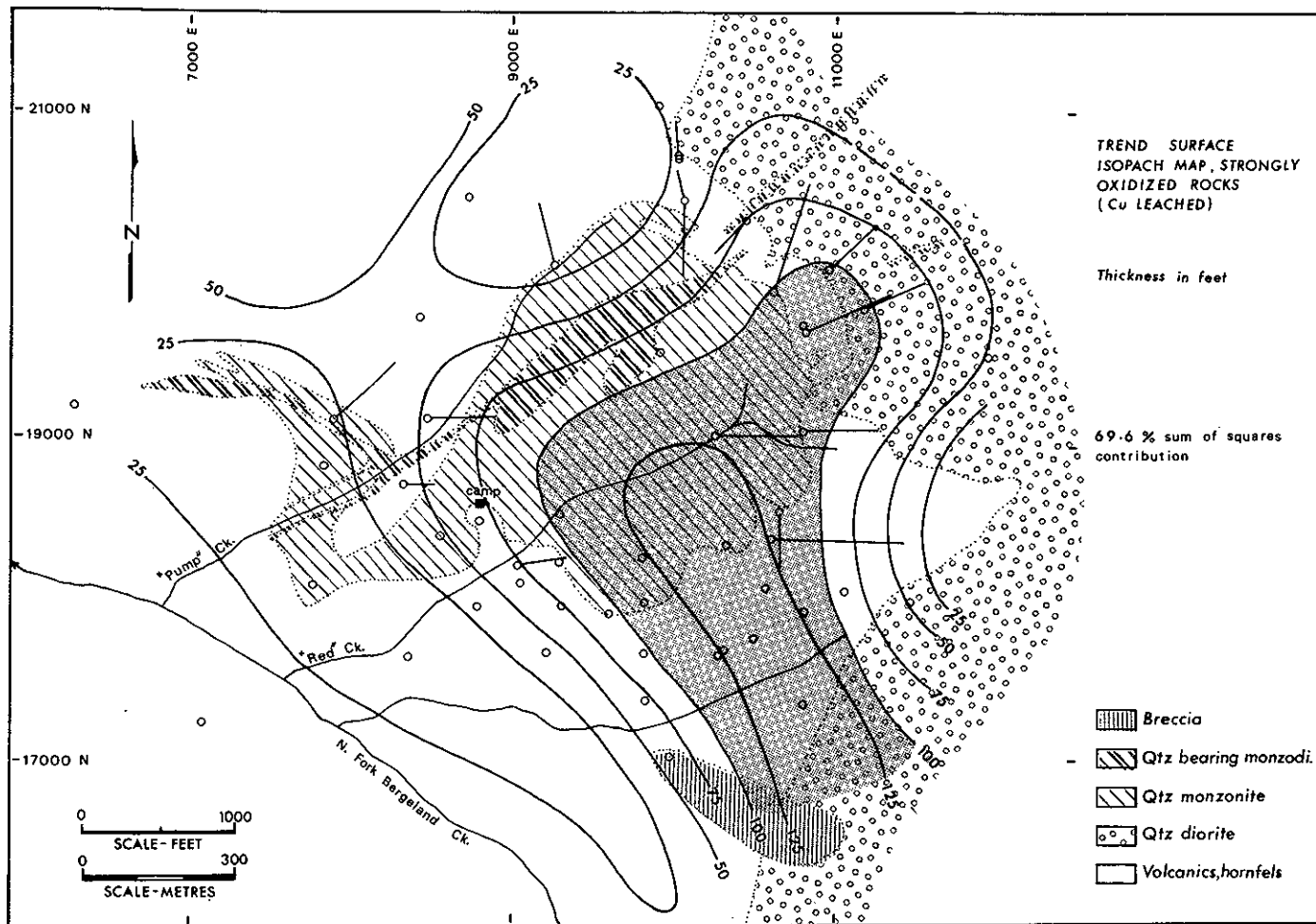


Figure 19. Trend surface isopach map, strongly oxidized rocks (Cu leached).

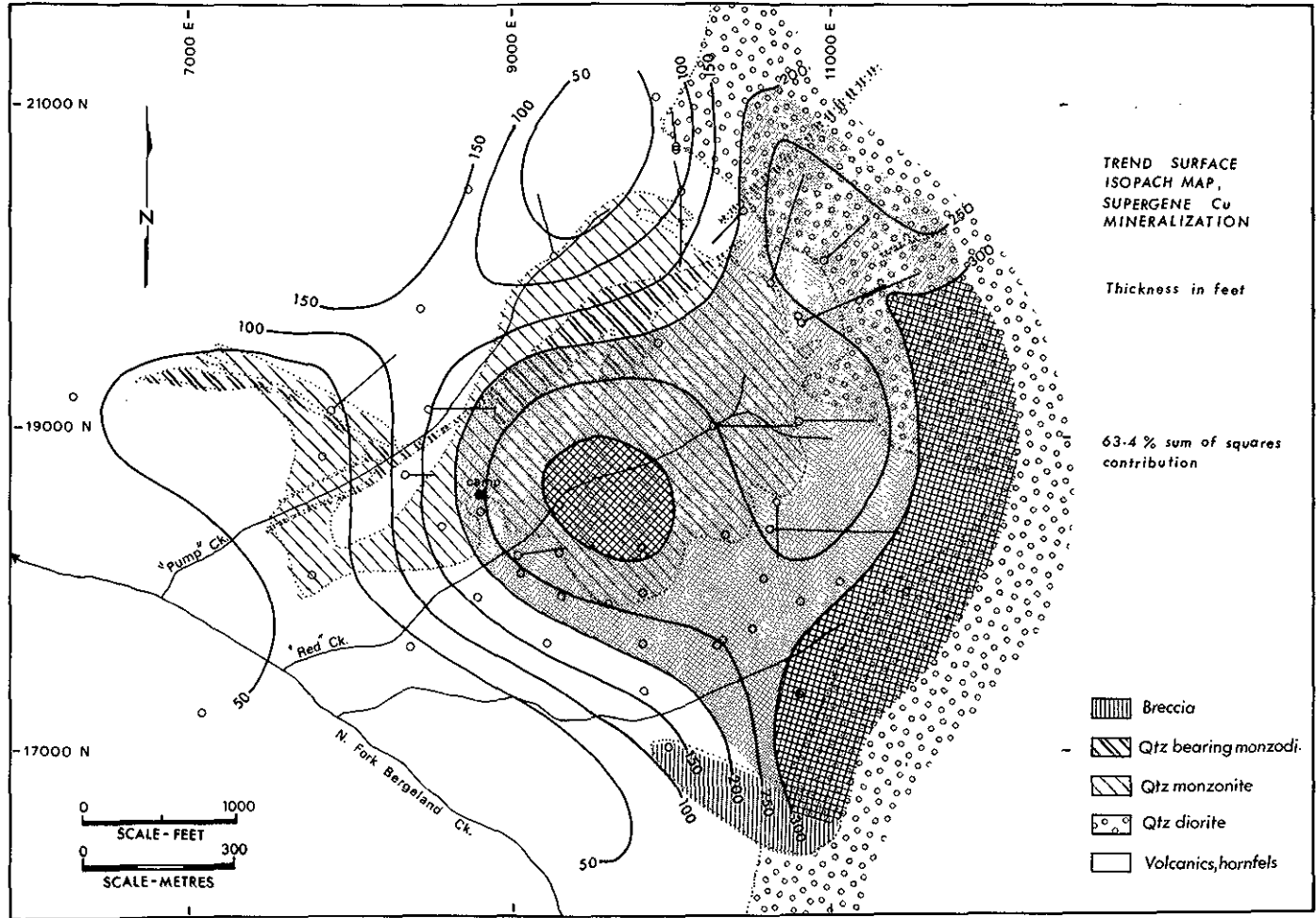


Figure 20. Trend surface isopach map, supergene Cu mineralization.

A trend surface isopach map of oxidized rocks from which copper is leached is shown on Figure 19 and one of supergene copper mineralization is shown on Figure 20. Similar trends are apparent with maximum thicknesses in the southeast and east sectors of the mineralized zone along the quartz monzonite contact and in hornfels adjoining quartz diorite. Strongest oxidation and most advanced leaching are seen in rocks in the vicinity of 'Red' Creek and its branches where the deeply incised creek efficiently conveys away surface runoff and shallow groundwaters from flanking slopes allowing intense oxidation. Deep oxidation takes place where acidic solutions from oxidizing pyrite-rich rocks penetrate the most highly fractured zones in hornfels between quartz monzonite and quartz diorite intrusions. Diurnal, periodic, and seasonal fluctuations in groundwater flow and chemistry facilitate deep, complete oxidation and sulphide leaching. The southeasterly extension of the deeply oxidized zone might be localized by increased permeability in northwest-southeast-trending zones of brecciation and faulting.

Supergene copper minerals are found in a zone that is more widespread than the zone of intense sulphide leaching. Maximum thickness of the supergene zone is developed along the eastern part of the mineralized zone between the major intrusions. A westward-projecting lobe indicated by thick supergene zones in two drill holes in the intrusive stock is coincident with quartz monzonite porphyry (Fig. 7, unit 3). Thickness of Figure 20 is exaggerated as values plotted are vertical drill hole intercepts on slopes that commonly approach 45 degrees. The pattern shown on Figure 20 is almost entirely a result of downslope migration of acidic copper-bearing leach solutions generated by oxidation of weakly cupriferous pyrite-rich rocks in the pyrite halo and interaction with a relatively stable water table in the zone of intense fracturing. The thickest zone of secondary copper sulphides in quartz monzonite is coincident with zones having most advanced sericite-quartz-pyrite alteration (mainly quartz monzonite porphyry and sericitized quartz plagioclase porphyry, Fig. 7, units 3 and 4).

MINERALOGY AND PROCESSES OF FORMATION

ZONE OF OXIDATION AND SULPHIDE LEACHING

Breakdown of sulphide minerals near surface has resulted in a leached capping consisting of mainly quartz, sericite, clay minerals, limonite, and opaline silica. Limonite is composed primarily of amorphous ferric hydroxide [hydrogoethite, $\text{Fe}(\text{OH})_3$], goethite (FeOOH), and minor hematite (Fe_2O_3) with locally developed jarosite [$\text{K}(\text{Fe}, \text{Al})_3(\text{SO}_4)_2(\text{OH})_6$]. Other minerals observed in small amounts in the zone of oxidation are cuprite, tenorite, native copper, malachite, azurite, brochantite, chalcantite, ferrimolybdate, possibly akaganeite (molybdenum-bearing beta limonite), and black amorphous iron-manganese oxides formed from lead-zinc-bearing carbonate veins. Owens (1968) has reported delafossite.

Freshly deposited limonite is amorphous 'active' hydrogoethite which changes with time to a more stable amorphous variety – 'inactive' hydrogoethite or crystalline goethite (McAndrew, *et al.*, 1975). Most limonite observed in outcrop is a pervasive or surficial pulverulent variety. Granular, coagulated, and caked, botryoidal, or flat crusts are seen in pits and fractures at depth. Some relief-type limonite and sintered crusts are present but cellular boxwork and sponges are rare or absent. According to the terminology of Locke (1926) and Blanchard (1968), most limonite studied would be classified as fringing (contiguous) or exotic (transported) types in which a specific source of iron cannot be identified. Indigenous limonites would be expected in quartz diorite with high chalcopyrite-pyrite ratios but none was observed. Instead, reddish brown, resinous 'pitch limonites' with high copper (and molybdenum) content are present. Fluffy, fibrous, star-shaped, and flake-like limonite is found in and proximal to basic (reducing) dykes along with amorphous, black, copper-bearing oxides (tenorite ?, melaconite ?) and cuprite.

Jarosite is present in various amounts throughout much of the deposit. It is most prominent at surface and shallow depths along the eastern margin of the quartz monzonite stock and along the mineralized quartz diorite contact. Locally jarosite is the dominant limonite constituent. Zones with jarosite in excess of goethite are coincident with the most intensely oxidized and leached rocks. Jarosite normally accompanied by ferrimolybdate imparts a bright yellow colour to the capping. At depth and in less intensely leached rocks away from the jarositic zone, colour of limonite changes progressively from yellow-brown to orange, brown, and dark brown characteristic of goethite.

The most abundant accumulation of limonite is ferricrete, a relatively homogeneous deposit of ferric hydroxide. Ferricrete is transported amorphous hydrogoethite and goethite precipitated on surface or in overburden as soft, porous, friable limonite. Ferricrete deposits commonly contain plant and rock fragments and other detritus. Some ferricrete forms a matrix in soil and talus deposits resulting in cemented soil and breccia-like deposits. At Berg, ferricrete is being deposited actively in creek gullies and along the base of slopes where groundwater discharges. Such deposits mantle much of the lower slopes along the north fork of Bergeland Creek over hundreds of square metres and locally are up to 2 metres in thickness.

Partial chemical analyses of limonites are listed in Table 4. Analyses show concentration of copper but values of molybdenum, manganese, and other metals are low. In bulk, Berg ferricrete closely resembles bog iron ores and goethitic 'soft ore' exploited at Steep Rock (Jolliffe, 1955) and elsewhere. It is higher in iron content and has less impurities than limonitic iron ores deposited as erosion and terrestrial-weathering products such as those being evaluated in Iraq (Skoček, *et al.*, 1971). However, despite similarities in composition, appearance, and possibly origin with some commercial iron deposits, Berg ferricrete is too limited in quantity and too high in sulphur content to be of present economic interest.

TABLE 4. PARTIAL ANALYSES OF IRON ORES AND BERG FERRICRETE (in per cent)				
	1 Berg Ferricrete (massive)	2 Berg Ferricrete Crusts (newly deposited)	3 Steep Rock Fe Ore	4 Wadi Husainiya, Iraq
Fe total	55.24	39.8	57.0	38.3
S	1.24	4.6	0.04	-----
P	0.043	0.08	0.020	0.065
Mn	0.08	0.001	0.20	0.014
Al ₂ O ₃	0.25	0.3	0.81	10.8
Cr	0.003	0.001	-----	0.009
TiO ₂	0.010	0.01	-----	1.59
CaO	0.05	0.12	0.32	6.3
MgO	0.05	0.01	0.27	0.41
SiO ₂	-----	1.0	3.1	15.3
Moisture	-----	-----	7.0	5.5
Loss on ignition	20.9	-----	7.6	-----

Note: ----- = not reported.

- 1 — Assay, Steep Rock Iron Mines, courtesy of A. W. Jolliffe, 1968.
- 2 — P. Ralph, Analyst, B.C. Ministry of Energy, Mines and Pet. Res., 1974.
- 3 — Anticipated average grade, H. M. Roberts and M. W. Bartley, *Econ. Geol.*, Vol. 38, 1943, pp. 1-24.
- 4 — Average of five samples, V. Skocek, *et al.*, *Econ. Geol.*, Vol. 66, 1971, pp. 986-994.

GEOCHEMICAL DETERMINATIONS, BERG FERRICRETES (in ppm)			
	1	2	3
Cu	2 875	461	270
Mo	115	333	300
Zn	39	100	---
Pb	32	100	---
Ag	3.4	5	---
Ni	12	100	---
Co	18	50	---
Mn	38	10	---

- 1 — H. Goddard, Analyst, Kennco Explorations, (Western) Limited, 1968.
- 2 — P. Ralph and R. Hibberson, Analysts, B.C. Ministry of Energy, Mines & Pet. Res., 1974.
- 3 — A. Mariano, Analyst, Ledgemont Laboratory, 1968.

Molybdenum is an important constituent of limonite at Berg deposit. Its presence in the capping in non-sulphide minerals is an important indicator of primary sulphide mineralization at depth. Locally molybdenum is concentrated in the zone of oxidation and grades exceed those of hypogene zones in underlying rocks as shown on Figure 17. These observations are in marked contrast to data presented by Pokalov and Orlov (1974) who state that molybdenum is consistently depleted from the zone of oxidation in molybdenum and copper-molybdenum deposits.

Molybdenum enrichment accompanying sulphide leaching and copper depletion near surface was noted early during exploration at Berg deposit. C. S. Ney, D. L. Norton, and G.O.M. Stewart found enrichment to be generally related to vitreous, brittle, violet-brown, lacquer-like limonite crusts referred to as 'Berg-X.' Studies by Norton and Mariano (1967) found 5 to 15 per cent molybdenum in select crusts of 'Berg-X' and widespread zones with limonite containing 1 to 2 per cent molybdenum. These results are consistent with observations made by Carpenter (1968) who reports up to 7.5 per cent molybdenum in limonite at Questa; also J. C. Wilson (unpublished report, Kennecott Copper Corporation, 1965) who states that up to 7 per cent molybdenum is present in limonites in a number of porphyry deposits and Pokalov and Orlov (1974) who report an average of 1.26 per cent molybdenum in limonite from a number of Soviet deposits. If sufficient amounts of such limonites accumulate in oxidized rocks, molybdenum enrichment would take place. It apparently has taken place at Questa where, according to Carpenter (1968), both chemical and mechanical concentration result in soils with 1 per cent residual molybdenum and gossans (presumably from sulphide-bearing veins) having greater than 27 per cent molybdenum content.

Identity of molybdenum-bearing substances at Berg deposit is only partially resolved. Ferrimolybdite is common and together with molybdenum-bearing ferric hydroxide might constitute a considerable proportion of total molybdenum in the capping. Some molybdenum may also be present in jarosite, which according to Pokalov and Orlov (1974) may contain up to 1.75 per cent molybdenum, probably as minute inclusions of MoO_3 . In addition, a series of molybdenum-bearing ferric hydroxides related to ferrimolybdite has been described by Carpenter (1968) and suggested to be present at Berg by Barakso and Bradshaw (1971). These are various pH dependent, amorphous to very fine-grained, orange-brown ferric molybdate hydrate phases having different Fe:Mo ratios. The brittle, wine-coloured 'Berg-X' is probably an altogether different and rarer limonite compound. Preliminary investigations by Norton and Mariano (1967) including electron microscopic, diffraction, and microprobe analyses suggest that 'Berg-X' may be, in part, 0.2 micron-sized crystallites of MoO_2 (tentatively called sibolaite) as well as a spinel mineral, probably Fe_2MoO_4 . No natural occurrences of MoO_2 are known but Jager, *et al.* (1959), Norton and Mariano (1967), as well as Pokalov and Orlov (1974), synthesized MoO_2 at low temperatures under laboratory conditions. Electron microprobe analysis of 'Berg-X' limonite crusts by this writer revealed periodic, intermittent molybdenum enrichment took place during deposition of banded limonite crusts. Zoning of molybdenum is evident within some individual limonite layers indicat-

ing progressively changing rates of molybdenum incorporation during deposition of limonite. Similar observations of periodic molybdenum enrichment in limonite at Questa have been made by Carpenter (1968).

Behaviour of sulphide minerals under oxidizing conditions and resulting products are summarized and illustrated on Figure 21. In porphyry deposits, conditions in the zone of oxidation commonly vary from pH 3 to 6 and oxidation potential (Eh) of 0.4 to 0.8 volt (Sato, 1960). More acidic conditions with pH 1.6 and lower are possible; oxidizing veins at Questa have measured pH of 1 to 1.5 (Carpenter, 1968). At Berg deposit Barakso and Bradshaw (1971) report pH of 3.1 to 5.9 and Eh from 0.4 to 0.9 volt in waters from streams, springs, and drill-hole discharge. Waters as acid as pH 2.8 were measured during prolonged summer dry spells. Eh of 0.9 volt implies the presence of bacteria (probably thiobacilli and ferrobacilli) according to Baas Becking, *et al.* (1960).

Under highly oxidizing conditions such as at Berg and other porphyry deposits, all sulphide minerals dissolve (that is, are leached) except rare sulphide grains where they are protected from leach solutions by nonreactive quartz gangue. Under milder oxidizing and less acidic conditions such as weathering of zones with little pyrite content, molybdenite remains stable and only copper and/or iron sulphide minerals are leached. Oxidation of sulphides, abetted to some degree by oxidizing bacteria, generates ferrous or ferric sulphate and sulphuric acid solutions. Copper as cuprous ion is mobile under acidic conditions and is removed in aqueous solutions. Iron precipitates through hydrolysis as ferric hydroxide and forms limonite, a mixture of mainly hydrogoethite and goethite. Hematite is a minor limonite constituent at Berg deposit. Under highly acidic oxidizing conditions (pH less than 3) and dependant on activities of potassium, sulphur, and iron, jarosite is stable (Brown, 1971). At Berg deposit, jarosite is widespread and locally is the dominant limonite constituent. Its presence coincides with zones of intensely leached rocks, probably where potassium is available by degradation of potassic alteration minerals. The widespread distribution and persistence of jarosite in the capping under moderately acidic conditions is explained by Brown (1971) as being due to sluggish reaction rates. Molybdenum released from solution of molybdenite is immobile under acidic conditions and is taken up by ferrimolybdite, limonite, and insoluble iron and molybdenum oxides as discussed earlier.

ZONE OF SUPERGENE ENRICHMENT

Supergene enrichment by secondary copper minerals takes place at or below the water table where downward-migrating acidic oxygenated leach solutions containing cuprous ion are reduced and neutralized. Secondary copper minerals selectively replace pre-existing sulphide minerals. Under certain conditions in the transition zone between the oxidizing and primary sulphide zone they precipitate as native copper, copper oxides, or copper carbonates. Native copper and oxide minerals may also form if groundwater table fluctuations expose secondary copper sulphide minerals and oxidation takes place while the water table is depressed.

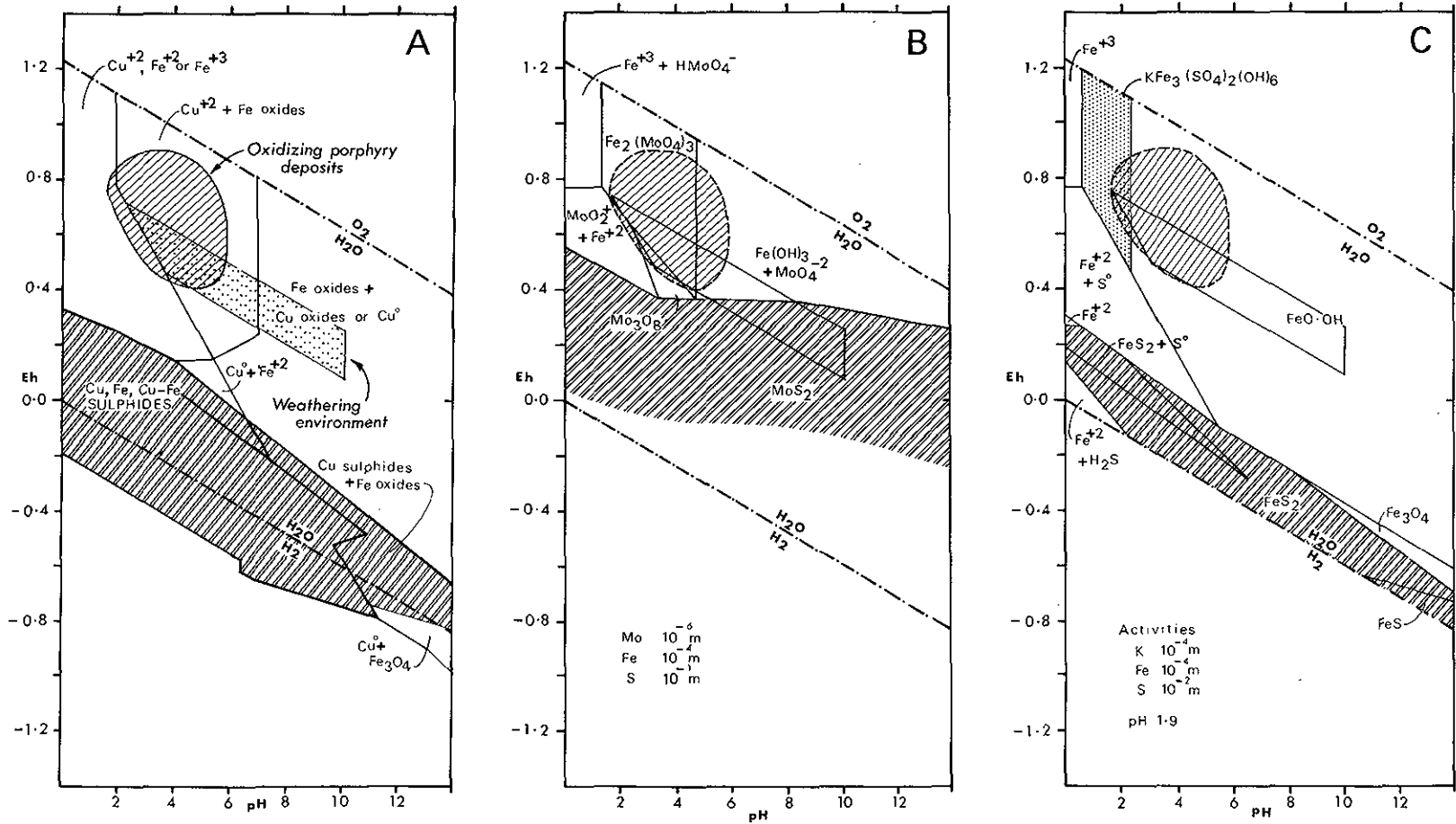


Figure 21. Mineral stability at 25° C and 1 ATM. A. Cu-Fe-S-O-H modified from Garrels (1960); B. Mo-Fe-S-O-H after Barakso and Bradshaw (1971); C. Fe-S-O-H in presence of K⁺ after Brown (1971). Field of weathering after Sato (1960).

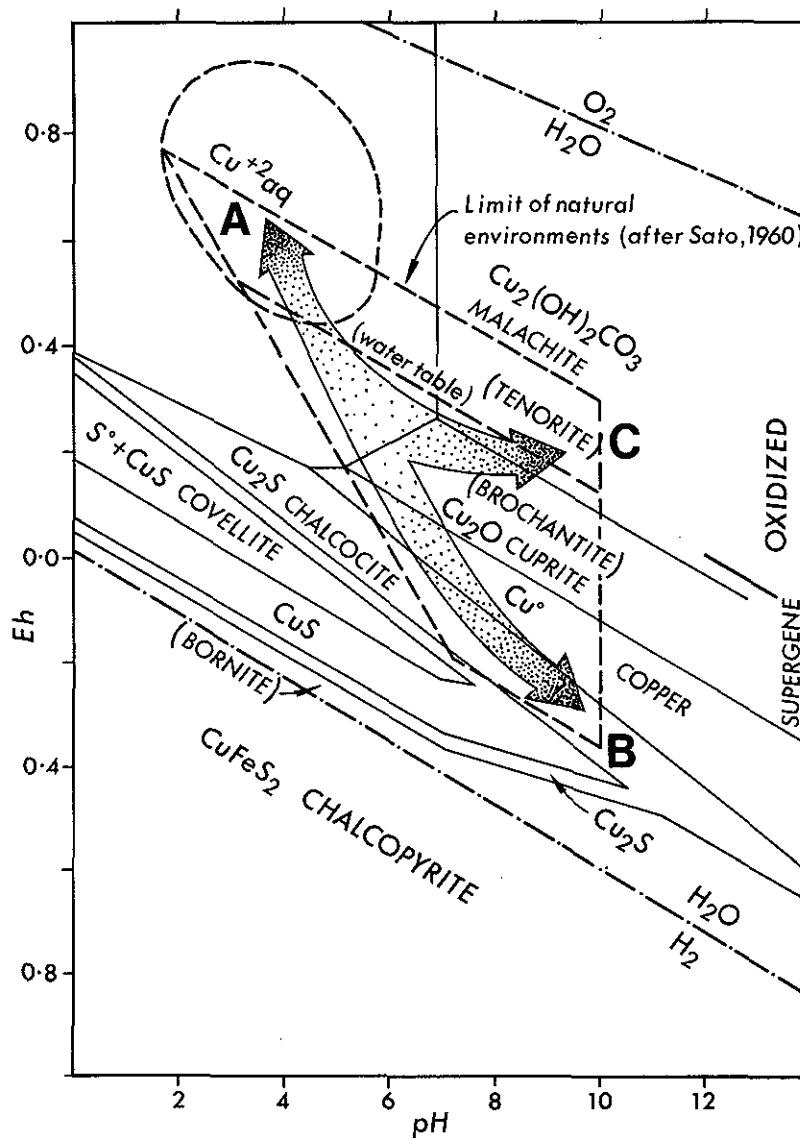


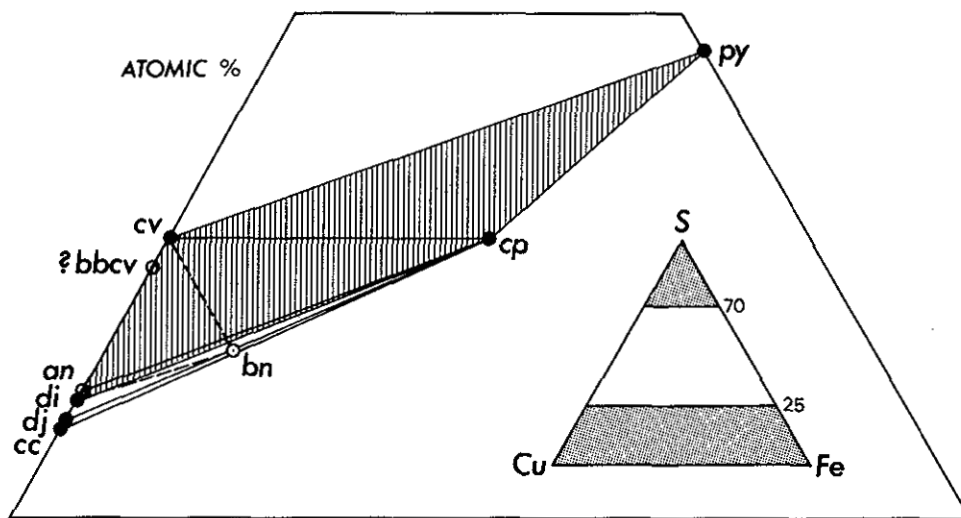
Figure 22. Stability fields in Cu-H₂O-CO₂-O₂-S system (including chalcopyrite) at 25° C and 1 ATM.

Reactions and products of the supergene process can be illustrated in a simplified manner in an Eh-pH diagram showing mineral stability fields of common minerals, as shown on Figure 22. Three processes can be envisioned as indicated by paths A → B, B → A, and A → C. More acidic conditions than those suggested by Sato (1960) and shown on Figure 22 probably occur in porphyry deposits. Thus points A and B may be shifted to the left in the diagram. A to B is the result of downward percolating leach solutions entering a relatively stable zone of groundwater saturation. Pre-existing sulphide minerals, first chalcopyrite (or bornite), later pyrite, are rimmed and replaced by 'chalcocite.' Near the water table neutralized solutions in the presence of oxygen may form tenorite or cuprite and native copper if reduction takes place. Path B to A is the result of *in situ* reactions

where sulphide minerals react with pore waters whose acidity and oxidation potential are increasing. This is the case where the water table is being depressed, and the zone of oxidation is encroaching on existing sulphide minerals, or groundwater flow patterns change resulting in additions of leach solutions. As acidity increases, iron and sulphur are leached from copper-iron sulphides in the presence of copper ions. Secondary copper sulphides are deposited starting with covellite, followed under ideal conditions by minerals with successively higher copper content, ideally anilite, digenite, djurleite, chalcocite, and possibly native copper and copper oxides. Path A to C is followed where leach solutions encounter reactive host rocks that neutralize and buffer solutions. Solutions in presence of calcite will not exceed pH 8.3 and, if hydrolysis of silicate minerals takes place, pH will range from 6 to 10 (Sato, 1960). Most commonly neutralizing reactions take place in limestone, along borders of basic dykes or other rocks with significant neutralizing potential and at depth where hydrolysis equilibria reactions take place in the zone of water-saturated primary mineralization. Cuprite, brochantite, tenorite, and native copper may form with 'fluffy' limonite as well as malachite and azurite where CO₂ concentration is high.

At Berg deposit, processes described by all three solution paths shown on Figure 22 are taking place simultaneously in different parts of the deposit. Path B to A takes place in the pyritic halo where propylitic pyrite-rich rocks are oxidizing. Initial conditions are described by area 'B' as oxidation begins in mineralized rocks exposed by erosion. As oxidation proceeds, solutions and products follow the path toward 'A.' Path B to A also describes ongoing processes within the supergene zone as erosion proceeds resulting in a downward-migrating groundwater table and encroachment of oxidation (weathering) conditions upon the zone of primary mineralization. Path A to B is followed by concentrated acidic leach solutions generated by oxidation (point 'A') which migrate downslope until they interact with the relatively stable groundwater table in the low-lying, highly fractured area around the quartz monzonite stock. Interaction of leach solutions with groundwaters results in migration of solutions from A to B (less acidic, more reducing conditions). Path A to C is followed locally where leach solutions encounter calcite-bearing dykes and are rapidly neutralized. This takes place both above and below the water table and accounts for copper enrichment by oxide and carbonate minerals in the zone of sulphide leaching and prevalence of cuprite (together with some brochantite) in andesite dykes.

Secondary copper sulphide minerals loosely described at Berg deposit as 'chalcocite' are identified by X-ray diffraction by Owens (1968) and this writer as covellite and digenite. Owens also reports traces of chalcocite and delafossite. Digenite and covellite are both found as partial replacement rims on chalcopyrite and pyrite. Complete replacement of small chalcopyrite grains up to 100 microns in size was seen by Owens (1968) but generally replacement rims are less than 10 microns thick and commonly are not more than a tarnish. In specimens examined by the writer covellite is more abundant than digenite, whereas Owens (1968) reports digenite in excess of covellite. Mineral associations found (Fig. 23) are chalcopyrite-pyrite-covellite and chalcopyrite-covellite-digenite-pyrite (a nonequilibrium assemblage). The observed supergene assemblages are com-



covellite	cv	CuS
blaubleibender covellite	bbc _v	Cu _{1.1} S - Cu _{1.4} S
anilite	an	Cu _{1.75} S
digenite	di	Cu _{1.765} S - Cu _{1.79} S
djurleite	dj	Cu _{1.96} S
chalcocite	cc	Cu ₂ S
chalcopyrite	cp	CuFeS ₂
bornite	bn	Cu ₅ FeS ₄

Figure 23. Mineral compositions showing possible phase relationships.

patible with phase relations suggested by studies in system Cu-Fe-S and Cu-S (Roseboom, 1966; Runnells, 1969; Morimoto and Koto, 1970; and Barton, 1973) and are consistent with the belief that supergene enrichment is an active process in its initial stages at Berg deposit. Result of supergene copper mineral deposition with an indicated enrichment factor of 1.25 or 25 per cent is shown on Figure 17. In plan (Fig. 24) zones underlain by 6.1 metres or more of 0.4 per cent copper in the supergene zone overlap extensively zones of primary or 'protore' with 0.2 per cent copper and thereby considerably expand ore reserves. Generalized cross-sections showing the relationship of the supergene zone to topography, the leached capping, and primary ore are shown on Figure 25.

Origin of the enrichment zone is debatable as to the time at which supergene processes were first initiated. Some workers believe that the enriched zone formed at least partially prior to glaciation. For example, Beaudoin and Mortensen (1973) report that approximately 90 metres of weak chalcocite enrichment is evident at high elevations on the eastern side of the pyrite halo. They conclude that this topographically high enrichment is pre-glacial in origin and remains as an early supergene zone that is perched above the present-day supergene blanket. Furthermore, they report that recent diamond drilling shows that lower limits of the chalcocite zone, at least locally, are independent of topography.

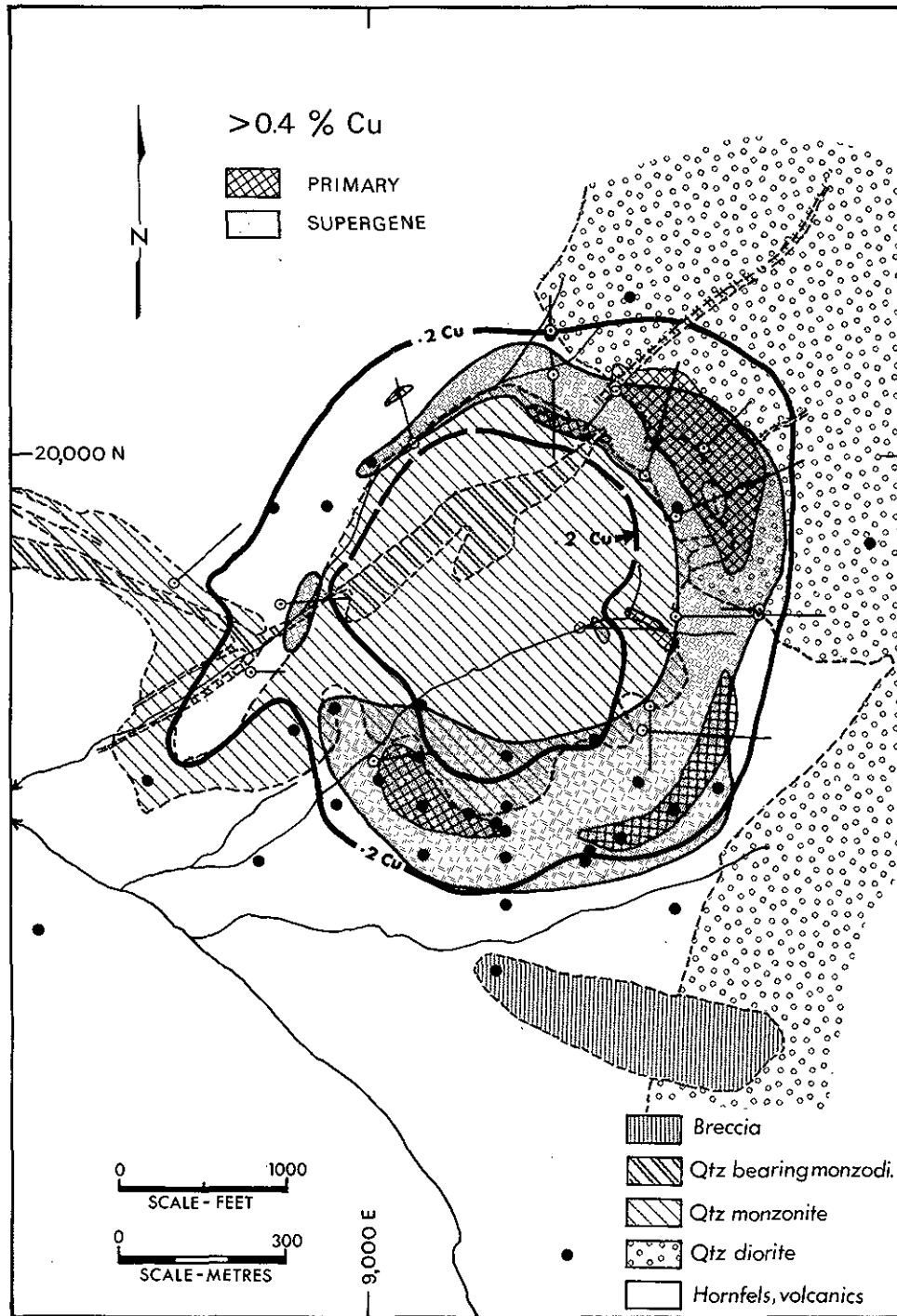


Figure 24. Primary and supergene copper minerals. Zones underlain by $\geq 0.4\% \text{ Cu}$.

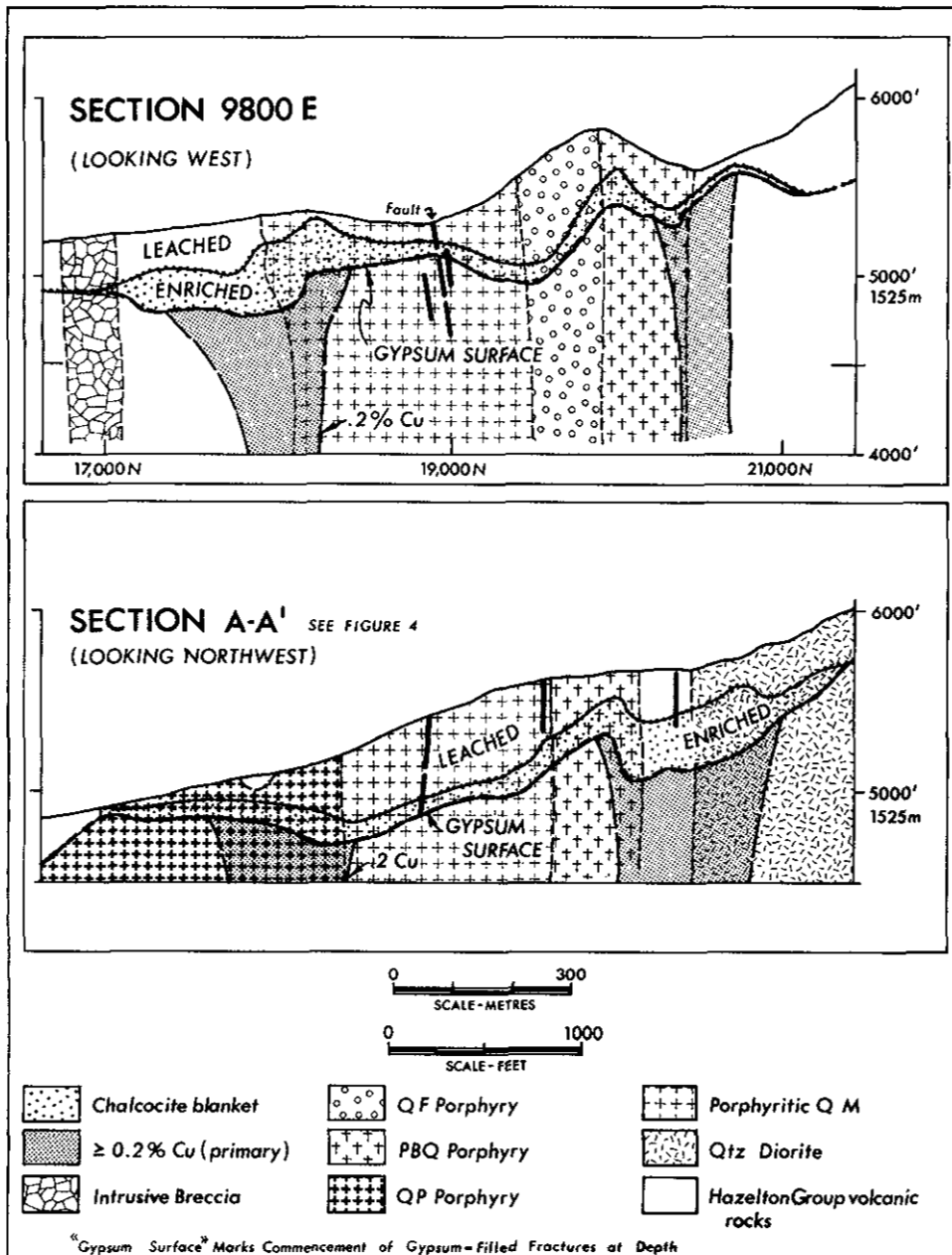


Figure 25. Berg deposit, idealized geologic sections.

This writer believes the supergene blanket is being formed by contemporary ongoing processes that represent a single-stage post-glacial phenomenon. The process began after Fraser (Wisconsin) glaciation or at earliest during deglaciation. It is difficult to envision other simple or more probable alternatives to how the enrichment blanket, which is so intimately related to present topography, could have survived repeated glaciation if it was pre-Pleistocene or an interglacial feature. Hematite, a common mineral in multiple-stage supergene zones, is generally absent at Berg deposit. Nonequilibrium assemblages and incipient replacement textures of secondary sulphide minerals suggest a short duration of supergene processes. Furthermore, the presence of Cretaceous rocks on ridges adjacent to the Berg deposit (*see* Fig. 3) makes it doubtful that the mineralized zone was exhumed by erosion prior to Pleistocene glaciation. Thus, as deduced from a map showing speculative ice-marginal positions (V. K. Prest, 1970, pp. 706, 707) supergene processes responsible for the observed chalcocite blanket were probably initiated not earlier than 10 000 to 12 000 BP.

Ten thousand years following glaciation is ample time for the observed supergene effects to be developed and the 38-metre-thick leached zone to form in the highly fractured, strongly dissected terrane at Berg deposit. Lovering (1948) calculated that at San Manuel total oxidation of 3.5 to 5 per cent pyrite could take place to depths of 150 to 180 metres (500 to 600 feet) in 40 000 to 47 000 years. Also, leach dumps in the southwestern United States (whose porosity is not much greater than that of weathered crackled zones in porphyry deposits) have complete oxidation of 5 per cent pyrite to a depth of 30 metres in a few tens of years (D. Norton, 1966, unpublished report, Kennecott Copper Corporation). Titley (1975) has described porphyry deposits in which extensive leached cappings and supergene enrichment blankets have formed in mineralized zones associated with intrusions as young as 1 110 000 years.

MINOR ELEMENTS IN PYRITE

INTRODUCTION

Minor element content of pyrite was investigated in order to:

- (a) Define concentration levels of minor elements in pyrite from a porphyry copper-molybdenum deposit.
- (b) Test if zoning of minor elements in pyrite is evident.
- (c) Relate zoning patterns and concentration ranges of minor elements in pyrite to mineralogical zoning (particularly the zone of primary copper sulphides).
- (d) Test if host rock compositions and different paragenetic types of pyrite influence the character or quantity of minor elements in pyrite.

Pyrite was selected because it is the most abundant sulphide mineral in porphyry copper deposits, is ubiquitous throughout mineralized areas, and is treated relatively easily to obtain a clean concentrate. Representative samples from the 45 available drill holes and 9 outcrops were taken to give maximum possible coverage of the mineralized area. In total, 135 analyses representing 100 sample sites were obtained. The samples do not constitute a random sample set because the diamond-drilling program tested specific areas with economic mineral potential rather than random areas. Bias is, thus, introduced into the statistical basis of the data by a preponderance of samples from the zone of copper-molybdenum mineralization. There is proportionally less representation of pyrite from the barren core, pyritic halo, and weakly mineralized peripheral rocks. However, any weakness introduced into the statistical basis of this study by nonrandom sampling is possibly overshadowed by having a maximum of information from the mineralized zone.

The samples were analysed by emission spectroscopy. Sampling procedures and rationalization, analytical methods, and statistical procedures used are described in detail in the original work (Panteleyev, 1976) and are summarized elsewhere by Gosh-Dastidar (1970), Dawson (1972), and Dawson and Sinclair (1974).

The sample set of 100 pyrites consists of 78 specimens of disseminated or fracture-controlled finely dispersed sulphides (hereafter collectively referred to as 'disseminated' pyrite) and 22 vein specimens. Of the 78 disseminated pyrites, 47 were taken from hornfels, 9 from quartz diorite, 18 from quartz monzonite, and 4 from peripheral volcanic rocks. Vein pyrite was mainly from quartz veins with various sulphide and gangue associations. In addition to pyrite, five chalcopyrite samples and one sphalerite sample were analysed to determine the effects of contamination by these minerals in pyrite (see Appendices A and B).

TABLE 5. ANALYTICAL PRECISION				
Error (Y) as a function of concentration (\bar{X}), (4 elements with sufficient data)				
Ag: $Y = -0.0885 + 0.323\bar{X}$				
Pb: $Y = 10.014 + 0.214\bar{X}$				
Ni: $Y = 0.723 + 0.123\bar{X}$				
Co: $Y = -43.2 + 0.372\bar{X}$				
PERCENTAGE RELATIVE ERROR (ALL DATA)				
Element	No. of pairs	Average concentration (\bar{X}) (ppm)	S.D.	Per cent relative error (SD/ \bar{X})
As	10	1 095.0	301.5	27.5
Bi	24	13.8	5.1	37.0
Co	31	463.0	199.7	43.1
Ni	31	185.8	71.1	38.3
Cu	16	340.4	66.6	19.6
Pb	31	114.5	48.5	42.3
Zn	27	80.9	56.3	69.6
Ag	31	12.2	11.3	92.7
Ti	18	255.9	79.5	31.1
Mo	20	23.6	16.0	67.8
Mn	18	31.6	8.9	28.2

Sample variability is readily evident; some can be explained by analytical (including sampling) error but precision and accuracy of the spectroscopic method used are sufficient for zoning to be demonstrated. A summary of analytical precision and estimate of relative error as a function of concentration, as calculated by P. Matysek after the method of Thompson and Howarth (1978) is given in Table 5. Accuracy of the spectroscopic method can be assessed by comparing results with those obtained independently by atomic absorption spectrometry (AA) as shown in Table 6.

TABLE 6. COMPARISON OF SPECTROGRAPHIC AND ATOMIC ABSORPTION ANALYSES* OF PYRITE CONCENTRATES

(All Analyses in ppm)

Sample No.	Mo	Cu	Zn	Pb	Ag	Ni	Co	Mn	Bi
15-187									
Spec i	6	500	16	20.5	2.5	168	115	5	2
Spec ii	1	490	21	12	2.5	142	93	5	4
AA	11	470	50	22	4.0	160	117	12	5
29-226									
Spec	6	330	53	18.5	8.0	62	620	5	1.5
AA	1	415	60	18	4.7	60	520	9	5
37-480									
Spec i	0	198	80	20.5	1.5	850	560	5	3
Spec ii	1	102	52	16	1.0	1 000	600	5.5	7.5
AA	1	122	44	21	2.1	1 000	415	45	5

*Atomic absorption analyses performed by Mr. H. Goddard, Kennco Explorations, (Western) Limited, 1968.

After examination of analytical precision and accuracy of the spectrographic method and consideration of analytical results, cobalt and nickel were found to be the most consistently useful elements present in pyrite. Lead and zinc were useful if no contamination of pyrite by other sulphide minerals was evident. Silver, bismuth, and manganese may be useful if sample variability is large as these elements suffer from low analytical precision. Arsenic is of limited use because of its high (300 ppm) detection limit. Copper, molybdenum, titanium, cadmium, and antimony suffer from contamination problems. Other elements were not detected in sufficient quantity to be meaningful (*see* Appendix A).

UNIVARIATE ANALYSIS

FREQUENCY DISTRIBUTION PLOTS (HISTOGRAMS)

Histograms illustrating distributions of minor elements in Berg pyrite are shown on Figures 26, 27, and 28. A normal curve, using the observed mean and standard deviation, is fitted to the transformed data on Figure 26. The mathematical expression for such Gaussian (normal) distributions and tables of numerical constants necessary for their calculation are taken from Dixon and Massey (1969). All data are summarized in Table 7 which gives the number of analyses, means (measure of central tendency), and standard deviations (measure of dispersion of the data). Both arithmetic and logarithmic values are given for comparison.

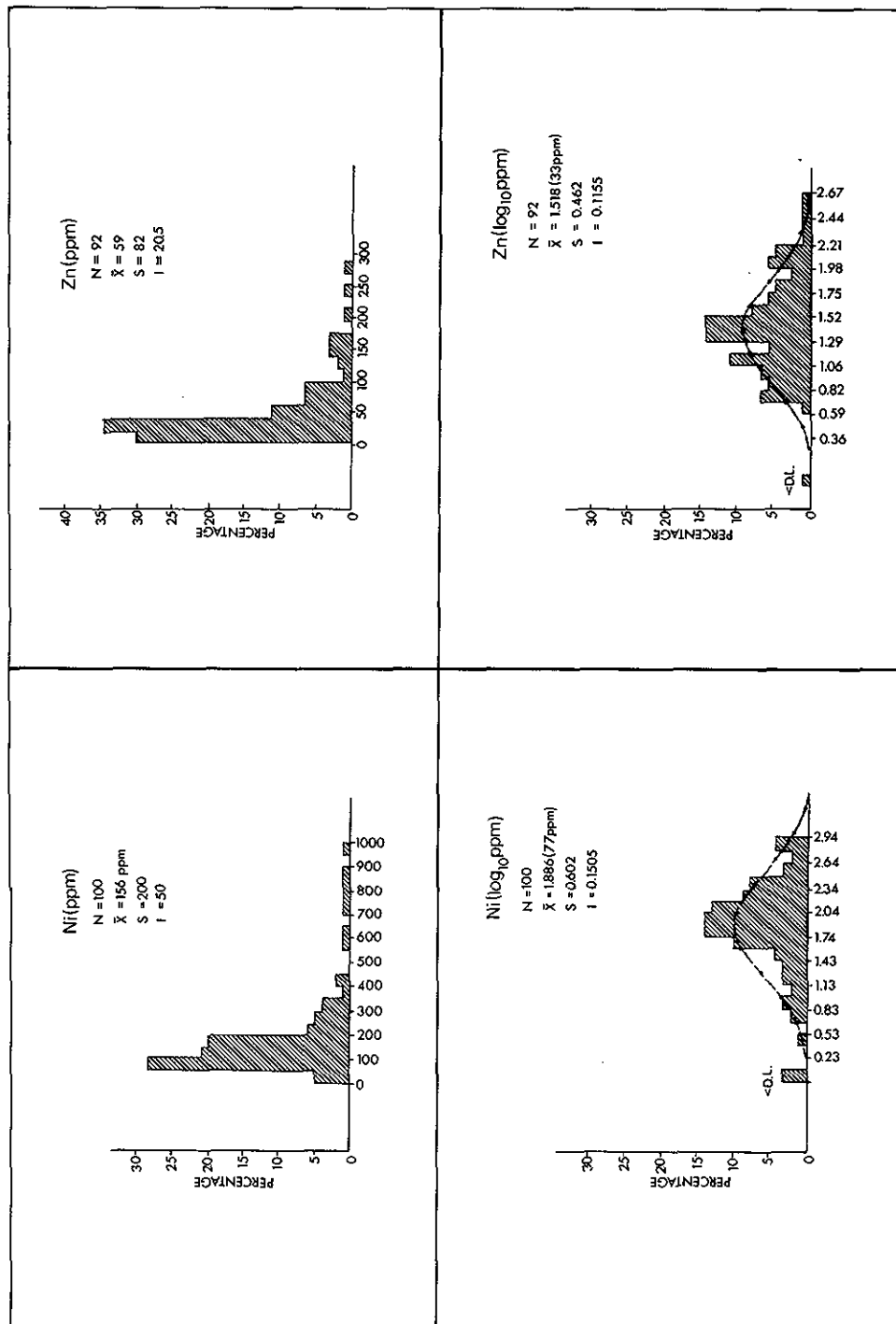


Figure 26. Ni and Zn content of pyrite. Normal curve fitted to \log_{10} data.

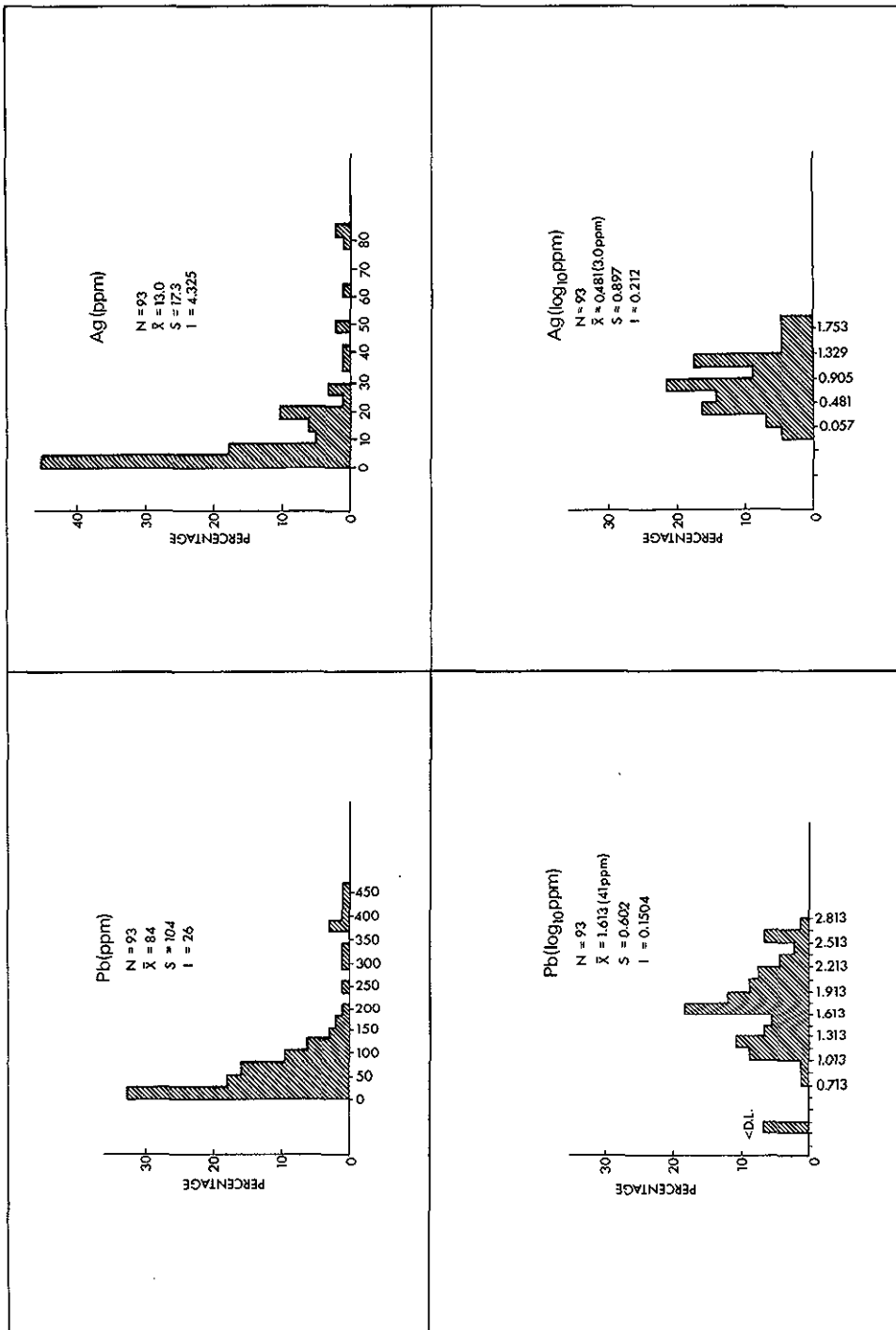


Figure 27. Pb and Ag content of pyrite.

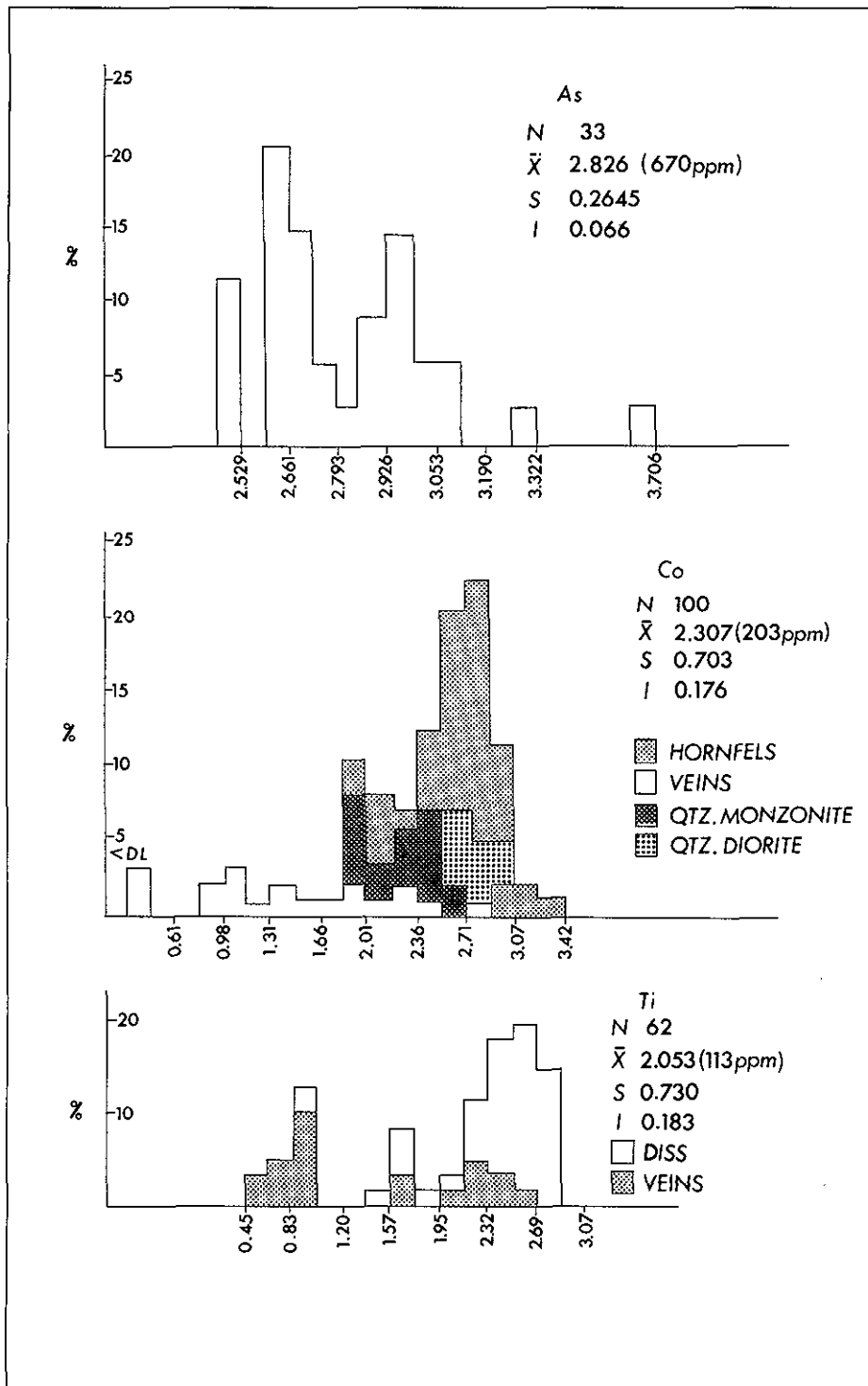


Figure 28. Frequency distributions of As, Co, and Ti.

TABLE 7. SUMMARY - MEAN AND STANDARD DEVIATION FOR ALL ANALYSES WITH DETECTABLE QUANTITIES (Maximum number = 100)					
Element	Samples Within Detection Limits	Arithmetic (ppm)		Logarithmic Log ₁₀ (ppm)	
		Mean	S. D.	Mean	S. D.
As	34	1 237	2 528	2.860 (725)	0.343
Bi	96	12.4	21.9	0.551 (3.6)	0.738
Co	100	406	354	2.307 (203)	0.703
Ni	100	156	200	1.886 (77)	0.587
Cu	55	263	194	2.257 (181 .)	0.461
Pb	93	84	104	1.613 (41)	0.602
Zn	92	59	82	1.518 (33)	0.462
Ag	93	13.0	17.3	0.481 (3.0)	0.847
Mo	75	13.0	20.0	0.3741 (2.4)	1.0335
Ti	62	256	255	2.053 (113 .)	0.730
Mn	89	5.5	10.5	0.001 (1.0)	0.960

It is evident in a few histograms (for instance, Fig. 28) that some minor element distributions might contain more than one population. Arsenic appears to be bimodal and cobalt could contain three populations. The two apparent populations of arsenic might be simply due to sampling error for the sample set contains only 33 analyses. Three populations of cobalt appear to be present and appear to be due to pyrite from different host rocks. Populations of cobalt from vein pyrite and two types of disseminated pyrite (one from quartz monzonite, the other from hornfels and quartz diorite) appear to be different populations. Titanium distribution is not readily explained; the two apparent populations are composed of pyrite from veins and all host rock types.

F AND t TESTS

One attribute of Berg minor element data shown by frequency distributions is that vein pyrite generally has lower concentrations of elements than disseminated pyrite. Thus, an hypothesis can be tested using t and F tests that one cause of polymodal distributions is mixing of vein pyrite and disseminated pyrite, both distinct populations. Figure 29 shows nickel distribution in which vein and disseminated pyrite is differentiated and tested by t and F tests. Table 8 summarizes t and F tests of vein versus disseminated pyrite for all elements determined.

The results summarized in Table 8 are definitive. F and t probabilities of cobalt, nickel, copper, zinc, titanium, and possibly lead, silver, molybdenum, and manganese are sufficiently low that it can be assumed populations of vein pyrite are distinct from those of disseminated pyrite. The only exceptions are arsenic and bismuth which are the only two of all elements determined that are believed to be incorporated in pyrite by anion substitution rather than cation substitution, inclusion in lattice defects, or location in interstitial sites.

TABLE 8. CALCULATED t and F PROBABILITY OF VEIN PYRITE VERSUS DISSEMINATED PYRITE (Based on log ₁₀ values of all available data)								
Element	Vein			Disseminated			F Prob.	t Prob.
	N	X	S.D.	N	X	S.D.		
As	6	2.898	0.242	24	2.808	0.272	.87	.46
Bi	22	0.532	0.746	66	0.697	0.595	.16	.36
Co	22	1.296	0.730	74	2.572	0.333	.00	.00
Ni	22	1.143	0.659	74	2.060	0.358	.00	.00
Cu	19	1.889	0.522	33	2.459	0.252	.00	.00
Pb	20	1.423	0.872	69	1.643	0.498	.00	.29
Zn	20	1.260	0.582	68	1.560	0.389	.02	.04
Ag	20	0.664	0.508	69	0.922	0.426	.29	.05
Mo	20	0.381	0.494	51	0.808	0.639	.22	.00
Ti	20	1.389	0.729	39	2.375	0.496	.04	.00
Mn	20	0.275	0.447	48	0.515	0.493	.65	.04

Polymodal distributions resulting from mixing of pyrite from different rock types are evident for certain elements, for example, cobalt on Figure 28. A more subtle expression of a polymodal distribution can be seen on Figure 29 where a number of (partially ?) coincident populations might be present. Figure 30 shows the distribution of nickel in disseminated pyrite (the disseminated pyrite portion of Fig. 29) with separate plots of pyrite from different sources.

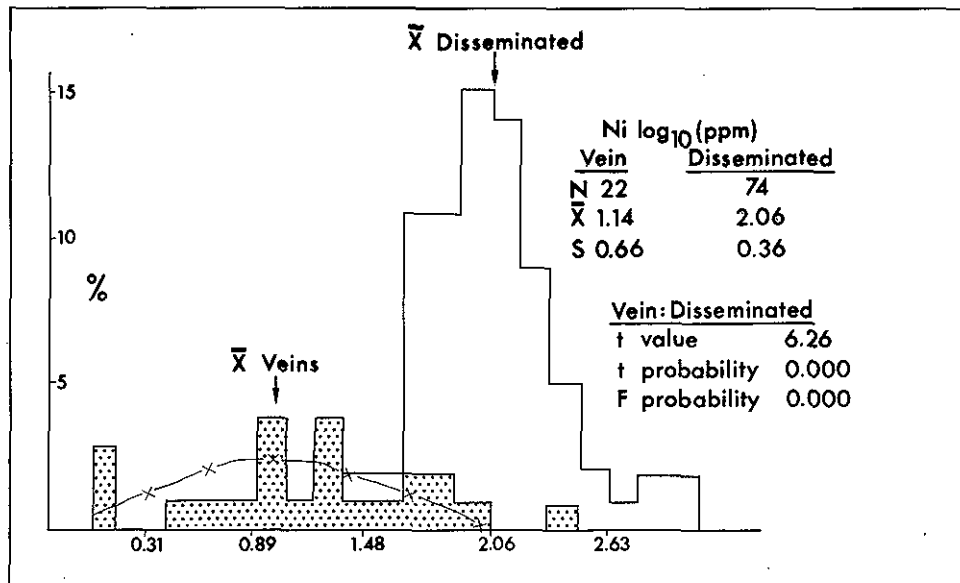


Figure 29. Bimodal distribution containing vein and disseminated pyrite populations (normal curves fitted to the data).

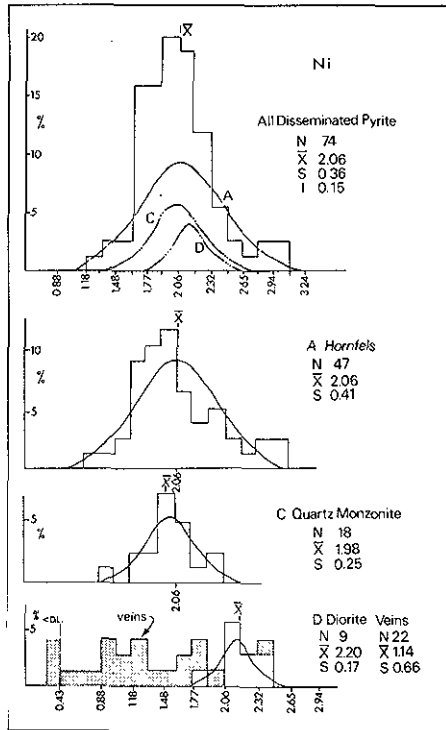


Figure 30. Distribution of Ni in pyrite. Data grouped according to host rock. A, C, D are fitted normal curves.

An hypothesis can be tested that the polymodal distribution of nickel in disseminated pyrite is due to a number of populations representing pyrite from different host rocks. t and F tests comparing distributions of pyrite from hornfels, quartz monzonite, and diorite are summarized in Table 9 and illustrated on Figure 30. Vein pyrites are also compared to pyrite from other host rocks.

TABLE 9. F and t TESTS - Ni IN PYRITE		
(No. of Samples: Hornfels, 47; Diorite, 9; Quartz Monzonite, 18; Veins, 22)		
Source	F Prob.	t Prob.
Hornfels: Quartz Monzonite	0.03	0.37
Hornfels: Diorite	0.01	0.10
Quartz Monzonite: Diorite	0.27	0.01
Hornfels: Veins	0.01	0.00
Quartz Monzonite: Veins	0.00	0.00
Diorite: Veins	0.00	0.00

The t and F tests indicate with a high confidence level (99 per cent or greater) that nickel in vein pyrite is a discrete population compared to nickel in disseminated pyrite from any of the three host rock types. The possibility of disseminated pyrite containing two or more populations of nickel is not nearly so certain. A 90-per-cent t and 99-per-cent F probability allows the conclusion that hornfels and diorite may contain distinct populations of nickel in pyrite, but pyrite from hornfels and quartz monzonite cannot be distinguished and may be part of the same population. A summary of t and F tests of all elements from pyrite in different rock types is given in Table 10.

Conclusions drawn from t and F tests (Tables 8, 9, and 10) are:

- (a) Vein pyrite is part of a population separate from disseminated pyrite on the basis of cobalt, nickel, copper, zinc, titanium, and possibly lead, silver, molybdenum, and manganese; but not arsenic and bismuth. However, except on the basis of cobalt and nickel, vein pyrite cannot be distinguished with any certainty from disseminated pyrite if disseminated pyrite is further subdivided into smaller groups according to host rock type. Larger sample sets from each type of host rock could possibly overcome this uncertainty.
- (b) Only a few elements in disseminated pyrite can be shown to constitute separate populations on the basis of host rock composition. For example, for zinc there is a 98-per-cent or greater t and F probability that pyrite from hornfels is distinct from that in quartz monzonite. Similar high probabilities for nickel and zinc indicate that separate populations of pyrite are present in hornfels and quartz diorite. Also, cobalt in pyrite from quartz diorite is distinct from that in quartz monzonite. In a number of other cases, separate populations are inferred by low F probabilities but t probabilities are high, and vice versa. Thus, no generalization can be made on the basis of t and F tests about populations of minor elements in disseminated pyrite from different host rocks. Polymodal distributions may, but need not be, caused by mixing samples from different host rocks. Each element must be looked at on an individual basis.

CUMULATIVE PROBABILITY PLOTS

Graphic description, interpretation, and resolution of polymodal data is possible, using cumulative probability plots. Form of cumulative probability curves can be used to determine if distributions are normal, lognormal, or polymodal. A second use is resolution of polymodal data into components (constituent populations) and definition of parameters of constituent populations. Use of probability plots is discussed in detail and clearly illustrated by Sinclair (1974, 1976).

In this study cumulative probability plots are used as a supplement to other univariate procedures of data analysis. If all Berg minor element data are plotted on a cumulative

TABLE 10. SUMMARY OF t AND F TESTS FOR ALL ELEMENTS
(Significance of host rock type)

Element	No. of Samplest	t Prob.	F Prob.	Element	No. of Samplest	t Prob.	F Prob.
HORNFELS : QUARTZ MONZONITE				VEINS: HORNFELS			
As	17 : 2	.02*	.41	As	6 : 17	.35	.75
Bi	46 : 18	.08	.58	Bi	22 : 46	.62	.13
Co	47 : 18	.00**	.69	Co	22 : 47	.00**	.00**
Ni	47 : 18	.37	.03*	Ni	22 : 47	.00**	.00**
Cu	22 : 9	.33	.78	Cu	19 : 22	.00**	.00**
Pb	45 : 16	.00**	.31	Pb	20 : 45	.78	.00**
Zn	45 : 16	.02*	.01**	Zn	20 : 45	.18	.00**
Ag	45 : 16	.78	.35	Ag	20 : 45	.12	.13
Mo	34 : 15	.21	.88	Mo	20 : 34	.05*	.22
Ti	33 : 5	.07	.28	Ti	20 : 33	.00**	.07
Mn	45 : 16	.45	.77	Mn	20 : 45	.17	.67
QUARTZ MONZONITE : DIORITE				VEINS : QUARTZ MONZONITE			
As	2 : 5	.14	.45	As	6 : 2	.26	.46
Bi	18 : 8	.20	.91	Bi	22 : 18	.07	.48
Co	18 : 9	.00**	.09	Co	22 : 18	.00**	.00**
Ni	18 : 9	.01**	.27	Ni	22 : 18	.00**	.00**
Cu	9 : 2	.62	.69	Cu	19 : 9	.00**	.06
Pb	16 : 8	.67	.35	Pb	20 : 16	.03*	.00**
Zn	16 : 7	.70	.81	Zn	20 : 16	.01**	.40
Ag	16 : 8	.06	.92	Ag	20 : 16	.15	.72
Mo	15 : 6	.53	.96	Mo	20 : 15	.01**	.37
Ti	5 : 1	---	---	Ti	20 : 5	.00**	.09
Mn	16 : 8	.20	.39	Mn	20 : 16	.09	.55
HORNFELS : DIORITE				VEINS : DIORITE			
As	17 : 5	.74	.85	As	6 : 5	.49	.93
Bi	46 : 8	.86	.80	Bi	22 : 8	.84	.53
Co	47 : 9	.20	.05	Co	22 : 9	.15	.00**
Ni	47 : 9	.10	.01**	Ni	19 : 9	.00**	.00**
Cu	22 : 2	.86	.60	Cu	20 : 2	.69	.76
Pb	45 : 8	.02*	.80	Pb	20 : 8	.87	.12
Zn	45 : 7	.08	.04*	Zn	20 : 7	.22	.71
Ag	45 : 8	.03*	.58	Ag	20 : 8	.17	.70
Mo	34 : 6	.14	.88	Mo	20 : 6	.01**	.56
Ti	33 : 1	---	---	Ti	20 : 1	---	---
Mn	45 : 8	.03*	.46	Mn	20 : 8	.00**	.65

†Number of samples varies because only samples with detectable (i.e., measurable) minor element concentrations can be compared.

Level of Significance: * = 95 per cent; ** = 99 per cent.

probability plot (except arsenic for which there is insufficient data), the following results are apparent:

- (a) Bismuth, cobalt, nickel, copper, lead, and zinc distributions appear to be polymodal, each consisting of at least two lognormal populations.
- (b) Silver and molybdenum appear to have single, lognormally distributed populations.
- (c) Titanium (not shown on Fig. 31) has a single, normally distributed population, or the distribution is a complex, polymodal mixture of lognormal populations.

Interpretation of polymodal cumulative probability curves suggests that bimodal populations of cobalt, nickel, copper, and lead consist of one large group of samples with generally higher values than the smaller population. This is readily interpreted to be a result of mixing disseminated and vein pyrite. Zinc distribution is polymodal but is difficult to interpret. Two populations of about equal proportions appear to be present, but the two are partly coincident and mask each other. Bismuth and manganese can be interpreted to consist of two populations: one with detectable amounts of metal; the other with amounts below the analytical detection limits. Normal distribution of titanium is anomalous. On the basis of its erratic behaviour it is suspected that titanium is present in included mineral grains. Normal distribution of analytical results might, therefore, be one criterion of contamination in minor element studies.

Resolution of polymodal data into component populations using cumulative probability plots is not necessary in this study since type of pyrite, its source, geological significance, mean, and variance of each sample group, and the proportions of all component populations are known from sampling. However, the method can be illustrated and conclusions from other univariate procedures can be double checked. F and t tests as well as histograms show, with the exception of bismuth, that vein and disseminated pyrites are distinct and, with very few exceptions, disseminated pyrite appears to constitute single populations of minor elements regardless of host rock.

Disseminated pyrite (Fig. 31) appears to approximate single, lognormally distributed, measured populations of copper, lead, silver, and possibly molybdenum, bismuth, and manganese. A second population of bismuth, manganese, and molybdenum can be postulated if samples with less than detectable amounts of these elements are considered. Exceptions are cobalt, nickel, and zinc which appear polymodal in the cumulative probability plot, but this was indicated earlier on the basis of t and F tests which suggested the following: cobalt in pyrite from diorite and quartz monzonite, nickel and zinc from hornfels and diorite, and zinc in pyrite from hornfels and quartz monzonite are distinct populations. Thus, probability plots are a powerful analytical method, in this case capable of resulting in similar conclusions as t and F tests in conjunction with frequency distribution data.

A third, small population containing high nickel and low cobalt values is suggested in histograms but is clearly shown in probability plots. The population is made up of only

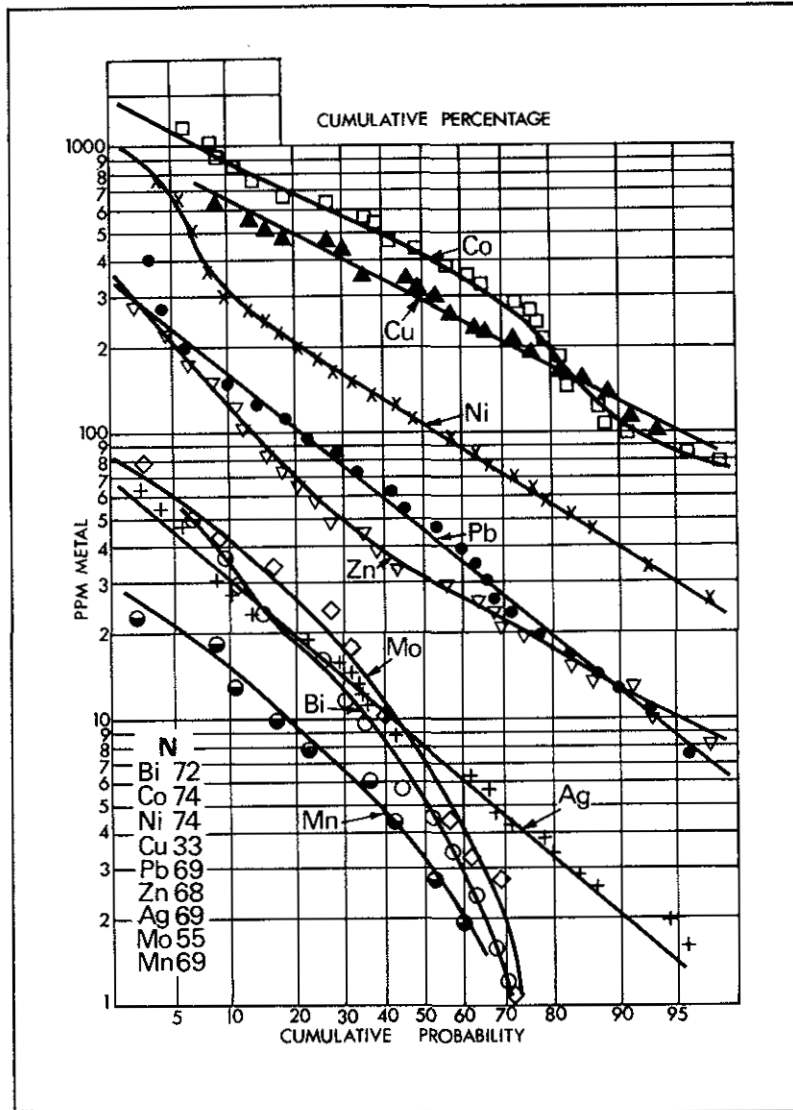


Figure 31. Cumulative probability. Minor elements in disseminated pyrite.

five samples but they are all from the pyritic halo zone. Further sampling might reveal that pyrite-rich rocks peripheral to the zone of copper-molybdenum mineralization are represented by nickel-rich pyrite that constitutes a separate population.

BIVARIATE ANALYSIS

CORRELATION AND SIMPLE REGRESSION

Bivariate analysis including correlation and simple regression was undertaken to examine relationships between paired variables. Correlation describes the interaction or

association of variables without causal effect. Correlation coefficients were computed for all pairs of variables (Table 11). The data were treated, first collectively, and then subdivided into groups according to source of pyrite to see if any trends or significant differences between various types of pyrite were apparent.

TABLE 11. CORRELATION OF PAIRED VARIABLES											
All Data N = 100											
Var.	As	Bi	Co	Ni	Cu	Pb	Zn	Ag	Mo	Ti	Mn
As	1.0000										
Bi	-0.1500	1.0000									
Co	0.0827	-0.0489	1.0000								
Ni	0.2143	0.0026	0.8574**	1.0000							
Cu	-0.1670	-0.0896	0.6342**	0.5356*	1.0000						
Pb	0.2261	0.4955**	0.1438	0.1745	-0.1522	1.0000					
Zn	0.1543	0.3254	0.3568	0.3619	0.1749	0.6762**	1.0000				
Ag	0.0717	0.5107**	0.3455	0.2066	0.1422	0.5229*	0.4437*	1.0000			
Mo	-0.2260	0.1196	0.3066	0.2490	0.1892	0.2564	0.1867	0.5285*	1.0000		
Ti	-0.5396	0.1457	0.4502	0.3681	0.5816*	0.0740	0.2330	0.0946	0.2055	1.0000	
Mn	0.2790	0.0538	0.2936	0.3301	-0.0186	0.3862	0.3962	0.2400	0.0614	0.1477	1.0000
Hornfels and Quartz Diorite N = 56											
Var.	As	Bi	Co	Ni	Cu	Pb	Zn	Ag	Mo	Ti	Mn
As	1.0000										
Bi	-0.2342	1.0000									
Co	0.1080	-0.1338	1.0000								
Ni	0.1953	0.0435	-0.5314*	1.0000							
Cu	0.2595	-0.3998	0.4382	-0.0988	1.0000						
Pb	-0.1129	0.4801	0.1740	-0.1469	0.0520	1.0000					
Zn	0.0013	0.2294	0.2538	0.1999	-0.0206	0.6335**	1.0000				
Ag	0.0118	0.4215	0.3849	-0.0827	0.4808	0.5696*	0.4510	1.0000			
Mo	-0.2950	0.1794	0.3192	0.2056	0.1358	0.3998	0.2568	0.5971	1.0000		
Ti	-0.1479	0.4864	-0.2577	-0.0980	-0.2966	0.2349	0.4308	0.1960	-0.0562	1.0000	
Mn	0.2526	0.0260	0.1968	0.2053	0.0104	0.3484	0.3091	0.3077	0.1901	-0.0546	1.0000
Quartz Monzonite N = 18											
Var.	As	Bi	Co	Ni	Cu	Pb	Zn	Ag	Mo	Ti	Mn
As	1.0000										
Bi		1.0000									
Co		-0.4595	1.0000								
Ni		-0.1865	0.7992*	1.0000							
Cu		-0.3645	0.2566	-0.2042	1.0000						
Pb		0.1528	0.3603	0.4926	-0.1257	1.0000					
Zn		-0.3599	0.3310	0.4328	-0.2084	0.5215	1.0000				
Ag		0.2298	0.4931	0.5741	0.0887	0.6861	0.2650	1.0000			
Mo		-0.1584	0.5021	0.3179	0.3146	0.1031	-0.0380	0.6777	1.0000		
Ti		-0.8157	0.3616	-0.2986	0.6492	-0.7887	-0.3107	-0.6585	0.2334	1.0000	
Mn		-0.0158	0.4083	0.4048	-0.0553	0.4306	0.3398	0.3731	0.1434	0.3759	1.0000
Veins N = 22											
Var.	As	Bi	Co	Ni	Cu	Pb	Zn	Ag	Mo	Ti	Mn
As	1.0000										
Bi	-0.2943	1.0000									
Co	0.3568	-0.0941	1.0000								
Ni	0.5479	-0.1753	0.8745**	1.0000							
Cu	0.2950	-0.0496	0.4397	0.5351	1.0000						
Pb	-0.7512	0.6052	-0.0275	-0.0702	-0.3390	1.0000					
Zn	0.1834	0.6813	0.2621	0.1282	0.1338	0.7222*	1.0000				
Ag	0.5528	0.7868*	0.3512	0.1665	0.1437	0.5481	0.7470*	1.0000			
Mo	0.3719	0.0860	0.2993	0.2742	0.0647	0.2008	0.3383	0.3015	1.0000		
Ti	-0.7326	-0.0978	-0.0200	-0.0314	0.4562	-0.3402	-0.1174	-0.1655	0.1782	1.0000	
Mn	-0.4897	0.0643	0.0761	-0.0103	-0.3954	0.3567	0.2185	0.2029	-0.0111	0.0452	1.0000

Level of Significance: * = 95 per cent; ** = 99 per cent.

TABLE 12. R ² AND F RATIOS FOR ALL DATA OF ALL PAIRS OF VARIABLES HAVING SIGNIFICANT CORRELATION		
Variables	F Ratio	R ²
Co : Ni	272	0.735**
Pb : Zn	75.8	0.457*
Co : Cu	35.7	0.402
Ni : Cu	21.3	0.287
Cu : Ti	19.4	0.338
Pb : Ag	34.3	0.273
Ag : Mo	27.9	0.279
Bi : Ag	31.8	0.261
Pb : Bi	29.3	0.246
Ag : Zn	22.1	0.197

Level of Significance: * = 95 per cent; ** = 99 per cent

Simple (linear) regression examines the interdependent relationships of paired variables and can be used to measure the amount or degree of variation in a variable due to variation in the other variable. The proportion of total variation or measure of variation explained by the interdependence of the variables compared to the total variation is called R². Table 12 lists R² and F ratios (variance ratios) for pairs of variables with significant correlation as listed in Table 11.

From preceding discussion it is apparent that the greatest amount of association at statistically significant levels is between cobalt and nickel, and also lead and zinc. A least squares regression line can be calculated for the paired variables as shown on Figure 32.

A regression plot of cobalt as a function of nickel is useful as a further means of discriminating between types of pyrite, as shown on Figure 33. Pyrite from different sources falls into separate fields on the diagram. Vein pyrite and disseminated pyrite are the most distinct types. Within the group of disseminated pyrite, samples from peripheral volcanic rocks, quartz diorite, quartz monzonite, and many samples from hornfels occur in separate fields, although pyrite from hornfels shows wide dispersion. Overlap of some vein and disseminated pyrite is to be expected since the group of 'disseminated' pyrite in the sample set includes both disseminated and fracture-controlled pyrite and the distinction between fracture-controlled and vein pyrite is entirely arbitrary. As a generalization, most of the disseminated pyrite in the field of mixed vein and disseminated pyrite on Figure 33 is from the pyritic halo, and the majority of pyrite in the disseminated field is from the zone of copper-molybdenum mineralization.

Differences in amounts of cobalt and nickel in pyrite appear to be proportional to amounts of these elements in the host rocks or vein-forming hydrothermal solutions. In general, cobalt and nickel decrease with increasing acidity of igneous rocks (Price, 1972). Similarly, original temperatures decrease from relatively high temperatures in basic volcanic rocks, lower ones in intermediate and acidic intrusions, and considerably

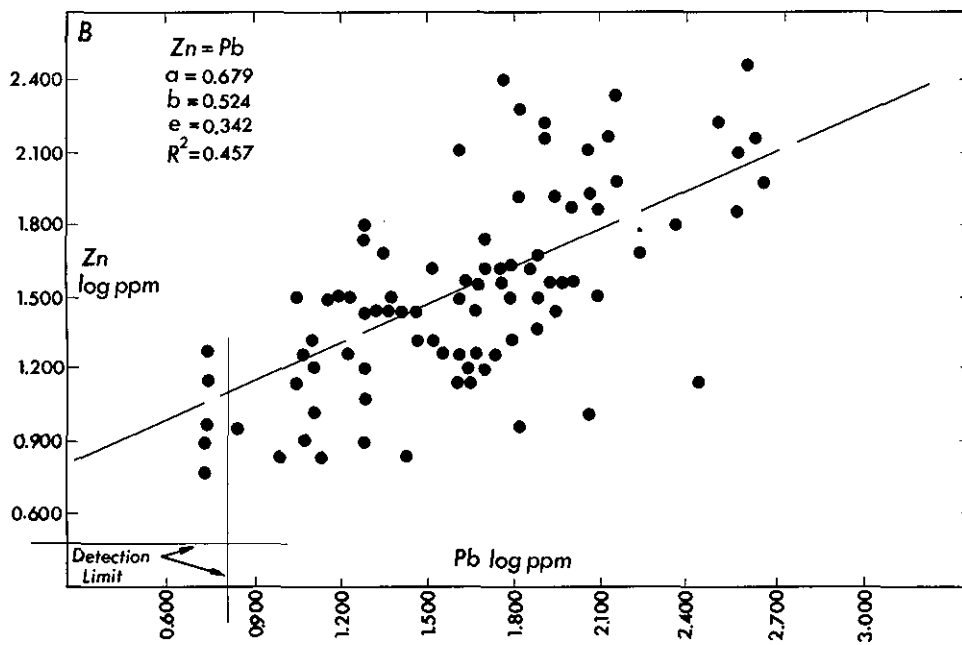
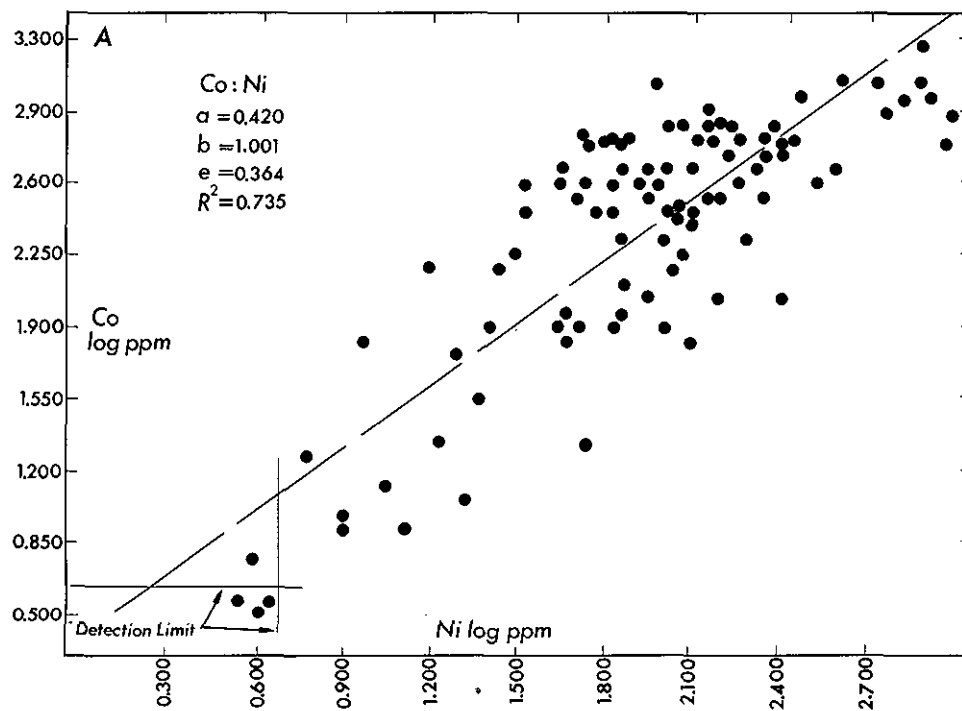


Figure 32. Linear least squares regression line ($Y = a + bX$) for Co:Ni(A) and Pb:Zn(B).

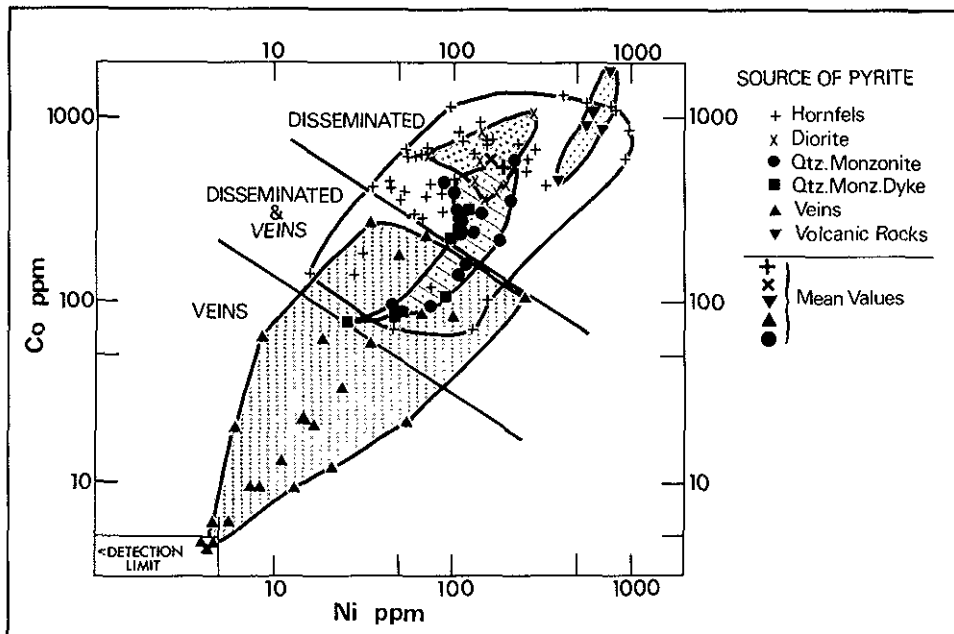


Figure 33. Cobalt-nickel scatter diagram showing pyrite according to source.

cooler ones in hydrothermal veins. Thus, differences in amount of cobalt and nickel seen on Figure 33 appear to correspond to changes in host rock composition and might also be influenced by temperatures at which pyrite crystallized.

COBALT-NICKEL RATIOS

Cobalt-nickel ratios (Fig. 34) in pyrite from veins and quartz monzonite are similar and are distinct from pyrite in hornfels, diorite, and possibly regional volcanic rocks, which are similar. The mean cobalt-nickel ratio for 96 samples with detectable amounts of both elements is 3:8. Price (1972) noted that this ratio is statistically indistinguishable from the mean cobalt-nickel ratio of pyrite from the large Endako and Casino porphyry deposits but is dissimilar to pyrites from smaller porphyry deposits at Tchentlo Lake and Moly mine, which have cobalt-nickel ratios of 31 and 27 respectively.

Some nickel enrichment is evident in vein pyrite ($Co/Ni = 2.40$) compared to disseminated pyrite ($Co/Ni = 4.28$). Since most veins are late-stage crosscutting features, late magmatic-hydrothermal fluids from which pyrite crystallized were evidently enriched in nickel as is the case in many other hydrothermal and advanced magmatic environments (Price, 1972). This implies that nickel-rich pyrite from the periphery of the pyritic halo may have formed during late mineralization as well (see Fig. 36 and discussion of zoning, pages 136-148).

Generally, use of cobalt-nickel ratios and quantities to characterize pyrite types or sources within individual deposits is limited due to large variations in minor element

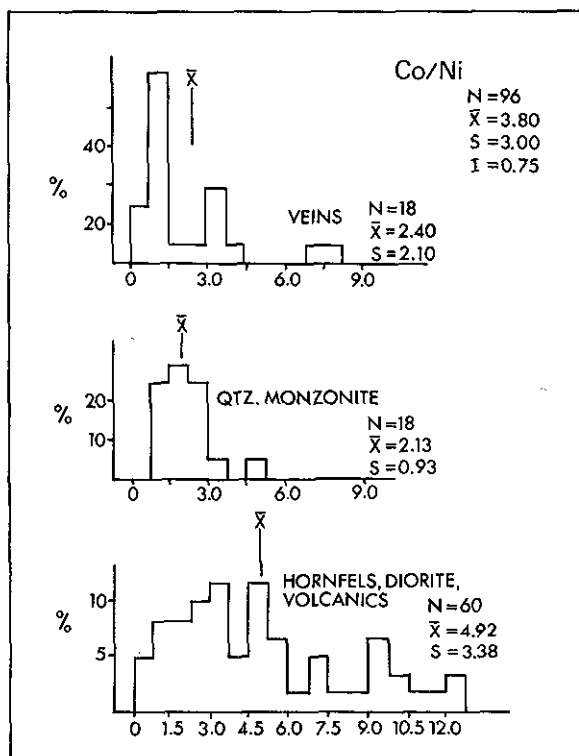


Figure 34. Co-Ni ratios of pyrite.

concentrations. Where differences are consistent and sufficiently large, such as between vein and disseminated pyrite at Berg deposit, concentration ranges and means of cobalt and nickel are characteristic and pyrite from unknown sources can be classified into fundamental groups.

Price (1972) has concluded that amounts of cobalt and nickel, and to a lesser extent cobalt-nickel ratios, are useful in distinguishing different types of pyrite from genetically distinct mineral deposits, namely: syngenetic (sedimentary), hydrothermal (including porphyry, vein, and skarn), and massive sulphide. Characteristic amounts of cobalt and nickel determined by Price are shown in Table 13.

TABLE 13. CHARACTERISTIC Co AND Ni CONCENTRATIONS IN PPM (After Price, 1972)			
	Syn- genetic	Hydro- thermal	Massive Sulphide
Co	41	141	486
Ni	65	121	56
Co/Ni63	1.17	8.7

Mean concentrations of cobalt (203 ppm) and nickel (77 ppm) of Berg pyrite are comparable to hydrothermal pyrite. Mean values of cobalt (374 ppm) and nickel (115 ppm) in disseminated pyrite can be distinguished with certainty only from syngenetic pyrite. Furthermore, when only vein pyrite is considered (cobalt = 20 ppm, nickel = 14 ppm), mean concentrations are most comparable to syngenetic pyrite but are also similar to hydrothermal (low temperature) lead-zinc deposits (Price, 1972). Therefore, any genetic classification of mineral deposits utilizing bivariate analysis and based on cobalt and nickel content of pyrite (and possibly any other pair of elements) is, at best, tenuous.

MULTIVARIATE ANALYSIS

Multivariate statistical analysis defines relationships between a number of variables or between samples for which three or more variables are measured. Factor analysis is a technique by which measured variables are combined in N-dimensional space into linear combinations of new variables (factors) by a mathematically sophisticated extension of correlation analysis. Relationships between variables are defined by R-mode analysis and those between samples or sample sites by Q-mode analysis. In this study Q-mode factor analysis is applied to the seven most frequently detected elements in the sample set — bismuth, cobalt, nickel, lead, zinc, silver, and manganese — as well as copper in vein pyrite. The technique has been described by Imbrie and Van Andel (1964) and Klován (1968), and applied to geochemical data by Nichol, *et al.* (1969), Wilson and Sinclair (1969), and Dawson and Sinclair (1974).

Treatment of pyrite geochemical data by Q-mode factor analysis accomplishes three main purposes:

- (a) The number of variables is reduced since the measured quantities are combined into multivariate 'factors.'
- (b) Associations and interrelations among variables are often realized that are not apparent on the basis of intuitive or subjective data examination.
- (c) The data generated are quantified and can be plotted on a map and contoured to reveal zoning patterns and areas of interest.

Data for factor analysis are divided into two fundamental groups, disseminated and vein pyrite, and the two groups are treated separately (Appendix C). Sixty-one sample sites of disseminated pyrite are plotted representing 74 analyses (Appendix D). Six factors account for 96.3 per cent of the variance but the four factors that explain 81 per cent of the variance are considered to be the most significant. These four factors define distinct zoning patterns and additional factors simply duplicate observed patterns and are redundant or are simply 'noise' that cannot be related to any geological cause or process. The successive varimax factor components computed are listed in Table 14 and the scores of the four factors plotted, in Table 15.

Factor	Components	% of Var.	Factor	Components	% of Var.
F1	-Ag, Co, (Mn, Zn, Pb, Ni) +Bi	25.3	F1	-Co, Ag, Zn, Pb, (Mn, Ni) +Bi	25.2
F2	-Bi, Mn, Ni, Pb +(Co, Zn, Ag)	21.0	F2	-Bi, Ni, Mn, (Pb, Zn) + (Co)	25.0
F3	-Mn +Bi, Zn, (Ag, Pb)	16.7	F3	-Co, Ni, (Mn) +Zn, Pb, (Ag, Bi)	15.7
F4	-Ag, (Mn, Bi, Pb, Zn) +Ni, Co	13.8	F4	-Bi, Ag, (Co) +Mn, (Zn, Ni)	14.9
F5	-Bi, Co, Ag +Zn, Pb, Ni, (Mn)	13.2		cum.	80.8
F6	-Zn, (Mn, Bi, Co) +Pb, (Ag)	6.3	F1	-Ni, Bi, Pb, Ag, Co, Mn, Zn	32.4
	cum.	96.3	F2	-Co, Ni, (Mn) +Bi, Pb, Zn	18.3
F1	-Ag, Co, (Mn, Pb, Ag, Ni) +Bi	25.0	F3	-Bi, (Co, Ni) +Zn, Mn, (Pb)	17.3
F2	-Mn, Bi, Ni, (Pb) +(Co, Ag)	21.1		cum.	68.0
F3	-Mn +Bi, Zn, Pb, (Ag, Ni)	17.3	F1	-Pb, Mn, Zn, Ni, Ag, (Co, Bi)	34.0
F4	-Bi, Ag, Co +Zn, Pb, (Mn)	13.9	F2	-Co, (Mn, Ni) +Bi, (Pb, Ag, Zn)	21.1
F5	-Ag, (Mn, Pb, Bi) +Co, Ni, (Zn)	13.8		cum.	55.1
	cum.	91.1			

Variable	Factor 1	Factor 2	Factor 3	Factor 4
Bi	0.910	-1.875*	0.152	-1.284
Co	-1.3576*	0.265	-1.551*	-0.623
Ni	-0.388	-1.178	-1.395*	0.278
Pb	-0.909	-0.882	0.949	-0.089
Zn	-1.171	-0.276	1.230	0.476
Ag	-1.341*	-0.008	0.414	-1.257
Mn	-0.441	-1.077	-0.203	1.754*
Variance per cent	25.2	25.0	15.7	14.9
Cumulative variance per cent	25.2	50.2	65.9	80.8

*Denotes important component factor.

All four factors, in a general way, outline annular zones centred on the quartz monzonite stock and have value maxima roughly coincident with the zone of copper-molybdenum mineralization. Zoning patterns are similar to those of individual elements but may be more significant in defining zoning trends as factors integrate behaviour of a number of elements. However, the geological significance of factors is not always obvious and

explanations or interpretations are subjective and may be speculative. No outstanding relationships between specific factors and ore or waste, such as that found at Endako (Dawson and Sinclair, 1974), are evident.

Factor 1 is characterized by high (negative) scores of cobalt and silver with moderate contributions from zinc and lead, and minor contributions from manganese and nickel. The only element that does not contribute to the (negative) factor value is bismuth and, thus, the factor can be interpreted as a measure of the amount of cation substitution in pyrite. Factor 2 is largely a measure of bismuth with moderate contributions from nickel, manganese, and lead scores. It complements factor 1 inasmuch as the most important factor components are those elements least significant in factor 1. Factor 2 also indicates the amount of minor element substitution in pyrite, but because bismuth is the main component in the factor value, the factor may be a measure of the amount of anion substitution. If indeed bismuth has a closer geochemical affinity in pyrite with anions rather than cations, factor 2 might indicate zones that supplied sulphur during mineralization.

TABLE 16. SUCCESSIVE Q-MODE VARIMAX FACTOR COMPONENTS VEIN PYRITE					
Factor	Components	% of Var.	Factor	Components	% of Var.
F1	-(Cu)		F1	-(Cu)	
	+Pb, Zn, Ag, (Bi, Mn, Co, Ni)	29.3		+Pb, Zn, Ag, Bi, (Mn, Co)	29.6
F2	-Bi, Mn, (Ag)		F2	-(Bi, Pb, Mn)	
	+Ni, Co, (Cu, Pb, Zn)	23.7		+Co, Ni, (Cu, Ag, Zn)	30.5
F3	-Mn, (Pb, Zn)	16.2	F3	-Mn, (Co, Pb)	
	+Bi, Cu, Ag			+Cu, Bi, (Ag, Zn)	18.8
F4	-Mn, Co, (Ni, Ag, Cu)	14.3	F4	-Cu, Mn, (Zn, Ag)	
	+Zn, Pb			+(Co, Pb, Ni)	10.2
F5	-Cu, Zn, Mn	9.9		cum.	89.1
	+(Co, Ni, Bi, Ag, Pb)				
F6	-Zn, Co	4.3	F1	-(Cu)	
	+Pb, (Cu, Ni, Mn, Ag)			+Pb, Zn, Ag, Bi, (Mn, Co)	30.1
	cum.	97.7	F2	-(Bi, Mn, Pb)	
				+Ni, Co, (Cu, Ag, Zn)	30.7
F1	-(Cu)		F3	-Mn, (Co, Ni, Pb)	
	+Pb, Zn, Ag, Bi, (Mn, Co, Ni)	29.4		+Cu, Bi, (Ag, Zn)	18.6
F2	-Bi, Mn, (Ag)			cum.	79.4
	+Ni, Co, (Cu, Zn, Pb)	23.5			
F3	-Mn, Pb, (Ni)		F1	+Bi, Pb, Zn, Ag, (Mn)	30.9
	+Bi, Cu, Ag, (Co)	17.0	F2	-(Bi, Mn, Pb)	
F4	-Mn, Co, Ag, Ni,			+Ni, Co, (Cu, Ag, Zn)	30.6
	+Pb, Zn	15.2		cum.	61.5
F5	-Cu, Mn, Zn	9.9			
	+(Co, Bi, Ni, Ag)	9.9			
	cum.	95.0			

Factor 3 is composed of two antithetic pairs of elements whose correlation was described in a preceding section: cobalt-nickel as a negative factor component and lead-zinc as a

positive one. The factor is possibly the most interesting from a zoning point of view as high (positive) factor values with high lead-zinc and low cobalt-nickel are found mainly in quartz monzonite and in hornfels or quartz diorite near the quartz monzonite contact. The high content of lead and zinc in pyrite from intrusive rocks was noted earlier in discussion of univariate minor element data. Thus, lead and zinc in factor 3 may be postulated to represent a hydrothermal contribution by quartz monzonite, whereas cobalt-nickel might be a contribution of elements to pyrite from country rocks (volcanic rocks and quartz diorite).

Factor 4 contains high (positive) manganese scores and modest (negative) bismuth and silver scores. High factor values are found in a series of isolated zones that encompass the quartz monzonite stock but are located at some distance from the contact. Highest (negative) factor values occur in biotite-bearing hornfels and quartz diorite. Factor 4 is possibly the best indicator of all four factors of the limits of the zone containing at least 0.2 per cent copper.

Factor analysis of vein pyrite (Table 16) includes values of copper (Appendix E). Two groups of elements account for most variance in vein pyrite — lead-zinc-silver (and bismuth) and cobalt-nickel. Two other factors, one composed largely of manganese, and the other of copper, account for much of the remaining variation. Together, these four factors account for 89 per cent of total variance.

Factors of vein pyrite are not the same as those of disseminated pyrite (Table 14), probably because the two types of pyrite are of different origins. Certainly combinations of elements from vein pyrite in factors provide geologically familiar and geochemically acceptable associations (for example, nickel and cobalt; bismuth, lead, zinc, silver), but otherwise very little is revealed about zoning of vein pyrite because of the erratic distribution of the small group of samples.

MINOR ELEMENT ZONING IN THE DEPOSIT

INTRODUCTION

Zoning, a systematic variation in space, of minor elements in pyrite is evident in plots of univariate and factor analysis data. Concentrations of impurity elements and high factor scores generally occur near the contact of the quartz monzonite stock, although the most intense concentration of all elements is in pyrite from quartz diorite in the well-mineralized northeast zone. Coincidence of high factor values and individual element concentrations with the zone of copper-molybdenum mineralization is remarkably consistent. Concentrations decrease away from the intrusive contact, both within the stock and intruded rocks. Five specimens of weakly altered peripheral volcanic rocks with only traces of pyrite do not fit the zoning pattern. These few samples suggest that

zoning of minor elements in pyrite is confined to the main zone of mineralized and hydrothermally altered rocks and pyrite from outside the pyritic halo can be recognized as being unrelated to the porphyry system.

Zoning patterns of most individual elements are centred on the quartz monzonite stock and are similar. Consistent patterns of different elements and factors in disseminated pyrite may indicate that a single, all-encompassing hydrothermal system prevailed during the main stages of mineralization. The variable most commonly considered to regulate incorporation of minor elements is temperature, and zoning is interpreted to be a response to temperature gradients. Undoubtedly there has been interplay of numerous other variables during sulphide deposition. These include: availability of elements, both metals and complexing ions; concentrations of elements and their partitioning between fluid and solid phases (Rose, 1970b); rates of precipitation, mobility (of elements) governed by fluid migration patterns, permeability, and diffusion rates; confining pressure, partial pressures of components in hydrothermal fluids, particularly those containing sulphur; changes in mineralizing solutions caused by interaction with groundwater and wallrock reactions; and many others.

Berg pyrite data were examined to see if there was any relation between quantity of pyrite and amount of minor elements in pyrite. It was concluded that the zoning observed reflects differences in absolute amounts of impurity elements and was not caused by dilution of a constant quantity of elements by different amounts of pyrite. Numerous studies have intimated that different paragenetic stages may have different contents of impurity elements. This fact has already been illustrated in this study by comparison of vein and disseminated pyrite. Therefore, zoning patterns considered here are based on analyses of carefully selected disseminated pyrite of the same paragenetic type and from rocks of apparently similar origin. Except for a few samples from the supergene zone, most samples analysed are from primary mineralization below the zone of oxidation. Regional metamorphism is low grade and mineralization has undergone a uniform post-depositional history.

Credibility of zoning patterns is based on the premise that minor element concentrations are not erratic at different depths but vary as a function of distance from the stock, and therefore, one or two samples per drill hole are representative of a large area. Vertical zoning of primary sulphide minerals and hypogene rock alteration was not recognized over depths of a few hundred metres but may be present over greater depths. Presumably minor element distributions behave in a similar manner.

The abundance of minor elements was found to be fairly consistent with depth, if specimens of similar rock and alteration types were compared. Table 17 illustrates variability of minor element concentrations at different depths. The specimens from drill hole 71 are all from hornfels but were selected to represent maximum variation in type and amount of rock alteration. In comparison, specimens from drill holes 16 (diorite) and 23 (biotite hornfels) are representative specimens from drill holes with uniform rock type and alteration throughout the length of the hole. As a group, pyrite from drill hole 71

TABLE 17. VERTICAL VARIATION OF MINOR ELEMENTS IN PYRITE										
Sample (Drill hole and footage)	As	Bi	Co	Ni	Pb	Zn	Ag	Mo	Ti	Mn
Biotite Hornfels										
71-420	N	N	720	230	1	8	4.0	N	55	N
71-667	N	1.0	950	140	7	9	7.0	28	8	20
71-738	N	1.0	560	168	1	18	2.5	N	450	N
Brecciated Hornfels										
71-533	N	1.0	430	330	64	20	5.5	26	10	N
71-569	530	17.0	400	98	36	19	9.0	10	64	6
Sericite Hornfels										
71-869	1 050	26.0	305	107	63	30	18.0	31	380	N
71-915	400	12.0	435	74	105	34	19.0	14	G	5
Diorite										
16-495	N	N	380	172	25	26	8.0	8	G	5.5
16-600	N	N	353	154	24	31	3.5	2	G	7.5
Biotite Hornfels										
23-328	N	N	615	55	13	10	6.5	N	40	N
23-434	575	N	640	67	24	28	7.0	6	270	12

N denotes less than detection limit; G denotes greater than detection limit.

shows considerable variation but specimens from similar alteration zones are comparable. As most pyrite in this study was taken from biotite hornfels of a superficially similar type, the amount of vertical variation indicated by hole 71 is possibly the maximum that would be expected.

It is concluded that similar zoning patterns can be reproduced at different depths if zones are defined by large, yet statistically meaningful, contour intervals such as values greater than the mean of all analyses (\bar{X}) and greater than the mean plus one standard deviation ($\bar{X} + SD$). Samples from different depths might change the detailed configurations of zones if different alteration zones were intersected but general patterns are not usually affected. For example, if each analysis from hole 71 was plotted successively, only about one-third would cause any change in the position of zone contours and most of the changes would be due to erratic behaviour of molybdenum, titanium, and manganese.

UNIVARIATE MINOR ELEMENT ZONING

Zoning patterns of individual minor element concentrations in pyrite are similar (see Figs. 35 and 36), with concentration maxima seen as annular zones about the quartz monzonite stock near the intrusive contact. Zones are not symmetrical about the stock as concentration contours bulge into diorite to the east and northeast of the quartz monzonite intrusion, and continuity of contours is disrupted in the southwest by irregular masses of quartz monzonite. This is similar to the distribution of copper.

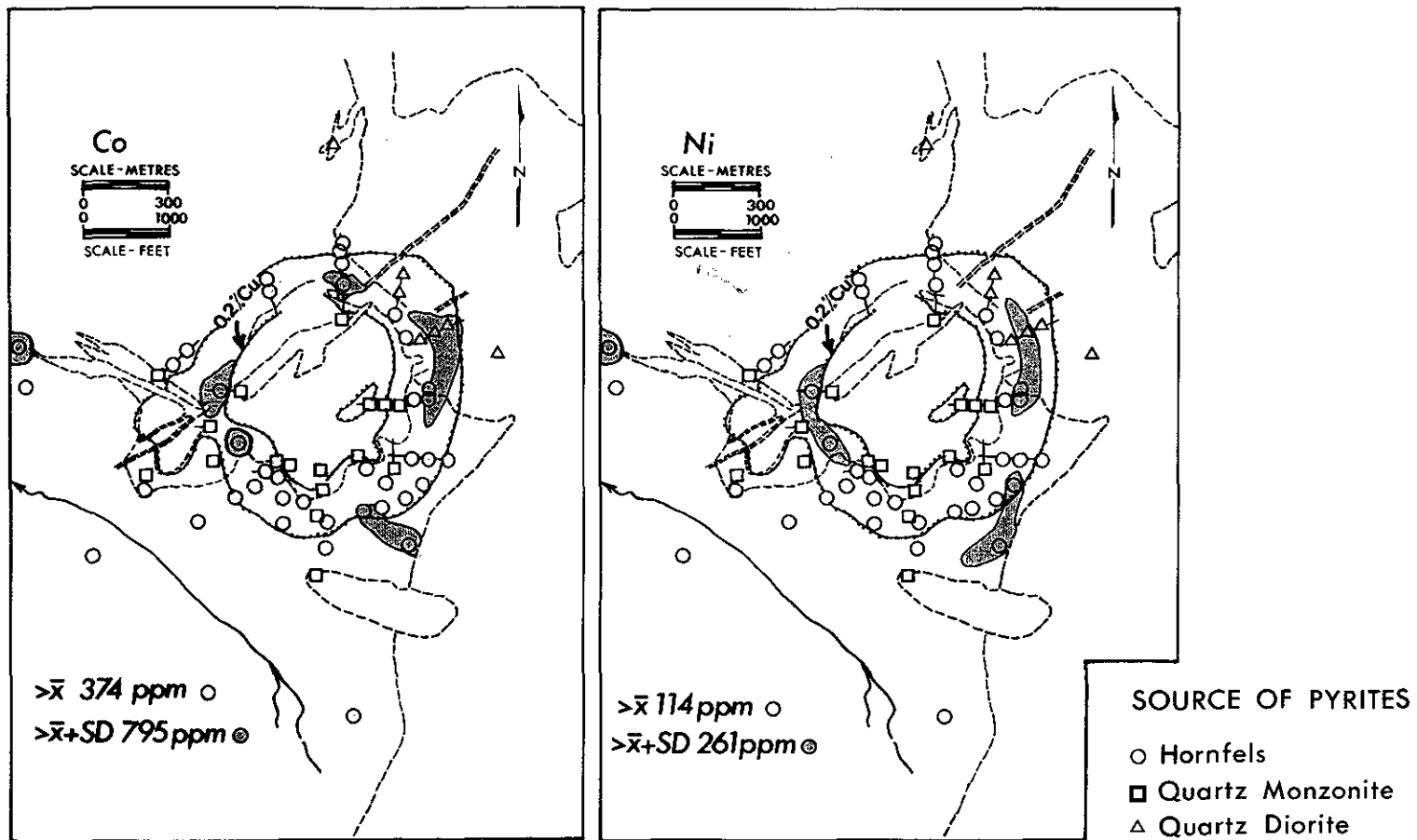


Figure 35. Zoning of minor elements in pyrite, Co and Ni.

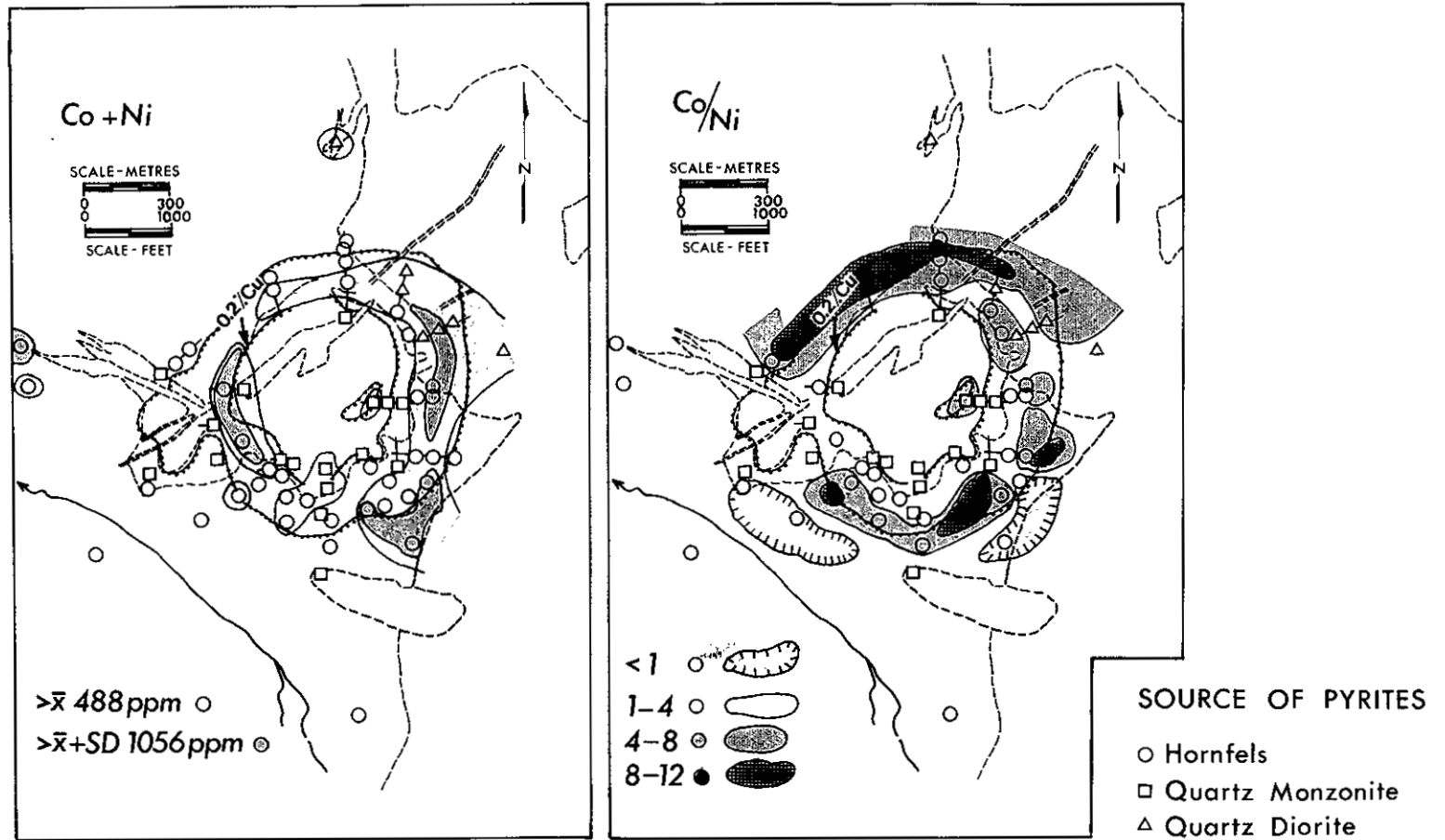


Figure 36. Zoning of minor elements in pyrite, Co and Ni and Co/Ni.

Cobalt, nickel, lead, zinc, silver, molybdenum, and manganese are concentrated in pyrite near the quartz monzonite intrusive contact with concentration maxima most common in the northeast zone of mineralization in hornfels and quartz diorite. Cobalt-nickel ratios have maximum values in hornfels about 150 metres from the contact. Four samples in the south suggest that nickel content increases outward from the zone of cobalt-nickel highs and pyrite south of this zone contains nickel in excess of cobalt over distances of about 100 metres. Bismuth distribution is much like that of other elements with high values found in a zone projecting out into the pyritic halo to the south. Bismuth (and possibly lead, zinc, and silver) may be concentrated there in pyrite related to north-south-trending structures. Detectable arsenic (>300 ppm) is found in all samples outside the main copper-bearing zone but small zones consisting of a few samples with detectable arsenic are coincident with the highest grades of copper within the area of copper mineralization. Additional sampling may reveal that arsenic is most abundant in pyrite from the pyritic halo and weakly mineralized peripheral volcanic rocks and therefore useful as a pathfinder element. Titanium concentrations are erratic and highest values (those above the detection limit) are associated with intrusive rocks or their contacts. Values of titanium below the mean of the sample group are found within zones of copper mineralization.

Concentration maxima of single elements or small groups of elements do not coincide exactly with best copper or molybdenum grades, but zones of best mineralization are clearly defined when all concentration highs are superimposed (Fig. 37). Ovchinnikov (1967) states: 'An increase in the quantity of the 'host' mineral is accompanied by a simultaneous increase in the relative concentration of the impurity elements in it.' Although this may be true in massive pyritic deposits, in this study and perhaps porphyry deposits in general, highest concentrations of minor elements in pyrite are intermediate between the pyritic halo and the sparsely mineralized intrusive core. At Berg deposit, concentration maxima of minor elements in pyrite are not coincident with maximum amounts of the host pyrite. Instead, highest minor element concentrations are more closely related to the amounts of copper and molybdenum minerals present within a zone containing 2 to 4 per cent pyrite.

A consistent zoning sequence is not evident. This may be, in part, because inhomogeneous stratified rocks are mineralized and rock compositions may have influenced composition of pyrite. Possibly minor element distributions in pyrite from homogeneous host rocks might display zoning sequences. There is some suggestion of this in diorite of the northeast copper zone where maxima of manganese, silver, and cobalt are clearly peripheral to highest nickel, bismuth, lead, and zinc values. A most noteworthy aspect of zoning of minor elements in pyrite is that minor elements do not imitate sulphide mineral zoning patterns in porphyry deposits. When lead, zinc, silver, and manganese minerals are found they most commonly occur in late-stage veinlets peripheral to the main zone of intrusion, alteration, and copper-molybdenum mineralization. However, as minor elements in pyrite, lead, zinc, silver, and manganese appear to be concentrated in pyrite from the ore zone, intrusive rocks, or rocks near the intrusive contact, whereas maxima of arsenic, cobalt, and nickel form peripheral highs in the pyritic halo.

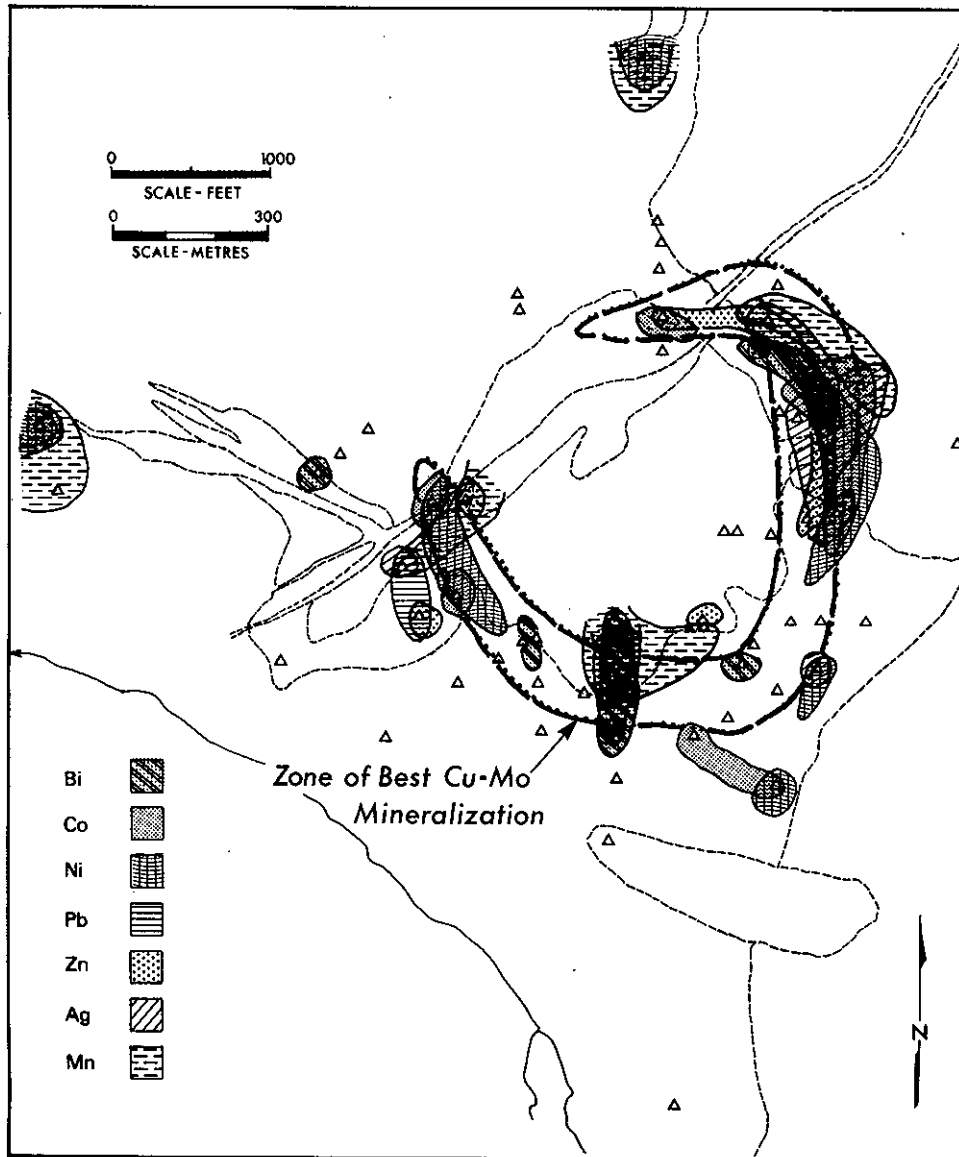


Figure 37. Composite of maximum minor element values.
(Greater than mean plus one standard deviation)

Depletion of minor elements or low element concentrations do not appear to have any defined patterns with the exception of manganese. Manganese lows are found only in areas with low concentrations of other minor elements in pyrite or areas with only few detectable elements. Zones with low manganese content (less than the detection limit) border zones of high concentrations of other minor elements. Manganese lows may be potentially useful, as in all cases observed, manganese lows border zones with best copper grades.

ZONING OF FACTORS (MULTIVARIATE ANALYSIS)

Contoured plots of factor values are shown on Figures 38 and 39. Factors have values ranging from 1 to -1 and are interpreted as follows: large negative values are caused by large amounts of negative variables and small amounts of positive variables. Similarly, large positive values imply large amounts of positive variables and small amounts of negative variables in the factors.

Factor 1 (negative) values define a broad, asymmetrical girdle about the quartz monzonite stock that coincides closely with the most highly altered and mineralized rocks. Highest (negative) factor values are associated with rocks containing about 3 to 4 per cent pyrite and occur in an area bounded by positive factor values that correspond to weakly mineralized rocks of the barren intrusive core and pyritic halo. Factor 2 has a similar zoning relationship as factor 1. Highest (negative) factor values occur in areas of copper mineralization and are flanked by positive factor values. Factor maxima lie in areas with less pyrite (about 2 per cent) than those of factor 1 and define smaller zones more closely related to intrusive contacts, particularly quartz diorite. If factor 2 is, indeed, an indicator of anion substitution in pyrite, it may be more closely allied to availability of sulphur in the mineralizing process. Thus, it would appear that the quartz diorite contact may have been a source area for sulphur during pyrite formation. Factors 1 and 2, because of their similar zoning patterns and close relationship to the zone of copper-molybdenum mineralization, may be made up of factor components contributed by the hydrothermal system and mineralizing processes.

Zones of factor 3 and 4 values do not correspond to any constant amount of pyrite and are more transgressive to pyrite contours. Factor 3 clearly exhibits mutually exclusive, antithetic zoning relationships between lead-zinc and cobalt-nickel, but zoning relationships to copper-molybdenum mineralization are not consistent. In the eastern part of the mineralized zone, positive factor values (high lead-zinc, low cobalt-nickel) define very closely the quartz monzonite contact in the adjoining zone of molybdenum-copper mineralization, whereas high negative values define the pyritic halo in hornfels and diorite. In southwest and west parts of the mineralized zone, high positive values again define the quartz monzonite contact but highest negative values correspond with copper-molybdenum mineralization in hornfels.

Zones of factor 4 values are the least continuous of the four factors and are seen as isolated areas with negative factor values (bismuth, silver component) spread around the quartz monzonite stock. Most areas are in copper-bearing hornfels with only a very few sample sites within intrusive rocks. The zone of mineralization defined is the copper zone, in most cases adjoining the shell of copper-molybdenum mineralization. The outer edge of areas with negative factor values defines approximately the furthest limit of 0.2 per cent copper mineralization and is coincident with the start of the pyritic halo.

Factors 3 and 4, in view of their somewhat transgressive relation to zones of constant pyrite content, yet consistent association with specific rock types, may represent factors

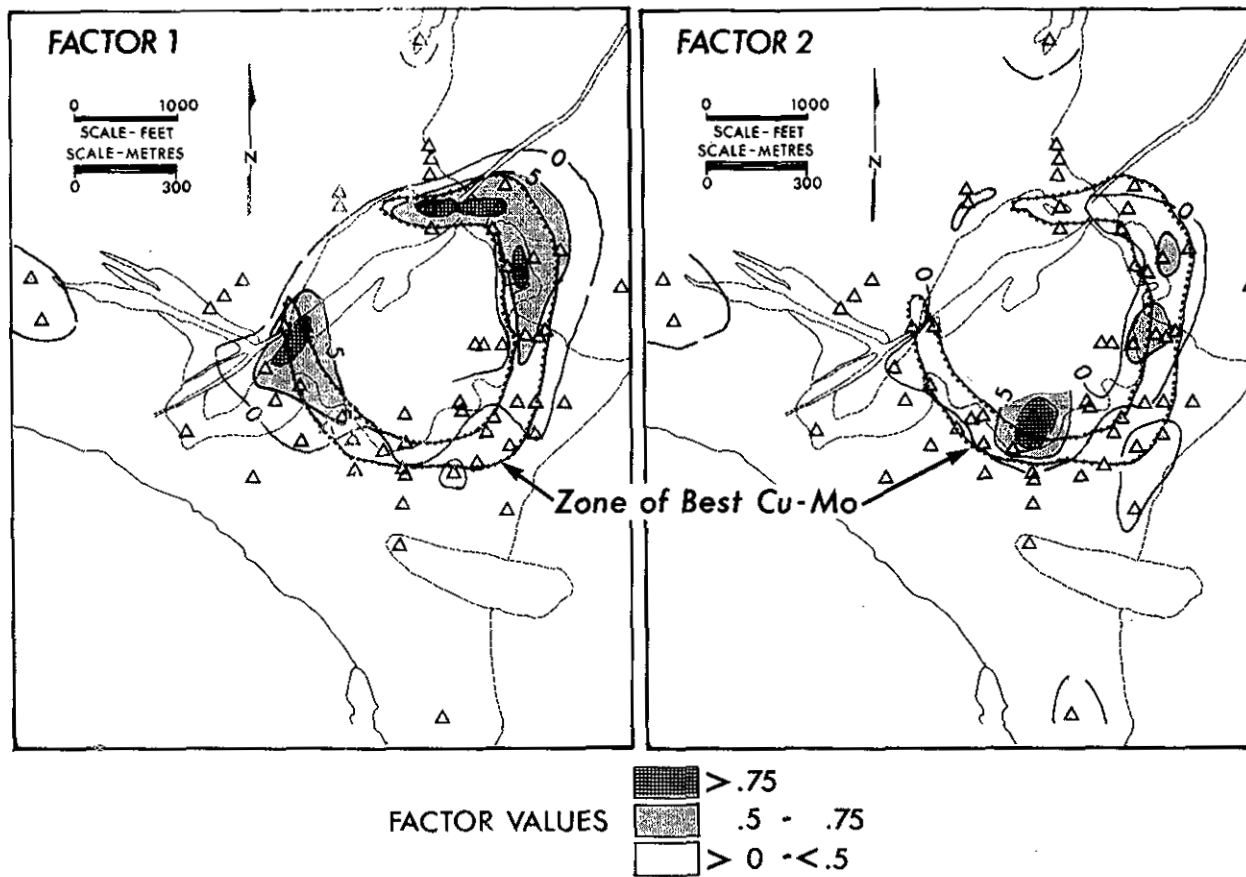


Figure 38. Contoured plan of Q-mode factor values — factors 1 and 2.

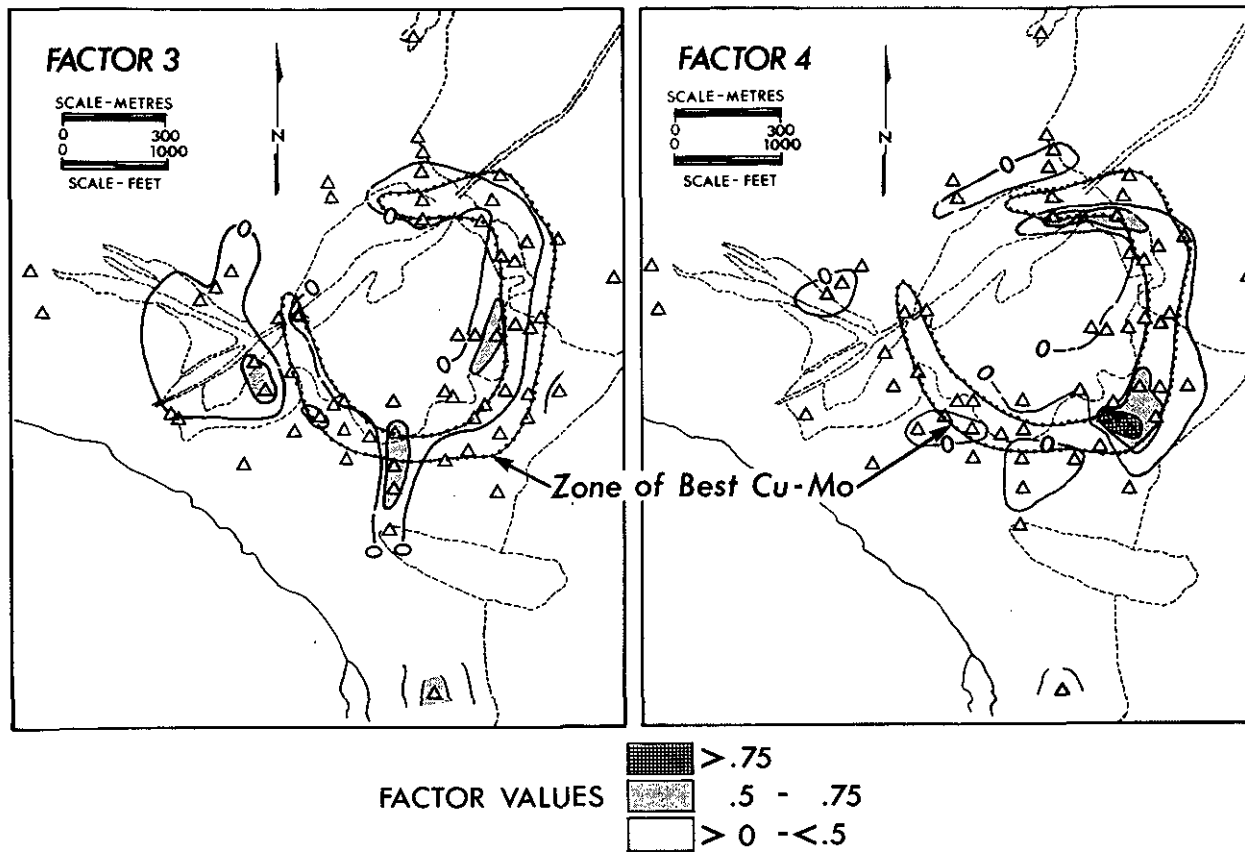


Figure 39. Contoured plan of Q-mode factor values — factors 3 and 4.

whose components are (partly) derived from country rocks during mineralization – in this case, lead-zinc from quartz monzonite, cobalt-nickel from hornfels and quartz diorite, and bismuth-silver from hornfels.

Zoning patterns of factors are generally similar to those of individual minor elements with factor maxima concentrated in an annulus about the quartz monzonite stock roughly coincident with the zone of copper and molybdenum sulphides (Fig. 40).

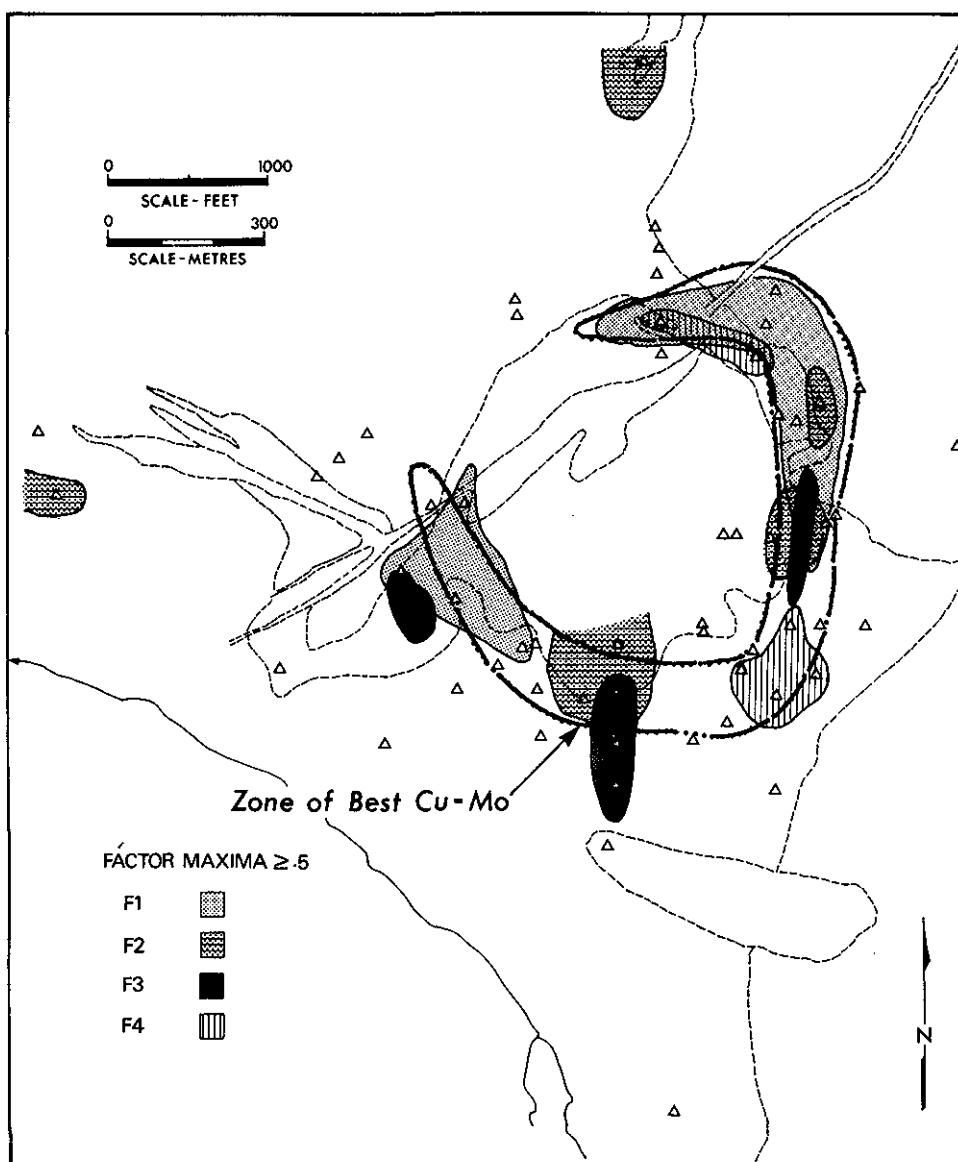


Figure 40. Composite of factors 1 to 4.

Composite highest factor values (≥ 0.5) shown on Figure 40 clearly coincide with the zone of best copper-molybdenum mineralization. Factor zoning patterns, while similar to those of individual minor elements or composites of minor element concentrations, appear to be useful in more precisely outlining the copper-molybdenum ore zone.

SUMMARY OF MINOR ELEMENT STUDY

Minor elements in pyrite display lateral zoning around the composite stock in a manner similar to alteration and sulphide zoning. Elements found to be most useful are cobalt and nickel, moderately useful are lead, zinc, silver, bismuth, and manganese, and possibly useful are arsenic, copper, molybdenum, and titanium.

Analytical data were examined and compared easily by plotting histograms. These inferred that minor elements are lognormally distributed and are polymodal. Another effective method of data presentation is using cumulative probability paper. Probability plots are effective in resolving and describing polymodal populations. One cause of polymodal data as indicated by histograms, t and F tests, and cumulative probability curves is mixing of vein and disseminated pyrite. There is an indication that the identity and quantity of some minor elements is influenced by host rock but this has not been demonstrated to be a general principle.

Associations between paired variables were demonstrated using correlation and simple regression analyses. Most significant correlation and interrelationships are between cobalt-nickel and lead-zinc. Cobalt-nickel ratios and regression plots show wide ranges in pyrite from Berg deposit. Use of such plots might enable different types of pyrite from the same deposit to be grouped but genetic classification of mineral deposits based on cobalt-nickel and probably other element ratios or quantities is tenuous.

Associations between samples based on multiple elements were demonstrated using Q-mode factor analysis. Four factors accounted for 81 per cent of total sample variability and were considered to be geologically meaningful. Two factors might be related to the amount of minor element substitution in pyrite, one measuring total cation substitution and the second measuring anion substitution in the pyrite lattice. The remaining two factors are interpreted to represent areas with significant concentration of certain minor elements from host rocks or hydrothermal fluids.

Contoured concentrations of individual and composite minor elements and factor values reveal zoning in which pyrite with highest minor element concentrations coincides with best copper-molybdenum mineralization and only modest amounts of pyrite. This refutes Ovchinnikov's (1967) statement that highest concentrations of minor elements in a host mineral will occur where that mineral is most abundant. Instead, it appears that minor elements are most abundant in zones of best mineralization, that is, zones where

other metal sulphides are abundant in addition to pyrite. This observation is in accord with studies by Kurz, *et al.* (1975) and Ryall (1977). Thus, a high degree of contamination of pyrite by impurity elements might be useful as a guide to ore and can be a favourable indication of ore potential.

APPENDICES

APPENDIX A. ELEMENTS DETECTED IN BERG PYRITE

APPENDIX B. ANALYTICAL RESULTS – MINOR ELEMENTS IN PYRITE

APPENDIX C. DATA PARAMETERS AND COMPUTED CHI SQUARE VALUES

APPENDIX D. VARIMAX FACTOR MATRIX, DISSEMINATED PYRITE

APPENDIX E. VARIMAX FACTOR MATRIX, VEIN PYRITE

APPENDICES

APPENDIX A. ELEMENTS DETECTED IN BERG PYRITE

Line spectra of a large number of elements were checked in a group of 16 pyrite concentrates constituting an orientation sample set. The samples were examined initially only on a qualitative basis. The following elements were detected in one or more samples. Undoubtedly, some are contaminants from admixed gangue and sulphide grains.

LIST OF 21 ELEMENTS		
Al	Co	Ag
Sb	Pb	Sr
As	Mg	Sn
Ba	Mn	Ti
Cd	Mo	V
Ca	Ni	Zn
Cr	Si	Zr

The following were not detected. These may be present but if so, concentrations are below spectrographic detection limits:

LIST OF 18 ELEMENTS		
Be	Au	Te
B	La	Th
Ce	Pt	W
Cb	Re	U
Ga	Sc	Yb
Ge	Se	Y

Detection limits of the spectrographic method used are approximately in the 0.1 to 1 000-ppm range, but each element behaves individually and has a characteristic upper and lower limit of detection. Characteristic wavelengths and 'index points' of elements for which standards were available are shown in Table 18. The 'index point' is simply a concentration convenient for describing calibration curves. Commonly maximum and minimum detection limits of elements shown are approximately 10 times and 0.10 of the 'index points.'

Contamination of pyrite concentrates by gangue and sulphide inclusions is inevitable. Si to 1 per cent, Al to 0.5 per cent, and some Sr, Ba, Mg, Ca, and Zr were detected and are believed to be due to quartz, feldspar, chlorite, calcite or gypsum, and zircon inclusions. Gangue minerals are not considered to be serious contaminants if they are present in minute quantities since most elements introduced are not contained in the pyrite lattice.

TABLE 18. SPECTROGRAPHIC ANALYSIS OF PYRITE ELEMENTS FOR WHICH CONCENTRATIONS WERE DETERMINED						
Standard Reference Line: Pd 3 421.2 A						
Element	Wavelength A	Index Point ppm		Element	Wavelength A	Index Point ppm
Sb	2 598.0	370		Pb	2 833.0	65
As	2 860.5	3 200		Mg	2 779.8	720
	2 780.2	1 800		Mn	2 798.0	54
Ba	4 554.0	4.2		Mo	3 170.3	96
	4 130.6	330		Ni	3 414.7	27
Be	3 130.4	11		Ag	3 382.8	4
Bi	3 067.7	12.5		Sr	4 077.7	2.4
B	2 497.7	92			3 464.5	225
Cd	3 261.2	49		Sn	3 175.0	32
Ca	3 158.9	2 100		Ti	3 361.2	32
Cr	4 254.3	18			2 942.0	1 500
Co	3 453.4	27		V	3 185.3	100
Cu	3 273.9	12.5		Zn	3 345.0	32
Ga	2 943.6	24			3 345.5	210
Ge	3 039.1	46		Zr	3 273.1	57

Contamination of pyrite by other sulphide minerals is the main source of concern. The main sulphide contaminant is chalcopyrite. Polished sections show that chalcopyrite is intimately intergrown with pyrite in the copper-molybdenum zone as minute 'encapsulated' grains within pyrite grain boundaries and as fillings in microfractures. Pyrite in peripheral volcanic rocks, the pyritic halo zone, and crystals from all types of veins generally have negligible chalcopyrite intergrowths. Five chalcopyrite samples from different areas within the deposit were analysed to determine effects of chalcopyrite contaminations. Results are shown in Table 19.

TABLE 19. MINOR ELEMENT CONTENT OF CHALCOPYRITE (in ppm)							
Sample No.	Pb	Zn	Ag	Mn	Mo	Ti	Sn
1	12	180	35.0	.5	---	164	14.0
2	38	365	43.0	8.0	---	>DL	5.0
3	23	680	1.0	52.0	1.0	38	---
4	10	16	20.0	21.0	12.0	---	---
5	23	620	14.5	26.0	1.0	4	8.0

Note: Sb, As, Bi, Co, Ni, and Cd were not detected.
 --- means less than detection limit.

From these data, assuming a maximum chalcopyrite content of 1 per cent in a pyrite concentrate, it appears that the only significant contribution to the analytical results by

chalcopyrite will be copper and possibly a minor amount of zinc (for example, 6.8 ppm in sample 3). Ag, Mn, Pb, and Ti present as contamination in pyrite from chalcopyrite will be below the detection limit.

Sphalerite is the second most abundant sulphide contaminant. It is found mainly in the vein and breccia specimens and a few samples from outside the copper-molybdenum zone. Analysis of a single sample of zoned, pale to medium brown sphalerite gave the following results:

Pb	1 000 ppm	Ti	80 ppm
As	6 300 ppm	Sb	990 ppm
Cu	6 800 ppm	Cd	22 000 ppm
Ag	250 ppm	Fe	10 000 ppm
Mn	2 350 ppm		

Note: Bi, Co, Ni, Mo, and Sn were not detected.

Sphalerite with this composition would contribute a number of elements in significant amounts to analytical results for pyrite. However, based on this and other analyses of mixed pyrite-sphalerite grains, Cd appears to be present always and is, thus, useful as an indicator of sphalerite contamination. Every pyrite analysis containing Cd (seven from the total 100 samples) also contains high values of Zn and commonly Mn, Pb, and Ag. In all these seven cases it is assumed that sphalerite is present and only analytical values of Bi, Co, Ni, Mo, and Sn (if present) were utilized.

Other potential contaminants are molybdenite, galena, tetrahedrite, and covellite, but these can be avoided by careful sample selection and hand picking of pyrite grains.

APPENDIX B. ANALYTICAL RESULTS - MINOR ELEMENTS IN PYRITE
(in ppm)

Sample	As	Bi	Co	Ni	Cu	Pb	Zn	Ag	Mo	Ti	Mn	Sn	Cd
HORNFELS													
1-280		1.0	728	106	500	92	216	14.0	8	210			
			740	106	460	52	134	10.0	2	245	5.0		
			900	108	C	97	120	8.5	12	C	13.0		
3-267			416	62	300	52	26	4.0	46	230		10.0	
			370	45	C	107	21	5.5	20	485			
4-220	620	3.0	1 100	820	C	46	36	3.0	C	C			
5-248			1 150	770	C	12	18	4.0	C	310	7.5		
8-271	510	16.0	760	162	C	140	95	18.0	C	C	7.0		
8-490	820	18.0	1 320	405	C	102	68	49.0	C	355	11.5		
10-253			48.0	740	114	C	52	55	7.0	C	600		
12-430			10.5	785	78	C	15	23	12.5	54	480	4.0	
			7.0	590	67	C	10	17	4.5	83	390	5.0	
12-697	700		410	44	C	15	33	5.0	6	310	4.0		
13-385			9.0	355	50	C	20	28	2.5	1	C		
13-693			142	16	370	12	8	3.0		190			
14-432			11.0	600	172	C	92	82	17.0	C	C		
14-727			5.0	700	128	C	13	31	3.5	63	148	5.0	
			8.0	820	175	C	8	29	35.0	11	215	12.0	
14-1163	400		2.0	420	35	650	22	46	7.0	C			
15-187			2.0	115	168	500	21	16	2.5	6	560		
			4.0	93	142	490	12	21	2.5	1	500		
17-105			3.0	70	128	100	13	15	1.5	C	7.0		
18-232			1.0	260	60	240	12	16	2.5	1	385	4.0	
			1.5	325	60	C	21	46	3.0	6	C	5.0	
19-465			9.0	460	244	160	75	36	3.5	17	395	5.0	
			18.0	570	265	C	110	36	4.5	35	C	9.5	
20-285			4.5	600	260	68	84	7.0		315	18.5		
22-197				448	44	215	11	13	7.5	6	475		
23-328				980	68	C	9	10	5.5	5	64		
				600	60	C	17	230	5.0	1	50		
				385	34	640	12	12	8.0		29		
				485	58	640	21	8	3.5		20		
23-434	600	1.0	650	70	630	25	33	8.0	19	300	10.0		
	450	2.0	630	63	C	23	22	6.0	1	240	5.0		
26-165		21.5	70	47	196	19	12	2.0	4				
26-437		11.0	188	32	181	28	17	8.0	1	395	5.0		
		10.0	180	31	C	64	51	12.0	4	C	9.0		
	1 200	3.0	55	17	38	30	7	5.0		7			
	500	2.5	64	21	10	26	7	4.0		6			
27-884	400	55.0	120	74	C	C	C	C	C	C	C		C
28-410	300	1.5	390	86	360	48	34	11.0	22	385			
29-226			620	62	330	19	53	8.0	6	100			
30-325		2.0	1 200	550	C	92	28	7.5	C	265	8.0		
32-277			640	132	C	42	13	4.0	C	29	4.0	28.0	
33A-558			2 050	114	880	52	20	7.0		47			
			1 280	90	760	44	18	6.5		43			
34-316		4.5	295	106	C	41	32	7.5	12	C	11.5		
35-387	500	52.0	670	54	C	58	42	16.0	C	640			
35-376		4.5	375	70	C	20	15	9.0	C	610			
36-582	400	19.0	550	108	C	58	27	20.0	86	C	4.0		
	450	9.0	392	94	C	37	25	11.0	31	C	4.0	4.0	
37-480		3.0	560	850	198	21	80	1.5	C	C			
		7.5	640	1 000	102	16	52	1.0	C	C			
43-281	450	C	285	66	C	57	41	84.0	C	C	9.0		
63-141	630	4.0	790	310	540	82	36	9.0		450	92.0		
	1 400	7.0	570	245	400	98	37	2.5		210	81.0		
65-129	3 050	3.0	340	78	430	320	C	17.0		C	140		41
	2 280	3.0	295	88	390	260	C	9.5		C	146		54
	C	3.5	350	100	590	235	C	8.0		900	110		28
	C	2.5	275	83	430	220	C	5.0		610	152		30
68-74	300	24.0	140	28	103	72	44	8.0		625	7.0		
71-420			720	230	C	1	8	4.0		55			
71-533		1.0	430	330	C	64	20	5.5	26	10			
71-569	530	17.0	400	98	360	36	19	9.0	10	64	6.0		
71-667		1.0	950	140	280	7	9	7.0	28	8	20.0		
71-738		1.0	560	168	C	1	18	2.5		450			
71-869	1 050	26.0	305	107	C	63	30	18.0	31	380			
71-915	400	12.0	435	74	600	105	34	19.0	14	C	5.0		
72-400		18.0	1 140	1 150	C	79	24	96.0	17	610			
		16.5	570	800	C	29	11	29.0	11	405	5.0		
DIORITE													
4-446	850	C	445	200	C	C	C	C	C	C		8.5	4
9-155	1 190	3.5	600	140	C	67	182	50.0	C	C	8.0		
9-430	300	34.0	1 040	285	C	C	100	86.0	C	C	5.0	18.0	
9-724	950	7.5	820	148	C	124	33	29.0	24	C	18.0		
10-510	500	3.0	560	214	C	192	620	21.0	94	C	16.0		
	400	4.0	510	225	C	173	367	18.5	86	C	9.5		

Note: Blank denotes less than detection limit; C denotes contamination.

APPENDIX B. ANALYTICAL RESULTS - MINOR ELEMENTS IN PYRITE (Continued)
(in ppm)

Sample	As	Bi	Co	Ni	Cu	Pb	Zn	Ag	Mo	Ti	Mn	Sn	Cd
DIORITE (Continued)													
10-803			660	71	C	76	32	19.0	27	C	7.0	4.0	
16-495			380	172	510	25	26	8.0	8	C	5.5		
16-600			300	144	215	16	24	2.0	1	C	5.0		
			405	164	C	32	37	4.5	8	C	15.0		
10.6.6		17.0	450	130	C	380	C	17.0	7	680	C	12.0	
QUARTZ MONZONITE													
1-547		7.5	300	106	C	116	10	20.0	15	C			
5-552		5.0	610	225	C	116	118	20.0	C	C	11.0		
6-350			450	91	540	34	20	4.0	36	960	4.0		
6-449		11.0	76	50	325	64	16	3.0	6	500			
		11.0	88	52	270	16	13	3.0	7	530			
		11.0	90	48	C	59	12	2.5	6	C			
6-724		13.0	225	104	C	78	49	11.5	C	C	4.0		
7-235			290	112	C	148	208	25.0	33	C	21.0		
10-683		89.0	77	25	250	C	C	C	3	C	C		34
11-404		9.5	104	92	C	30	20	5.5	20	C	C		
13-134		21.0	90	74	360	21	27	2.5	C	C			
17-290		2.0	90	47	132	35	44	1.5	3	C	4.0		
20-512		3.5	310	122	420	122	69	3.0	4	320	8.0		
21-502	1 325	40.0	216	194	55	30	48	0.5	1	500	5.0		
	1 110	34.0	216	184	94	73	37	4.5	30	C	8.5		
24-541		40.0	160	132	C	270	38	39.0	C	C	20.0	13.0	
		56.0	120	84	C	196	85	13.0	C	C	38.0	6.0	
25-396		21.0	164	120	180	430	148	17.0	6	172			
27-358		27.0	86	46	C	C	C	C	13	C	C		4
31-337		1.5	256	132	175	80	330	3.0		670	5.0		
		2.0	230	122	325	270	520	8.0		C	9.5		
34-368		2.0	325	140	C	58	260	13.0	87	C		4.0	
69-463	1 030	54.0	390	220	C	212	50	65.0	51	C	15.0		
	900	38.0	332	205	C	141	42	29.0	88	C	12.5		
VEIN													
1-596			180	50	116	41	18	3.5	C	5			
12-191	600	35.0	10	8	67	380	72	18.0		C			
14-261		72.0	21	17	600	45	16	17.5	7.5	144		4.0	
23-545			9	8	590	1	9	4.0		52			
24-355			9	13	102	1	6	0.5		260			
25-165			1	1	15	1	1	0.5		9			
26-437	850	3.0	60	19	24	28	7	4.5		4			
30-363	900	29.0	29	54	C	360	C	27.0			C		26
	700	50.0	14	56	430	440	215	34.0		C			
33A-558		1.0	13	11	30	14	7	1.5			8		
35-627	900	24.0	64	9	180	136	148	36.0		5	6.5		
37-390			83	100	122	53	15	8.0	20	7	4.0		
43-355		7.0	1	1	600	19	8	2.5	C	235			
63-251		148.0	20	6	20	410	300	80.0	11	7	9.5		
68-68	400	1.5	5	5	6	290	13	1.5	3	C	20.0		
69-480			272	34	140	1	14	3.0	6	90			
70-515			74	54	500	16	34	4.0	38	174			
			77	80	305	15	31	3.0	24	122			
71-580		2.0	106	260	600	30	26	3.0		6		1.0	
71-804			225	72	134	10	7	8.0		174	8.0		
M.24.6			1	1	60	70	9	1.5		8			
Fissure	1 980		15	24	30	290	520	12.0	C	6	13.5		11
	2 100		9	18	50	415	C	3.0		6	5.0		11
M3		22.0	5	5	53	210	122	3.5	12	17			84
		26.0	18	5	C	450	205	7.0	1	59			
3.22.7			33	24	144	57	34	4.0	3	140	8.0		
VOLCANIC ROCKS													
3.25.7	C	3.0	2 400	940	42	380	154	11.0	6	C	30.0		
	C	3.0	1 300	550	74	350	104	13.0	1	5	40.0		
1.8.6	350	2.0	920	570	650	42	128	1.0		148	24.0		
3.21.6	600	2.0	880	680	C	84	173	1.0		220	52.0		
3.24.6		39.0	550	400	300	130	78	27.0	6	230	38.0		
			395	360	350	97	98	25.0	5	215	34.0		
CHALCOPYRITE													
1-596					Major	12	180	35.0		164	5.0	14.0	28
10-510					Major	38	365	43.0		C	8.0	5.0	5
14-1003					Major	23	680	1.0	1	38	53.0		56
26-437					Major	10	16	20.0	12		21.0		34
71-677					Major	23	620	14.5	1	4	26.0	8.0	
SPHALERITE													
30-363	6 300				6 800	Major	Major	250		80	2 350		
		Also: Sb 990 ppm											
		Fe 1%											
		Cd 2.2%											

Note: Blank denotes less than detection limit; C denotes contamination.

APPENDIX C. DATA PARAMETERS AND COMPUTED CHI SQUARE VALUES			
A. PANTELEYEV--FACTOR ANALYSIS--8 VARIABLES--MARCH 06 1972--			
DATA PARAMETERS			
VARIABLE	MEAN	STAN DEV	CHI
BI	15.8750	34.9593	43.5098
VEIN PYRITE CO	59.7499	77.3401	29.7480
NI	35.4500	58.1347	15.6186
N = 20 CU	200.2999	215.7057	25.5140
PB	56.6499	133.1234	25.7593
ZN	45.3499	73.2641	21.5763
AG	10.3000	17.9801	35.1719
MN	2.8700	5.0892	47.9430
TRANSFORMED DATA PARAMETERS			
VARIABLE	MEAN	STAN DEV	CHI
BI	0.5056	0.7160	28.7609
CO	1.3046	0.7468	6.7097
NI	1.1044	0.6594	5.9948
CU	1.9999	0.5653	15.1119
PB	1.4226	0.8496	18.3775
ZN	1.2603	0.5674	12.6403
AG	0.6644	0.4952	7.8990
MN	0.2750	0.4354	49.9290

A. PANTELEYEV--FACTOR ANALYSIS--7 VARIABLES--MARCH 06 1972			
DATA PARAMETERS			
VARIABLE	MEAN	STAN DEV	CHI
BI	9.8410	12.4378	55.1237
DISSEMINATED PYRITE CO	497.9795	312.4673	14.2432
NI	189.2782	213.1245	49.7227
PB	76.6718	83.7864	30.8166
N = 61 ZN	66.4915	87.6576	48.4221
AG	14.5852	18.2134	40.6231
MN	7.3655	12.5966	41.3416
TRANSFORMED DATA PARAMETERS			
VARIABLE	MEAN	STAN DEV	CHI
BI	0.6784	0.5514	28.4411
CO	2.5909	0.3326	12.8796
NI	2.0945	0.3751	5.3034
PB	1.7048	0.3903	6.5861
ZN	1.6188	0.3841	5.3026
AG	0.9199	0.4526	3.4562
MN	0.5792	0.4999	55.8327

APPENDIX D. VARIMAX FACTOR MATRIX, DISSEMINATED PYRITE

A. PANTELEYEV--FACTOR ANALYSIS--7 VARIABLES--MARCH 06 1972

VARIMAX FACTOR MATRIX

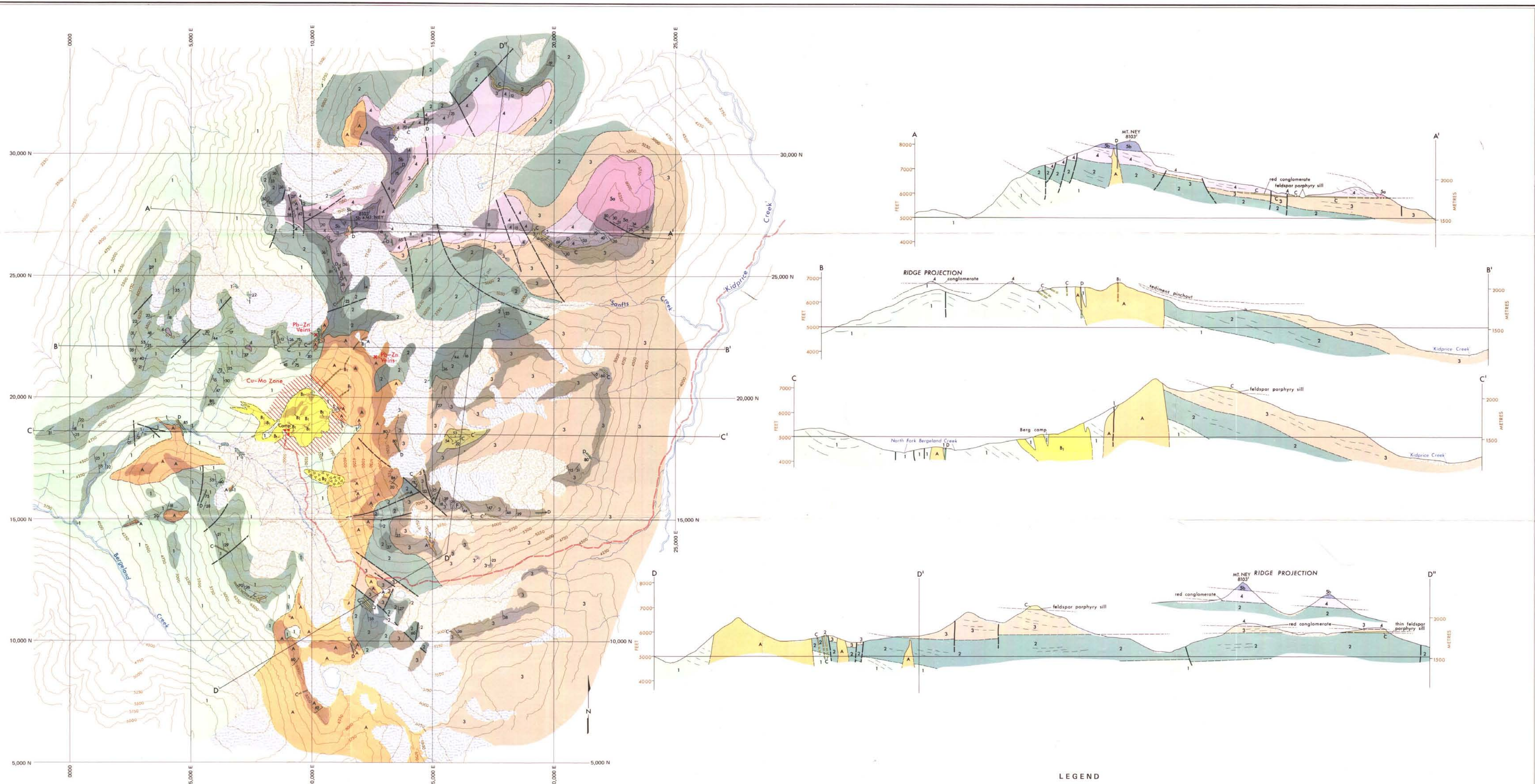
NO	ID	X	Y	COMP.	1	2	3	4	
1	H126	1008	2028	0.6122	-0.8460	0.1461	0.3509	0.2281	
2	H326	1006	2060	0.6377	0.1252	0.1515	-0.0685	0.7709	
3	H422	1117	1508	0.5310	-0.1071	-0.7158	-0.0829	-0.0137	
4	H524	866	1911	0.6462	-0.0633	-0.9082	0.3145	0.1360	
5	H827	1098	1903	0.9277	-0.6557	0.1378	-0.2333	-0.6515	
6	H849	1112	1903	0.9647	-0.6844	-0.2675	-0.2623	-0.5966	
7	H102	1067	2006	0.6650	0.1443	-0.0481	-0.7370	-0.3141	
8	H124	919	2032	0.6645	0.3958	-0.4737	-0.3999	0.3514	
9	H125	917	2042	0.6569	0.2384	-0.0743	0.3201	0.8319	
10	H133	808	1942	0.7941	0.7489	-0.0078	-0.2641	0.4044	
11	H126	225	1957	0.9481	0.6426	0.1051	0.0158	0.7237	
12	H144	1089	1837	0.7779	-0.4341	0.1583	-0.7207	-0.2122	
13	H147	1108	1837	0.4168	-0.0528	-0.6027	-0.1936	0.1154	
14	H141	1135	1837	0.8949	0.2142	0.2074	-0.2175	0.8711	
15	H151	836	1763	0.7764	0.8098	-0.0300	0.0953	0.3327	
16	H171	771	1810	0.9196	0.8133	-0.0316	0.4909	0.1270	
17	H182	1004	2088	0.9568	0.5491	-0.0484	0.2563	0.7663	
18	H194	960	1791	0.7237	0.0831	-0.3557	0.0256	-0.7679	
19	H202	922	1823	0.9587	-0.5395	-0.2203	0.5719	-0.5405	
20	H221	1007	2075	0.5608	0.3573	-0.2322	-0.1553	0.8690	
21	H23A	1049	1777	0.7418	0.0672	-0.3979	0.3224	0.6887	
22	H251	580	1766	0.9964	0.9598	0.2117	-0.1339	0.1112	
23	H264	980	1738	0.6588	0.4897	0.6600	-0.1312	0.0781	
24	H284	906	1812	0.8645	-0.0466	0.1122	-0.3388	0.8573	
25	H252	881	1757	0.8856	-0.0671	-0.0801	-0.1277	0.9265	
26	H303	880	1852	0.8665	-0.5141	-0.7133	0.2108	-0.2212	
27	H322	933	1768	0.7754	0.1166	-0.6268	0.2882	0.5347	
28	H235	1028	1765	0.8235	-0.2099	-0.5078	-0.1657	0.7030	
29	H343	1033	1833	0.5305	0.2678	-0.0059	0.6521	-0.1829	
30	H35A	1058	1810	0.8967	0.3158	0.0521	-0.8890	0.0620	
31	H365	1080	1752	0.5134	0.1712	-0.0721	-0.9286	-0.1288	
32	H374	1079	1735	0.3490	0.1750	-0.5557	0.0585	-0.0789	
33	H422	1081	1970	0.4370	-0.5017	0.3184	0.0209	0.2889	
34	H631	631	1919	0.6564	-0.3021	-0.3275	0.5818	-0.5651	
35	H680	1017	1535	0.7720	0.4371	0.7216	-0.0452	-0.2412	
36	H71A	931	1757	0.8105	0.2325	-0.7667	-0.2650	-0.3135	
37	H724	1105	1807	0.8058	-0.2837	-0.5209	-0.5492	-0.3904	
38	D915	1093	1965	0.8334	-0.8591	0.2655	-0.0381	-0.1459	
39	D943	1107	1577	0.9775	-0.6587	0.1245	-0.4278	-0.5874	
40	D972	1132	1866	0.6412	-0.6261	-0.1432	-0.0572	-0.4747	
41	D105	1073	2026	0.9190	-0.7740	0.3589	0.2432	-0.3634	
42	D803	1079	2048	0.6377	-0.6292	-0.0129	0.1476	0.4689	
43	D16A	1193	1945	0.8946	0.0727	-0.4528	0.6516	0.5056	
44	Q154	1008	2007	0.4887	0.2037	0.0497	-0.6650	0.0497	
45	Q555	886	1914	0.9226	-0.8405	0.1129	0.1435	-0.5029	
46	Q635	1049	1894	0.9022	0.2293	-0.3713	0.4287	0.7266	
47	Q649	1053	1854	0.9334	0.8784	0.3462	-0.1472	0.1427	
48	Q672	1076	1894	0.9677	0.2058	0.7046	-0.2724	-0.5955	
49	Q723	805	1872	0.9698	-0.7073	0.4955	0.4633	-0.6970	
50	Q114	1065	1821	0.8853	0.8549	0.2689	-0.2481	0.1436	
51	Q131	794	1930	0.6420	0.9189	0.2720	-0.1503	0.0324	
52	Q172	770	1809	0.9858	0.6411	0.4483	0.5223	0.3180	
53	Q205	930	1825	0.6828	-0.0780	0.3450	0.6849	-0.2930	
54	Q215	975	1699	0.8958	0.6442	0.0544	0.0435	-0.6898	
55	Q245	981	1756	0.8499	-0.0848	0.5151	0.0238	-0.7595	
56	Q253	980	1764	0.8156	-0.1788	0.7072	-0.3514	-0.4000	
57	Q313	857	1840	0.7370	-0.4438	0.5688	0.4653	0.0052	
58	Q343	1033	1835	0.4919	-0.4468	0.4771	-0.0802	0.2411	
59	Q694	981	1825	0.6599	-0.3175	0.1807	-0.2733	-0.8073	
60	HS18	615	1959	0.7695	-0.2189	-0.4258	0.6931	-0.2445	
61	HS32	996	2190	0.9291	-0.4131	0.0006	0.0666	-0.8684	
VARIANCE					25.197	15.677	14.933	24.947	
CUM.VAR.					25.197	40.874	55.807	80.754	

A. PANTELEYEV--FACTOR ANALYSIS--7 VARIABLES--MARCH 06 1972
VARIMAX FACTOR SCORE MATRIX

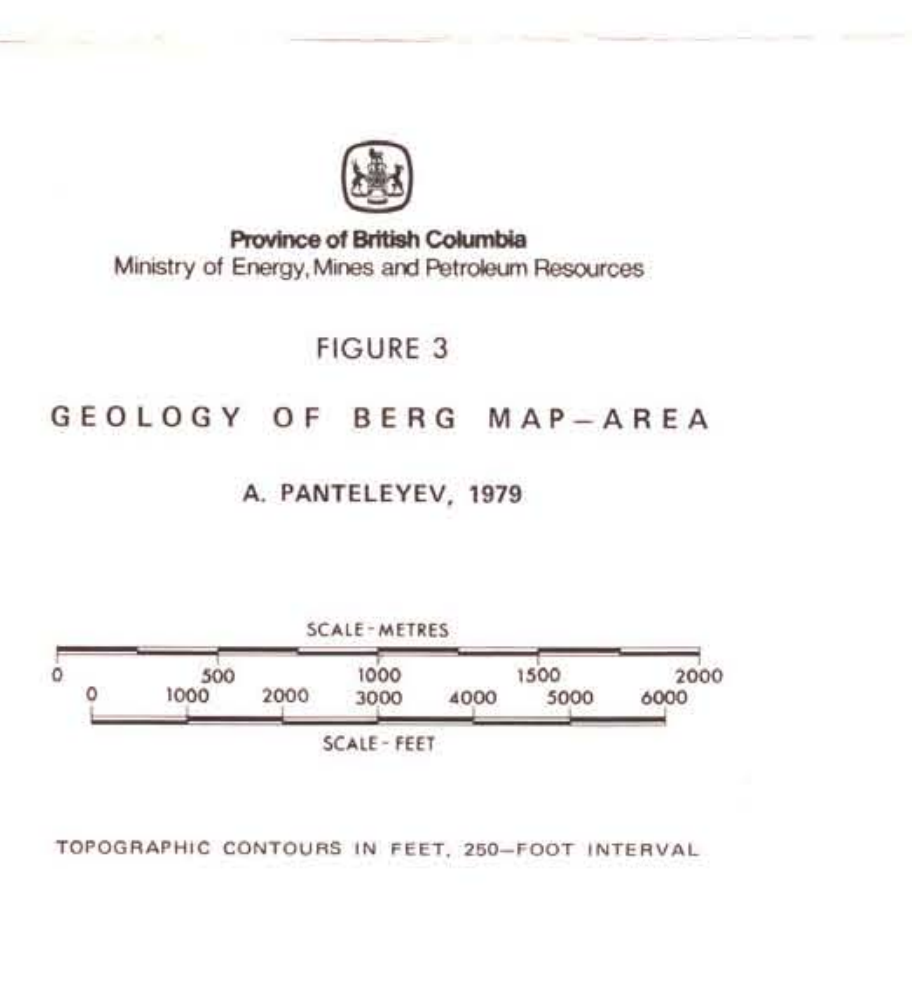
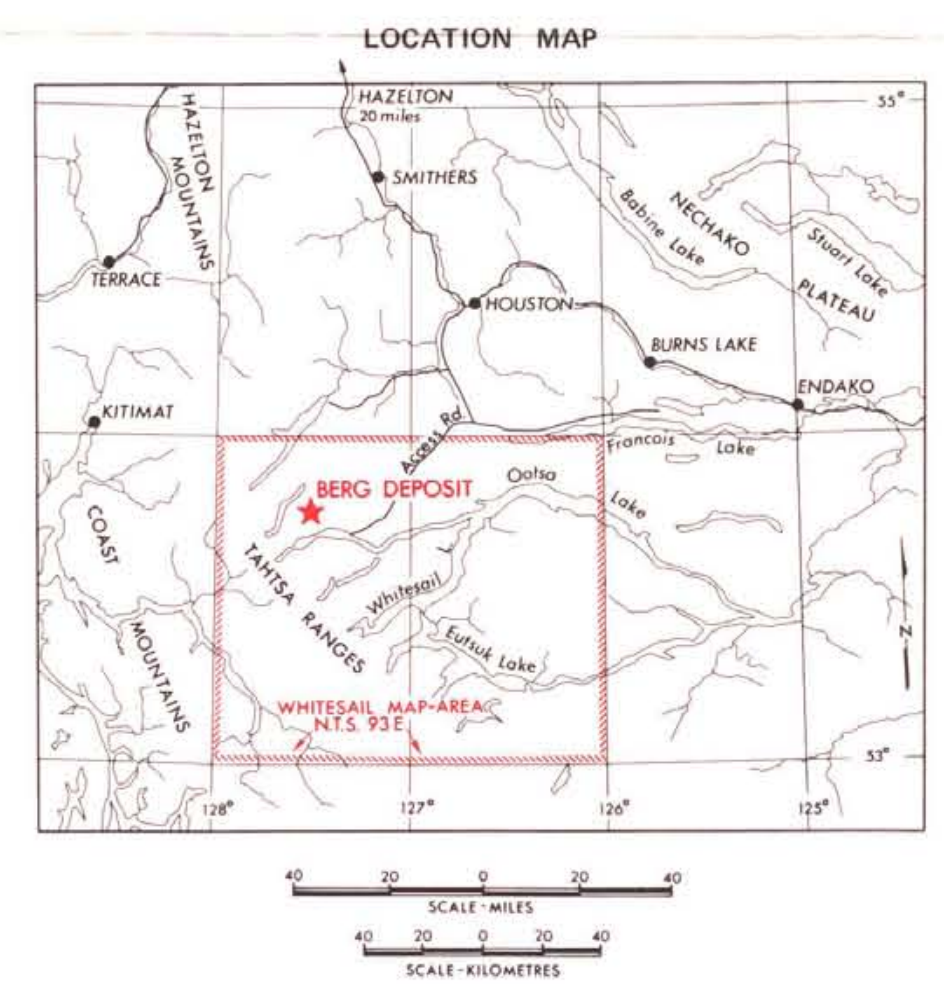
VARIABLE	FACTOR			
	1	2	3	4
BI	0.9095	0.1523	-1.2841	-1.8750
CO	-1.3566	-1.5509	-0.6232	0.2649
NI	-0.3880	-1.3953	0.2777	-1.1781
PB	-0.9091	0.9490	-0.0891	-0.8821
ZN	-1.1705	1.2300	0.4755	-0.2761
AG	-1.3411	0.4139	-1.2566	-0.0075
MN	-0.4406	-0.2025	1.7537	-1.0769

APPENDIX E. VARIMAX FACTOR MATRIX, VEIN PYRITE								
A. PANTELEYEV--FACTOR ANALYSIS--8 VARIABLES--MARCH 06 1972--								
VARIMAX FACTOR MATRIX								
NO.	ID	X	Y	COMM.	1	2	3	4
1	V159	1009	2004	0.8831	-0.1569	0.8576	0.0191	0.3502
2	V121	922	2017	0.9922	0.8321	-0.2500	0.4681	0.1347
3	V142	1078	1837	0.7618	0.3651	0.0708	0.7544	-0.2268
4	V235	1049	1777	0.9283	-0.8168	0.0068	0.3592	-0.3635
5	V243	981	1796	0.9347	-0.9547	-0.1049	-0.0278	0.1070
6	V291	980	1766	0.9666	-0.6771	-0.6211	-0.1718	0.3047
7	V264	980	1738	0.9378	-0.1116	0.1909	-0.1418	0.9321
8	V33A	1028	1765	0.9831	-0.3705	-0.2348	-0.8875	0.0542
9	V356	1058	1810	0.9274	0.8700	0.1330	0.2083	-0.3307
10	V373	1079	1735	0.8426	-0.0031	0.8644	0.1027	0.2915
11	V433	1081	1970	0.9275	-0.3564	-0.7049	0.4468	-0.3225
12	V632	631	1919	0.9148	0.9362	-0.1639	-0.0251	-0.1038
13	V686	1017	1535	0.9664	0.2259	-0.4365	-0.8454	0.0990
14	V654	581	1825	0.7914	-0.5907	0.6507	0.0543	0.1269
15	V705	931	1854	0.8769	-0.2982	0.8206	0.2948	-0.1665
16	V715	930	1798	0.8366	-0.1503	0.8490	0.2788	-0.1245
17	V718	932	1796	0.8260	-0.0809	0.7071	-0.5285	-0.2002
18	VHS1	1035	2242	0.7957	-0.3411	-0.8112	-0.0158	0.1449
19	VHS2	1115	2178	0.8023	0.6591	-0.4871	0.3475	0.0994
20	VHS3	512	1677	0.9316	0.2221	0.3473	-0.6849	-0.5409
VARIANCE					29.593	30.521	18.809	10.210
CUM. VAR.					29.593	60.114	78.923	89.133

A. PANTELEYEV--FACTOR ANALYSIS--8 VARIABLES--MARCH 06 1972--				
VARIMAX FACTOR SCORE MATRIX				
VARIABLE	FACTOR			
		2	3	4
BI	1.1872	-0.6399	1.0534	0.0484
CO	0.3202	1.8517	-0.2424	0.6007
NI	0.0611	1.8828	-0.1691	0.2145
CU	-0.5821	0.6526	1.3282	-2.0786
PE	1.6074	-0.1436	-0.1506	0.4573
ZK	1.2403	0.2182	0.3754	-0.7314
AG	1.2493	0.3739	0.6263	-0.1881
MN	0.6687	-0.1075	-2.1136	-1.5791



LEGEND

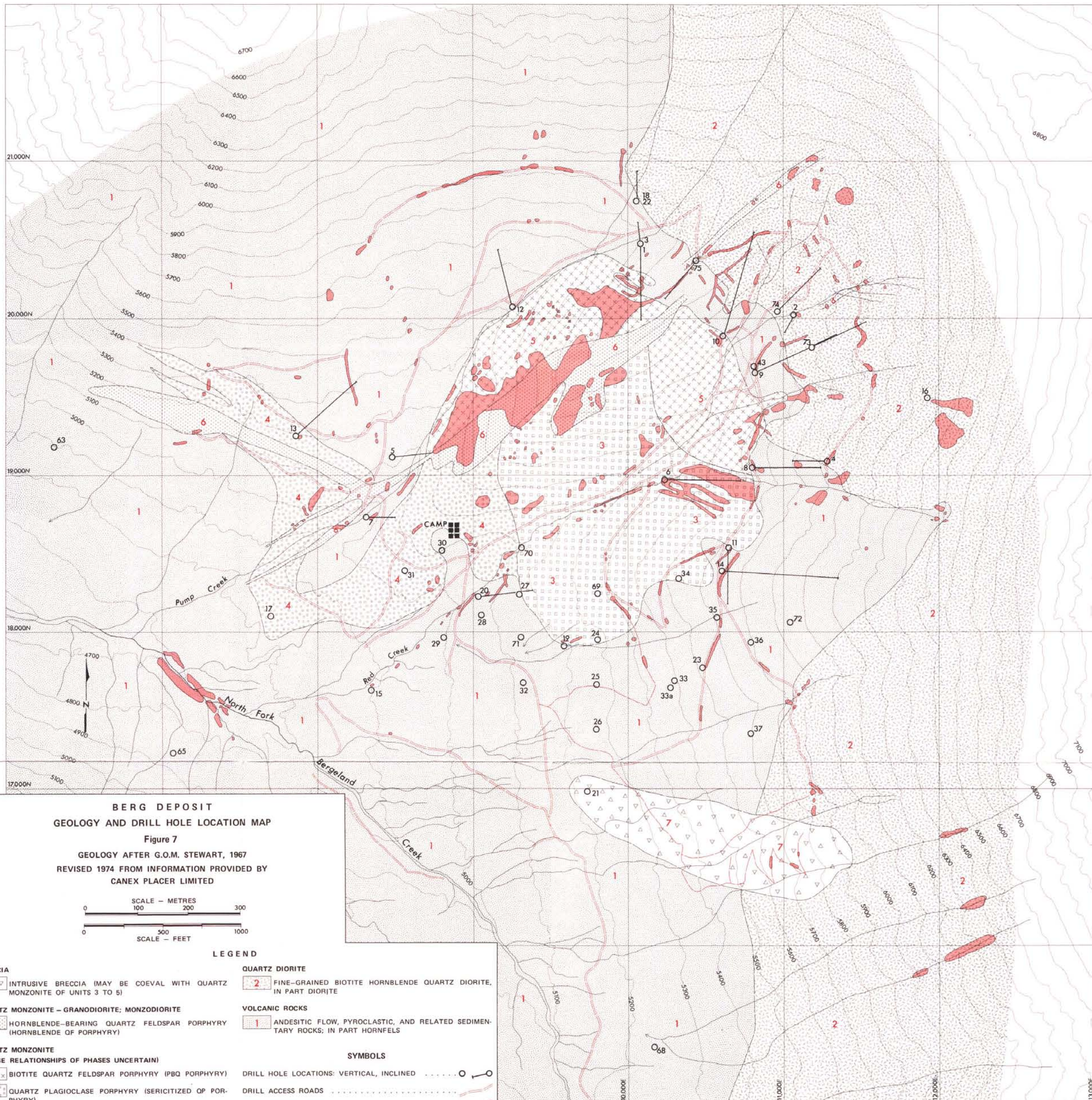


- PLEISTOCENE AND RECENT**
- FLUVIATILE GRAVEL, SAND, SILT; GLACIAL OUTWASH, TILL, MORAINÉ
- LATEST LOWER CRETACEOUS TO UPPER CRETACEOUS**
- 'KASALKA GROUP' (NAME PROPOSED BY MacINTYRE, 1976)**
- 5a** BUFF TO PALE GREY RHYOLITE, RHYODACITE BRECCIA, FLOWS ('BERGETTE FORMATION' OF MacINTYRE, 1976)
 - 5b** GREY, PURPLE, PALE GREY TO CHALK WHITE RHYOLITE, RHYODACITE, DACITE BRECCIA, AGGLOMERATE, VITRIC TUFF, LESSER FELDSPAR CRYSTAL TUFF, ANDESITE PORPHYRY BRECCIA (MAY BE LATERAL EQUIVALENT TO UNIT 5a)
 - 4** DARK GREEN, MAROON, RED BASALT, ANDESITE, LATITE, LAHAR, LITHIC TUFF, BRECCIA; BASAL RED BED CONGLOMERATE ('SWING PEAK FORMATION' OF MacINTYRE, 1976)
- LOWER CRETACEOUS (ALBIAN)**
- SKEENA GROUP**
- 3** SANDSTONE, SILTSTONE, SHALE, MINOR CONGLOMERATE
 - 2** GREY, BLuish GREY, PURPLE, AND GREEN BASALT, ANDESITE FLOWS, BRECCIA, COMMONLY AMYGDALOIDAL, RARELY PORPHYRYTIC

- MIDDLE JURASSIC**
- HAZELTON GROUP**
- 1** GREEN, GREY, RED, MAROON, PURPLE ANDESITIC PYROCLASTIC AND FLOW ROCKS, LESSER DACITIC BRECCIA, VITRIC TUFF, AND SEDIMENTARY ROCKS
- INTRUSIVE ROCKS**
- TERTIARY**
- D** BASIC DYKES
- Eocene (IN PART CRETACEOUS)**
- C** FELDSPAR PORPHYRY, QUARTZ FELDSPAR PORPHYRY, RHYOLITE
- Eocene**
- BERG INTRUSION**
- B₁** INTRUSIVE BRECCIA
 - B₂** QUARTZ MONZONITE PORPHYRY, QUARTZ PLAGIOCLASE PORPHYRY, PLAGIOCLASE BIOTITE QUARTZ PORPHYRY, HORNBLende QUARTZ FELDSPAR PORPHYRY
- Eocene or Older**
- A** QUARTZ DIORITE, DIORITE

- SYMBOLS**
- BEDDING:** INCLINED, HORIZONTAL
 - JOINTING**
 - FOLIATION**
 - FAULT:** DEFINED, INFERRED
 - DYKE, DIP INDICATED**
 - GEOLOGICAL CONTACT:** DEFINED, INFERRED
 - FOSSIL LOCALITY**
 - MAIN OUTCROP AREAS**
 - ACCESS ROAD**

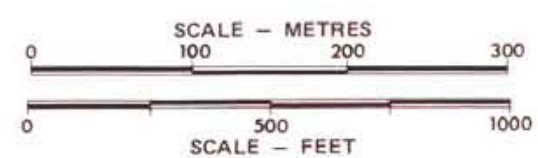
#66 ①



**BERG DEPOSIT
GEOLOGY AND DRILL HOLE LOCATION MAP**

Figure 7

GEOLOGY AFTER G.O.M. STEWART, 1967
REVISED 1974 FROM INFORMATION PROVIDED BY
CANEX PLACER LIMITED



LEGEND

- | | |
|--|--|
| BRECCIA | QUARTZ DIORITE |
| 7 INTRUSIVE BRECCIA (MAY BE COEVAL WITH QUARTZ MONZONITE OF UNITS 3 TO 5) | 2 FINE-GRAINED BIOTITE HORNBLENDE QUARTZ DIORITE, IN PART DIORITE |
| QUARTZ MONZONITE - GRANODIORITE; MONZODIORITE | VOLCANIC ROCKS |
| 6 HORNBLENDE-BEARING QUARTZ FELDSPAR PORPHYRY (HORNBLENDE OF PORPHYRY) | 1 ANDESITIC FLOW, PYROCLASTIC, AND RELATED SEDIMENTARY ROCKS; IN PART HORNBELLS |
| QUARTZ MONZONITE
(AGE RELATIONSHIPS OF PHASES UNCERTAIN) | SYMBOLS |
| 5 BIOTITE QUARTZ FELDSPAR PORPHYRY (PBQ PORPHYRY) | DRILL HOLE LOCATIONS: VERTICAL, INCLINED |
| 4 QUARTZ PLAGIOCLASE PORPHYRY (SERICITIZED QP PORPHYRY) | DRILL ACCESS ROADS |
| 3 QUARTZ FELDSPAR PORPHYRY (QM PORPHYRY) | OUTCROP |
| | CONTACTS: DEFINED, APPROXIMATE |